STRUCTURAL BEHAVIOUR OF STAINLESS STEEL BOLTED BEAM TO COLUMN JOINTS

By

MOHAMED A HUSSAEN ELFLAH

A thesis submitted to the University of Birmingham
for the degree of Doctor of Philosophy

Department of Civil Engineering, School of Engineering

University of Birmingham

Edgbaston B15 2TT, Birmingham, UK

May 2018

List of Publications

The present PhD study has led to a list of journal papers and conference papers as follows:

Journal Papers:

1. Elflah, M., Theofanous, M., Dirar, S. and Yuan, H., 2018. Behaviour of stainless steel beam-to-column joints—Part 1: Experimental investigation. Journal of Constructional Steel Research.

2. Elflah, M., Theofanous, M. and , Dirar, S., 2018. Behaviour of stainless steel beam-to-column joints—Part 2: Numerical modelling parametric study. Journal of Constructional Steel Research.

3. Elflah, M., Theofanous, M. and Dirar S. Behaviour of stainless steel semi-rigid open beam-to-tubular columns joints under monotonic loading. Engineering Structures (in preparation)

4. Elflah, M., Theofanous, M. and Dirar S. A mechanical model for the design of stainless steel T-stubs. Engineering Structures (in preparation)

Conference Papers:

1. Elflah, M., Theofanous, M. and Dirar S .(2015). Structural Performance of stainless steel beam to column joints .in: Proceedings of the 6th Annual BEAR PGR Conference 2016, University of Birmingham, UK.

2. Elflah, M., Theofanous, M. and Dirar S .(2016). Structural Performance of stainless steel beam to column joints .in: Proceedings of the 7th Annual BEAR PGR Conference 2016, University of Birmingham, UK.

3. Elflah, M., Theofanous, M. and Dirar S .(2016). Structural Performance of stainless steel beam to column joints .in: Proceedings of the 7th Annual BEAR PGR Conference 2016, University of Birmingham, UK.

4. Elflah, M., Theofanous, M. and Dirar S (2016). Structural response of stainless steel open beam to tubular column connection .in: Proceedings of the EPS Research Conference 2016, University of Birmingham, UK.

5. Elflah, M. , Theofanous, M. and Dirar S. Structural Performance of stainless steel beam to column joints , Poster conference, Engineering School 2015, University of Birmingham, UK .

6. Elflah, M., Theofanous, M. and Dirar S . Behaviour of stainless steel beam-to column joints-Part 1: experimental investigation. In: Proceedings of the Fifth International Experts Seminar 20171, 18-19 September, London, UK.

7. Elflah, M., Theofanous, M. and Dirar S. Behaviour of stainless steel beam-to column joints-Part 2: numerical modelling and design recommendations, In: Proceedings of the Fifth International Experts Seminar 20171, 18-19 September, London, UK.

Acknowledgements

First of all, I wish to express my sincere gratitude to my supervisor, Dr Marios Theofanous for his dedication, guidance, support, and encouragement throughout my research. His valuable suggestions and time spent with me during my research enabled me to accomplish a highly successful thesis. I am indebted to him and will always remember his contribution throughout my career.

I would also like to gratefully acknowledge the funding received from the Libyan government, in order for me to accomplish my PhD and likewise to Lindapter International for providing the blind bolts to undertake my research.

For my extended family, I can never say enough words to express how grateful I am for the endless support from them. My parents have always provided me with unconditional love, and support needed for me to undertake such a challenge. Without their faith in me, I could not have made it this far.

Special and profound thanks to my brothers and sisters who offered invaluable support and encouragement along my journey and to each of them for their absolute faith in me.

Dedicated to the memory of my father in law, Mr idris, who always believed in my ability to be successful in the academic arena and although no longer with us, his belief in me has made this journey possible. Without any hesitation I extend the same respect and appreciation to my mother in law Fathia.

Most importantly, my deepest gratitude goes to my wife, Narjis, who always stands by me when I encounter problems in my research and her continuous, unconditional encouragement and support. Thanks to my daughter, Salma, and son, Abdul-Razek, who unknowingly gave me the inspiration I always wanted to be to them as a role model father.

Abstract

Research on stainless steel structures has primarily focused on the structural response of individual members, whilst the response of joints has received far less attention to date . To this end, this research aims to investigate the structural performance of common typologies of stainless steel beam-to-column joints under monotonic static loads thus allowing the assessment of current European design guidance (EN 1993-1-8, 2005; EN 1993-1-4, 2015) and the development of novel design rules in line with the observed structural response. The employed methodology includes experimental testing and numerical (Finite Element – FE) modelling. The material grades considered in this study belong to the austenitic and duplex families.

Initially, two experimental programmes studying the structural behaviour of stainless steel beam-to-open column joints and beam-to-tubular column joints under static loads are reported in detail. The joint configurations tested include flush and extended end plate connections, top and seat cleat connections and top, seat and web cleat connections. All connected members and connecting parts including bolts, angle cleats and end plates are in Grade EN 1.4301 stainless steel . The full moment-rotation characteristics, developed strains in critical locations and failure modes are reported in details. It is observed that the connections displayed excellent ductility, superior than that of equivalent carbon steel connections, and attained loads much higher than the ones predicted by design standards for carbon steel joints .

Following the twelve full-scale tests reported in this study, nonlinear FE models have been developed and validated against the experimental results. The FE models are shown to accurately replicate the experimentally determined, initial stiffness, ultimate resistance, overall moment-rotation response and observed failure modes. For this purpose, the FE method was used to generate additional data on key parameters. Hence, a comprehensive parametric study is conducted and the structural response of 132 beam-to-open column joints and 127 beam-to-tubular column joints has been obtained numerically. This information was subsequently used to review the specification of EN 1993-1-8 and also used to propose a simplified mechanical model for the moment-rotation response of stainless steel joints.

Based on both experimental and numerical results, the design rules for stainless steel connections, which are based on the specifications of EN 1993-1-8 for carbon steel joints, are reviewed and are found to be overly conservative in terms of strength and inaccurate in terms of stiffness thus necessitating the development of novel design guidance in line with the observed structural response . Hence, simplified mechanical models in line with the observed response are developed. These models maintain consistency with the component methodology specified in EN 1993-1-8 (2005), whilst taking into account the effect of key material parameters such as strain-hardening on the joint behaviour in a simplified manner. Emphasis is placed on the response of T-stubs , which according to the tests are the critical joint components for the joint configurations considered. The proposed method offers better prediction of the overall joint response and is seen to lead to efficient yet safe design. Finally conclusions are drawn and suggestions for future research are included in the final part of this thesis.

Table of contents

List of figures

List of tables

Nomenclature

A	cross-sectional area
A_{cor}	corner area of cross-section
A_s	tensile stress area of the bolt
CSM	continuous strength method
COV	coefficient of variation
D	outer depth of the section
d	the nominal bolt diameter
d_o	the hole diameter for a bolt
E	Young's modulus
$E_{0.2}$	tangent modulus at 0.2% offset strain
e_1	the end distance from the centre of a fastener hole to the adjacent end of any part, measured in the direction of load transfer
e_2	the edge distance from the centre of a fastener hole to the adjacent edge of any part, measured at right angles to the direction of load transfer
FE	finite element
$F_{T,Rd}$	the tension resistance of an equivalent T-stub flange
F_u	ultimate load
$F_{u,FE}$	predicted ultimate load based on finite element analysis
$F_{u,pred}$	predicted ultimate load

F_y	yield stress
I	second moment of area
L	beam length between centerlines of load and column face
$LVDT$	linearly varying displacement transducer
SHS	square hollow section
t_a	thickness of the angle cleat
t_p	thickness of the plate under the bolt or the nut
t_{wb}	thickness of the beam web
t_{wc}	thickness of the column web
M	bending moment
M_{el}	elastic moment resistance
M_{pl}	plastic moment resistance
$M_{j,Rd}$	the design moment resistance of a joint
N	axial force
n	strain hardening exponent used in Ramberg-Osgood model
$n'_{0.2,1.0}$	strain hardening exponent used in compound Ramberg-Osgood model
p_1	spacing between centres of fasteners in a line in the direction of load transfer
p_2	spacing measured perpendicular to the load transfer direction between adjacent lines of fasteners
r	bolt row number
$R-O$	Ramberg-Osgood
Z	the lever arm

δ	vertical displacement
δ_u	end-shortening at ultimate load
ε	strain, or material factor defined in EN 1993-1-4
ε_f	plastic strain at fracture
ε_{nom}	engineering strain
$\varepsilon_{t0.2}$	total strain at $\sigma_0.2$
$\varepsilon_{t1.0}$	total strain at $\sigma_1.0$
ν	Poisson's ratio
σ	stress
σ_{nom}	engineering stress
σ_{true}	true stress
σ_u	ultimate tensile stress
$\sigma_{u,mill}$	ultimate tensile stress as given in the mill certificate
$\sigma_{0.2}$	proof stress at 0.2% offset strain
$\sigma_{0.2,mill}$	proof stress at 0.2% offset strain as given in the mill certificate
$\sigma_{1.0,mill}$	proof stress at 1.0% offset strain as given in the mill certificate
Φ	the rotation of a joint

Chapter 1

Introduction

1.1 Background

The term stainless steel refers to a broad family of iron-chromium (Fe-Cr) alloys containing a minimum of 10.5% by mass chromium. The chromium reacts with the atmospheric oxygen forming a self-repairing passivation layer of chromium oxide (Cr_2O_3) on the surface of the alloy thus protecting it from corrosion. Higher chromium content leads to an increase in corrosion resistance, and the addition of nickel and other alloying elements such as molybdenum can increase the protection offered by the passivation layer in various environments. Its resistance to corrosion has made stainless steel a very versatile material with applications in different fields such as food, medicine, construction and automotive, among others. The term Inox, which is short for inoxidable, is often used interchangeably with the term "stainless" for such steels even though corrosion does occur, albeit at a very slow rate, whilst the term carbon steel is used to differentiate the standard structural steel grades from stainless steels.

From a metallurgical viewpoint, five subcategories of stainless steels exist, namely austenitic, ferritic, duplex (austenitic-ferritic), martensitic and precipitation hardening. Each of these families has a different chemical composition and crystalline structure, hence

different material characteristics (Euro Inox, 1994). Among the hundreds of existing stainless steel grades, each of which is tailored for optimal performance under different conditions, only a few dozen grades are suitable for structural applications and are covered by international structural design standards. All structural stainless steel grades belong to the austenitic, the ferritic, or the duplex stainless steel subgroup, whilst martensitic and precipitation hardening stainless steels possess poor ductility and weldability characteristics, which render them unsuitable for structural applications.

The increasing importance of sustainability and a transition towards whole life costing has led to an increased interest in the use of stainless steel as a primary structural material (Gardner, 2005; Baddoo, 2008; Rossi, 2014, Elflah, et al., 2018 a). In addition to its excellent corrosion resistance, which leads to minimal maintenance requirements even in aggressive environments, stainless steel possesses high strength, ductility and stiffness and adequate weldability comparable or even superior to that of carbon steel. Furthermore, its superior retention of strength and stiffness at elevated temperatures (EN1993-1-2, 2005; Gardner and Baddoo, 2006) lead to superior fire resistance compared to carbon steel. A recent study on stainless steel memebes, the comparison between stainless and carbon steel composite columns filled with unreinforced concrete was investigated under fire condition. The results show that carbon steel columns buckle at a lower load than stainless steel columns of identical size and length (Gardner and Baddoo , 2006). Additionally, the availability of several surface finishes ranging from dull mill to mirror polished finish (EN 10088-4, 2009; EN 10088-5, 2009) for stainless steel structural products, renders stainless steel a versatile material suitable for elegant and aesthetically appealing architectural applications, like the cladding of the Chrysler building depicted in Figure 1.1. More recently, stainless steel has been used as the principal structural material in numerous road bridges and footbridges (Gedge, 2008), an example of which is shown in Figure 1.2.

In steel constructions, the connections are vital components. In stainless steel structures, it is known that the areas most susceptible to corrosion are the connection zones. This is considered to be the result of the drilling of bolt holes, a process that induces fine cracks in the steel (Salih et al, 2010). This is an additional reason why careful attention needs to be paid to the design of connections; to safeguard against corrosion and ensure effective corrosion resistance. The SCI/Euro Inox Design Manual for structural stainless steel (2006) provides numerous proposals concerning connections; i.e., it recommends avoiding galvanic corrosion either by not including carbon steel (or any other metallic material), or taking precautions such as insulating the stainless or carbon steel by inserting non-metallic bushes, gaskets or washers. This document also advises the complete avoidance of any combination of stainless steel elements and carbon steel bolts.

Figure 1.1 Chrysler Building 1930

Figure 1.2 The Millennium Bridge, York, UK, 2001

Key to any structural application is the material response of the employed structural material. Figure 1.3, shows the material response of typical stainless steel and carbon steel grades at small strains. Contrary to carbon steel, stainless steel grades are seen not to exhibit a well-defined yield point, but a gradual rather than sharp loss of stiffness with increasing strains and significant strain-hardening.

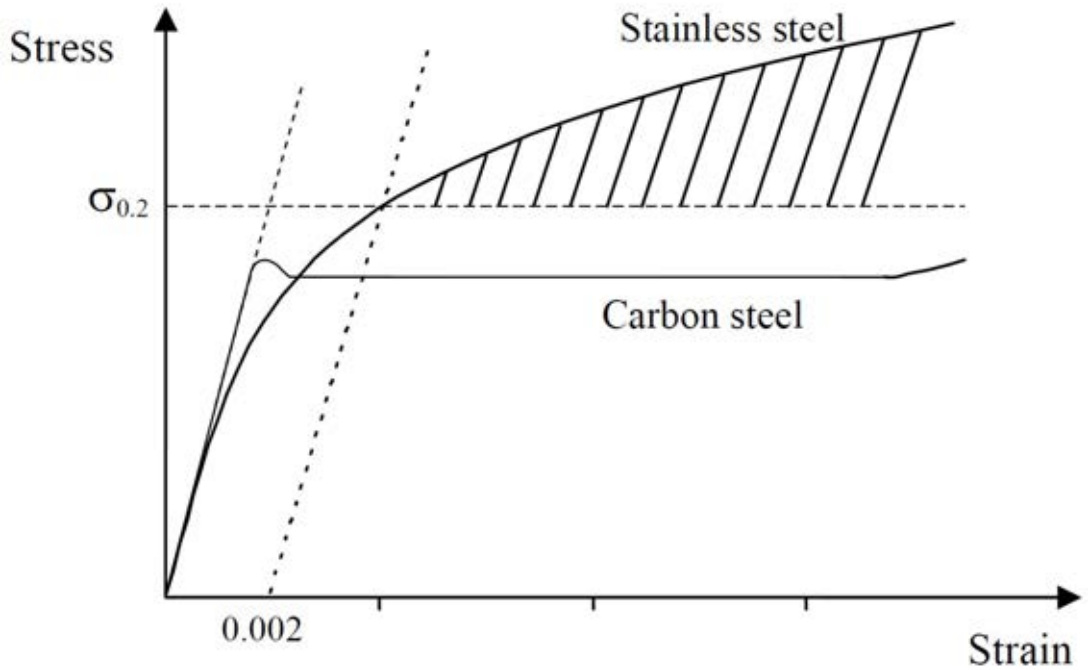

Figure 1.3 stress-strains, tension curves for common stainless and carbon steel grades (Euro Inox, 2006)

The design of stainless steel structures has traditionally relied upon assumed analogies with carbon steel design thus not accounting for the actual material response which exhibits significant strain hardening and absence of a yield plateau . In all international design specifications , including the European EN 1993-1-4 (2015), the Australian AS/NZS 4673(2001) and the American SEI/ASCE 8-02 (2002) and AISC 27 (2013), assume an elastic perfectly plastic material response for stainless steel and adopt a the stress corresponding to 0.2% plastic strain (i.e. $\sigma_{0.2}$) as a conventional yield stress for design in order to maintain consistency with the equivalent design codes for carbon steel structures . Neglecting the significant strain-hardening exhibited by stainless steel has been shown to lead to overly conservative ultimate capacity predictions particularly for stocky stainless steel sections (Afshan and Gardner, 2013; Gardner and Theofanous, 2008) and hence uneconomic design.

Deficiencies in current design guidance put stainless steel at a disadvantage compared to other materials thereby hindering its use in applications where it might be the optimal solution. Given the high material cost of stainless steel, full advantage of its structural merits has to be taken, in order to enable designers to make informed decisions when selecting a structural material for a given application. Hence research into the response of structural stainless steel design is warranted in order to develop improved design guidance to be developed. To date, research on structural stainless steel design has primarily focused on the response of individual stainless steel components, with the response of stainless steel joints having received far less attention. Due to lack of available research, current design rules covering stainless steel joints are essentially identical to the ones adopted for ordinary carbon steel joints, despite stainless steel's pronounced strain-hardening and superior ductility. It is the intention of this project to generate much needed research into the response of stainless steel connections focusing on beam-to-column joints, for which no experimental data have reported to date in the published literature. No significant difference between stainless steel and carbon steel joints is expected in terms of the initial stiffness, as the Young's modulus of both materials is similar. Contrary, due to the

higher material ductility and significant strain-hardening of stainless steel, significant gains in terms of strength and rotation capacity are expected, however they have not been quantified to date (Elflah et al, 2018 a).

1.2 Aim and scope

The aim of this project is to investigate the structural performance of common typologies of stainless steel beam-to-column joints under monotonic static loads thus allowing the assessment of current European design guidance (EN 1993-1-8, 2005; EN 1993-1-4, 2015) and the development of novel design rules in line with the observed structural response. The employed methodology includes experimental testing and numerical (Finite Element – FE) modelling. The material grades considered in this study belong to the austenitic and duplex families, whilst the response of ferritic stainless steels has not been considered given their inferior strain-hardening characteristics and ductility which resemble that of carbon steel. The experimental study focuses on both conventional connections to open column sections and blind-bolted connections to tubular column sections in a typical austenitic stainless steel grade. The experimental results are augmented with FE simulations, thus allowing the response of stainless steel joints over a large range of geometric configurations to be investigated and design recommendations to be made.

1.3 Objectives

To achieve the stated aim, the following research objectives need to be met:

1. To investigate the material properties of all components of the joints, including the connected members, the bolts, the angle cleats and the plates.

2. To investigate experimentally the structural response of common typologies of beam-to-open column joints under monotonic loads.

3. To investigate experimentally the structural response of common typologies of beam-to-tubular column connections utilising Hollo-Bolts under monotonic loads.

4. To develop and to validate numerical models against the obtained experimental results

5. To conduct parametric studies thus augmenting the pool of experimental data with numerical data.

6. To review the current European design rules for stainless steel joints specified in EN 1993-1-8 (2005), as well as other design methods reported in the literature.

7. To propose novel design rules that better accord with the observed response that allow improved ultimate capacity predictions to be made.

1.4 Outline of the thesis

In this chapter, an overview of stainless steel, its material response and structural applications has been given and the aim, scope and objectives of this research project have been stated.

In Chapter 2, a broad literature review on the response of connections is carried out. The very few available experimental and numerical data on stainless steel connections are initially discussed, followed by a review on the structural response of bolted beam to column joints, which in the absence of stainless steel data focuses on carbon steel data. A review on available techniques, methods, and fasteners for the execution of bolted connections where access is available from one side only (i.e. bolted connections to tubular columns) is also included. A more focused review on specialized topics, including design

methods and modelling techniques is included in the relevant chapters.

Chapter 3 reports a comprehensive experimental investigation into the structural response of stainless steel bolted beam-to-open column joints. The execution of six full-scale tests on commonly employed joint typologies subjected to static monotonic loads is described and the obtained results are reported in detail and compared against the codified provisions of EN1993-1-8 (2005).

Chapter 4 focuses on an experimental study on beam-to tubular column joints subjected to static monotonic loads. As in Chapter 3, the full load-deformation response is reported and compared against relevant design provisions.

Chapter 5 states the modelling assumptions and describes the development of 3D non-linear FE models that can accurately replicate the experimental response of the specimens reported in Chapters 3 and 4. Parametric studies are then conducted to investigate the response of stainless steel joints in terms of stiffness, strength, failure modes and ductility over a wide range of geometric configurations. The effect of material response on the joint behaviour is also investigated and the accuracy of design provisions is assessed.

Chapter 6 utilises all results obtained in Chapters 3-5 to develop a simplified predictive model for the response of stainless steel joints, taking into account key features such as strain-hardening in a simplified manner. Emphasis is placed on the response of T-stubs which according to the tests are the critical joint components.

Finally, Chapter 7 contains a summary of the findings of this study and gives an overview of the contribution of this research project to structural stainless steel design. Suggestions for further research, some of which is already underway, are also provided.

Chapter 2

Literature review

2.1 Introduction

In this chapter a broad review of previous research relevant to this project is carried out. Initially the very limited pool of available experimental and numerical test data on stainless steel joints of various types is summarized and discussed. Thereafter, a more focused literature review on conventional carbon steel beam-to-open section column joints, pertinent to the tests reported in Chapter 3, is conducted and the relevant European design provisions of EN 1993-1-8 (2005) are presented. The next part of the literature review is devoted to the behaviour of beam-to-tubular column joints and includes a review of available techniques, methods, and fasteners for the execution of bolted connections when there is access only from one side (i.e. blind bolted connections). Finally, concluding remarks are made and knowledge gaps are identified. Additional discussions of specific aspects of past studies are included in the relevant chapters as appropriate.

2.2 Types of beam-to-column connections

For steel frame construction, it is common practice to connect beams to columns on site. A variety of connections are used. These connections usually involve some combination of bolting and welding. Normally, it is preferred that bolts are used on site with welding undertaken in fabrication shops.

Welding on site is generally to be avoided if possible and any welding required for a connection is done in shop, under better quality control conditions than can be achieved on site. Site-welded moment connections are not popular for a number of reasons, including; (i) expense, (ii) erection difficulties, it may not be possible with welded steel frames to pack the joints together so as to facilitate a fully aligned structure, and (iii) in many locations, there are limitation to welding due to climatic conditions. Bolted connections are usually more flexible than fully welded joints, thus accentuating the need for semi-rigid design methods.

The eight connection types shown in Figure 2.1 were the subject of a survey (PASK, 1982) of beam-to-column connections used by the construction industry in the UK. The behaviour characteristics of the connections, the joints, fall into the following categories currently used in industry: flexible, semi-rigid and rigid. The survey suggests that the most frequently used beam-column connection is the flush end plate (FEP); 96% of the replies claimed to use this connection "frequently". The extended end plate (EEP) is also popular, presumably because of its extensive use in portal frame construction. For connections using angle flange cleats; Top, Seat and double Web Cleat connection (TSWAC) and Top and Seat Angle Cleat connection (TSAC) are more popular than Web and Seat Angle Cleat connection. For 'no moment' connections, the web cleat is popular but the 'flexible' end plate is not much used. Directly welded with horizontal stiffener connections has limited use because it involves site-welding. Hence, the flush end plate connection (FEP), the extended end plate (EEP), the Top, Seat and double Web Cleat connection (TSWAC), and the Top and Seat Angle Cleat connection (TSAC) were selected, have been studied herein, and are as described below: :

- The flush end plate (FEP) and the extended end plate (EEP) connections are invariably welded to the beam's web and flanges in a workshop, and subsequently bolted on site to the column. EEP connections are divided into types, see Figures

2.1.f and 2.1.g (Chen, 2011), where the end-plate is extended only on the tension side, or extended on both the tension and compression sides.

- The combinations of Top, Seat and double Web Cleat connections (TSWAC): are shown in Figure 2.1.c. Double Web Angle is used to increase the moment resistance of connections and for shear transfer (Chen, 2011).

- The Top and Seat Angle Cleat connection (TSAC): this type of connection has top and seat angles as shown in Figure 2.1.b. The top angle is used to transfer the top vertical forces of the beam to the column while the seat angle is used to support the compression flange of a beam laterally (Chen, 2011).

2.3 Previous studies on stainless steel connections

Most of the published research underpinning the development or revision of stainless steel design codes has focused on the response of structural members, whilst the design and response of stainless steel connections has received significantly less attention, even though the high ductility and significant high strain-hardening of stainless steel is expected to significantly affect their strength and overall response (Salih et al., 2013). The first experimental research on stainless steel bolted and welded connections were reported by Errera et al. (1974), who confirmed the suitability of the design equations previously proposed for cold-formed steel by Winter (1956), for the determination of the strength of austenitic stainless steel lap joints. Van der Merwe (1987) investigated experimentally the response of bolted ferritic stainless steel lap joints in single or double shear. The number of bolts employed in his studies varied from 1 to 4.

A further of 31 experimental tests was conducted on austenitic and duplex stainless steel lap joints in single shear by the Steel Construction Institute. The adoption of a reduced ultimate stress value for the connected plates was recommended when checking bearing

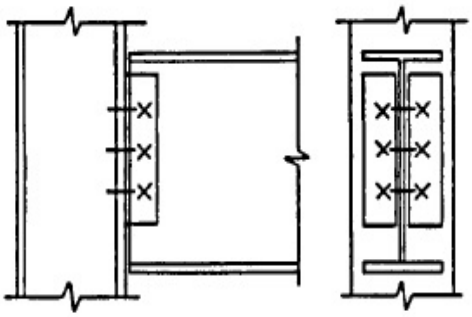

(a) Web Angle Cleat connection

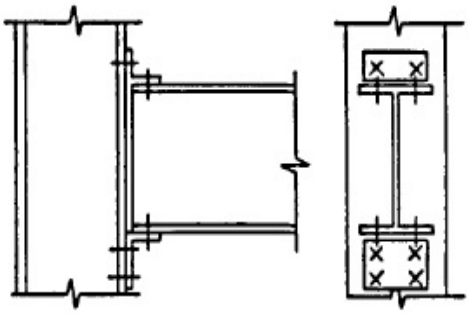

(b) Top and Seat Angle Cleat connection

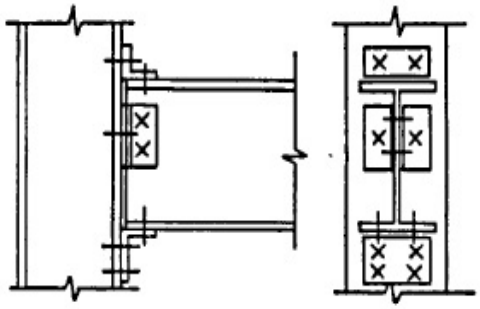

(c) Top, Seat and Double Web Cleat connection

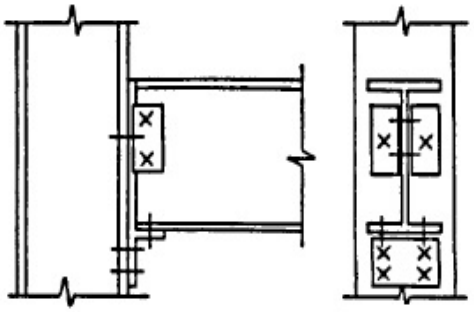

(d) Web and Seat Angle Cleat connection

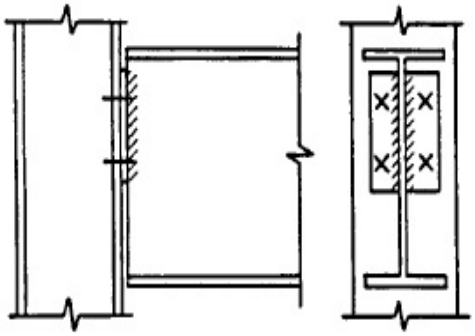

(e) Flexible End Plate connection

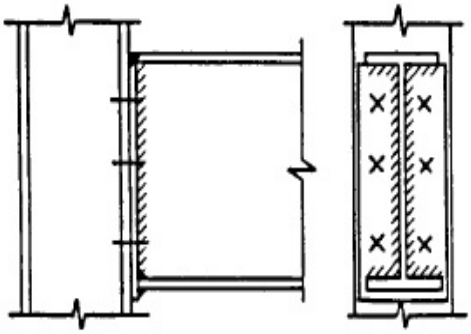

(f) Flush End Plate connection

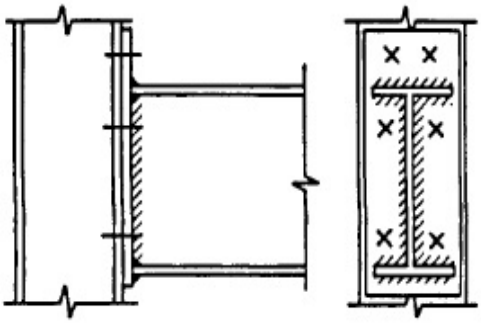

(g) Extended End Plate connection

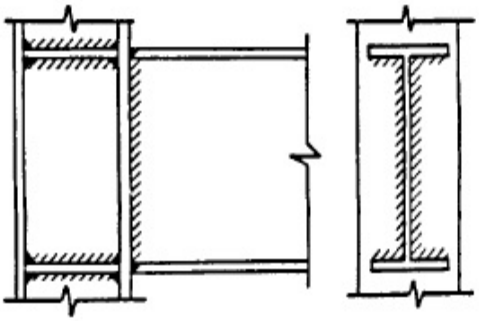

(h) Directly welded with horizontal stiffeners connection (PASK, 1982)

Figure 2.1 Common beam-to-column connection types.

resistance to limit the ovalisation of bolt holes (i.e. plastic deformation) within acceptable limits. A summary of these tests can be found in the commentary to the 2nd edition of the Design Manual for structural stainless steel (SCI/EuroInox, 2003). Ryan (1999) conducted 36 tests on austenitic, ferritic and duplex stainless steel bolted lap joints (12 tests per material grade) subjected to double shear and observed that in all cases failure was ultimately triggered by bolt failure in shear, with the net section resistance of the connected stainless steel plates exceeding the predicted value due to the high ductility of the plates. A plastic deformation limit of 5 mm and 1.75 mm was specified for ultimate and serviceability limit states respectively. This is in accordance with the recommendations by SCI/EuroInox (2003) and demonstrates that due to the significant strain-hardening and ductility exhibited by stainless steels (particularly the austenitic and duplex grades), deformation considerations are likely to govern the design of connections even at the ultimate limit state.

Based on the experimental test results reported by Ryan (1999), Buchair et al. (2008) and Salih et al (2010; 2011; 2013) validated numerical models and conducted extensive parametric studies investigating the net section failure (Salih et al., 2010), bearing failure (Salih et al., 2011) and response of gusset plate connections (Salih et al., 2013). Considering both the experimental and numerical results, Salih et al. (2010; 2011; 2013) highlighted the conservatism of the then valid European design recommendations EN 1993-1-4 (2006) and proposed more efficient design equations.

More recently, Kuwamura and Isozaki (2002) conducted 90 experiments on austenitic stainless steel joints in single shear to investigate the effect of curling. The original source document reporting the tests is in Japanese, but information on the experiments can be found in subsequent publications by Kim and Kuwamura (2007; 2011) and Kim et al. (2008), where they report numerical studies based on models validated against the test results by Kuwamura and Isozaki (2002).

Talja and Torkar (2014) reported an extensive experimental investigation on ferritic stainless steel bolted and screwed lap joints of relatively thin material (thickness ranging from 0.5 mm to 4.5 mm). They proportioned the dimensions of the specimens is such a way that all possible failure modes could be studied within their test series. A total of 11 tests were performed to determine the net section resistance of flat austenitic stainless steel bars, whilst a further 3 tests were conducted on ferritic stainless steel angles cleats. The resistance of bolt groups to bearing and block tearing was investigated via 23 and 11 relevant tests respectively. 54 tests were performed on screwed lap joints between thin plates (0.5 mm to 1.2 mm). Their main conclusions confirmed the validity of design guidance developed for carbon steel for the design of bolted and screwed ferritic stainless steel lap joints except where block tearing of bolted connections and load bearing of screwed connections where an extra reduction factor of 0.9 needs be introduced for safe design.

Cai and Young (2014b) conducted a total of 49 tests on austenitic and lean duplex stainless steel lap joints in both single and double shear with 1, 2 and 3 bolts. Furthermore, they tested 100 lap joints in single shear (Cai and Young, 2014a) and 194 lap joints in double shear (Cai and Young, 2015) at elevated temperatures and complemented their experimental studies with extensive FE investigations (Cai and Young, 2016), providing, for the first time, design rules for stainless steel bolted lap joints at elevated temperatures. In addition to the response of bolted stainless steel lap joints, 54 fillet welded stainless steel lap joints and 7 full and partial penetration butt welded joints have also been tested and an overview of these tests can be found in SCI/Euro Inox (2003). A summary of all test data on bolted and welded lap joints collected from the literature is given in Table 2.1. In cases where the original documents reporting the experimental tests were difficult to obtain, the SCI/Euro Inox (2003) design manual is cited as the source document since it is readily available.

Table 2.1 Available test data on stainless steel bolted and welded lap joints

Source	Material grade	Type of tests	No of specimens
Errera et al. (1974)	austenitic	single/double shear	15
Van der Merwe (1987)	ferritic	single/double shear	66
Ryan (2001)	austenitic, duplex and ferritic	double shear	36
Kuwamura and Isozaki (2002)	austenitic	single shear	90
SCI/Euro Inox (2003)	austenitic and duplex	single shear	31
SCI/Euro Inox (2003)	austenitic and duplex	longitudinal, inclined and transverse fillet welded, and butt welded joints	61
Talja and Torkar (2014)	ferritic	single and double shear bolted and single shear screwed lap joints	48 bolted and 54 screwed lap joints
Cai and Young (2014a)	austenitic and lean duplex	single shear at elevated temperatures	100
Cai and Young (2014b)	austenitic and lean duplex	single and double shear	49
Cai and Young (2015)	austenitic and lean duplex	double shear at elevated temperatures	194

Departing from studies on simple lap joints, Feng and Young (2008 a,b)have extensively investigated the structural behaviour, fatigue and failure modes of welded connections between empty and concrete filled stainless steel tubular (RHS/SHS) members representative of typical truss joints between the chord and diagonal members. They reported 22 and 27 experimental results on stainless steel welded T-joints between empty (Feng and Young, 2008a) and concrete filled (Feng and Young, 2008b) SHS and RHS respectively. Furthermore, they conducted 32 experimental tests on bare stainless steel (Feng and Young, 2010) and 25 experimental results on concrete filled stainless steel (Feng and Young, 2009) X-joints as well as an experimental investigation on the stress concentrations in welded stainless steel X-joints with the aim to provide fatigue guidelines (Feng and Young, 2013). Feng and Young (2011) augmented their experimental results with a comprehensive FE study, based on which they proposed improved design rules for welded stainless steel joints

between tubular members. No other experimental study on welded stainless steel tubular joints exist.

Tao et al (2017) recently published a paper on the response of blind bolted beam-to concrete filled stainless steel tubular column connections. 4 SHS and 3 CHS concrete filled stainless steel sections were tested under monotonic or cyclic loading with or without the presence of a concrete slab. All tested joints involved a concrete-filled stainless steel column and hence do not lend themselves for the assessment of design provisions for stainless steel joints, as the presence of concrete slab and the interaction of concrete infill and blind bolts complicate the response and affect the developed failure modes (Elflah et al, 2018 a). Given the inherent scatter of experimental results where concrete is present, deducing the response of stainless steel joints based on the tests of Tao et al. (2017) is not possible .

An attempt to study numerically the response of top and seat cleat stainless steel beam-to-column joints was recently reported by Hasan et al. (2017). However, due to the absence of relevant test data, the validation of the numerical models was based on existing carbon steel experimental results, and assumptions regarding the material response and the interaction of the various stainless steel components in the numerical model were made (Elflah et al, 2018 a). The validation of the FE model developed by Hasan et al. (2017) against carbon steel test data demonstrates the urgent need for relevant stainless steel test data.

Finally, Yuan et al. (2018) reported a comprehensive experimental study on the structural response of austenitic and lean duplex stainless steel T-stubs in tension considering the effect of bolt size, material grade, T-stub thickness and applied preload of the bolts. Although not full-scale experiments, these tests are the first ever to be reported which characterize the response of stainless steel T-stubs, arguably the most significant component of beam-to-open section column joints. Since they are closely related to this

project, the tests reported by Yuan et al. (2018) are extensively utilized in Chapter 6 where design equations for stainless steel joints are devised. This brief literature survey clearly highlights the need for full-scale tests on stainless steel beam-to-column joints which has led to the project reported in this thesis .

2.4 Behaviour and design of beam-to-column joints

The definition of connections or joints is the physical tying of the adjacent members together, to facilitate a change in direction or splice together shorter elements. The main function of a joint is to transmit loads between the connected members; in the case of a beam-to-column joint to transmit forces and moments from the supported member (beams) to the supporting members (columns). Traditionally, beam-to-open column joints are the most widely adopted moment resisting connections, since I-section beams and H or I-section columns are extensively employed in construction. No experimental studies on stainless steel beam-to-column joints exist to date, hence international design codes like EN1993-1-4 (2015) refer to the relevant design guidance for carbon steel joints EN1993-1-8 (2005) with only minimal additional requirements reflecting the effect of stainless steel. Consequently, the design guidance and underpinning research on carbon steel beam-to-column joints is reviewed herein in the absence of specific guidelines for stainless steel joints.

2.4.1 Joint behaviour and classification according to EN1993-1-8

The structural behaviour of beam-to-column joints is characterized by its respective moment-rotation curves, which is a graphical representation of the moment transmitted from one member to another with increasing relative rotation between the two members. A typical moment rotation graph is shown in Figure 2.2 where the moment-rotation curve of an extended end plate beam-to-column joint is schematically depicted. As shown in Figure

2.2, for small rotations the response is linear, whilst there is a progressive loss of stiffness with increasing rotation until the maximum moment resistance is reached, whereupon the curve descends. The three main characteristics of all beam-to-column joints as annotated in Figure 2.2 are the rotational stiffness (i.e. slope of initial linear branch of the curve), the moment resistance, which corresponds to the strength of the connection assumed in design and the rotation capacity which is a measure of ductility, i.e. ability of the connection to undergo large inelastic deformations without a significant loss of moment resistance (SCI/BCCA, 1995). It should be noted that the moment resistance of a joint assumed in design does not correspond to the maximum moment that the connection can attain before failure, but to the so-called pseudo plastic moment resistance of the joints $M_{j,R}$, which corresponds to the strength of the joint when its weakest joint component yields, rather than the ultimate moment resistance (Beg et al., 2004). This is further discussed in Chapter 3.

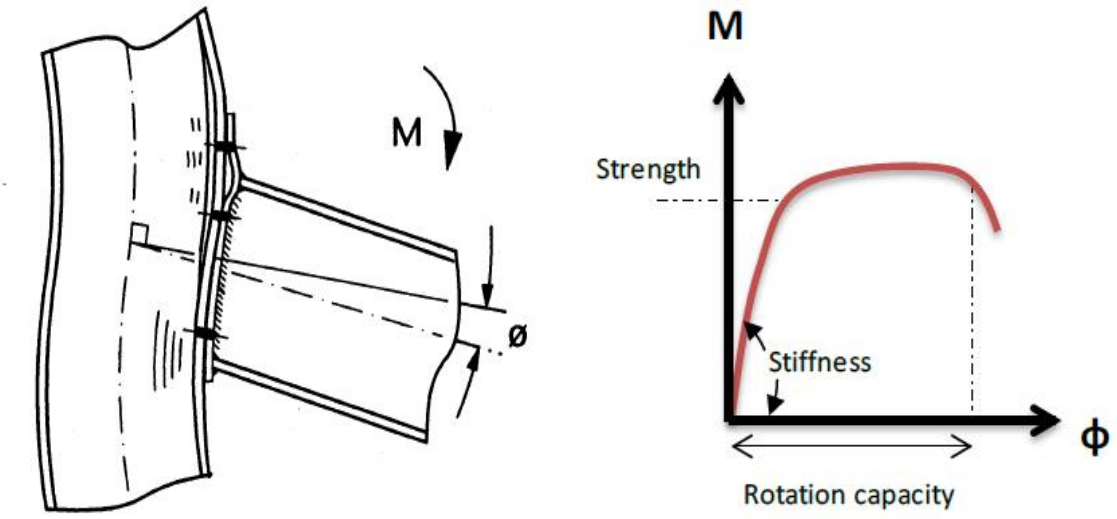

Figure 2.2 Extended end plate beam to column joint a schematic representation of corresponding moment-rotation response (Pitrakkos, 2012).

EN 1993-1-8 (2005) classifies the connections with respect to strength, stiffness and ductility and specifies appropriate design methods and relevant assumptions for global analysis. Table 2.2 and the curves plotted in Figure 2.3 illustrate six examples of joint response and how they fit within the classification boundaries for strength and stiffness specified in EN1993-1-8 (2005).

As shown in Figure 2.3a, a joint can be classified as full-strength (joints A, B, D), partial strength (joints C and E) or nominally pinned such as joint F. Full-strength joints have a moment resistance at least equal to the moment resistance of the weakest of the connected parts, whereas nominally pinned joints can carry a moment no more than 25% of the moment resistance of the weakest of the connected parts (SCI/BCCA, 1995). The moment resistance of nominally pinned joints is usually ignored and they are assumed to only transmit forces. Joints the strength of which lies between the limiting values for nominally pinned and full-strength joints are classified as partial-strength joints (SCI/BCCA, 1995).

With reference to Figure 2.3b, a joint can be characterized as rigid (joints A, B, C and D), semi-rigid (joint E) or nominally pinned like joint F with respect to its stiffness. Nominally pinned joints are assumed to allow free rotation of the beam's end with respect to the connected column and hence possess infinite rotation capacity, whereas rigid joints are assumed to prevent any relative rotation between the connected parts.

Figure 2.4 is extracted from EN 1993-1-8 (2005) and shows how joints are classified with respect to how the joint stiffness compares to the beam stiffness. When the joint stiffness is less than 50% of the stiffness of the connected beam (zone 3 of Figure 2.4), the joint is assumed pinned (i.e. nominally pinned) and its stiffness may be ignored in design. Ignoring the moment transmitted by nominally pinned or even semi-rigid joints has been shown to lead to safe design for all but a few unrealistic structures, provided the connections possess sufficient rotation capacity (i.e. yielding of the connected parts occurs

prior to failure of bolts or welds) (Brahman and Jaspart, 2004). On the contrary, when the joint stiffness exceeds a limiting stiffness value associated with the beam stiffness, full continuity between the connected beam and column may be assumed and the differential rotation between the connected parts is neglected (zone 1 of Figure 2.4). Different limiting values for the beam stiffness are adopted for braced and non-braced frames, with more stringent requirements imposed on frames that do not rely on a bracing system for their lateral stiffness. Joints that do not meet the requirements to be characterized as nominally pinned or rigid are classified as semi-rigid (zone 2 of Figure 2.4).

In the case of either nominally pinned or rigid joints explicit consideration of the joint stiffness is not required in the structural analysis. Hence the analysis and design of the members can be conducted independently of the design of the connections, which are designed at a later stage to accommodate the assumptions made in the global analysis (i.e. as rigid or pinned connections). On the contrary, semi-rigid joints, lying between these two extremes, necessitate the explicit determination of the joint stiffness and are simulated in analysis by means of rotational springs. Although computationally more demanding, the adoption of semi-rigid joints has been shown to results in more economic design solutions compared to pinned or rigid joints (Jaspart, 2000). Therefore, numerous researchers have studied the influence of semi-rigid joints on the structural response of frames (Jaspart, 1988; Jaspart and Maquoi, 1990) and the effect of connection stiffness on column buckling (Nethercot and Chen, 1988).

Table 2.2 Joint classification and design assumptions (SCI/BCSA, 1995)

Design method		Connection response	
Type of joint model	Method of global analysis	Properties	Figure 2.3 Examples
Simple	Elastic	Nominally pinned	F
Continuous	Elastic	Rigid	A, B , C and D
	Rigid-Plastic	Full-strength	A , B and D
	Elastic-Plastic	Rigid and full-strength	A , B and D
Semi-continuous	Elastic	Semi-rigid	E and F
	Rigid-Plastic	Partial-strength and Ductile	E and F
	Elastic-Plastic	Semi-rigid and/or Partial-strength	Any

.

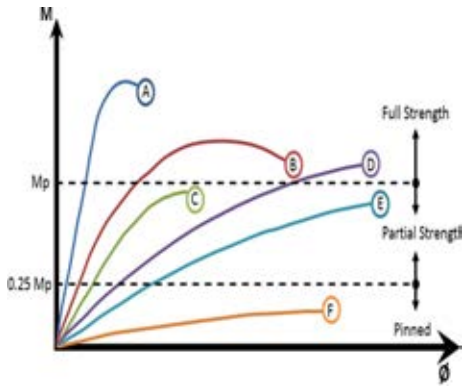

(a) Classification by strength

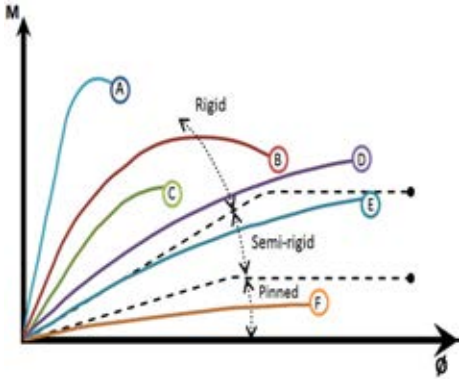

(b) Classification by stiffness

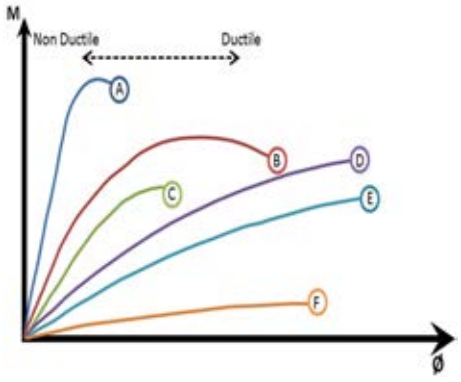

(c) Classification by Ductility

Figure 2.3 Classification of Joints According to SCI/BCCA (1995)

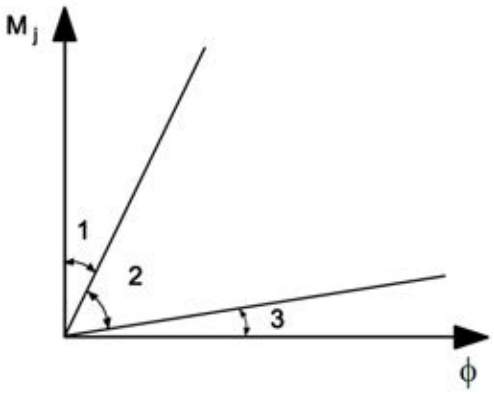

Zone 1: rigid, if $S_{j,ini} \geq k_b EI_b / L_b$

where:

$k_b = 8$ for frames where the bracing system reduces the horizontal displacement by at least 80 %

$k_b = 25$ for other frames, provided that in every storey $K_b/K_c \geq 0{,}1$ *)

Zone 2: semi-rigid

All joints in zone 2 should be classified as semi-rigid. Joints in zones 1 or 3 may optionally also be treated as semi-rigid.

Zone 3: nominally pinned, if $S_{j,ini} \leq 0{,}5\, EI_b / L_b$

*) For frames where $K_b/K_c < 0{,}1$ the joints should be classified as semi-rigid.

Figure 2.4 Classification of joints with respect to stiffness (EN1993-1-8, 2005)

where : E is the young's modulus of beam;

- $S_{j,ini}$ is the initial rotational stiffness of the joint;
- M_j is the bending moment of the joint;
- Φ is the rotation capacity of joint;
- K_b is the mean value of I_b/L_b for all the beams at the top of that storey;
- K_c is the mean value of I_c/L_c for all the columns in that storey;
- I_c is the second moment of area of a beam;
- I_c is the second moment of area of a column;
- L_b is the span of a beam (centre-to-centre of columns);

Significant differences in joint rotation capacity can be observed in Figure 2.3c, where the amount rotation capacity accommodated prior to failure of the various joints varies significantly, depending of the ductility of the failure mode of the joints. Contrary to strength and stiffness, EN 1993-1-8 (2005) does not specify any means of quantifying the supplied rotation of a connection, nor does it define any strict limits for the classification of joints with respect to their ductility. Instead, it is specified that a bolted beam-to-column

joint may be assumed to possess sufficient rotation capacity provided that its failure is governed by a ductile failure mode (e.g. column web panel in shear, column flange in bending, end plate or angle cleat in bending) and brittle modes associated with bolt failure or weld failure are prevented.

2.4.2 Typical behaviour of common beam-to-column joints

Figure 2.5 depicts schematically several joint configurations commonly used in practice and their associated moment-rotation responses. It is evident that some joint types display higher stiffness and/or strength compared to others (e.g. fully welded joints with stiffeners display the stiffest response, whilst bolted connections are more flexible due to among others the tolerance between the bolts and the bolt holes).

Davison et al. (1987) reported 17 full scale bolted beam-to-column joint tests with the focus lying in determining the rotational stiffness of various commonly employed bolted joint configurations, including web cleats, top and seat angle cleats, seat and web cleats, flush end plates, extended end plates and header plates. Figure 2.6 shows the obtained response of the tested configurations and can be seen to accord well with the typical moment rotation curves schematically shown in Figure 2.5. It can be observed that among all joint configurations considered the extended end plate (EEP) and the flush end plate (FEP) joints display the highest stiffness and strength, whilst the top and seat angle cleat (TSAC) joints (termed flange cleats in Figure 2.9) have a markedly lower stiffness and strength and experience a gradual loss of stiffness and a very limited linear response. Similar observations are made in Chapter 3 where tests on EEP, FEP and TSAC stainless steel joints are reported. Unfortunately, the focus of Davison et al. (1987) was on the stiffness and no information on ultimate strength or rotation capacity is given as the reported curves shown in Figure 2.6 do not extend beyond the rather low joint rotation of 20 mrad.

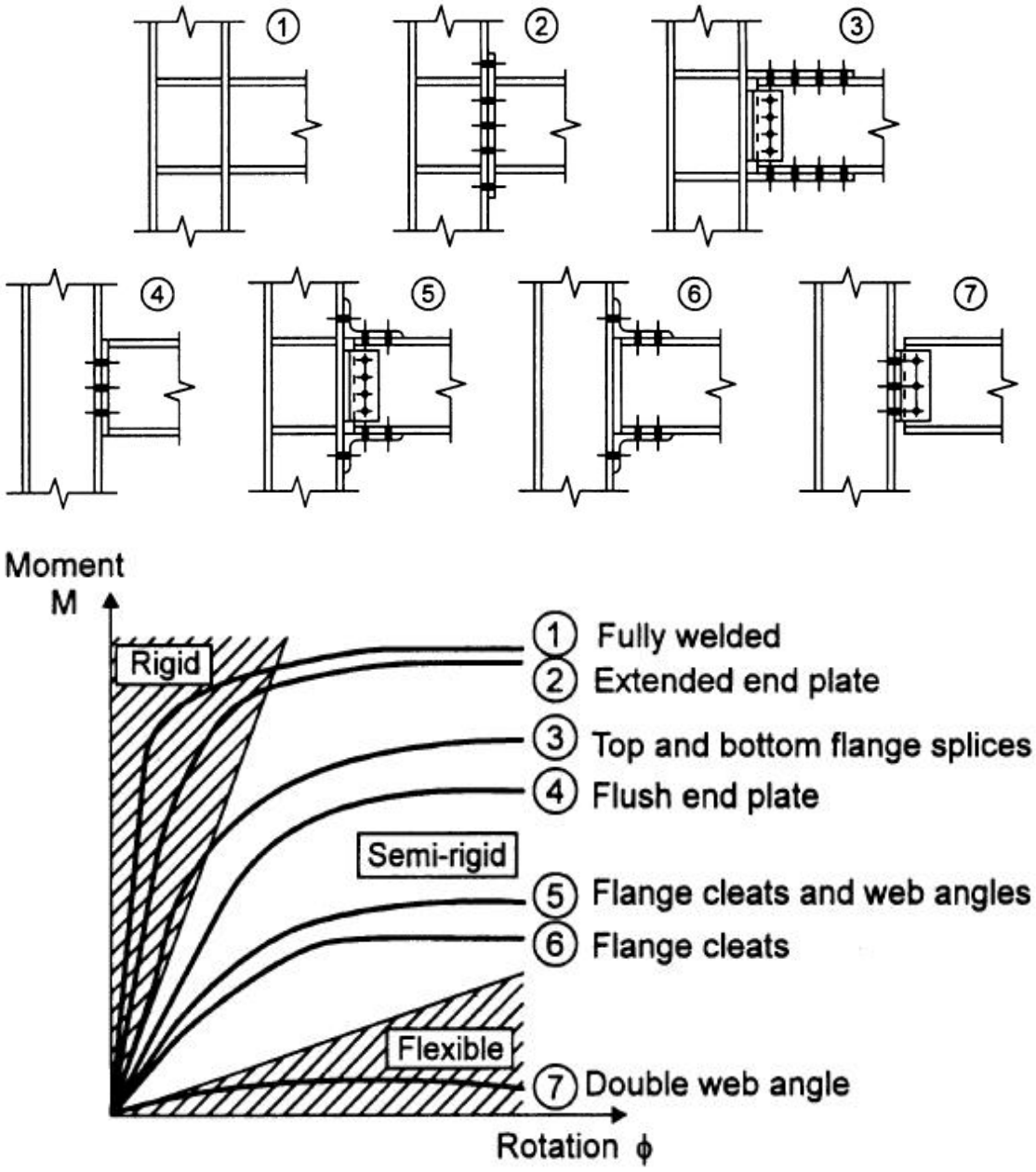

Figure 2.5 Typical moment- rotation curves for common joint configurations (Ivanyi, 2000)

From Figures 2.5 and 2.6, it can be observed that different joint typologies are associated with a certain joint response, for example joints employing extended end plates are usually associated with rigid behaviour, whilst joints with flush end plates and flange and web cleats usually fall within the semi-rigid regime. However, it should be emphasized that joints belonging to the same type can display significant differences in strength,

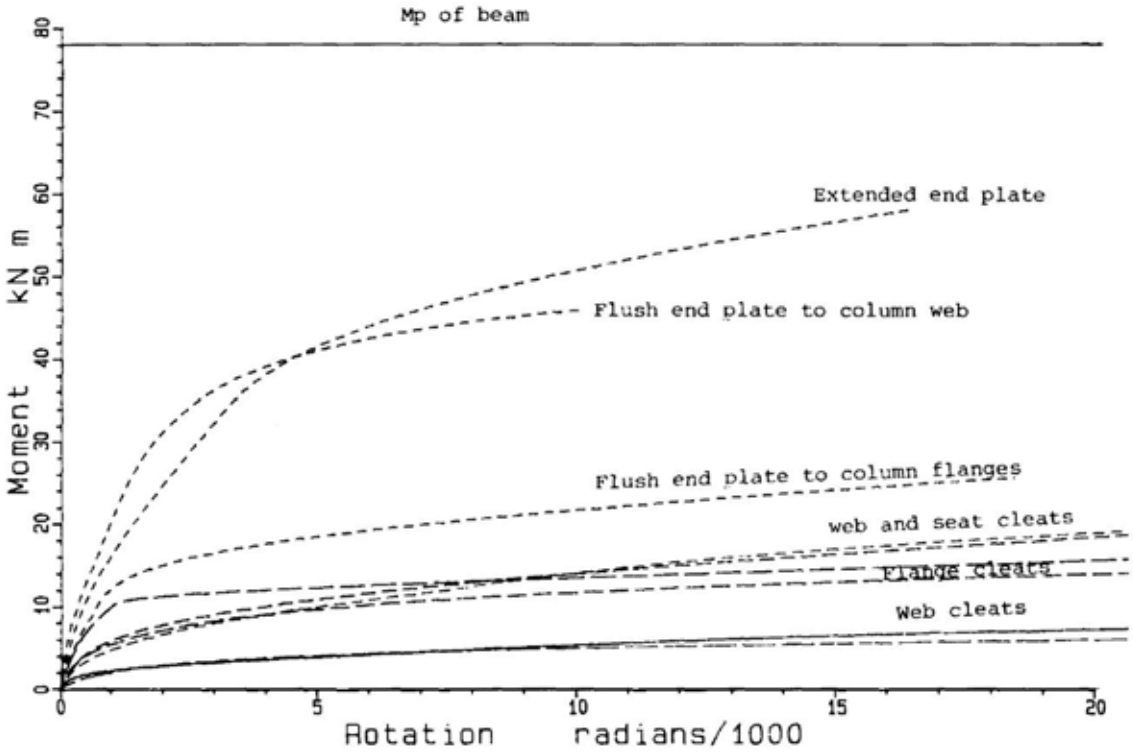

Figure 2.6 Experimental moment-rotation curves for common joint configurations (Davison et al., 1987)

stiffness and ductility since the actual geometric configuration of a joint (i.e. thickness of end plates and angle cleats, bolt size and spacing, provision of stiffeners) significantly affects its overall response and obtained failure modes (Chan and Chui, 1999; Ivanyi, 2000).

This can be clearly observed in Figure 2.7 (extracted from Kishi et al., 1997) where the moment-rotation response in a non-dimensional format (i.e. both the moment and rotation of the joints have been normalized by the respective beam moment resistance and rotation) of hundreds of joints has been collated from various experimental studies. On the same graphs the boundaries between pinned, semi-rigid and rigid joint response are denoted as dotted lines. Massive differences in the observed response occur within the same joint typology. Hence the explicit determination of a joint's stiffness and strength is required for its classification. Within the framework of EN 1993-1-8 (2005), this is done following the so-called component method, as subsequently discussed.

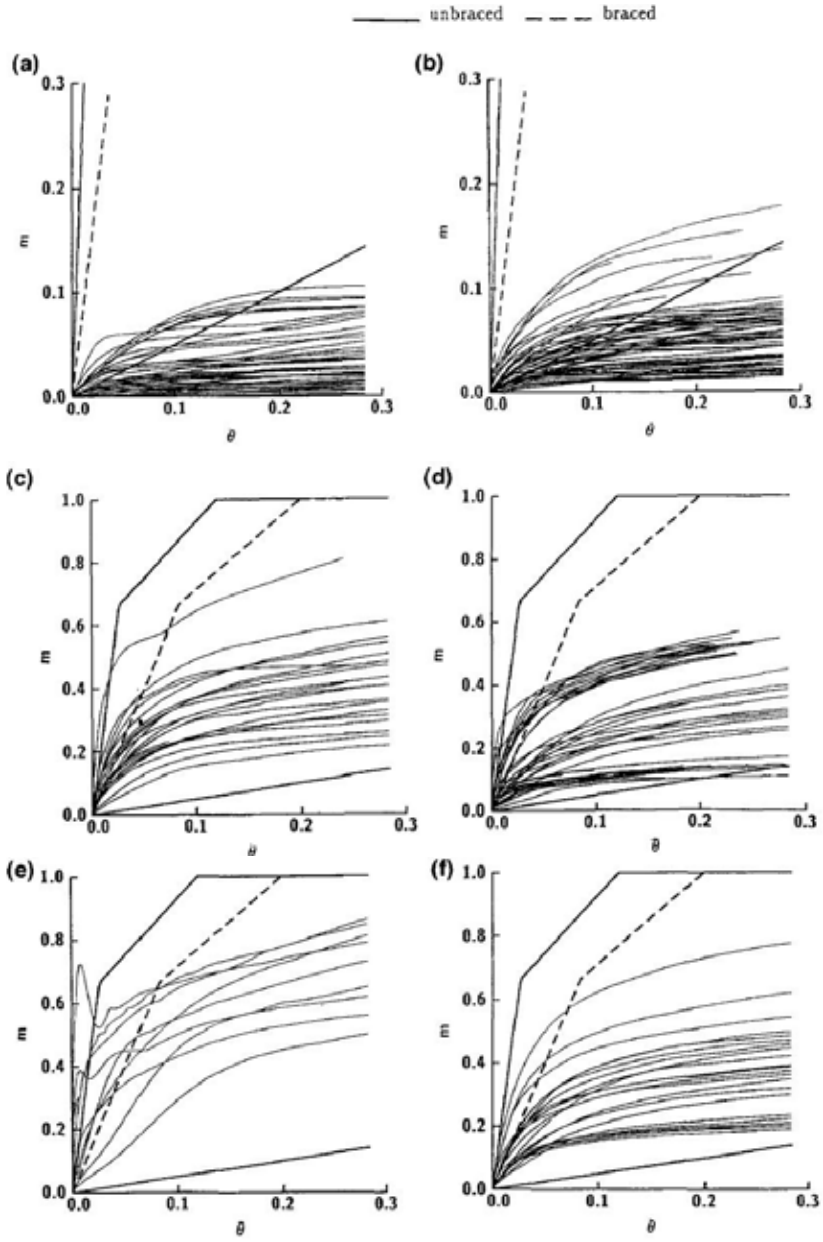

Figure 2.7 Non-dimensional moment-rotation response for joints of different configurations: a) single web angle cleat, b) double web angle cleat, c) top, seat and double web angle cleats (TSWAC), d) top and seat angle cleats (TSAC), e) extended end plate (EEP), f) flush end plate (FEP). (Kishi et al., 1997)

2.4.3 The component method

The component method is a semi-analytical framework based on the work of Jaspart (1991) and Weynard et al. (1996), that allows the characterization of the response of connections without the need of expensive experimental testing or tedious numerical modelling. A mechanical model consisting of rigid links and springs that simulate the response of the

various idealized components comprising the joint is assumed to reflect the response of the whole joint. EN 1993-1-8 (2005) provides explicit design equations for the determination of the stiffness and strength of each critical component of which the joints consists. Upon the determination of the response of each component, the response of the joint is assembled following the provisions of EN 1993-1-8 (2005).

Hence, there are 3 main steps in the component method: (1) identification of the joint components, (2) determination of the behaviour (i.e. stiffness and strength) of the components and (3) assembly of the joint response from the response of the constituent components. This procedure is schematically shown in Figure 2.8 (Jaspart, 2000) for a welded beam-to-column joint.

The strength of the component method lies in its versatility and its ability to accommodate many different joint configurations within a single procedure, which is based on the assumption that the response of a joint relates to the response of the various idealized components which comprise the joint. An example of the numerous active joint components for an extended end plate beam-to-column joint is shown in Figure 2.9, where the associated critical components are identified.

In its simplest form, the component method involves the determination of the strength and stiffness properties of a number of springs, which are suitably assembled to simulate the idealized joint response as shown in Figures 2.10 and 2.11, where the geometry of a welded beam-to-column joint and an extended end plate beam-to-column joint together with their respective mechanical model idealizations based on the component method are displayed respectively. By comparing the two figures it is evident that the more components are involved in the response of a connection and hence the more possible failure modes, the more complicated the simplified mechanical model becomes.

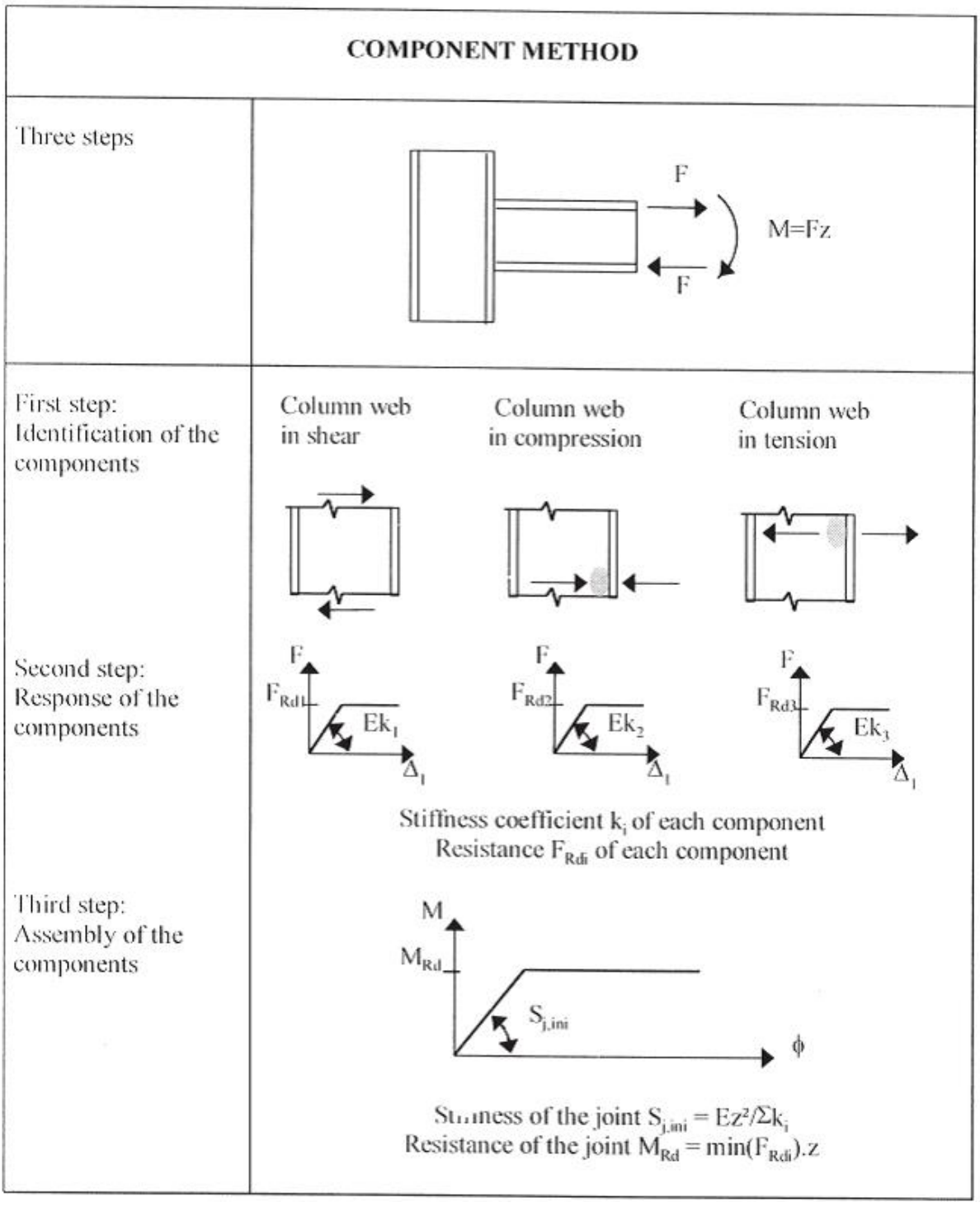

Figure 2.8 Component method as applied to a welded beam-to-column joint (after Jaspart , 2000)

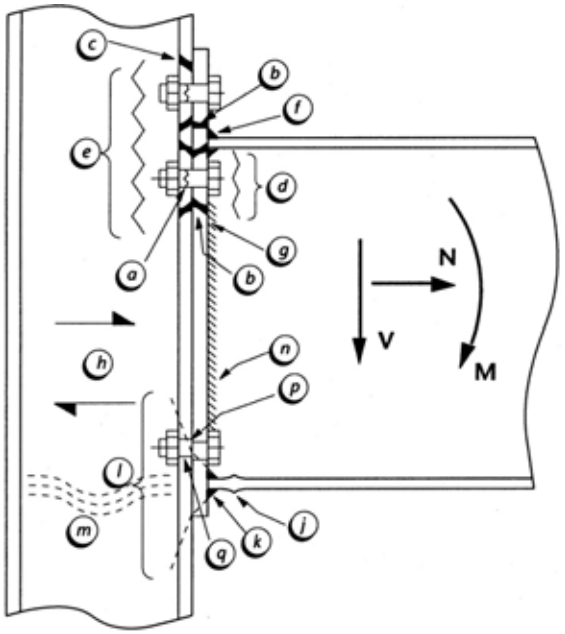

ZONE	REF	CHECKLIST ITEM
TENSION	a	Bolt tension
	b	End plate bending
	c	Column flange bending
	d	Beam web tension
	e	Column web tension
	f	Flange to end plate weld
	g	Web to end plate weld
HORIZONTAL SHEAR	h	Column web panel shear
COMPRESSION	j	Beam flange compression
	k	Beam flange weld
	l	Column web crushing
	m	Column web buckling
VERTICAL SHEAR	n	Web to end plate weld
	p	Bolt shear
	q	Bolt bearing (plate or flange)

Figure 2.9 Components of an extended end plate beam-to-column joint (ESDEP COURSE)

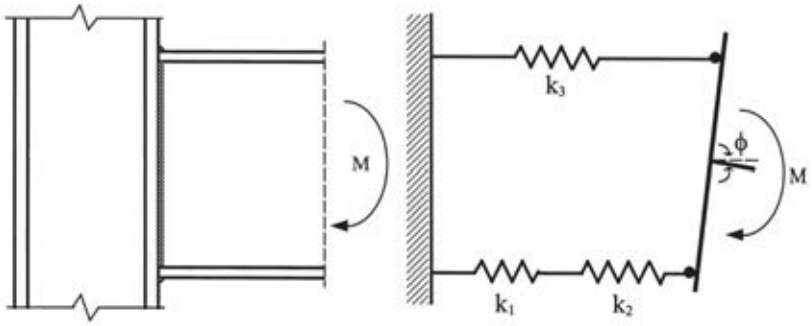

Figure 2.10 Welded beam-to-column joint and associated mechanical model (after Simoes da Silva and Girao Coelho, 2002)

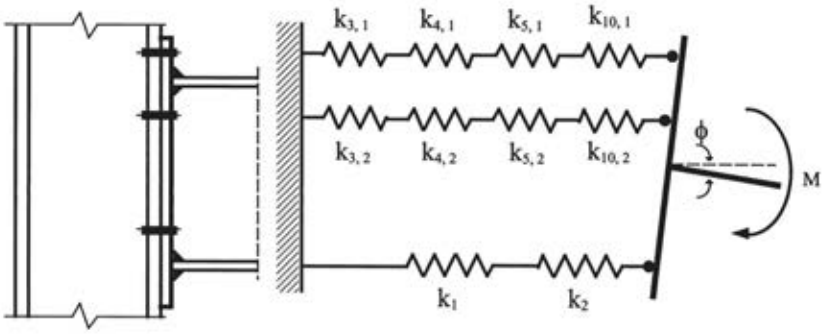

Figure 2.11 Extended end plate beam-to-column joint and associated mechanical model (Simoes da Silva and Girao Coelho, 2002)

Regardless of the number of components and the complexity of the mechanical model, based on the EN 1993-1-8 (2005) provisions, only the initial stiffness S_j and the moment resistance M_j of the joint can be determined but no quantifiable measure of rotation capacity can be obtained. Only equations for the stiffness and strength of the joint components are provided with the underpinning assumption being that the springs simulating the joint components behave linearly until their design resistance is reached, whereupon the joint fails. Hence failure of the joint coincides with failure of the weakest constituent spring of the mechanical model simulating the joint.

The design equations given in EN 1993-1-8 (2005) for the strength and stiffness of the components of a joint predominantly loaded in bending are only valid for coexisting axial forces smaller than 5% of the joint axial capacity. For higher axial loads a linear interaction between axial and flexural strength needs be considered, whilst no specific guidelines are provided for the determination the rotational stiffness in presence of an axial load higher than 10% of the joint axial resistance. A further limitation pertinent to the research reported herein relates to the joint components covered by EN 1993-1-8 (2005), which do not include connections with contributions from web cleats or blind bolted connections.

2.5 Past research on beam-to-open column joints

The behaviour and design of bolted steel beam-to-column joints has attracted considerable attention from many researchers worldwide, with the focus primarily being on the characterization of the strength, stiffness and rotation capacity of commonly employed configurations via experiments. An extensive review of available test data reported between 1936 and 1984 has been conducted by Nethercot (1985), who collated hundreds of test data from the US, UK, Canada, Australia, Netherlands and Germany. Comprehensive

databases containing hundreds of data on beam-to-column semi-rigid connections have been compiled by Kishi and Chen (1986) and Weynard et al (1992). A more focused database on the behaviour of steel and composite beam-to-column joints in seismic regions (i.e. subjected to cyclic loads) has been compiled by Cruz et al. (1998). Overall thousands of test data on a wide range of steel and composite joint configurations have been reported, none of which is on stainless steel joints.

Some of the original source documents reporting the data collated in the aforementioned databases are hard to obtain. Moreover, the tested steel grades, the testing procedures and available data acquisition techniques of the earlier tests are not representative of the modern ones and in several cases the experimental setup, material properties or recorded test results are not documented in detail. It is beyond the scope of this thesis to give an account of all previous experimental research on steel joints and no detailed discussion on the earlier tests is attempted. Thus, the literature review on past research on beam-to-open column joints is not intended to be exhaustive but to set the scene for the later chapters by discussing a few selected sources that informed the research reported in Chapters 3 and 5. Therefore only studies focusing on joints subjected to monotonic static loads have been considered and are subsequently discussed. Research on the response of beam-to-column joints under cyclic loads (Krawinkler and Mohasseb, 1987; Broderick and Thomson, 2002) or at elevated temperatures (Al-Jabri et al., 2008) has also been conducted but is beyond the scope of this thesis.

Azizinamini et al. (1985) conducted 18 tests to determine the stiffness of semi-rigid bolted beam-to-column joints employing top, seat and web cleats (TSWAC) and subsequently (Azizinamini et al., 1987) developed an analytical model to predict the rotational stiffness of this type of semi-rigid joints. Considering among others the tests by Azizinamini et al. (1985), Kishi and Chen (1990) developed analytical equations for the stiffness and strength of joints employing single or double web clears, top and seat cleats (TSAC) and

top, seat and web cleats (TSWAC). Moreover, they developed an empirical power model based on least squares curve fitting to simulate the full moment-rotation response of the studied joints. Further tests on TSWAC beam-to-column joints have been performed according to Kong and Kim (2017 b).

The above mentioned studies were developed prior to the emergence of the component method as a generic and powerful design procedure for beam-to-column joints. Despite this, the response of joints involving web angle cleats is not explicitly covered in EN 1993-1-8 (2005) and no design equations for the contribution of web cleats to the joint stiffness and strength are available. Kong and Kim (2017a) developed semi-analytical design expressions for joints with a single web angle cleat as well as TSWAC joints (Kong and Kim, 2017b) considering all available test data and using curve fitting. Pucinotti (2001) elaborated on the work by both Weynard (1995) and Kishi and Chen (1986) and developed an analytical model within the framework of the component method to extend the applicability of the design provisions of EN 1993-1-8 (2005) to connections with top, seat and web cleats, considering both the stiffness and strength of these joints in a manner compatible with the provisions of EN 1993-1-8 (2005). The mechanical model, depicted in Figure 2.12, and design expressions for strength and stiffness of the constituent springs developed by Pucinotti (2001) have been utilized herein to derive the Eurocode compatible strength and stiffness predictions of the stainless steel TSWAC joints studied in Chapters 3-5.

The response of flush and extended end plate connections has been extensively studied and documented in several publications. The work reported by Girao Coelho et al. (2004b) and Girao Coelho and Bijlaard (2007) on the behaviour and design of end plate beam-to-column joints in carbon and high strength steel is in the author's opinion the most well documented set of experimental data and therefore largely informs the experimental setup and instrumentation reported in Chapter 3 and 4. In most cases the tension zone of

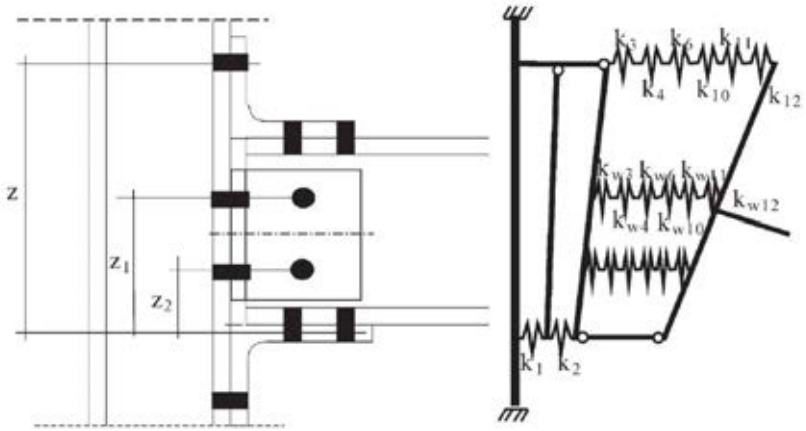

Figure 2.12 Mechanical model for top, seat and web angle cleat (TSWAC) joints (Pucinotti, 2001)

the connection, simulated as a T-stub in tension (Zoetemeijer, 1974) governs the overall response and a more focused literature review on that matter is given in Chapter 6.

In addition to the flexural behaviour of joints, several researchers have conducted experimental and analytical research to incorporate the effect of moment-axial load interaction in mechanical idealizations of connections. Simoes da Silva et al. (2004) and de Lima et al. (2004) carried out experimental investigations on the response of flush and extended endplate connections subjected to combined bending and axial forces and concluded that low to moderate coexisting compression enhances the moment resistance, whilst high compressive forces or the presence of tensile forces decreases the strength and stiffness of the joints. Urbonas and Daniunas (2006, 2008) proposed a mechanical model based on the component method for the design of joints under combined bending and high axial loads. Simoes da Silva and Girao Coelho (2001a) developed a refined mechanical model based on an energy formulation that considers the post ultimate response of the constituent components and demonstrated its applicability to a welded beam-to-column joint under combined moment and axial compression. Simoes da Silva (2008) reviewed relevant experimental, numerical and analytical research and proposed a design framework for joints under general loads, whilst Del Savio et al. (2009) developed a generic component method based approach for beam-to-column joints in tension and compression considering

a trilinear force-displacement relationship for the constituent components.

Comprehensive research on simulating joint ductility and an analytical framework for its quantification in line with the component method of EN 1993-1-8 (2005) for beam-to-column end plate joints has been conducted by Simoes da Silva and Girao Coelho (2001b), Simoes da Silva et al. (2002) and Beg et al. (2004). They proposed the use elastic-linear hardening springs in place of the elastic-perfectly plastic ones specified by EN 1993-1-8 (2005) for joint components the failure of which is considered ductile, such as the yielding of the T-stub in bending or the yielding of the column web panel in shear. The use of a modified spring response for the ductile components results in the determination of the nonlinear moment-rotation response of the joint, which explicitly incorporates the gradual loss of stiffness of the joint as joint components yield successively and failure occurs when a non-ductile component fails. Hence the nonlinear response of any steel joints can be reproduced as long as the response of the joint components is adequately characterized, and the yielding sequence is identified (Simoes da Silva and Girao Coelho, 2001b).

The previous discussion demonstrates that the determination of the moment-rotation response of a joint relies on adequate characterization of the key properties (i.e. stiffness, strength, post-yield stiffness and ductility) of the constituent components. Therefore, studies focusing on the response of some of the key joint components, including the so called T-stubs and the column web panel in shear (Girao Coelho et al., 2009; Augusto et al., 2016) have been widely reported in the literature. A comprehensive review on the response of T-stubs in tension, commonly employed to idealize the behaviour of tension zone of bolted connections, is given in Chapter 6, where a design method for the response of stainless steel T-stubs in tension is proposed based on recently published test data by Yuan et al. (2018).

2.6 Beam-to-tubular column joints

2.6.1 Tubular construction

Tubular structural members are a major area of interest within the field of steel and stainless steel structures and are preferred by many architects due to their aesthetic appeal (Baddoo et al., 1997). In addition to the traditional family of Square, Rectangular and Circular Hollow Sections (SHS, RHS, CHS), Elliptical Hollow Sections (EHS) are available in both carbon (Chan and Gardner, 2008) and stainless steel (Theofanous et al., 2009). Among the advantages of hollow section members are their high stiffness about both principal axes, which makes them an attractive choice for compression members and their high torsional stiffness, which makes them efficient to resist torsion and lateral torsional buckling. Moreover, the possibility of filling the tubular columns with concrete thereby creating composite columns (concrete filled tubes) possessing high strength, stiffness and ductility has made tubular columns popular in high-rise building construction (Roeder et al., 1999; Giakoumelis and Lam, 2004). However, the closed nature of either bare steel or concrete filled tubular columns complicates the assembly of bolted connections, since hollow section columns allow access from only one side. Hence, despite their optimal geometry for structural members subjected primarily to compression, open sections (e.g. UC) are often preferred as connections to open members are less cumbersome to fabricate.

Several researchers have investigated various connection configurations between beam and tubular columns. Early research was conducted by White and Fang (1966), who carried out five experimental tests on carbon steel beam-to-tubular column joints employing angle cleats, fin plates and T-sections welded on the column face and bolted to the beam section in various different configurations. They concluded that the stiffness of the joint was significantly affected by the variation of the width and thickness of the column face. Dawe and Grondin (1990) reported ten tests on carbon steel joints using angle cleats welded to the tubular columns and bolted to the beams and discussed the various failure modes

obtained. Sherman and Ales (1991) tested 12 carbon steel joints using a fin plate welded on the tubular column face and bolted to the beam section. The width-to-thickness ratio of tubular columns ranged from 8 to 48. It was demonstrated that the minimum thickness of the column face should be related to the thickness of the fin plate to induce yielding of the fin plate prior to failure of the column face by punching shear. Maquoi et al. (1984) tested connections with threaded studs welded to the tubular column. In addition to the low ductility exhibited by these connections, possible damage of the welded studs during transportation of the columns made this technique less favourable for practical applications as pointed out by Korol et al (1993).

More recently, Málaga-Chuquitaype and Elghazouli (2010a) conducted tests on and derived a component characterization for bolted connections utilising a reverse channel section welded on the tubular column face, as shown in Figure 2.13. This configuration allowed bolted connections to be assembled with standard bolts as the presence of the reverse channel section allowed access from both sides of the bolt. The test results demonstrated that this joint configuration possesses high ductility, but its strength and stiffness are adversely affected by the strength and stiffness of the channel section.

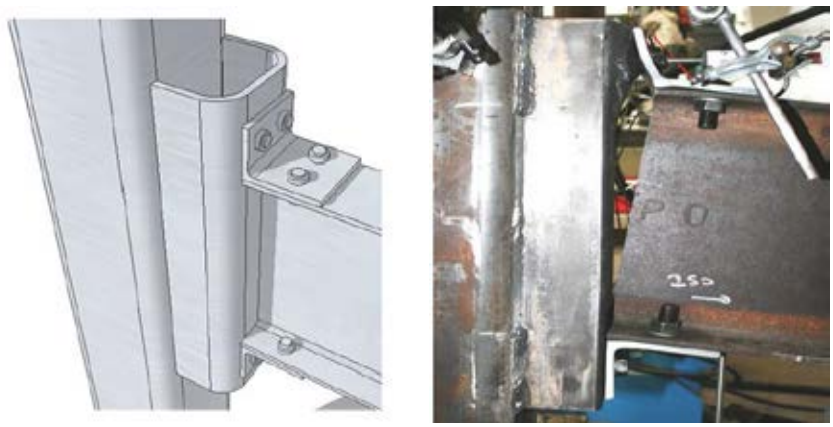

Figure 2.13 Bolted angle/reverse channel joint (Málaga-Chuquitaype and Elghazouli, 2010a)

The use strengthening measures in the form of external diaphragm plates (i.e. collars) welded to concrete filled CHS or SHS was investigated by Schneider and Alostaz1(1998) and Han et al. (2008) respectively, who considered the response of the resulting moment resisting connections to cyclic loads. Other possible joint configurations involving the use of through plates and stiffeners have been studied by Yang et al. (2015) and Hoang et al. (2014) for both empty and concrete filled tubular columns, as shown in Figure 2.14, whilst a typical joint configuration of the external collar type is shown in Figure 2-15.The use of through section beam joints, where slots with the shape of the beam section are made on the column to allow the connected beam to pass through has been studied by Azizinamini et al. (1995) and Elremaily and Azizinamini (2001).

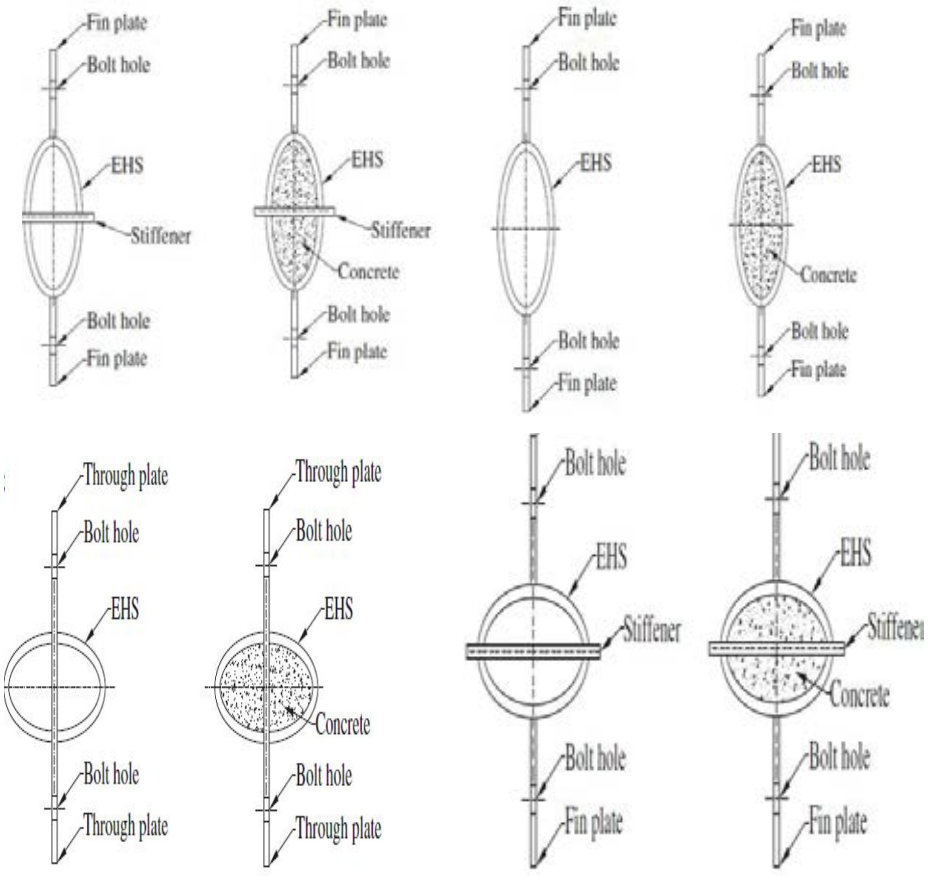

Figure 2.14 Beam-to-tubular column connections using stiffeners and internal plates (Yang et al., 2015).

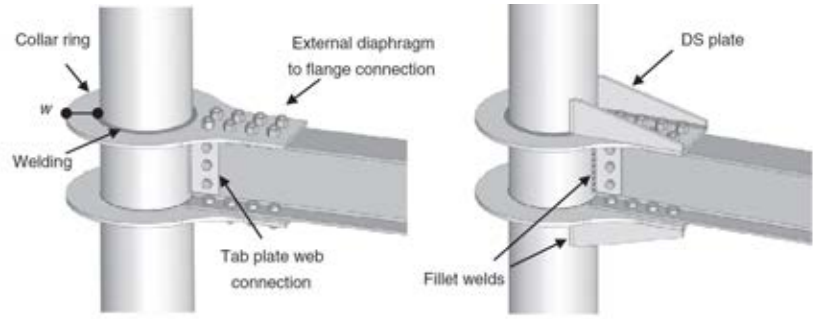

Figure 2.15 Beam-to-tubular column connections with collars (Sabbagh et al., 2013).

The aforementioned connection details have been shown to result in satisfactory joint response but are associated with costly and cumbersome fabrication as extensive precision cutting and welding is required. Other less fabrication-intensive connection details have also been explored involving various bolting techniques. A conceptually simple bolted connection involving bolts long enough to go through the column section has been experimentally investigated by Hoang et al. (2013) for concrete filled SHS. However, the resulting connection detail is difficult to execute on site and could induce additional cost as Hoang et al. (2013) pointed out. The use of bolted connections on site is desirable provided that the resulting details are easy to execute on site and result in good structural performance. To this end various types of the so-called blind-bolted connections allowing bolted connections to be assembled without requiring access to both sides of the bolts have been developed as discussed hereafter.

2.6.2 Fasteners for blind-bolted connections and relevant research

The different joint configurations discussed in the previous section have been associated with increased complexity and additional fabrication cost. The need to execute bolted connections with only one side of the column being accessible led to the development and utilization of special types of bolts or processes that allow bolting from one side. Many types of fasteners employing a type of sleeve, the expansion of which after installation

allows single-sided bolting, have been developed by several companies. Table 2-3 gives an overview of all such fasteners that are commercially available. All pictures of the fasteners were extracted from the manufacturers' websites.

Table 2.3 Available fasteners for blind-bolted connections

Commercial name	Manufacturer	Size range	Origin	Image of typical fastener
Flowdrill	Flowdrill	M2-M20	Netherlands	
BOM or HSBB	Huck International	M6-M24	USA	
Hollo-bolt	Lindapter	M8-M20	UK	
Lindibolt	Lindapter	M10-M24	UK	
Molabolt	Advanced Bolting Solutions	M8-M24	UK	
Ajax One-side	Ajax Fasteners	M16-M24	Australia	
Blind bolt	Blindbolt	M8-M30	UK	

The application of the thermal drilling technique (i.e. the flowdrill process) to connect thin-walled tubular columns to beams with partial or full depth end plates as simple connections and thicker endplate beams as moment-resisting connections has been studied by France et al. (1999a; 1999b). Essentially the installation procedure consists of creating a threaded hole on the column face with a special tool, thus allowing bolting without the need of a nut, as shown in Figure 2-16. Although the results of this study indicated the suitability of this technique for the execution of simple connections, the flowdrill process has a limiting column thickness ranging from 5mm to 12.5mm, is time consuming and cumbersome, thus hindering its more widespread usage in practice (Elghazouli et al., 2009).

Figure 2.16 Application of the flowdrill process (Flowdrill, 2018)

Alternative connection methods involve the use of special fasteners, like the Oversized Mechanical Bolts (BOM) and Huck High Strength Blind Bolt (HSBB) produced by Huck International Inc. Their installation process involves inserting the fasteners in oversized holes and plastically deforming the fastener's sleeve with thus hindering the pull-out of the fastner, as shown in Figure 2-17. The structural performance of Oversized Mechanical Bolts (BOM) and Huck High Strength Blind Bolts (HSBB) has been investigated via five joint tests utilising flush end plates by Korol et al. (1993). It was concluded that employing the HSBB fasteners lead to joint response comparable to similar joints using conventional bolts, whilst joints employing the BOM fasteners were observed to possess lower resistance.

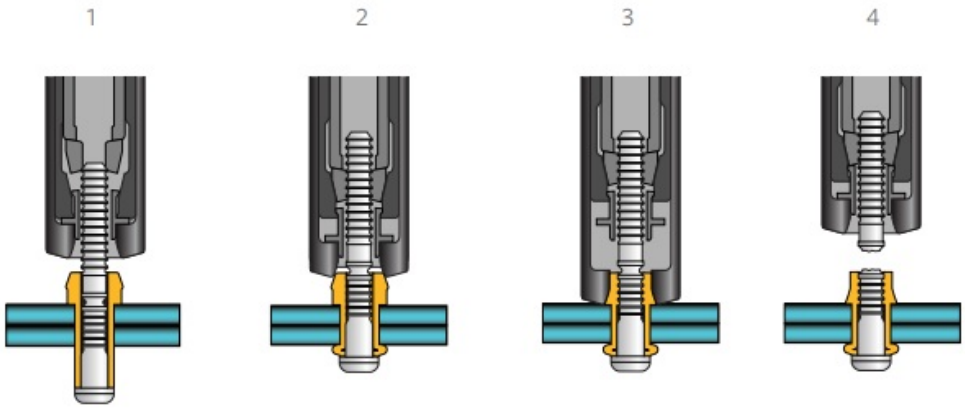

Figure 2.17 Installation of BOM fastener (BOM fastener, 2018)

Experimental and numerical studies on a new type of blind bolt called Oneside and developed by Ajax were conducted by Lee et al. (2010), who also developed a design approach within the component method for the calculation of the joints's strength and stiffness. However, they only conducted 3 experimental tests and no other journal paper documenting the response of Oneside has been found in the published literature.

Arguably the most well-studied type of blind bolts is Hollo-bolt developed by Lindapter. Its installation process is shown in Figure 2-18, it is conceptually simple and, contrary to many other blind bolt types, does not require special equipment.

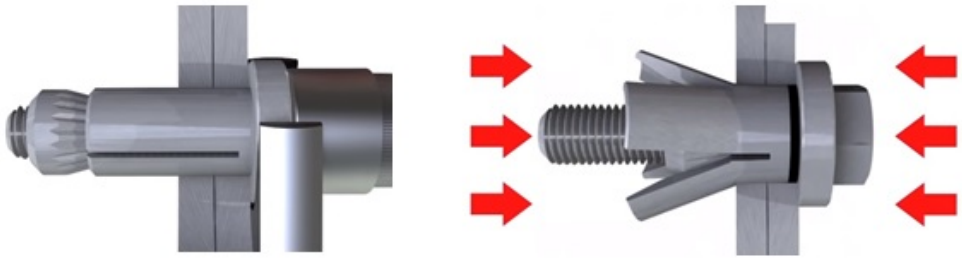

Figure 2.18 Hollo-bolt installation and deformation of sleeve. (LINDAPTER ,2018)

The response of the Hollo-bolt in tension as well as the strength and stiffness of T-stubs employing Hollo-bolts was numerically investigated by Wang et al. (2010), who proposed a rather complicated analytical predictive model. Elghazouli et al. (2009) studied the

behaviour of top and bottom seated angle cleat connection employing different grades and configurations of Hollo-bolts under monotonic and cyclic loading. The results of this study indicated that the bolt configuration affected the behaviour of the studied connections in terms of obtained failure modes, strength and stiffness. Liu et al. (2012a) and Liu et al. (2012b) performed a similar series of experiments and numerical simulations to investigate the response of open beam to tubular column connections under extreme shear or axial loads (i.e. applied at high strain rates). The findings suggest that in general the angle dimensions and the thickness of the column face significantly affect the response characteristics. Málaga-Chuquitaype and Elghazouli (2010b) formulated design equations for the strength and stiffness of both the Hollo-bolt and the column face in bending according to the component-based approach. Wang and Wang (2016) conducted a series of experimental and numerical studies on T-stubs bolted on SHS with Hollo-bolts subjected to tension, thus idealising the response of the tension region of a moment resisting connection. To improve the performance of blind-bolted joints using Hollo-bolts, the Extended Hollobolt (EHB) was recently developed Tizani et al. (2013) and Tizani and Pitrakkos (2015). This EHB is specifically designed for concrete filled columns as the bolt extension provides an anchor in the concrete leading to the bolt developing its full tensile strength as opposed to the alternative where the blind bolt pulls out prematurely.

2.6.3 Design procedures for blind-bolted joints

Despite the existence of several types of blind bolts during the time that EN 1993-1-8 (2005) was drafted, no design equations are provided for the stiffness and strength of the joint components/springs simulating the face of a tubular column in blind-bolted joint. Hence the design of carbon steel blind bolted joints is based either on design recommendations made by researchers or manufacturers, which however do not have the status of codified design provisions. All available design recommendations for the strength of the column face in bending are based on yield line analysis of the face of the tubular column and

involve analytical or numerical determination of the yield line pattern of the column face.

Originally developed for the determination of the strength of blind-bolted connections executed with the flowdrill process, Yeomans (1994 ; 1996) developed a design equation which was later adapted to blind-bolted connections using Hollo-bolts. This equation has been adopted by CIDECT in its design guidance on connections to hollow section columns (Kurobane et al., 2004). A similar equation (Eq. 2-1) was developed by the SCI (Steel Construction Institute) and the BCSA (British Constructional Steel Association) (SCI, 2014).

$$F_{y,SCI} = \frac{2\sigma_y t_c^2}{1-\beta_1}\left[\frac{(\eta_1 - 1)p - 0.5\eta_1 d_{bh}}{b_0 - 3t_c} + 1.5(1-\beta_1)^{0.5}(1-\gamma_1)^{0.5}\right] \tag{2.1}$$

where σ_y is the material yield stress, p is the bolt pitch distance, β_1 =g/(b_0-3t_c) and γ_1=d_{bh}/(b_0-3t_c), g being the gauge width (i.e. distance) between the bolts, b_0 the outer width of the tubular column face to which the connection is made, t_c the thickness of the face of the tubular columns and d_{bh} the diameter of the clearance hole of the Hollo-bolts.

The main difference between the equation developed by Yeomans (1994) and Eq. (2.1) is that it considers the diameter of the clearance hole and the flat width of the column face rather than the diameter of the sleeve and the mid-line width of the column face in the design equation and that it takes into account the interaction between the various bolt rows, thus resulting in similar but slightly more conservative results. This design equation will be utilized determine the strength of the column face in bending when discussing the response of beam-to-tubular column joints in Chapters 4 and 5.

Gomes et al. (1996) proposed a design model for the moment resistance of beam-to-open column joints with the column being bent about its minor axis. They identified two failure

mechanisms, one related to failure of the column web in bending ("flexural mechanism") and one related to punching shear ("punching shear mechanism") and proposed design equations for both. Despite the difference between a column face of a tubular column and the web of an I-section, the response of both components is in principle similar, since both are subjected to similar support and loading conditions and deform in a similar manner. Although not developed for blind-bolted joints, the method proposed by Gomes et al. (1996) is considered a good starting point for the determination of the resistance of the face of a tubular column (Wang and Wang, 2016). However, the design approach proposed by Gomes et al. (1996) was shown to produce consistently unsafe results (Wang and Wang, 2016; Jiang, 2018), hence it will not be considered in the remainder of this thesis.

A good overview of the aforementioned design methods for the strength of the column face of a tubular column in bending is given by Wang and Wang (2016), who also proposed their own model for the yield strength and ultimate strength of the face of a tubular column in bending. The design method proposed by Wang and Wang (2016) was shown (Jiang, 2018) to accurately predict the test results reported by its developers, but to overestimate the resistance of specimens tested by Liu et al. (2012).

2.7 Concluding remarks and knowledge gap

In this chapter past experimental and numerical research on stainless steel bolted and welded connections as well as past studies on carbon steel beam-to-column conventional joints and blind-bolted joints have been reviewed. From the review of past research, it can be concluded that very limited experimental and numerical research has been carried out on stainless steel joints to date with only one publication reporting experimental tests on full-scale blind-bolted joints (Tao et al., 2017) and one study reporting tests on stainless steel T-stubs (Yuan et al., 2018). No experimental investigation on stainless steel beam to

open section joints has been reported to date. This brief literature survey clearly highlights the need for full-scale tests on stainless steel beam-to-column joints, given the current worldwide trend towards sustainability , which is expected to favour the more widespread use of stainless steel in construction (Baddoo,2008 and Rossi, 2014). Such as the important advantage of the use of stainless steel in construction is has corrosion resistance and therefore longer service life and low maintenance and also is its high recycled content and recapture rate as well as the possibility of material reuse in the case of renovation (Rossi, 2014).

Experimental characterization of the behaviour of stainless steel joints will allow the suitability of current design provisions of EN 1993-1-8 (2005), originally derived for and based on the response of carbon steel joints, for stainless steel joints to be assessed (Elflah et al, 2018 a). Moreover, it is envisaged that certain restrictions of EN 1993-1-4 (2015), as for example the fact that plastic global analysis is currently not allowed in the absence of experimental evidence as "there should be evidence that the joints are capable of resisting the increase in internal moments and forces due to strain hardening" can be overcome in light of appropriate experimental and numerical research. The experimental and numerical studies reported in Chapters 3-5 are an important step towards the development of design guidance on stainless steel beam-to-column joints (Elflah et al, 2018 a ,b).

Chapter 3

Experimental investigation of stainless steel open beam-to-open column joints

3.1 Introduction

Traditionally the design of stainless steel structures has been based on equivalent design rules for carbon steel. Since the material response of stainless steel does not display a yield plateau and hence no well-defined yield point exists, the stress corresponding to 0.2% plastic strain termed $\sigma_{0.2}$ proof stress has been historically adopted in lieu of a yield stress and the pronounced strain-hardening exhibited by stainless steel has been ignored. The selection of the proof stress appears arbitrary as nothing drastically changes in terms of material response at this stress value, but it is a necessary compromise to maintain the design approach followed for carbon steel structures, which designers are familiar with, thereby facilitating an easy transition when designing in stainless steel.

Research on the behaviour and design of stainless steel members (Gardner and Nethercot, 2004,b; Gardner and Theofanous, 2008, Afshan and Gardner, 2013; Saliba et al., 2014)

has highlighted deficiencies associated with overly conservative ultimate capacity prediction for stocky stainless steel cross-sections and members, stemming from simplifying the nonlinear material response of stainless steel as an elastic-perfectly plastic one. Numerous international design standards (e.g. EN 1993-1-4, 2015; AS/NZS 4673, 2001; SEI/ASCE 8-02, 2002; AISC 27, 2013) have been recently revised to reflect the observed structural response and yield more favourable and less scattered structural response predictions.

Compared to research conducted on stainless steel members, research on stainless steel joints is lagging a very small number of relevant experimental studies exists as discussed in Chapter 2. Joints, being areas of a structure with high stress concentrations, where locally inelastic deformations occur, are expected to be affected more significantly by material response than members. This Chapter reports in detail the first ever set of tests on full-scale stainless steel beam-to-column joints. The research published herein was conducted as part of my PhD studies and has been submitted and recently accepted for publication by the Journal of Constructional Steel Research (Elflah et al, 2018 b). To conform with University regulations on self-plagiarism (!), the text has been reworded, however what is reported, and the conclusions remain unaffected.

3.2 Experimental investigation

3.2.1 Specimen design and fabrication

In designing the beam-to-open section joint tests, the specimen characteristics are determined in accord with the parameters of the existing test set up; load capacity of actuator (400 kN, with a maximum stroke of 250 mm), load cell (200 kN), and geometrical properties, including the displacement capacity of the inductive displacement transducers. The main geometric dimensions of the specimens are presented in Figure 3.5. To be able to achieve the intended measures on the specimens, preliminary calculation were undertaken.

The moment resistance of joints can be determined as the minimum resistances of the possible failure modes. The resistance of the connection was easily calculated according to EN1993-1-8 (2005). Regarding material properties, austenitic stainless steel (yield stress = 250 MPa) and bolts of strength Grade A80 (stainless steel) were adopted for the calculations. The selection of the thickness for the end plates and the angle cleats was based on the maximum recommended thickness of an end plate or angle cleat as given in EN 1993-1- 8.

A fabricated stainless steel I-section with an outer depth h of 240 mm, a flange width b of 120 mm, flange thickness t_f equal to12 mm and web thickness t_w equal to 10 mm (i.e. I 240×120×12×10) has been used both for the column and the beam of the tested connections. Out of a multitude of different joining options utilized in structural applications, four connection typologies often employed in steel structures (e.g. steel buildings), have been selected and are studied herein. These are:

- the extended end plate connection (EEP-O)
- the flush end plate connection (FEP-O)
- the top and seat angle cleat connections (TSAC-O)
- the top, seat and double web cleat connection (TSWAC-O)

"In the nomenclature and symbols used herein, the letter “O” refers to beam-to-open column joints. Hence, TSAC-O employs the top and seat angle cleat configuration for a connection of a beam to an open section column"

Following the discussion on the behaviour of equivalent carbon steel connections in Chapter 2, the TSWAC-O and EEP-O joints usually fall within the rigid or the stiff side of the semi-rigid range when classifying connections with respect to stiffness, whilst the TSAC-O and the FEP-O joints are more flexible and depending on the actual geometry of the fasteners and connected parts can be either pinned or semi-rigid (Kishi et al., 1997).

With respect to connection classification according to strength, all of the tested connections were designed to be partial strength, as a full-strength joint would lead to premature beam failure and thus would not allow the strength of the connection to be determined.

The dimensions and overall configuration of the tested connections is depicted in Figure 3.1. Grade A80 stainless steel bolts have been used throughout this study. This bolt grade is similar to the commonly used Grade 8.8 carbon steel. The bolt diameter was 16 mm (M16), hence 18 mm holes were used throughout. Identical configuration in terms of bolt-hole locations were used for the TSAC-O and TSWAC-O configurations, whilst the top and seat angle cleats were cut from the same member length. Since the joint response strongly depends on the thickness of the employed angle cleats and end plates, two variations of angle cleat thickness were employed for TSAC-O and TSWAC-O joints to generate a range of joint responses in terms of stiffness, strength, rotation capacity and failure mode and allow reliable FE models, able to predict different failure modes to be validated as discussed in Chapter 5. The reasoning underpinning the choice of the thickness of the angle cleats and end plates is based on Equation 3.1, which according to EN 1993-1-8 (2005) defines the maximum thickness t of a carbon steel angle cleat or end plate with a yield strength f_y for a given bolt diameter d and strength $f_{u,b}$ if sufficient joint rotation capacity is desired.

$$t = 0.36d\sqrt{\frac{f_{u,b}}{f_y}} \tag{3.1}$$

Since at the point of ordering the specimens, no material coupon tests could be conducted, the material properties stated in the mill certificates and nominal bolt strength were used in Equation (3.1) to estimate the required thickness t. The 0.2% proof stress $\sigma_{0.2}$, the 1% proof stress $\sigma_{1.0}$, the ultimate tensile stress σ_u and the strain at fracture ε_f are reported in Table 3.1. Based on these values, Equation (3.1) yields a maximum thickness of 8.4 mm for the angle cleats and 8.9mm for the end plates. Hence two angle cleat thicknesses, one below and one above this limiting value (8mm and 10 mm) were

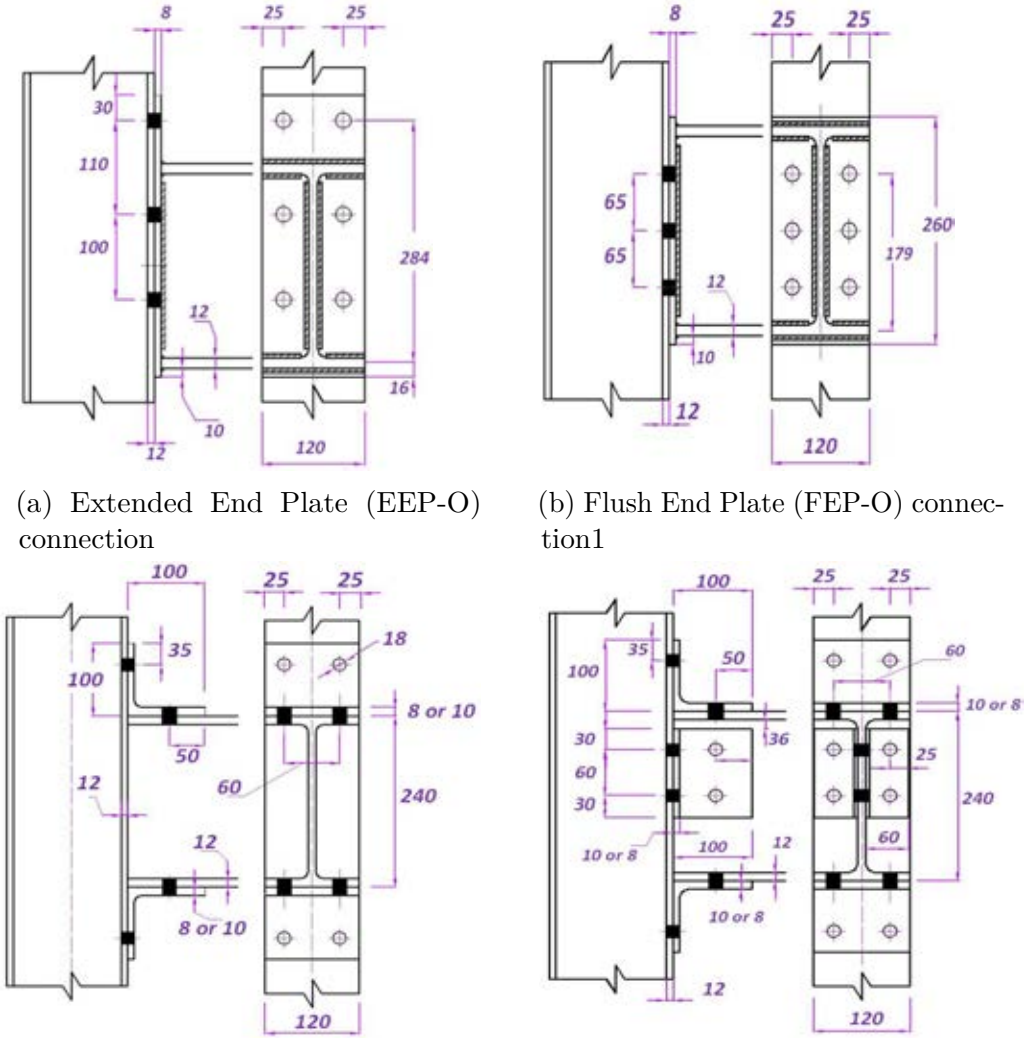

(a) Extended End Plate (EEP-O) connection

(b) Flush End Plate (FEP-O) connection1

(c) Top and Seat Angle Cleat (TSAC-O) connection

(d) Top, Seat and double Web Cleat (TSWAC-O) connection

Figure 3.1 Geometry of the tested specimens (Elflah et al, 2018 b)

chosen for the angle cleats .

Table 3.1 Material properties according to mill certificates (Elflah et al, 2018 b)

Specimen	$\sigma_{0.2}$ (N/mm^2)	$\sigma_{1.0}$ (N/mm^2)	σ_u (N/mm^2)	ε_f %
I-240×120×12×10	341	369	635	53
L-100X100X8	373	441	675	54
L-100X100X10	378	445	673	55
Endplate (thickness 8mm)	335	379	630	54

3.2.2 Coupon testing and material response

Material coupons were cut from the web and flange of the I-section employed as beam and column, from the angle cleats and from the same material from which the end plates were extracted. Strain control with an applied strain rate of 0.007 %/s up to the 0.2% proof stress $\sigma_{0.2}$ and subsequently a strain rate of 0.025%/s until coupon failure was applied during testing following the provisions of BS EN ISO 6892-1 (2016). In Figure 3.2 the obtained stress-strain curves for the web and flange material of the I-section and the angle cleats are reported (Elflah et al, 2018 b).

Stainless steel bolts from the same batch as the ones used in the tests were tested in tension and in shear to obtain their material response and facilitate the discussion of the results and the FE simulations discussed in Chapter 5.The procedure of tensile testing bolts in their full size is recognised and adopted by by many standardising bodies, including the International Organisation for Standardisation (ISO), British Standards Institution, Standards Association of Australia, American Society for Testing and Materials (ASTM) and Society of Automotive Engineers (SAE). The tensile test was carried out in accordance with ISO 6892-1 (2009) .The bolt was screwed into a tapped attachment leaving six complete threads unengaged between the self-aligning grips and the bolt head is initially supported on a parallel collar. The load is applied axially. Bolt elongation was measured to determine yield strength by the offset method with the offset specified (0.2). A gage length of 4 diameters of the test specimen was used. The speed of testing, as determined with a free running cross head, shall not exceed 25 mm/min. The tensile test was continued until fracture occurs. Following the ISO 6892-1 (2009), failure must occur in the body or threaded section, with no failure at the junction of the body and the head. Figures 3.3 and 3.4 show the experimentally determined axial force vs elongation, the shear force vs shear deformation and the corresponding failure modes for bolts tested in double shear and in tension respectively .

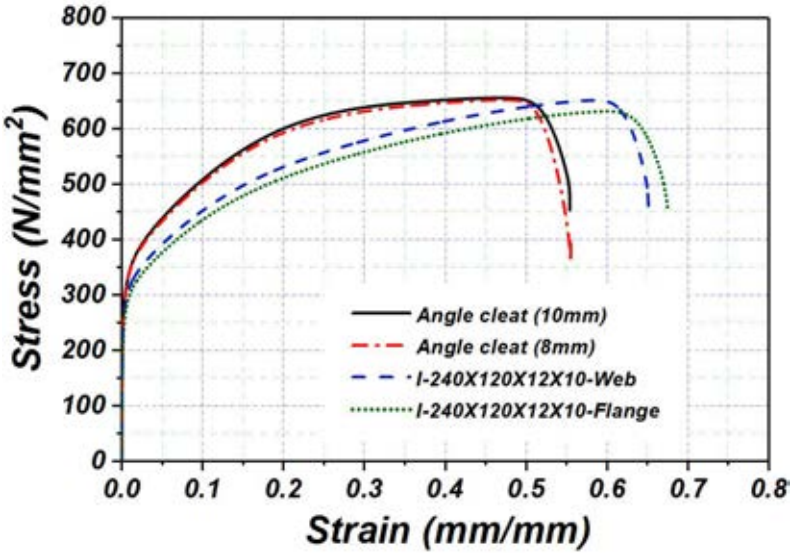

Figure 3.2 Typical stress strain curves of tested stainless steel tensile coupons (Elflah et al, 2018 b)

In Table 3.2 key material properties as derived from the tensile tests are reported. Both the proof stress and ultimate tensile stress reported in Table 3.2 can be seen to be lower than the corresponding values reported in the mill certificate for all material. Given the pronounced anisotropy exhibited by stainless steels (Becque and Rasmussen, 2009), possible differences in the orientation in which the material was tested by the mill can explain this discrepancy. A further explanation relates to the higher strain rates at which mill certificate tests are conducted compared to the ones performed for academic research, as the ones reported herein. In the remainder of this thesis, the material properties reported in Table 3.2 will be used. Finally, it is noted that using the measured material properties as reported in Table 3.2, Equation (3.1) yields 9.7 mm as the maximum thickness value recommended for angle cleats/end plates when high rotation capacity is required.

3.2.3 Details of experimental set-up

Figure 3.5 depicts the setup and employed instrumentation used in all tests. The beam and column members used in all tests were 1.5 m long. The dimensions of the connected beam and column as well as the applied boundary conditions imposed, ensure that all plastic deformations are limited within the joint region where failure occurs, whilst the

Table 3.2 Material properties from tensile tests (Elflah et al, 2018 b)

Specimen	E (N/mm^2)	$\sigma_{0.2}$ (N/mm^2)	$\sigma_{1.0}$ (N/mm^2)	σ_u (N/mm^2)	ε_f %
I-240×120×12×10 - flange	196500	248	306	630	66
I-240×120×12×10 - web	205700	263	320	651	65
Angle cleat (8 mm)	197600	280	344	654	55
Angle cleat (10 mm)	192800	289	353	656	56
End plate	198000	282	343	655	54
M16 bolt (A4-80)	191500	617	703	805	12

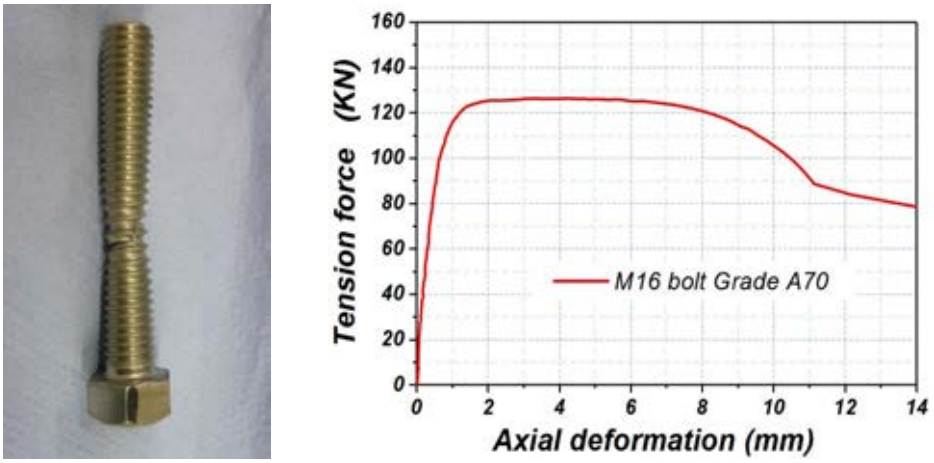

Figure 3.3 Load-elongation curve and failure mode of M16 bolt Grade A4-80 loaded in tension (Elflah et al, 2018 b)

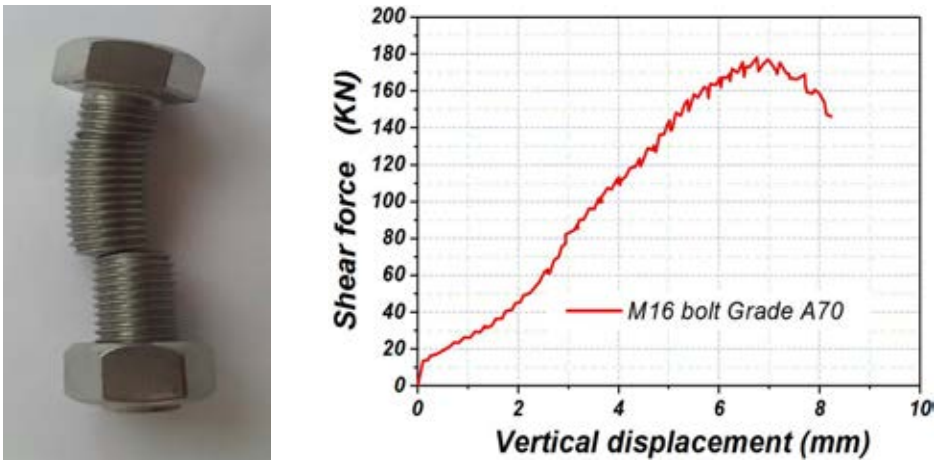

Figure 3.4 Load-deflection curve and failure mode of M16 bolt Grade A4-80 loaded in double shear (Elflah et al, 2018 b)

connected beam remains virtually elastic and hence undamaged, so that it can be reused in more than one tests. The stress pattern developed in the tested joints is typical of

common single-sided beam-to-column joints.

As shown in Figure 3.6, where TSWAC-O-8 during testing is depicted, the bottom end of the column inserted in a fabricated steel sleeve which was rigidly clamped to the strong floor of the lab by four 50 mm diameter grade A490 bolts, thereby facilitating fixed end conditions and also LVTD 10 was used to monitor the horizontal displacement of the bottom end of the column and verified that the adopted support conditions were rigid as intended. A reaction frame was utilized to restrain the top of the column against horizontal displacement in the plane of loading. A hydraulic actuator was used to apply a vertical load at 1.47m from the column face. In all tests lateral torsional buckling of the beam was prevented and no out of plane deformations of the beam were observed, by using suitable support conditions. As shown in Figure 3.6, the actuator was applying the load via a pin connected to a steel bracket which allowed rotation of the loaded end of the beam in the plane of loading, but prevented the rotation about the beam axis, thus providing support against lateral torsional buckling.

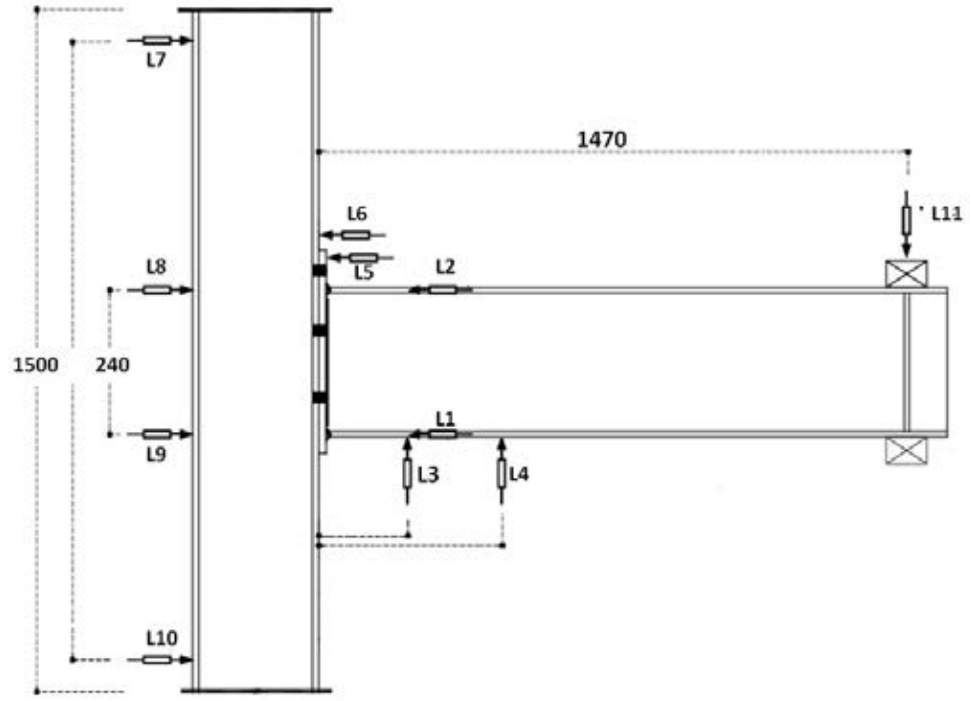

Figure 3.5 Sketch of setup and instrumentation(Elflah et al, 2018 b)

Figure 3.6 TSWAC-O-8 during testing

Figures 3.5 and 3.6 illustrate the instrumentation used in the experimental campaign. Eleven LVDTs were employed to capture and record key horizontal and vertical displacements in critical locations. Figure 3.5 shows the location and direction of the LVDTs, which are marked on the sketch with the letter "L" followed by a number. The rotation of the beam end connected to the column Φ_b was determined separately from the following pairs of LVDTs: L1 -L2, L3-L4 and L3-L11, as discussed in the following section of this Chapter. The rotation of the panel zone of the column (i.e. part of the column between the flanges of the connected beam) Φ_c was determined from LVDTs L8 and L9. Bolt elongation or thread stripping of the bolts in tension may lead to the potential separation between the connected parts in the tension zone of the joint (i.e. end plate/angle cleat from the column flange in the vicinity of the top flange of the beam). This was monitored by subtracting the values of the displacements recorded by L5 and L6; in all cases the separation was negligible. LVDTs L7 and L10 were used to monitor the horizontal displacement of the top and bottom ends of the column and verified that the adopted support conditions were rigid as intended.

A load cell was utilized to monitor the horizontal reaction force offered by the reaction frame to the top end of the column, whilst the applied vertical load was monitored and recorded by the load cell which was embedded in the hydraulic actuator. Finally, the development of strains was monitored by the array of strain gauges affixed in critical locations of the angle cleats and end plates, as depicted in Figure 3.7. Before testing the joints, the critical locations (large inelastic deformations take place) of the angle cleats and end plate were determined from Finite element models. The evolution of strains informs the subsequent discussion and allows areas of strain concentration and hence plastic deformation to be identified. Load cells, LVDTs and strain gauges were connected to a data acquisition system and the obtained readings were recorded at 2s intervals . Load cells was calibrated after each test on a uniaxial Tinius machine. Linear Variable Differential Transformers were calibrated for use in the laboratory to ensure reliable linear measurements and the calibration procedure incorporating precision gauge blocks and a micrometer fixture.

3.2.4 Load application

Upon inserting and steel wedging the bottom end of the column into the fabricated sleeve connected to the strong floor, as depicted in Figure 3.6, the beam was bolted to the column flange according to the tested configuration. In all cases the bolts were hand-tightened, which resulted in the so-called snug tight condition. Hence, no bolt preload was applied since the behaviour of preloaded stainless steel joints were not meant to be studied within the project. As reported by Yuan et al. (2018) for stainless steel T-stubs in tension, preloading results in marked differences in the initial rotational stiffness but has no effect on the strength of the joints. The hydraulic actuator used in this experimental programme had a nominal capacity of 400 kN whilst the maximum travel of the stroke was 250 mm. This proved sufficient for all tests, as joint failure was obtained in all cases. A constant loading rate of 1.5mm/minute was adopted for all tests. To obtain the quasi-static response

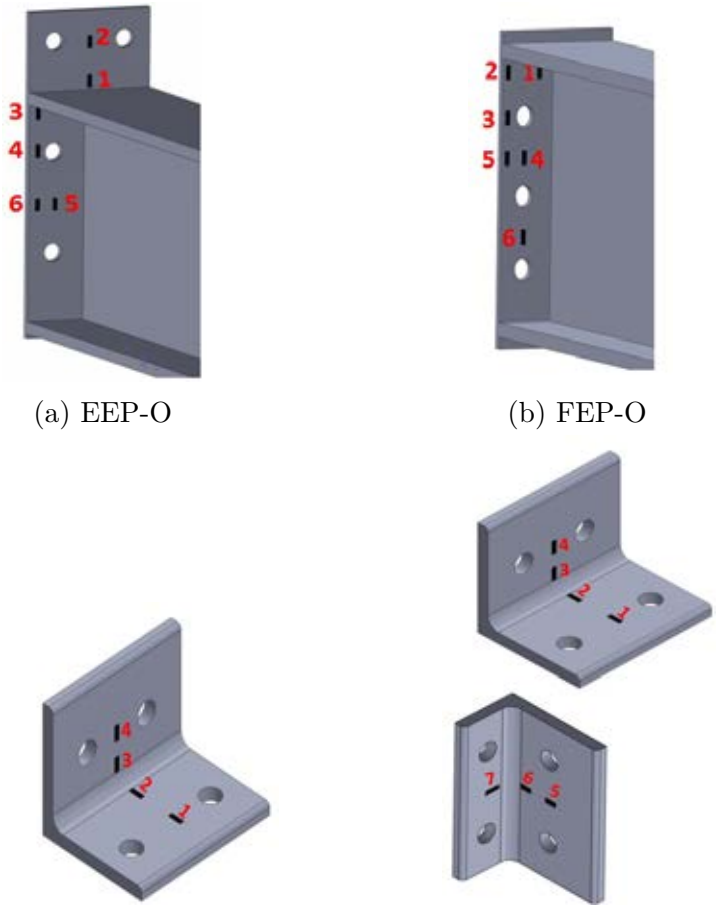

(a) EEP-O

(b) FEP-O

(c) TSAC-O-10 and TSAC-O-8

(d) TSWAC-O-10 and TSWAC-O-8

Figure 3.7 Location of strain gauges for each specimen

of the joints and eliminate any potential strain rate effects, the loading procedure was halted for at least 2 minutes regularly at intervals of approximately 10% of the expected failure load. During the time that the testing was paused, photos of the specimens were taken and the recorded LVDT and strain-gauge readings were checked for consistency to ensure that the test was progressing as expected. Moreover, the beam was constantly inspected visually for any signs of lateral displacements that would indicate the occurrence of lateral torsional buckling. A slower loading rate of 1mm/min was adopted and more regular halting of the test was applied when approaching the failure load and collapse seemed imminent. In all cases the tests progressed until the maximum load was obtained and were terminated when the applied load was seen to clearly decrease with increasing stroke of the actuator. As subsequently discussed, the initiation of bolt fracture either in

tension or in shear triggered overall joint failure. This was verified by visual inspection of the most heavily loaded bolts, where either bolt fracture or large inelastic deformations accompanied by clear indication of crack initiation were observed.

3.3 Results

This section contains a comprehensive discussion of the recorded experimental results with the focus being on the overall joint response in terms of the obtained moment–rotation behaviour and observed failure modes. The applied moment is calculated by multiplying the acting force at the beam end by the distance between the point of load application and the column face, which was 1.47 m for all specimens. The corresponding joint rotation is obtained as the recorded beam rotation Φ_b minus the recorded column shear panel rotation Φ_c . Both these rotations are determined as the difference of relevant LVDT readings divided by the distance between the LVDTs, as previously stated. Figure 3.8 depicts the obtained moment-rotation response for the EEP-O specimen. Based on the readings of three pairs of LVDTs (i.e. L1 -L2, L3-L4 and L3-L11), three different estimations for the beam end displacement can be obtained, however the difference between them is seen to be negligible. The same conclusion was drawn for all tests. Therefore, all subsequently reported rotations have been determined from the reading of L1 and L2 alone, whilst the remaining LVDT values yield almost identical results. A detailed discussion of the obtained results follows for each joint configuration tested.

3.3.1 FEP-O and EEP-O

Figure 3.9 shows the moment-rotation behaviour recorded from the tests on the specimens with the FEP-O and EEP-O configurations. Both specimens demonstrate a similar behaviour with an initially linear moment-rotation behaviour up to about one third of the ultimate moment resistance $M_{j,u}$ followed by a rounded curve indicating a progressive loss

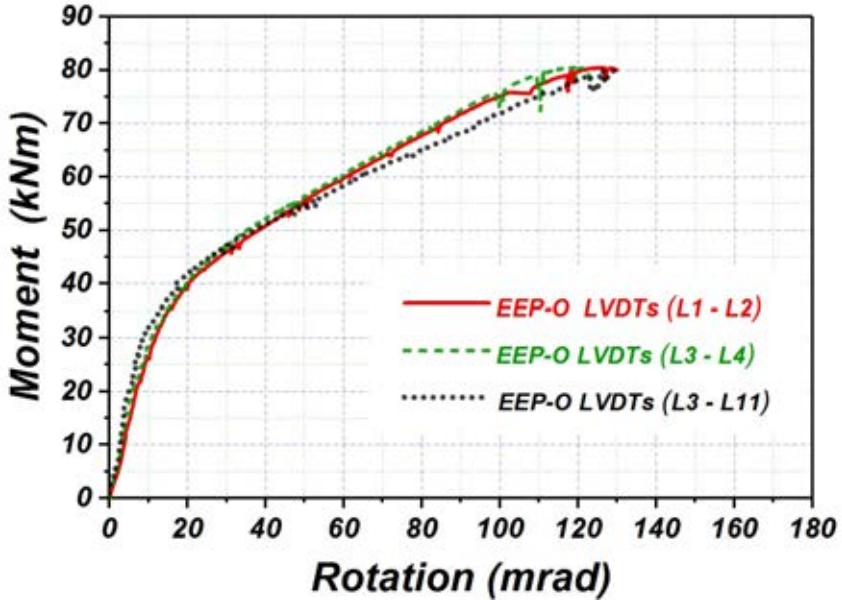

Figure 3.8 Moment rotation curves of EEP-O with different definitions of beam rotation Φ_b

of stiffness and a second linear branch up to failure. The second linear branch terminates sharply upon $M_{j,u}$ is reached and is followed by a rapid loss of strength. The end of the falling branch of the curve coincides with either bolt fracture, as was the case for the FEP-O specimens or the termination of the test shortly after signs of bolt fracture were observed in the case of the EEP-O specimen.

The EEP-O having a greater distance between its centre of rotation (i.e. centre of the compression zone) and the bolts in tension exhibits both higher stiffness and strength compared to the FEP-O specimen. On the other hand, FEP-O exhibits a clearly higher rotation capacity with its rotation$\Phi_{j,u}$ at the maximum moment $M_{j,u}$ being 30 mrad higher compared to the EEP-O specimen. In any case, both specimens are characterized by a very high rotation capacity and a distinctly increasing moment resistance with increasing joint rotation, presumably due to the high ductility and strain-hardening of austenitic stainless steel.

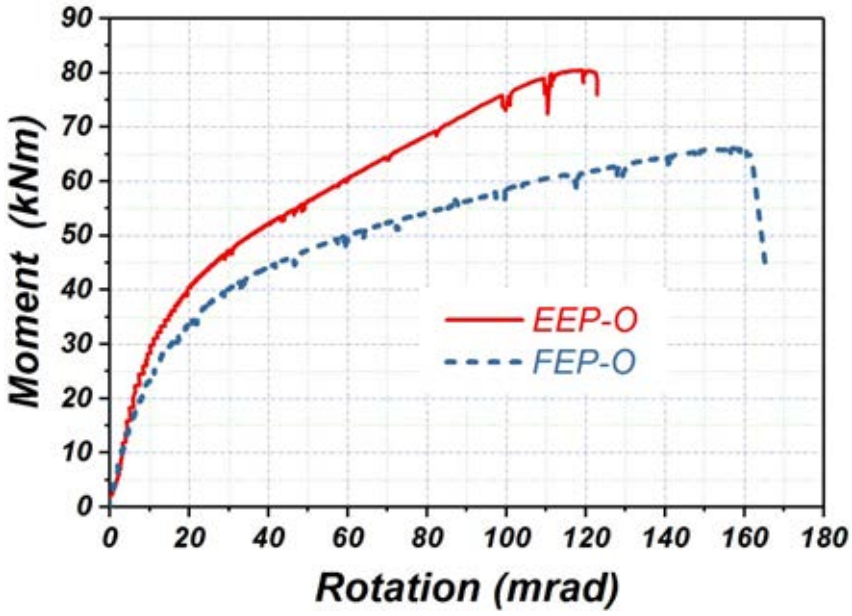

Figure 3.9 Moment-rotation response for FEP-O and EEP-O specimens

Figures 3.10a and 3.10b illustrate the obtained failure modes for both FEP-O and EEP-O specimens accompanied by the most severely damaged bolts the failure of which led to the overall joint failure. For the FEP-O specimen, significant inelastic deformations in both the end plate and the column flanges attached to it are clearly observed. Hence significant bending of the column flanges in both the tension and the compression zone of the joint as well as of the end plate has clearly occurred prior to the bolt fracture which ultimately led to failure. An inspection of the fracture of the bolt reveals that the failure occurred near the head of the bolt in the threaded shank. No significant inelastic defamation or necking of the bolt can be observed. The failure mode of the EEP-O specimen illustrated in Figure 3.10b the classical deformation pattern of a T-stub in tension. The T-stub comprises the end plate between the top two bolt rows which is being pulled by the beam tension flange welded on the end plate. Clear plastic deformations of the end plate in the vicinity of the beam flange and of the bolts can be observed and the T-stub deformation depicted is typical of a mode 1 deformation pattern, which is characterized by high ductility. A comprehensive discussion on T-stubs in tension is contained in Chapter 6. In contrast to the tension zone of the extended end plate (i.e. the T-stub), the column flange connected to it does not show signs of significant deformation,

presumably due to the very high stiffness of the flange compared to the end plate since the flange thickness is 50% higher than the end plate thickness. However, in the compression zone of the joint bending of the column flange can be clearly observed.

(a) Flush End Plate (FEP-O) connection failure mode and fractured top bolt

(b) Extended End Plate (EEP-O) connection failure mode and deformed top bolt

Figure 3.10 Failure modes of FEP-O and EEP-O specimens

In Figure 3.10b the most heavily stressed bolt of the EEP-O joint (i.e. the bolts of the top row) exhibits clear sings of inelastic deformation in shear and tension, whilst a closer inspection reveals a hairline crack in the bolt shank indicating the initiation of bolt fracture. None of the two specimens (EEP-O, FEP-O) showed any sings of weld fracture and ultimately failure was due to bolt failure, which however occurred after large inelastic deformations had occurred in the more ductile parts of the joints (end plates, and column

flange in bending).

Figures 3.11(a) and 3.11(b) depict the development of strains as rotation is increased for specimens FEP-O and EEP-O respectively. The location of the strain-gauges and their numbering have been reported in Figure 3.7. Tensile strains have been assigned a negative sign, whilst compressive strains have been assigned a positive sign. This sign convention was followed by Liu et al. (2012(a); 2012(b)) and has been also adopted in Chapter 4, were the tests on the blind-bolted beam-to-tubular column connections are reported.

Figure 3.11(a) reveals that high plastic tensile strains occur in locations 1, 2, which were located the farthest from the centre of rotation of the joint. The recorded tensile strains can be observed to progressively decrease with decreasing distance from the centre of location of the joint (locations 4, 5 and 6) since these parts of the end plate deformed less. In agreement with the mode of deformation of the flush plate observed in Figure 3.10(a), significant plastic compressive strains can be observed in location 3, which lies in the concave part of the curved flush end plate, where compressive strains and stresses develop. Figure 3.11(b) shows the development of significant tensile strains between the top two bolt rows (i.e. in locations 1 and 3) due to the bending of the end plate. The tensile strains clearly decrease between the second and the bottom row of bolts (i.e. locations 5 and 6). In locations 2 and 4 compressive strains occur as these locations lie in the concave part of the bent (i.e. curved) extended end plate, where plastic hinges develop in the T-stub.

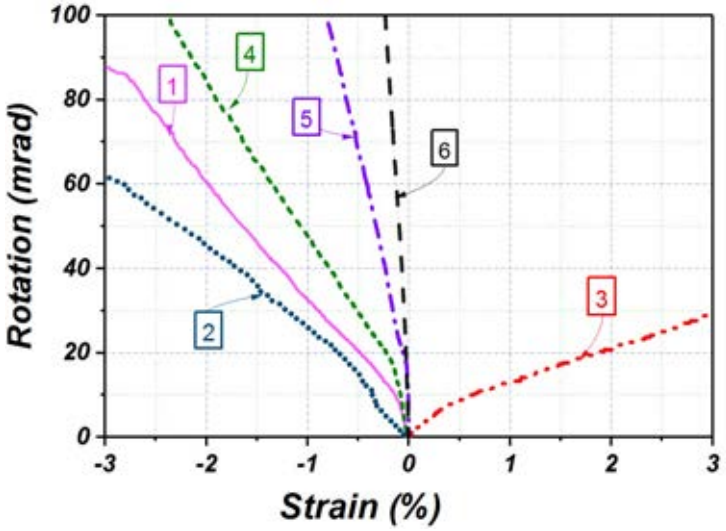

(a) Measured strain for FEP-O specimen

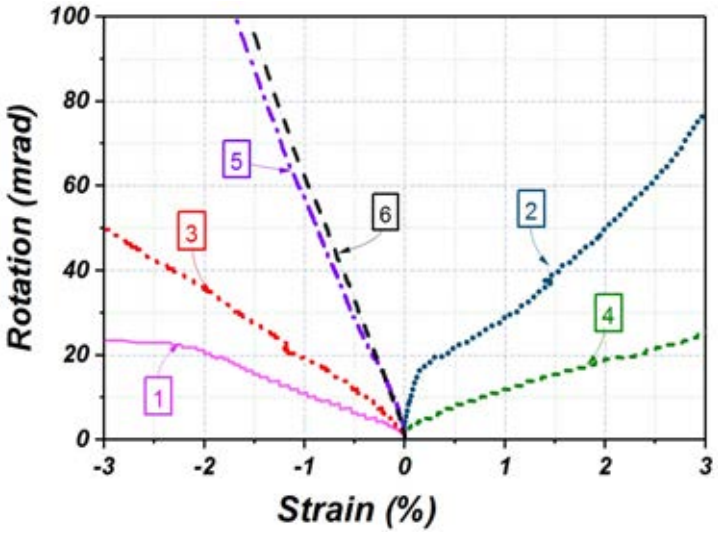

(b) Measured strain for EEP-O specimen

Figure 3.11 Strain – rotation response for FEP-O and EEP-O specimens

3.3.2 TSAC-O

Following the previous discussion on the FEP-O and EEP-O joint results, the results obtained for the TSAC-O specimens are discussed herein. Figure 3.12 depicts the recorded moment-rotation behaviour obtained from the tests on the TSAC-O-8 and TSAC-O-10 specimens. A non-linear response with increasing stiffness can be initially observed for both specimens, as the various gaps between the connected parts and the bolts and the bolt holes begin to close and then the initial elastic rotation stiffness is attained. As with

the EEP-O and FEP-O specimens, the linear elastic response is followed by a gradual loss of stiffness indicated by the rounded part following the first linear branch of the moment-rotation curves. This progressive loss of stiffness is attributable to the bending of the top angle cleat in the tension zone of the joints. Thereafter a second linear branch follows as the increasing plastic deformations are accompanied by strain hardening of the deformed angle cleats. TSAC-O-8, which employs thinner angle cleats (8 mm) exhibits a hardening response following the second linear branch prior to failure. This can be attributed to the progressive flattening of the thin top angle cleat, whereupon forces are transferred by tension rather than bending, hence the joint exhibiting a stiffer response. Specimen TSAC-O-10, which employs the thicker (10 mm) angle cleats, exhibits both higher strength and higher stiffness than the thinner TSAC-O-8 specimen. No significant differences in the rotation capacity of the two specimens can be observed, with the rotation $\Phi_{j,u}$ corresponding to the ultimate moment $M_{j,u}$ being close to 150 mrad for both TSAC-O-8 and TSAC-O-10.

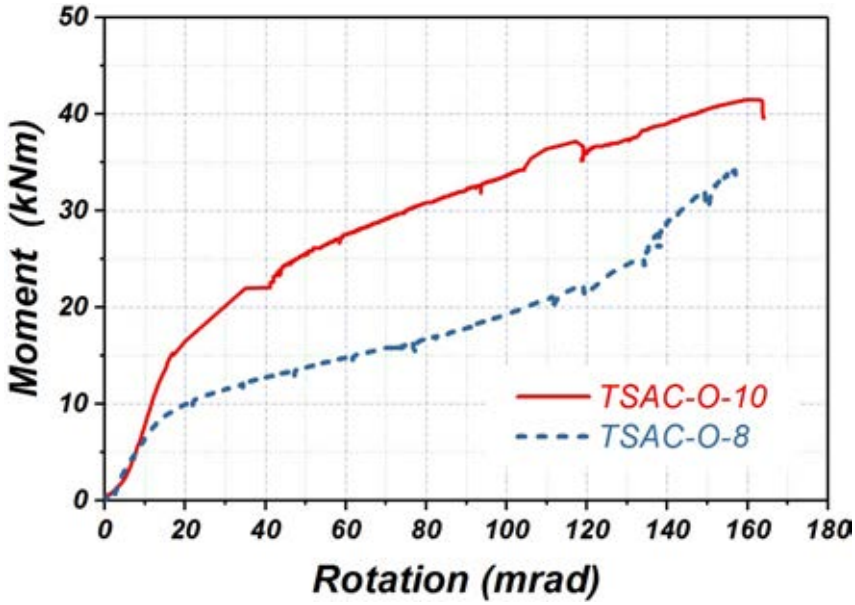

Figure 3.12 Moment-rotation response for TSAC-O-8 and TSAC-O-10 specimens

In Figures 3.13(a) and 3.13(b) the obtained failure modes are illustrated for TSAC-O-8 and TSAC-O-10 respectively. High plastic deformations can be observed in the tension

(a) TSAC-O-8 connection failure mode and deformed top bolt

(b) TSAC-O-10 connection failure mode and deformed top bolt with crack initiation

Figure 3.13 Failure modes of TSAC-O-8 and TSAC-O-10 specimens

zone of both specimens with the top cleats exhibiting clear signs of inelastic bending (i.e. flattening). In the compression zone of both specimens, the seat cleats are bent, whilst the column flange shows limited plastic deformation due to the compression forces transferred from the bottom flange of the connected beam via contact. The bolts connecting the top cleats to the column flange can be seen to be plastically deformed in single shear and tension, whilst the bolt shown in Figure 3.13(b) exhibits a hairline crack in the shearing plane, which ultimate caused the failure of the joint. These observations agree with the ones made previously for the EEP-O and FEP-O tests.

In Figures 3.14(a) and 3.14(b) the development of strains in the top angle cleats connecting the tension flange of the beam to the flange of the column with increasing joint

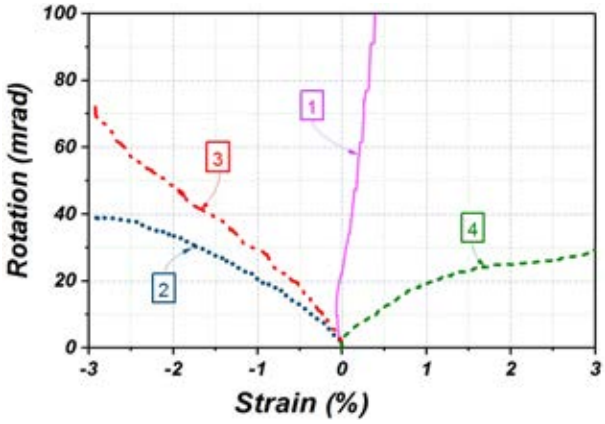

(a) Measured strain for TSAC-O-8 specimen

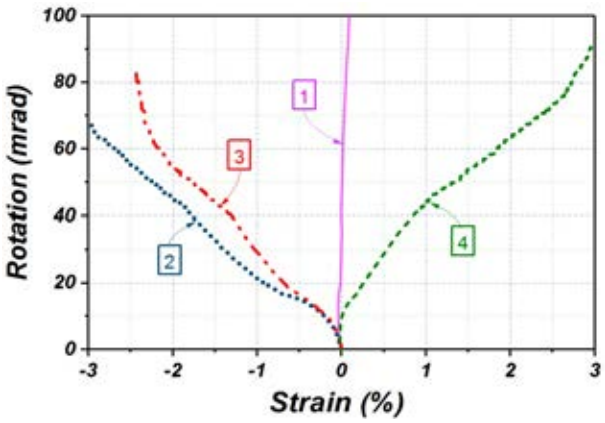

(b) Measured strain for TSAC-O-10 specimen

Figure 3.14 Strain evolution with increasing rotation for TSAC-O-8 and TSAC-O-10 specimens

rotation is reported for specimens TSAC-O-8 and TSAC-O-10 respectively. The same sign convention as before is assumed. The evolution of strains is qualitatively similar for both specimens, with high tensile strains on either side of the corner of the angle cleat (locations 2 and 3), where significant plastic strains due to the plastic bending (i.e. flattening) of the angle cleats develop. High compressive strains are observed in location 4 in accordance with the deformed shape of the specimens, from which location 4 can be seen to be on the concave side of the bend angle cleats. Finally, very small deformations and strains are seen to develop between the bolt holes on the horizontal leg of the top angle cleat.

3.3.3 TSWAC-O

In Figure 3.15 the moment-rotation behaviour obtained from the tests on the TSWAC-O-8 and TSWAC-O-10 specimens is reported. Similar to the TSAC-O specimens, the TSWAC-O specimens demonstrate an initially nonlinear response until all gaps between the connected parts (e.g. bolts and bolt holes) are closed. Due to the web cleats connecting the beam to the column via to additional bolt rows, the TSWAC-O specimens are seen to demonstrate superior rotational stiffness and strength compared to their TSAC-O counterparts, as was expected. The angle cleat thickness has a significant effect on both the stiffness and the rotation capacity of the tested TSWAC-O specimens with TSWAC-O-8 exhibiting reduced stiffness but higher ductility compared to its TSWAC-O-10 counterpart. On the contrary, and rather unexpectedly, the strength seems to remain unaffected with both specimens reaching similar values of ultimate moment resistance $M_{j,u}$ albeit at different corresponding rotation values $\Phi_{j,u}$.

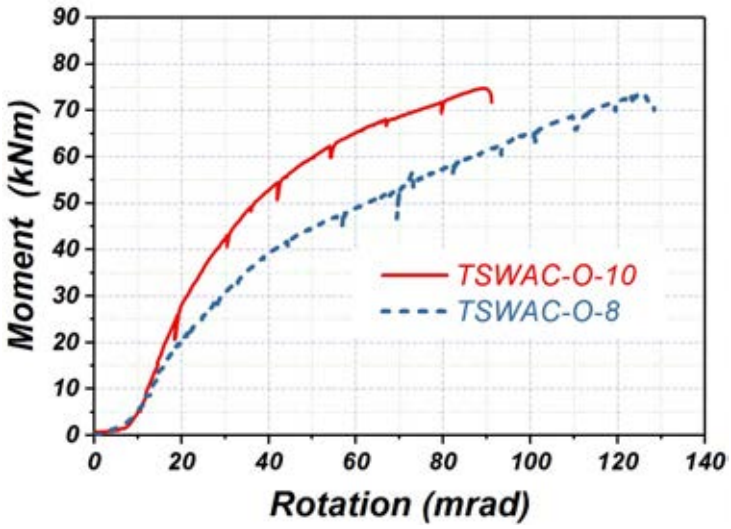

Figure 3.15 Moment-rotation response for TSWAC-O-8 and TSWAC-O-10 specimens (Elflah et al, 2018 b)

In both TSWAC-O-8 and TSWAC-O-10 specimens failure was ultimately triggered by the top bolt connecting the web cleat to the beam web failing in double shear. This is highlighted by Figure 3.16(b), where a typical failure mode of a bolt in double shear


(a) TSWAC-O-8 connection failure mode and deformed top bolt


(b) TSWAC-O-10 failure mode and bolt in double shear

Figure 3.16 Failure modes of TSWAC-O-8 and TSWAC-O-10 specimens

can be observed for the bolt connecting the web angle cleat to the beam web in specimen TSWAC-O-10; significant plastic deformation of the bolt shank can be clearly seen along two well-defined shear planes the distance of which is equal to the thickness of the beam web. Clear evidence of plastic deformation due to bending of the column flange can be clearly observed in the compression zone of the joint. These occurred upon the attainment of high rotations, due to the corresponding high compression forces developed in the compression zone of the joint. Finally the bolts connecting the top cleat to the column flange was visibly deformed plastically as shown in Figure 3.16(a).

In Figures 3.17(a) and 3.17(b) the development of strains in the web cleats of the tension zone of the joint (top and web cleat) is depicted for TSWAC-O-8 and TSWAC-O-10

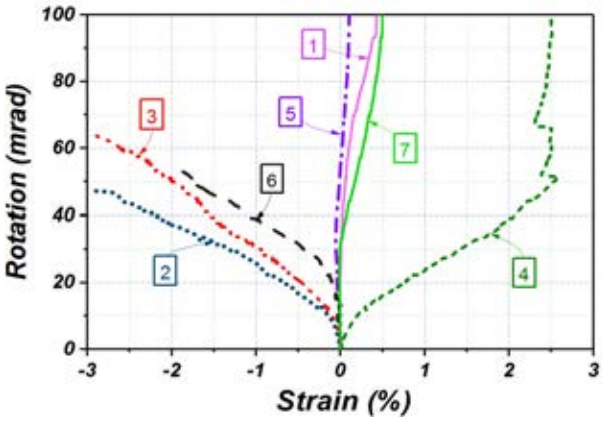

(a) Measured strain for TSWAC-O-8 specimenn

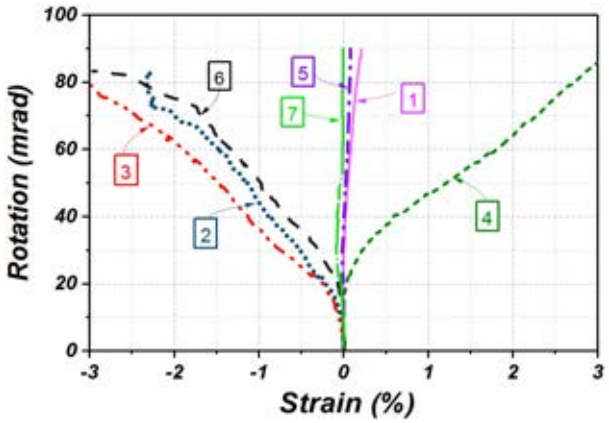

(b) Measured strain for TSWAC-O-10 specimen

Figure 3.17 Strain evolution with increasing rotation for TSWAC-O-8 and TSWAC-O-10 specimens (Elflah et al, 2018 b)

respectively. The observations previously made in the discussion of Figure 3.14 regarding the strain evolution recorded for the top cleat of the TSAC-O specimens hold for the evolution of strains in locations 1-4 (top cleat) observed for the TSWAC-O specimens.

Regarding the evolution of strains in the web cleat connecting the beam web to the column flange, it can be observed that high plastic strains develop in location 6 (web cleat corner on the side of the beam), whilst the strains in location 5 are negligible indicating that this part of the web cleat remains virtually undeformed. In location 7 no strain develops for the TSWAC-O-8 specimen, whilst some compressive strains are observed for TSWAC-O-10 specimen.

3.3.4 Key joint behaviour parameters

Table 3.3 reports a summary of key parameters pertinent to the connection response, which allows the behaviour exhibited by the tested connections to be quantified in terms of rotational stiffness, strength (plastic moment resistance) and rotation capacity. Quantified key joint response characteristics facilitate the discussion and comparison of the response of the tested joints as well as the comparison with the design predictions according to EN 1993-1-8 (2005). The symbols used in Table 3.3 are compatible with the ones in EN 1993-1-8 (2005) and are:

- $S_{j,ini}$, for initial rotational stiffness of the joint
- $M_{j,R}$, for the pseudo-plastic moment resistance of the joint
- $M_{j,u}$, for the ultimate moment resistance (maximum recorded moment during testing)
- $M_{j,30}$, for the moment resistance corresponding to a rotation of 30mrad
- $\Phi_{j,u}$, for rotation corresponding to $M_{j,u}$
- Φ_c, for the maximum rotation recorded during testing

Table 3.3 Key parameters from test results (Elflah et al, 2018 b)

Specimen	Initial stiffness $S_{j,ini}$ (kNm/mrad)	Ultimate moment $M_{j,u}$ (kNm)	Moment at 30 mrad $M_{j,30}$ (kNm)	Plastic moment resistance $M_{j,R}$ (kNm)	Rotation Φ (mrad)	
					Maximum moment $\Phi_{j,u}$	Maximum recorded Φ_c
FEP-O	3913	65.4	41	40	157	165
EEP-O	4464	80.4	48	42	119	121
TSAC-O-8	1237	34.1	12	12	157	157
TSAC-O-10	1521	41.5	21	23	162	162
TSWAC-O-8	1920	73.3	30	39	125	131
TSWAC-O-10	2769	74.7	44	55	91	95

All above mentioned parameters can be extracted from the reported moment-rotation curves. The initial rotational stiffness $S_{j,ini}$ is simply the slope of the first linear branch of

the curves, as determined by means of linear regression analysis. A linear trendline is used to approximate the initial part of the curve and the slope of the best fit line is reported in Table3.3 as the initial rotation stiffness. For specimens FEP-O and EEP-O for which the initial part of the curves is linear from the onset of loading, the slope can be unambiguously determined. With respect to the TSAC-O and the TSWAC-O specimens, that exhibit an initial nonlinear region prior to the attainment of the initial rotational stiffness the initial nonlinear part of the curves is ignored, and regression analysis is performed after the rotational stiffness slope has become stable. The ultimate moment recorded during testing $M_{j,u}$, the rotation corresponding to that moment $\Phi_{j,u}$, the moment at 30 mrad rotation $M_{j,30}$ and the maximum rotation recorded during testing Φ_c are also determined by extracting the corresponding readings from the graphs.

The selection of the rotation of 30 mrad as a key rotation value at which the moment $M_{j,30}$ is reported is based on similar studies by many researchers performing tests on carbon steel joints (Girão and Bijlaard, 2007; Girão and Bijlaard, 2007; Wilkinson et al., 2006). It is noteworthy that the European design guidance for earthquake resistant structures EN 1998-1-1 (2004) specifies joint rotation values of 25 mrad and 35 mrad as the minimum rotation capacity required (i.e. ductility demand) for steel connections that are required to dissipate energy under a seismic action for structures classified as ductility class medium (DCM) and ductility class high (DCH) respectively. The joint rotation of 30 mrad lies in-between and hence joints reaching or exceeding this value can be considered as joints possessing high rotation capacity.

Some ambiguity arises when the pseudo-plastic moment resistance $M_{j,R}$ needs to be determined from experimentally derived moment-rotation curves. As discussed in Chapter 2, $M_{j,R}$ is the joint moment resistance at which the weakest joint component plastifies/fails. When the weakest joint component exhibits a ductile failure, significant redistribution of stresses occurs, and higher moment resistances can be reached. This is not considered

by EN 1993-1-8 (2005). Hence $M_{j,R}$ does not and is not meant to correspond to the maximum moment resistance of the joint but to a moment value at which pronounced plastic deformation occurs.

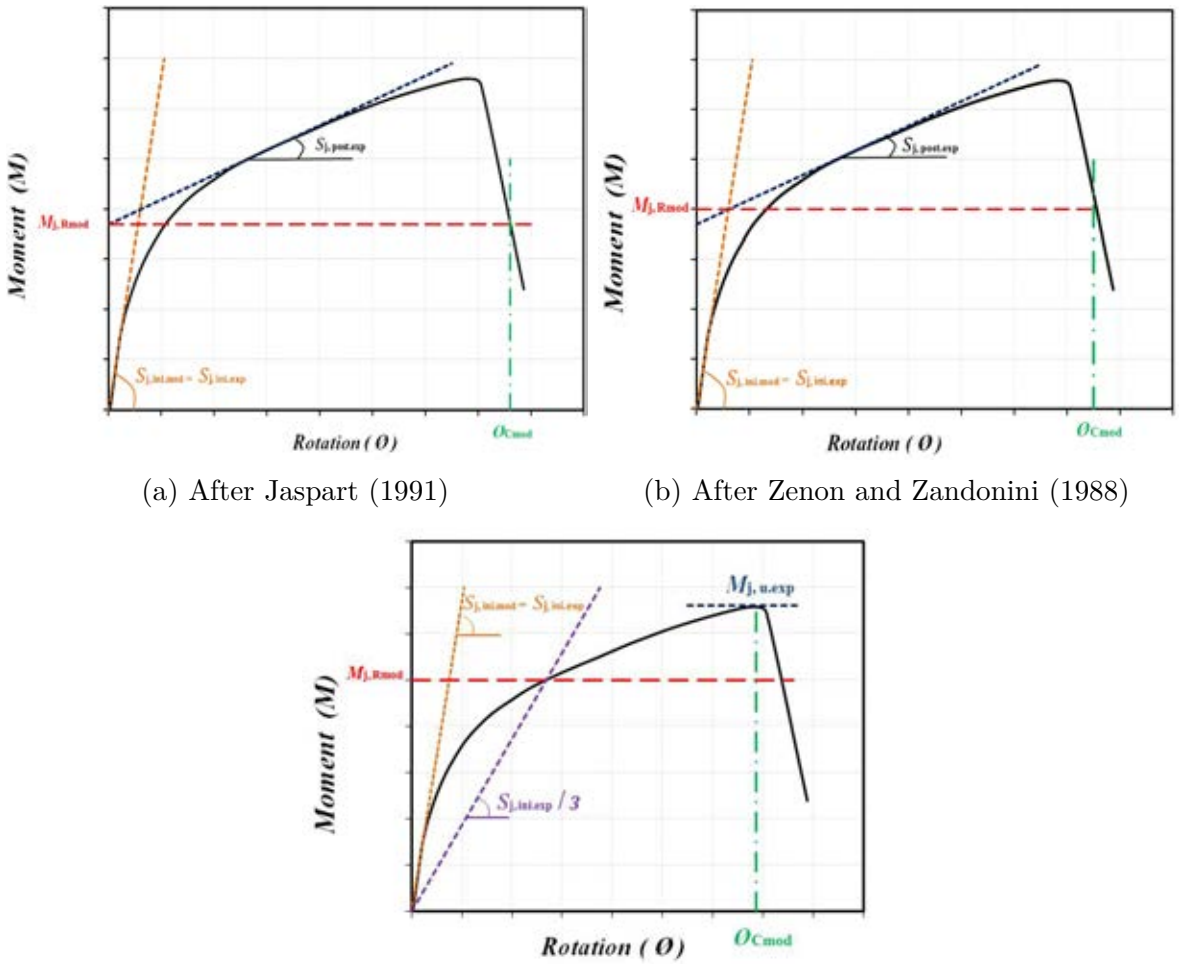

(a) After Jaspart (1991)

(b) After Zenon and Zandonini (1988)

(c) After Weynard (1997)

Figure 3.18 Various definitions of plastic moment resistance (Elflah et al, 2018 b)

Where the symbols used in Figure 3.18 are :

- $S_{j,ini.exp}$ is the expermintal initial rotational stiffness of the joint
- $S_{j,post.exp}$ is the expermintal post rotational stiffness of the joint
- $M_{j,R.mod}$ is the plastic moment resistance of the joint

- $M_{j,u.exp}$ is the expermintal ultimate moment resistance (maximum recorded moment during testing)

- $\Phi_{C.mod}$, for rotation corresponding to $M_{j,u.exp}$

Figure 3.18 depicts schematically three possible definitions of $M_{j,R}$ based on the research work by Jaspart (1991), Zanon and Zandonini (1988) and Weynand (1997). The procedure recommended by Jaspart (1991) relies on determining $M_{j,R}$ as the intersection of the second linear branch following the curved region of the joint response with the y-axis of the moment-rotation curve. According to the recommendation by Zanon and Zandonini (1988) the pseudo-plastic moment resistance $M_{j,R}$ is defined as the intersection of the two linear branches of the curve. Finally Weynard et al. (1997) propose the definition of $M_{j,R}$ as the intersection of a secant stiffness with the moment-rotation curve. In accordance with similar studies on carbon steel joints by Girão and Bijlaard (2007) and Girão et al. (2004,b), the definition of $M_{j,R}$ according to Zanon and Zandonini (1988) (i.e. Figure 3.18(b) is adopted throughout this thesis. These $M_{j,R}$ values are later on compared against the relevant predictions codified in EN 1993-1-8 (2005).

3.4 Discussion of results

After reporting the key results obtained from the experiments, the design predictions for the initial rotational stiffness, strength and ductility according to the provisions of EN 1993-1-8 (2005) for carbon steel joints are compared against the experimentally determined ones. A discussion on the observed failure modes is also included. In all calculations the measured geometric and material properties were used for the joint components and all safety factors were set to unity. The design provisions codified in EN 1993-1-8 (2005) fully cover the strength and stiffness calculations for carbon steel joints employing the EEP-O, FEP-O and TSAC-O configurations, whilst the TSWAC-O configuration is not full covered. As discussed in the literature review, the recommendations by Pucinotti

(2001), which extend the scope of application of the EN 1993-1-8 (2005) are adopted herein for the determination of the strength and stiffness of the TSWAC-O specimens.

3.4.1 Joint stiffness

EN 1993-1-8 (2005) specifies that the initial rotational stiffness $S_{j,ini}$ of a joint determined according to Equation (3.2):

$$S_{j,ini} = \frac{Ez^2}{\sum_{i=1} \frac{1}{k_i}} \tag{3.2}$$

In the above equation E is the Young's modulus of the material of the joint, z is defined as distance between the centre of compression and the centre of tension of the joint (also termed lever arm) and k_i is the elastic stiffness of springs simulating each basic joint component i. All equations for the stiffness coefficients are explicitly given in EN 1993-1-8 (2005). The joint components considered in the determination of the stiffness and strength for all joints include the column web in tension, the column web in compression, the column flange in bending and the bolts in tension. For the FEP-O and EEP-O joints the end plate in bending is also considered, whilst the bending of the angle cleats, the bearing of the beam flanges and shearing of the bolts was taken into account for the joints employing the TSAC-O configuration. Additionally, bearing of the beam web and bending of the web cleat considered for the TSWAC-O specimens (Elflah et al, 2018 b).

In Table 3.4 the predictions for the initial rotational stiffness according to EN 1993-1-8 (2005) $S_{j,ini}$ (EC3) for the tested specimens and the corresponding predicted over experimental ratios are reported. In accordance with similar studies on carbon steel joints

Table 3.4 Assessment of EC3 design predictions (Elflah et al, 2018 b)

Specimen	Initial stiffness $S_{j,ini}$ (kNm/mrad)			Moment Capacity Mj (kNm)		
	$S_{j,ini}$ (EC3)	$S_{j,ini}$ (Test)	EC3/Test	$M_{j,R}$ (EC3)	$M_{j,R}$ (Test)	EC3/Test
FEP-O	5740	3913	1.47	18.6	40	0.47
EEP-O	9360	4464	2.1	27.2	42	0.65
TSAC-O-8	1800	1237	1.48	6.6	12	0.55
TSAC-O-10	2520	1521	1.68	11.1	23	0.48
TSWAC-O-8	5240	1920	2.73	19.2	39	0.49
TSWAC-O-10	6140	2769	2.22	30.3	55	0.55
MEAN			1.94			0.53
COV			0.25			0.13

with end plates (Girão and Bijlaard, 2007; Weynand, 1997), TSAC-O and TSWAC-O (Kong and Kim, 2017; Pucinotti, 2001), significant discrepancies between the predicted and experimentally determined initial rotational stiffness values are observed, with the predictions overestimating the experimentally determined stiffness by 94%, whilst a coefficient of variation of 0.25. It is thus believed that the observed discrepancies relate primarily to the inherent scatter in stiffness exhibited by bolted joints employing non-preloaded bolts, due to gaps and slips that initially occur between the connected components until contact between all connected members has been established. Such complex interactions are not easily accounted for by any design standard, as hard to quantify parameters such as the exact location of the bolts in the clearance holes may significantly affect the stiffness.

Worked example

The selected example is provided in this section to show how to calculate the initial stiffness of joinT. Determination of the rotational stiffness for the top and seat angle cleat connections (TSAC-O-8) as follows: :

All Cross-section geometric and material properties were reported and shown in Figure 3.1 and Table 3.2 and The symbols are used as given in Table 6.11 of EN 1993-1-8 .

The first step consists in estimating stiffness coefficients for the different components of the joint, according to Table 6.11 of EN 1993-1-8.

- Column web panel in shear

$$k_1 = \frac{0.38\, A_{vc}}{\beta\, Z} = \frac{0.38 * 2331.4}{1 * 309} = 2.85$$

where Z : is the lever arm,

β : is the transformation parameter

- Column web in compression

$$k_2 = \frac{0.7\, b_{eff,c,wc}\, t_{wc}}{d_c} = \frac{0.7 * 90.8 * 10}{212} = 3.00$$

where $b_{eff,c,wc}$: is the effective width in compression,

t_{wc} : is the thickness of the column web

d_c : the clear depth of the column web

- Column web in tension

$$k_3 = \frac{0.7\, b_{eff,t,wc}\, t_{wc}}{d_c} = \frac{0.7 * 144.8 * 10}{212} = 4.78$$

where $b_{eff,t,wc}$: is the effective width in tension,

t_{wc} : is the thickness of the column web

d_c : the clear depth of the column web

- Column flange in bending

$$k_4 = \frac{0.9\, l_{eff}\, t_{fc}^3}{m^3} = \frac{0.9 * 144.8 * 12^3}{28.4^3} = 9.83$$

where l_{eff} : is the smallest of the effective lengths for this bolt-row,

t_{fc} : the thickness of the column flange

m : is as defined in Figure 6.8 of EN 1993-1-8

- Flange cleat in bending

$$k_6 = \frac{0.9\, l_{eff}\, t_a^3}{m^3} = \frac{0.9 * 60 * 8^3}{50.6^3} = 0.21$$

where l_{eff} : is the effective length of the flange cleat,

t_a : the thickness of the cleat

m : is as defined in Figure 6.8 of EN 1993-1-8

- Bolts in tension

$$k_{10} = \frac{1.6\, A_s}{L_b} = \frac{2 * 1.6 * 157}{35} = 14.35$$

where A_s : is the tensile stress area of the bolt,

L_b : is the bolt elongation length

- Bolts in shear

$$k_{11,1} = \frac{16\, n_b\, d^2\, f_{ub}}{E\, d_{M16}} = \frac{16 * 1 * 16^2 * 805}{191500 * 16} = 1.07$$

$$k_{11,2} = \frac{16\, n_b\, d^2\, f_{ub}}{E\, d_{M16}} = \frac{16 * 1 * 16^2 * 805}{191500 * 16} = 1.07$$

where d_{M16} : is the nominal diameter of an M16 bolt,

d : is the nominal diameter of a bolt

n_b : is the number of bolt-rows in shear

- Bolts in bearing (for top and bottom beam flange)

$$k_{12,1} = \frac{24\, n_b\, k_b\, k_t\, d\, f_u}{E} = \frac{24 * 1 * 1.25 * 1.13 * 16 * 630}{196500} = 1.73$$

$$k_{12,2} = \frac{24\, n_b\, k_b\, k_t\, d\, f_u}{E} = \frac{24 * 1 * 1.25 * 1.13 * 16 * 630}{196500} = 1.73$$

- Bolts in bearing (for top and bottom flange cleat)

$$k_{12,1} = \frac{24\, n_b\, k_b\, k_t\, d\, f_u}{E} = \frac{24 * 1 * 1.25 * 0.75 * 16 * 654}{197600} = 1.19$$

$$k_{12,2} = \frac{24\, n_b\, k_b\, k_t\, d\, f_u}{E} = \frac{24 * 1 * 1.25 * 0.75 * 16 * 654}{197600} = 1.19$$

where k_b : $\leqslant 1.25$ according to Table 6.11 of EN 1993-1-8,

k_t : $\leqslant 2.5$ according to Table 6.11 of EN 1993-1-8,

f_u : is the ultimate tensile strength of the steel

In a second step, the joint stiffness is then computed through the use of formula 6.27 of EN 1993-1-8:

$$\begin{aligned} S_{j,ini} &= \frac{E\, z^2}{\sum_{i=1} \frac{1}{k_i}} \\ &= \frac{197600 * 309^2}{\frac{1}{2.85} + \frac{1}{3.00} + \frac{1}{4.78} + \frac{1}{9.83} + \frac{1}{0.21} + \frac{1}{14.23} + \frac{2}{1.07} + \frac{2}{1.73} + \frac{2}{1.19}} * 10^{-6} \\ &= 1800\, kNm/mrad \end{aligned} \tag{3.3}$$

3.4.2 Joint moment resistance

Using the provisions of EN 1993-1-8 (2005) and the measured $\sigma_{0.2}$ values in lieu of the yield stress of the joint components the pseudo-plastic moment resistance predictions $M_{j,R}$(EC3) is reported in Table 3.4 for all tested joints. The predicted-to-experimental ratio for the moment resistance is also reported and is on average 0.53 with a coefficient of variation 0.13. A similar level of conservatism of the EN 1993-1-8 (2005) design predictions was reported for stainless steel T-stubs in tension by Yuan et al. (2018), where the predicted-over-experimental resistance was 0.51 with a coefficient of variation of 0.13. The close agreement with the results reported by Yuan et al. (2018) is not surprising, given that in most cases the joint component controlling the overall joint response was the T-stub in tension. In both cases the underestimations of the experimental resistance can be attributed to the significant strain-hardening exhibited by austenitic stainless steels, which is not accounted for. High but smaller levels of conservatism exhibited by the Eurocode design predictions have been reported for stainless steel cross-sections in bending and compression (Gardner and Theofanous, 2008) (Elflah et al, 2018 b).

3.4.3 Observed failure modes and ductility

As previously stated, EN 1993-1-8 (2005) does not provide any quantified measure of rotation capacity or any procedure to predict the available rotation capacity of a steel connection but specifies a set of simple design recommendations that have to be followed if a joint is to be considered to possess adequate rotation capacity. These include limiting the thickness of the end plate (or angle cleat) or flange of the tension zone according to Equation (3.1) and designing a joint so that a ductile failure mode governs $M_{j,R}$. All tested joints adhered to these design recommendations and indeed developed high rotation capacities ranging from 95 mrad to 165 mrad, as reported in Table 3.3.

In Table 3.5 the failure modes determined according to the EN 1993-1-8 (2005) provisions are reported together with the ones observed during the tests at the maximum recorded load. In all cases the predicted failure modes, which were determined as the modes corresponding to the resistance of the weakest joint component, involved bending of an angle cleat/end plate and are hence deemed ductile. This observation agrees well with the recorded high rotations at failure as well as with the deformed specimens prior to failure, which all exhibited marked inelastic deformations of the end plates or angle cleats in the tension zone of the joints. From the previous discussion of the tests it was concluded that in all cases bolt failure in tension of in shear triggered joint failure in all cases. Bolt fracture is usually associated with brittle failure. However, bolt failure occurred upon significant inelastic deformations had already developed in other parts of the joints.

In addition to the joint rotation at failure, the ratio of the ultimate moment resistance $M_{j,R}$ over the plastic moment resistance $M_{j,u}$ can be considered as another quantifiable measure of ductility and is reported in Table 3.5. It can be seen that this ratio ranges from 1.36 for the TSWAC-O-10 specimen, which failed at the lowest recorded rotation, to 2.83 for the TSAC-O specimen which reached higher rotation prior to failure.

Table 3.5 Failure modes and measures of ductility (Elflah et al, 2018 b)

Specimen	Predicted failure mode	Actual failure mode	maximum recorded rotation Φ_c (mrad)	$M_{j,max}/M_{j,R}$
FEP-O	End plate in bending	Fracture of bolt in tension	165	1.63
EEP-O	End plate in bending	Bolt failure in tension	121	1.91
TSAC-O-8	Bending of flange cleat/mode1	Bolt failure in tension and shear	157	2.83
TSAC-O-10	Bending of flange cleat/mode 1	Bolt failure in tension and shear	162	1.80
TSWAC-O-8	Bending of flange/mode 1- bending of web cleat /mode 1	Bolt failure in tension and shear (flange cleat bolt)	131	1.88
TSWAC-O-10	Bending of flange/mode 1- bending of web cleat /mode 1	Bolt failure in shear (top bolt connecting web cleat to beam web)	95	1.36

3.5 Conclusions

In this chapter six full-scale beam-to-open column connections employing the FEP-O, EEP-O, TSAC-O and TSWAC-O configurations have been reported in detail. These configurations are representative of common joint typologies employed in practice. The recorded moment-rotation curves, evolution of strains with increasing rotation and observed failure modes have been discussed. In all cases the joints exhibited significant inelastic deformations prior to failure with rotations at failure ranging from 95 mrad to 165 mrad, far beyond the limit of 35 mrad required for dissipative joints in structures classified as DCH (ductility class high). Failure was triggered for all tests by bolt failure since all other parts of the joints had a significantly higher ductility, as can be seen in Table 3.2, where the strain at fracture ε_f is 12% for the bolts and over 50% for all other parts of the joint.

The design procedures codified in EN 1993-1-8 (2005) for the determination of the stiffness and the moment resistance of the joints, originally developed for carbon steel

joints, but applicable to stainless steel joints have been assessed based on the six test data reported herein. The predicted rotational stiffness was significantly higher than the experimental one and displayed high scatter. This observation has also been made in the past for carbon steel joints. With respect to the moment resistance, the design predictions were found to significantly and consistently underestimate the observed response, thus confirming a recent study on stainless steel T-stubs in tension (Yuan et al., 2018).

It is noteworthy that the six tests reported herein are the first to ever be conducted on stainless steel beam-to-column joints as such are expected to be extensively utilized by other researchers. A FE model is developed and validated against these test data in Chapter 5, thus allowing additional structural performance data to be generated and the design provisions of EN 1993-1-8 (2005) to be assessed on the basis of a larger pool of data.

Chapter 4

Experimental investigation of stainless steel beam-to-tubular column joints

4.1 Introduction

In the previous Chapter six full-scale tests on stainless steel beam-to-open column connections have been reported in detail and the conservatism exhibited by the EN 1993-1-8 (2005) design provisions when used to predict the moment resistance of stainless steel joints has been highlighted. This Chapter reports six full scale tests on bolted stainless steel beam-to-tubular column joints. As discussed in Chapter 2, tubular members are the most common stainless steel members used in construction but insufficient access due to the closed form of the hollow sections complicates the execution of bolted connections. Among the various fasteners available the execution of blind-bolted connections discussed in Chapter 2, the use of stainless steel Hollo-bolts (Lindapter, 2018) was decided. The main reasons for this decision are the following:

- Lindapter is the indsutry leader in the UK for blind-bolted connections and Hollo-bolts are readily available in a suitable stainless steel Grade (EN 1.4401), hence they are suitable for joints where the parent metal is stainless steel.

- A lot of published research on the response of carbon-steel blind-bolted connections using Hollo-bolts is available (Elghazouli et al., 2009; Wang et al., 2010; Liu et al., 2012,a,b ; Tizani et al., 2013; Wang and Wang, 2016), hence the behaviour of Hollo-bolts is well-documented in terms of both experimental testing and numerical modelling.

- Lindapter donated all Hollo-bolts required for this research project and provided experimental data on the tensile response of the bolt itself and the bolt sleeve.

4.2 Experimental investigation

4.2.1 Specimens

Similar to the tests reported in Chapter 3, all tested beam-to-tubular column specimens employed a fabricated stainless steel I-section with an outer depth h of 240 mm, a flange width b of 120 mm, flange thickness t_f equal to 12 mm and web thickness t_w equal to 10 mm (i.e. I 240×120×12×10) for the beam at the end of which the load was applied. Two square hollow sections (SHS) with the same outer dimensions (150×150) but different wall thickness (6mm or 10 mm) were as columns. Three connection typologies often employed in steel structures (e.g. steel buildings), have been selected and are studied herein. These are:

- the flush end plate connection (FEP-T)

- the top and seat angle cleat connections (TSAC-T)

- the top, seat and double web cleat connection (TSWAC-T)

"In the nomenclature and symbols used herein, the letter “T” refers to beam-to-tubular column joints (i.e. blind bolted joints). Hence, a model designated as TSAC-T, refers to top and seat angle cleat joint between a beam and a tubular column."

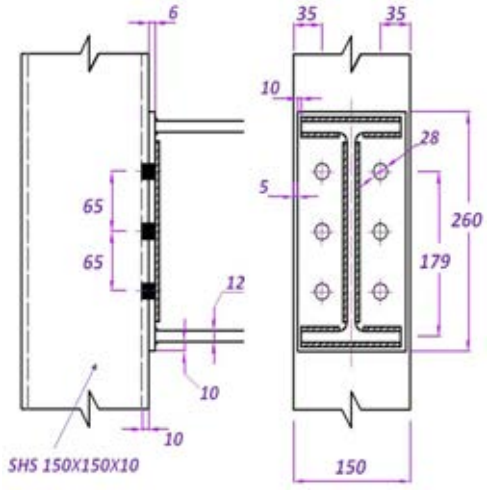

(a) Flush End Plate (FEP-T-1) connection

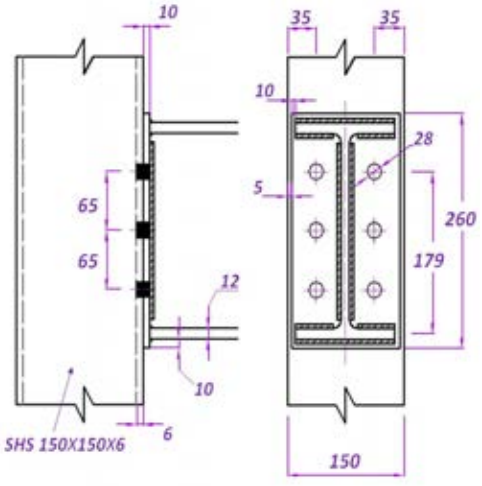

(b) Flush End Plate (FEP-T-2) connection

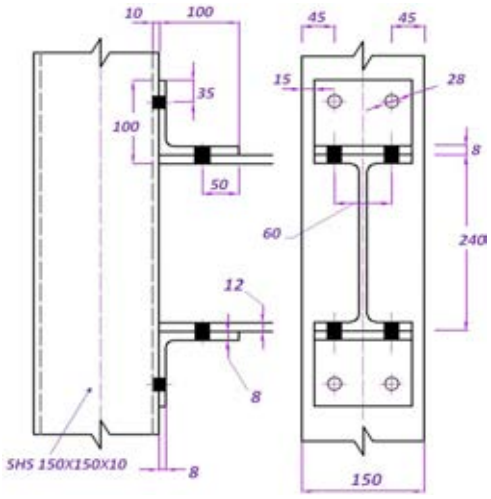

(c) Top and Seat Angle Cleat connection (TSAC-T-1)

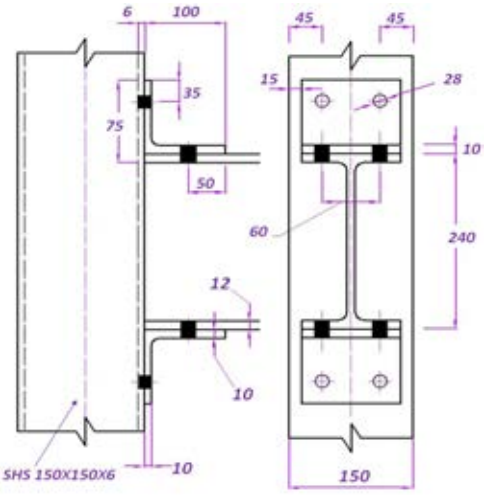

(d) Top and Seat Angle Cleat connection (TSAC-T-2)

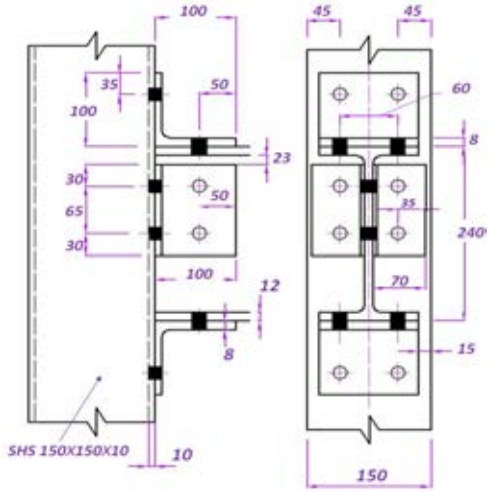

(e) Top, Seat and double Web Cleat connection (TSWAC-T-1)

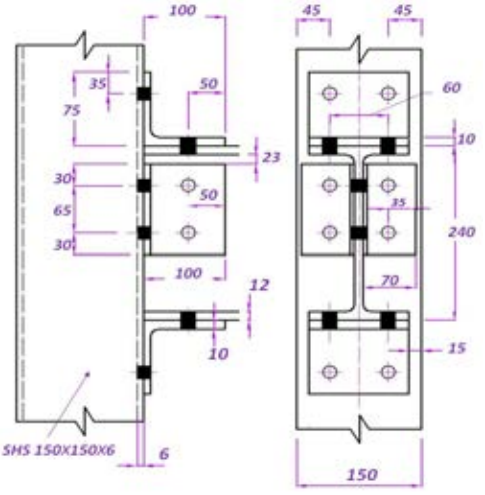

(f) Top, Seat and double Web Cleat connection (TSWAC-T-2)

Figure 4.1 Geometry of the tested specimens

To induce variations in the obtained structural response and observed failure modes for each joint typology two specimens were tested: one where a thicker (10 mm) SHS was connected to the beam via thinner end plates/angle cleats (specimen 1) and one with a relatively thin-walled (6 mm) SHS connected to the beam via thicker (10 mm) end plates/angle cleats thus promoting failure of the column face (specimen 2), as shown in Figure 4.1 where the geometry of the tested specimens is reported.

Following the discussion on the behaviour of equivalent carbon steel connections in Chapter 2, both the FEP-T (Tizani et al., 2013) and TSAC-T and TSWAC-T (Elghazouli et al., 2009; Málaga-Chuquitaype and Elghazouli, 2010; Liu et al., 2012 a,b) joint typologies fall within the semi-rigid range when classifying connections with respect to stiffness. With respect to connection classification according to strength, all of the tested connections were designed to be partial strength so that failure of the connection occurs prior to failure of the connected members.

As in the experimental programme reported in Chapter 3, M16 in Grade A80 stainless steel bolts have been used in 18 mm clearance holes to connect the angle cleats to the beam section. Identical configuration in terms of bolt-hole locations were used for the TSAC-T and TSWAC-T configurations, whilst the top and seat angle cleats were cut from the same member length. Since access from one side only was available when bolting the angle cleats or end plates to the column, stainless steel Hollo-bolts were used to facilitate blind bolted connections, as shown in Figure 4.2. All Hollo-bolts used were M16 in Grade EN 1.4401. In accordance with the specifications by Lindapter (2018), 26 mm clearance holes were drilled to accommodate the 25.75 mm outer diameter of the sleeve.

The selection of the thicknesses of the angle cleats and end plates for the chosen bolt size and grade followed the same reasoning as the one described in Chapter 3 and aims at obtaining a ductile joint response. Since no specific design recommendations for either

stainless or carbon steel blind-bolted joints are specified in EN 1993-1-8 (2005), it was assumed that the same fastener thicknesses as the ones adopted for the conventional bolted joints would suffice, given that the adopted Hollo-bolts have the same tensile resistance as the conventional bolts.

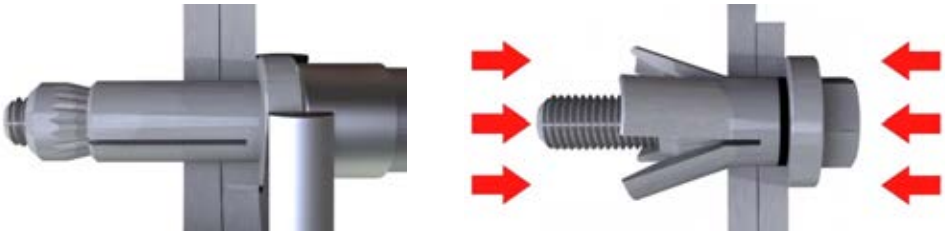

Figure 4.2 Hollo-bolt installation and deformation of sleeve. (LINDAPTER ,2018)

4.2.2 Material response

The material response of the I-sections used as beams, the angle cleats and the conventional bolts connecting the angle cleats to the beams was reported in Chapter 3.2.2. As part of the experimental programme reported herein, additional material coupons were tested in tension to characterize the material response of the columns, the end plates and the flared sleeves of the Hollo-bolts. The coupons were extracted from the top part of the columns, which remained undeformed upon the completion of the tests, from the plates from which the end plates were machined and from the flared sleeves of Hollo-bolts taken from the same batch as the ones used in all joints. Both flat and corner coupons were extracted from both SHS (i.e. SHS 150×150×6 and SHS 150×150×10) employed in the joint tests. Since the focus of this study lies in the joint response, flat coupons were extracted only from the column face to which the beam was connected and from an adjacent corner to that face. Figure 4.3 depicts a flat coupon during the test and at the formation of necking and a corner coupon at the initiation of the formation of the necking prior to failure.

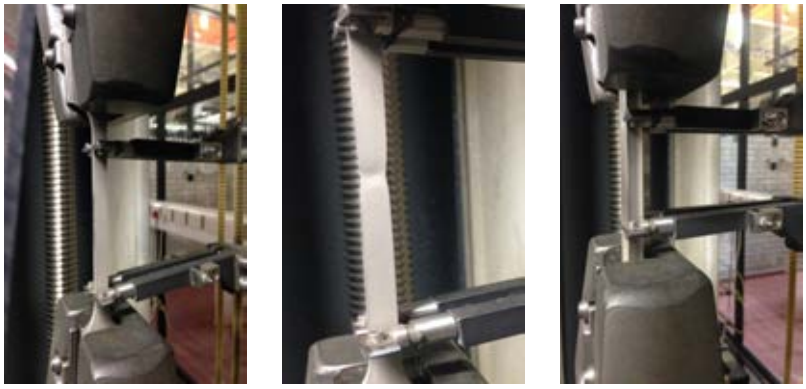

Figure 4.3 Flat and corner coupons tested in tension

As reported in Chapter 3, strain control with an applied strain rate of 0.007%/s up to the 0.2% proof stress $\sigma_{0.2}$ and subsequently a strain rate of 0.025%/s until coupon failure was applied during testing following the provisions of BS EN ISO 6892-1 (1999). In Figure 4.4 the obtained stress-strain curves for the flat and corner coupons of the SHS and for the material of the sleeve of the Hollo-bolts are reported. Similar curves were obtained for all tested material.

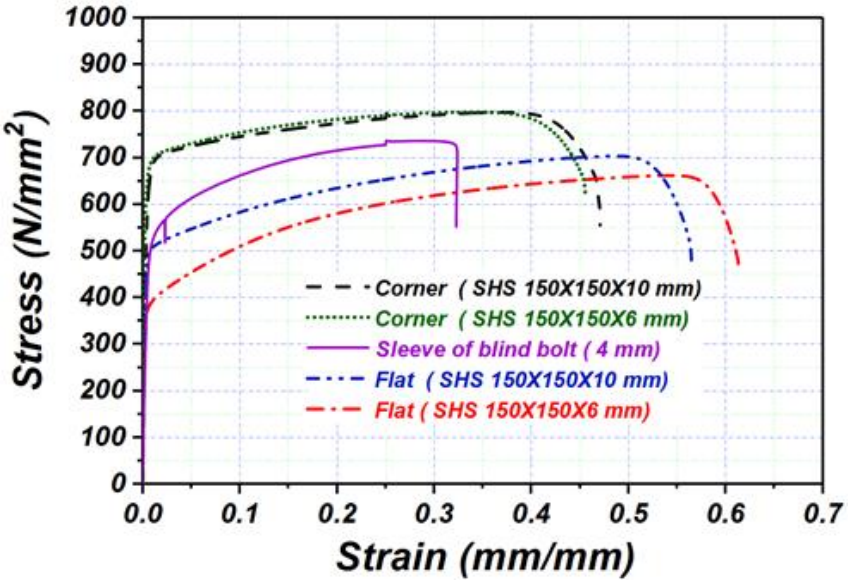

Figure 4.4 Material response of Hollo-bolt sleeve and SHS

Table 4.1 Material properties according to mill certificates

Specimen	$\sigma_{0.2}$ (N/mm^2)	$\sigma_{1.0}$ (N/mm^2)	σ_u (N/mm^2)	ε_f
I-240×120×12×10	341	369	635	53
L-100X100X8	373	441	675	54
L-100X100X10	378	445	673	55
Endplate (6 mm)	387	419	644	50
Endplate (10 mm)	334	376	620	53
SHS 150×150×6	284	338	612	56
SHS 150×150×10	336	377	617	53

Table 4.2 Material properties from tensile tests

Specimen	E (N/mm^2)	$\sigma_{0.2}$ (N/mm^2)	$\sigma_{1.0}$ (N/mm^2)	σ_u (N/mm^2)	ε_f
I-240×120×12×10 - flange	196 500	248	306	630	66
I-240×120×12×10 - web	205 700	263	320	651	65
Angle cleat (8 mm)	197 600	280	344	654	55
Angle cleat (10 mm)	192 800	289	354	656	56
End plate (6 mm)	201000	289	357	658	62
End plate (10 mm)	195000	276	339	636	51
SHS 150×150×6 - flat	189650	334	373	640	63
SHS 150×150×6 - corner	210420	647	703	795	46
SHS 150×150×10 - flat	200020	507	540	730	51
SHS 150×150×10 - corner	198000	608	692	796	47
Sleeve of blind bolt (4 mm)	180000	381	533	735	32

Key material characteristics as stated in the mill certificates and as obtained from the tensile tests are reported in Tables 4.1 and 4.2 respectively, where all symbols have been previously defined in Chapter 3. For completeness, the properties of the angle cleats and beam flange and web reported in Chapter 3 are repeated.

Significant discrepancies in the obtained material responses as quantified in terms of the reported proof stress and ultimate tensile stress values can be observed, particularly for the SHS 150×150×10 section, the $\sigma_{0.2}$ of which is seen to be 50% higher in Table 4.2 compared to the value reported in the mill certificates. Smaller discrepancies are observed for the ultimate tensile stress. This is attributed to the cold-forming process, which significantly alters the material response and enhances the proof stress and ultimate

tensile stress values of cold-formed stainless steel sections, compared to the ones of the virgin material from which the sections were rolled (Afshan et al., 2013; Rossi et al., 2013). Additional reasons for the observed discrepancies between values reported in the mill certificates and the ones obtained from this study for proof stresses, ultimate tensile stress and strain at fracture have already been discussed and are attributed to potential differences in material orientation and applied strain rates when the tests were conducted.

Figure 4.5 depicts the applied tensile force vs axial deformation of a Hollo-bolt being pulled from a hollow section. This test result was provided by Lindapter (2016) and corresponds to a bolt from the same batch as the ones used in this study. The failure mode was pull-out of the Hollo-bolt upon significant bending of the flaring sleeve. In Figure 4.5 a significant reduction in stiffness is observed to occur at relatively small loads, contrary to the response of standard bolts in tension (Figure 3.3) where the initial stiffness is maintained until relatively high stresses and the observed progressive loss of stiffness is due to material yielding. Similar conclusions have been reported by Wang et al. (2010) who have highlighted the highly nonlinear response of carbon steel Hollo-bolts and identified the deformation of the sleeve as the main source of deformation of the Hollo-bolt.

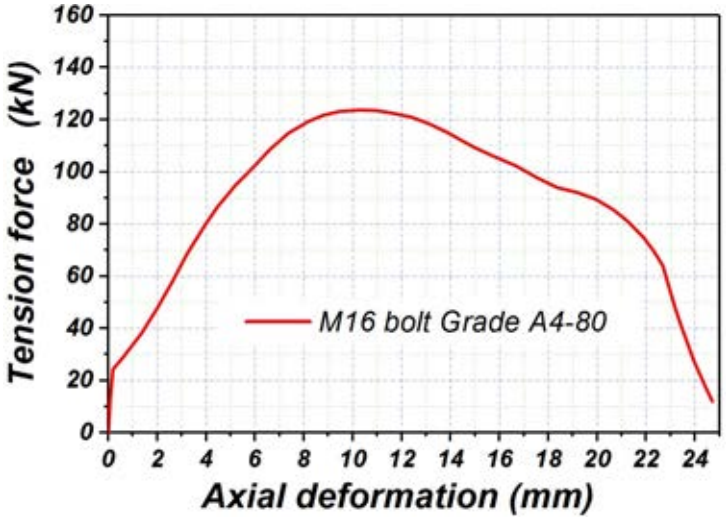

Figure 4.5 Tensile force vs axial deformation of Hollo-bolt

Since plastic bending of the flared sleeve rather than axial deformation of the bolt is the main source of deformation of the Hollo-bolt, axial load vs elongation curves cannot be directly converted into a stress-strain response. Being the most important (i.e. experiencing the highest stresses and deformations) part of the Hollo-bolt connection, the material response of the sleeve requires special consideration. For this reason, a material coupon was extracted from the sleeve and tested in tension as previously reported.

4.2.3 Experimental set-up and instrumentation

Figures 4.6 and 4.7 depict the setup and employed instrumentation used in all tests, which is identical to the one reported in Chapter 3 for the beam-to-open column joints. The beam and column members used in all tests were 1.5 m long. The dimensions of the employed beams and columns as well as the applied boundary conditions imposed, ensure that all plastic deformations are limited within the joint region where failure occurs.

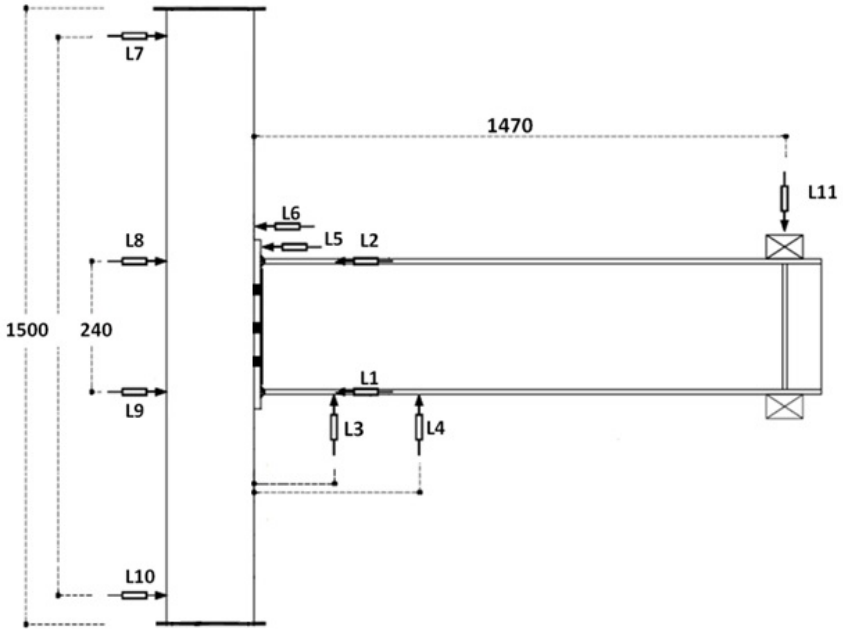

Figure 4.6 General arrangement of experimental setup and instrumentation

All details reported in Chapter 3 regarding the overall setup, load application, column and beam support conditions and employed instrumentation have been replicated for the tests reported in this Chapter and therefore their description is not repeated. The location and numbering of the strain gauges affixed on the end plates and angle cleats of the tested

specimens is shown in Figure 4.8. No strain gauges were affixed on the column face of the columns as they would have been damaged by the end plates/angle cleats in contact.

Figure 4.7 Experimental setup and testing of FEP-T-2

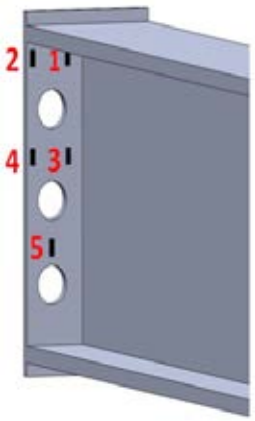

(a) FEP-T-1 and FEP-T-2

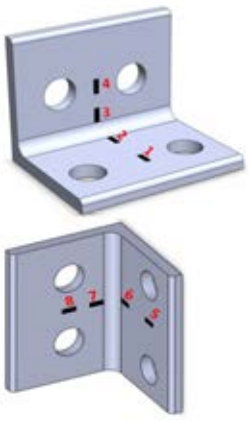

(b) TSWAC-T-1 and TSWAC-T-2

(c) TSAC-T-1 and TSAC-T-2

Figure 4.8 Location and numbering of strain-gauges for each specimen

4.2.4 Assembly and load application

The assembly of the specimens followed the same procedures as the ones reported in Chapter 3 for beam-to-open column joints and the same testing rig has been used. All conventional bolted connections were non-preloaded (i.e. snug-tight). Following the manufacturers specifications (Lindapter, 2018), a 190 Nm tightening torque was applied on the Hollo-bolts using a calibrated torque wrench to plastically deform the sleeve as required and form the connection. As for the beam-to-open section joint tests, a 400 kN hydraulic actuator with a maximum stroke of 250 mm was used in all tests reported in this Chapter. A constant loading rate of 1.5mm/minute was adopted to obtain the quasi-static response of the joints and eliminate any potential strain rate effects, whilst the loading procedure was halted for at least 2 minutes at regular intervals to visually inspect the specimen and check the recorded results for consistency. A slower loading rate of 1mm/min was applied when significant inelastic deformations developed in the joints, primarily due to concerns relating to a potential sudden bolt pull-out.

Contrary to the tests reported in Chapter 3, which were performed to failure, the tests reported in this Chapter were not conducted to failure due to health and safety concerns associated with the sudden nature of the bolt pull-out failure and the high potential energy stored in the bolts during testing. The tests were terminated once significant joint rotations and inelastic deformations occurred in either the column face or the end plates and angle cleats. A joint rotation of 105 mrad, 3 times the minimum rotation value of 35 mrad required by EN 1998-1-1 (2005) for dissipative joints in structures characterized as ductility class high (DCH), was deemed high enough for all intents and purposes, whilst it also suffices to characterize the joints' response in terms of stiffness and strength.

4.3 Results and discussion

This section contains a comprehensive discussion of the recorded experimental results with the focus being on the overall joint response in terms of the obtained moment–rotation behaviour and observed failure modes. Since the tests were not conducted to failure, the term failure mode is used herein as synonymous to observed localization of plastic deformation. Based on the observations made in Chapter 3 and given the extremely high ductility of austenitic stainless steel, it is expected that in all cases bolt failure either by sleeve fracture or by pull-out would trigger the overall failure of the specimens.

As for the beam-to-open section column joint tests reported in Chapter 3, the applied moment is determined as the applied force times 1.47, whilst the corresponding joint rotation is defined as the rotation of the beam end Φ_b minus the recorded column shear panel rotation Φ_c. Three pairs of LVDTs (i.e. L1 -L2, L3-L4 and L3-L11) were used for the determination of the beam rotation (i.e. rotation equals the difference of the LVDT readings divided by the distance between the LVDTs), which yielded identical results, as depicted in Figure 4.9, where moment rotation curves for FEP-T-2 specimen are depicted. All subsequently reported rotations have been determined from the reading of L1 and L2 alone, whilst the remaining LVDT values yield almost identical results. A detailed discussion of the obtained results follows for each joint configuration tested.

4.3.1 FEP-T-1 and FEP-T-2

Figure 4.10 shows the moment-rotation behaviour recorded from the tests on the specimens with the flush end plate (FEP-T) configuration. FEP-T-1 specimen employs a larger column section (SHS 150×150×10) and a thinner (6 mm) plate, whilst FEP-T-2 employs a thicker end plate (10 mm) but a thinner column section (SHS 150×150×6). Both specimens demonstrate a qualitatively similar overall response with a well-defined initially linear moment-rotation behaviour, followed by a rounded curve indicating a progressive loss of stiffness and a second linear branch until the termination of the tests.

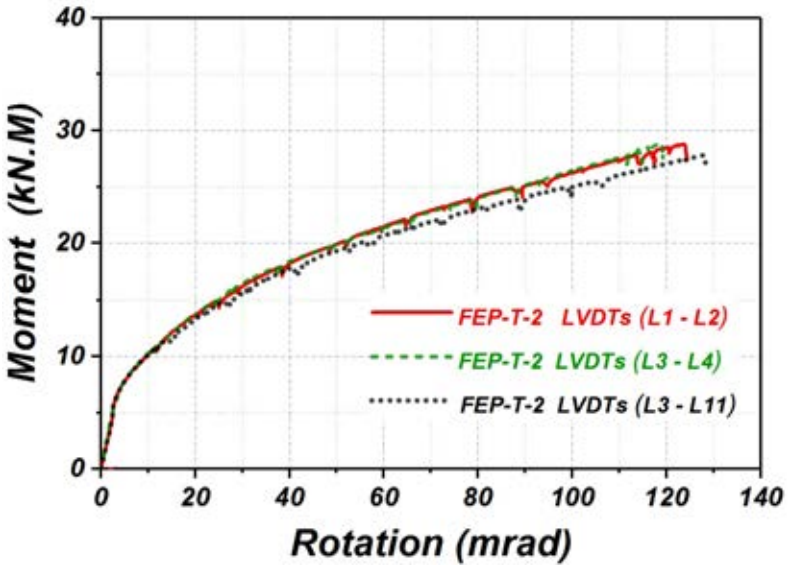

Figure 4.9 Moment rotation curves of FEP-T-2 based on different definitions of beam rotation Φ_b

The test was terminated at a rotation of 106.4 mrad and 119.2 mrad for the FEP-T-1 and FEP-T-2 specimens respectively. By comparing the response of the two specimens it can be observed that the FEP-T-1 specimen having a thicker column section displays a better retention of stiffness until approximately half of the maximum recorded load, whilst FEP-T-2 shows signs of loss of stiffness from about one third of its maximum recorded load.

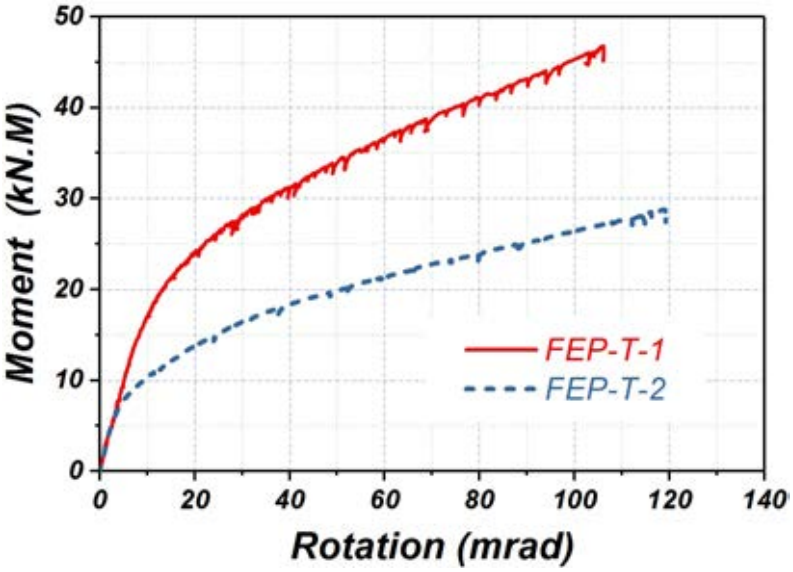

Figure 4.10 Moment-rotation response for FEP-T-1 and FEP-T-2 specimens

Figures 4.11a and 4.11b illustrate the observed deformation modes as recorded at the end of the test for both specimens. As intended, two distinct failure modes (i.e. modes of localization of plastic deformation) were obtained. Significant plastic deformation occurred in the thinner end plate of specimen FEP-T-1, whilst its much thicker column face remained virtually undeformed. As depicted in Figure 4.10(a), where a close-up of the end plate is also included, plastic bending of the end plate occurred primarily in the vicinity of the top bolt row where higher tensile stresses developed. On the contrary, the thicker (10 mm) end plate of specimen FEP-T-2 did not show signs of bending and remained undeformed as shown in Figure 4.11 (b), where the end plate rotates about the centre of rotation of the connection almost like a rigid body. Very limited plastic deformation was also observed in the vicinity of the bolt holes on the thinner column face. It can thus be deduced in the case of the FEP-T-2 specimen, plastic deformation was primarily located in the sleeves of the top row of the Hollo-bolts. No signs of plastic deformation were observed in either the compression zone or the shear panel of either of the joints.

Figure 4.12 illustrates the separation of the top of the end plate from the column face with increasing moment for specimen FEP-T-2, determined as the difference between the recordings of LVRTs L5 and L6. An initially linear response is followed by a region of progressive loss of stiffness, in agreement with the overall moment rotation response. Recording of the separation ceased at about 12 mm, as the LVDT ran out of stroke. Since the end plate rotated almost in a rigid-body like manner, the opening of the gap between the end plate and column face can be directly translated into the rotation of the whole joint.

Figures 4.13(a) and 4.13(b) depict the development of strains as rotation is increased for specimens FEP-T-1 and FEP-T-2 respectively. The location of the strain-gauges and their numbering have been reported in Figure 4.8 and the sign convention adopted in Chapter 3 is followed.

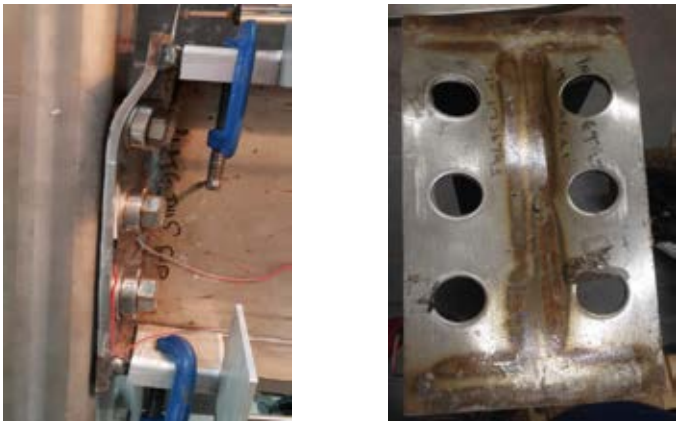

(a) FEP-T-1: plastic deformation of the end plate and closeup of the deformed end plate

(b) FEP-T-2: pull-out of top Hollo-bolts

Figure 4.11 Failure modes of FEP-T-1 and FEP-T-2 specimens

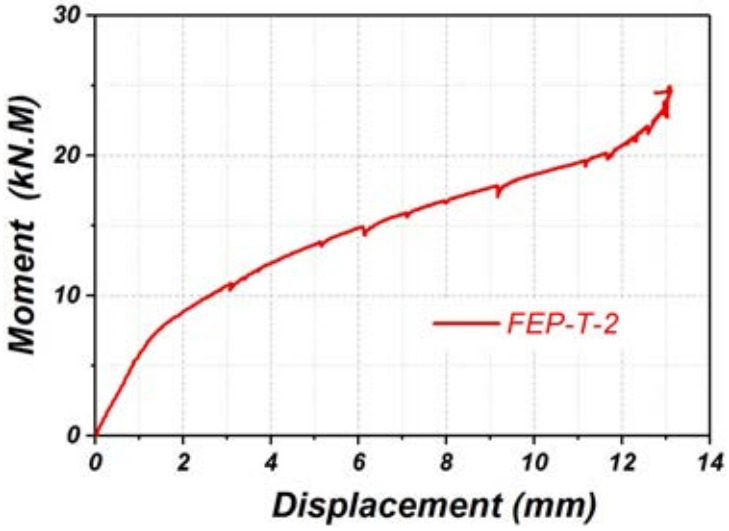

Figure 4.12 Moment vs gap opening between end plate and column face for FEP-T-2

Figure 4.13(a) reveals that high plastic tensile strains occur in locations 1, 2, 3 of specimen FEP-T-1 which were located the farthest from the centre of rotation of the joint and accord well with the deformation mode (i.e. bending) of the plate shown in Figure 4.11 (a). On the contrary, Figure 4.13 (b) reveals that only small strains developed in the end plate of specimen FEP-T-2. The small magnitude of the strains and the linear relationship between the strains and the applied rotation verify that the strains of the end plate in specimen FEP-T-2 were mostly elastic and that as observed in Figure 4.11(b) the end plate rotated as rigid body (i.e. remained virtually undeformed).

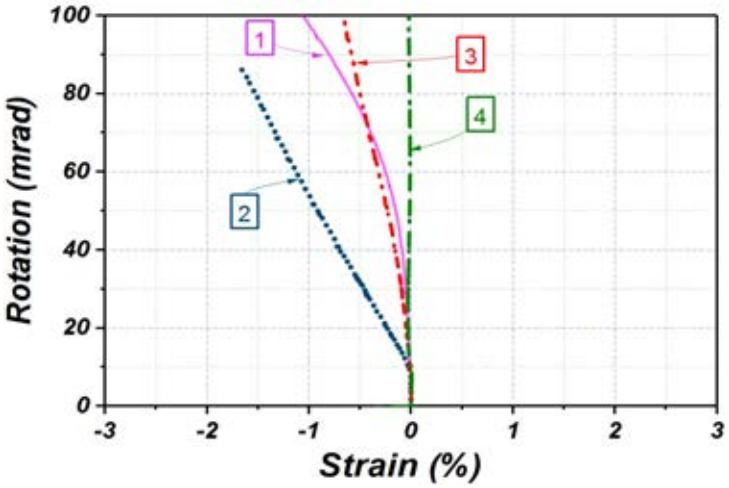

(a) Measured strains for FEP-T-1 specimen

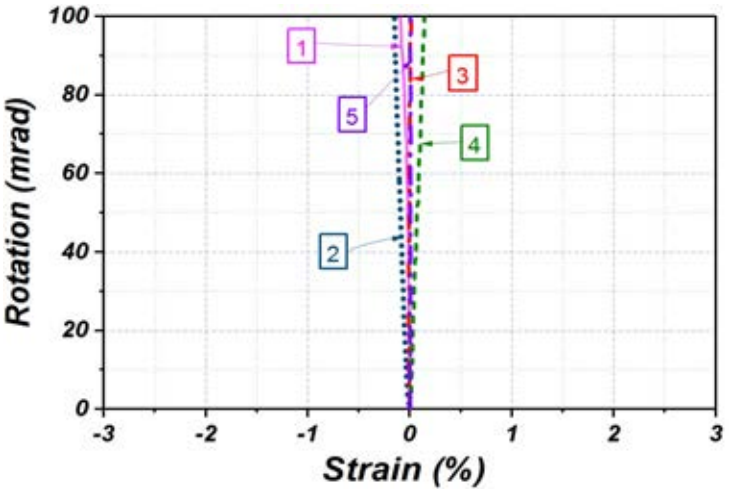

(b) Measured strains for FEP-T-2 specimen

Figure 4.13 Strain evolution with increasing rotation for FEP-T specimens

4.3.2 TSAC-T

Following the previous discussion on the FEP-T joint results, the results obtained for the TSAC-T specimens are discussed herein. Figure 4.14 depicts the recorded moment-rotation behaviour obtained from the tests on the TSAC-T-1 and TSAC-T-2 specimens. In agreement with the observations made in Chapter 3 for the TSAC-T-8 and TSAC-T-10 specimens, a non-linear response with increasing stiffness can be initially observed for both specimens, as the various gaps between the connected parts and the bolts and the bolt holes begin to close and then the initial elastic rotation stiffness is attained. The initially linear elastic response is followed by a gradual loss of stiffness indicated by the rounded part following the first linear branch of the moment-rotation curves. Thereafter a second linear branch follows as the increasing plastic deformations are accompanied by strain hardening of the plastically deformed regions of the joint. TSAC-T-1, which employs thinner angle cleats (8 mm) exhibits a hardening response following the second linear branch attributable to the progressive flattening of the thin top angle cleat, whereupon forces are transferred by tension rather than bending, hence the joint exhibiting a stiffer response. This observation accords with the response exhibited by specimen TSAC-T-8 as reported in Chapter 3. Specimen TSAC-T-2, which employs the thicker (10 mm) angle cleats, exhibits both higher strength and higher stiffness than the thinner TSAC-T-1 specimen.

Similar to the FEP-T specimens, the TSAC-T specimens were proportioned such that different failure modes would result. In Figure 4.15(a) and 4.15(b) the deformed shape of the TSAC-T-1 and TSAC-T-2 joints is depicted at the end of the tests. In Figure 4.15 (a) the deformed shape of specimen TSAC-O-8 is included for comparison purposes. High plastic deformations can be observed in the tension zone of both specimens, whilst in the compression zone of both specimens, the seat cleats are bent. However, the source of the plastic deformation is different in each specimen. It can be clearly seen that specimen TSAC-T-1, having a thicker column face than angle cleat, exhibited localization of plastic

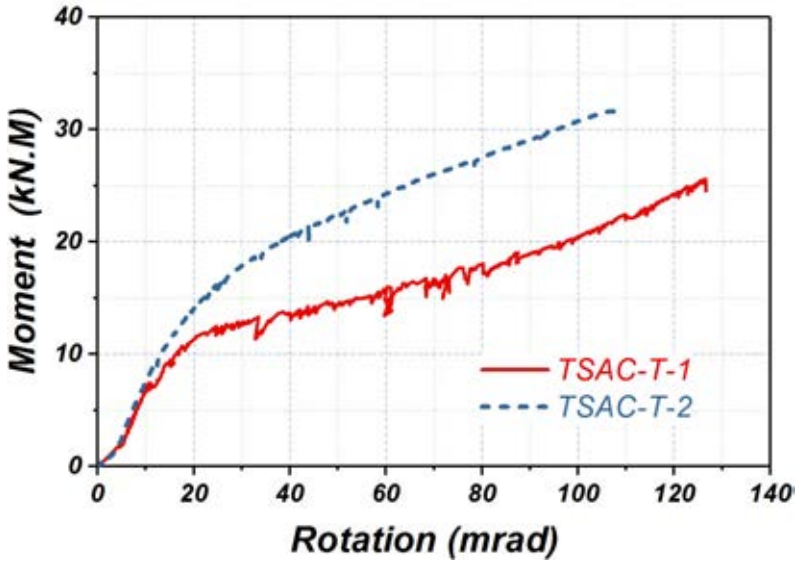

Figure 4.14 Moment-rotation response for TSAC-T specimens

deformation exclusively in the top angle cleat which bent significantly. Neither, the bolts connecting the top angle cleat to the column face, nor the column face itself show any evidence of plastic deformation and there is no separation between the top cleat and the column face near the connecting bolts. It is noteworthy that both the overall moment-rotation response and the deformation mode of specimen TSAC-T-1 are identical to the ones of specimen TSAC-O-8 reported in Chapter 3, since both specimens employed the same angle cleats, which were the critical components (i.e. weakest components) governing the joint response.

In the case of specimen TSAC-T-2, which employs thicker (10mm) angle cleats and a thinner column face (6 mm), plastic deformations occur not only at the top angle cleat but extend to the column face and the sleeve of the Hollo-bolt, as can be seen in Figure 4.15(b). This can be clearly observed in Figure 4.16(a), where a closeup of the tension zone of TSAC-2 as well as plastic bending of the column face in the vicinity of the top bolt row is depicted. This is due to the thicker and hence stiffer angle cleats attracting higher tensile stresses in the tension zone which lead to plastic deformation of the column face and Hollo-bolt sleeve and partial pull-out of the Hollo-bolt. The low tensile stresses

(a) TSAC-T-1 and TSAC-O-8: bending of top angle cleat

(b) TSAC-T-2: deformation of angle cleat, column face and sleeve Hollo-bolt

Figure 4.15 Failure modes of TSAC-T specimens

developing in the tension zone of specimen TSAC-1 do not suffice to cause pull-out of the Hollo-bolt, but cause indentations in the sleeve and some plastic deformation of the Hollo-bolt head, as observed in Figure 4.16(b). Both the Hollo-bolts and the column face are sufficiently stronger than the angle cleat to ensure that the vertical leg of the top cleat remains connected to the column face whilst it undergoes significant plastic bending, which allows further rotation of the joint.

Figure 4.17 illustrates the separation of the top of the end plate from the column face with increasing moment for specimen TSAC-2, determined as the difference between the recordings of LVRTs L5 and L6. The values recorded for the separation reflect the

(a) TSAC-2: plastic bending of the column face and partial pull-out of the Hollo-bolts in the tension zone

(b) TSAC-1: Hollo-bolt in the tension zone

Figure 4.16 Closeup of TSAC specimens

cumulative effect of both plastic bending of the column face and the pull-out of the bolts. No separation is observed until approximately 12 kNm, whereafter a rounded region indicating progressive loss of stiffness followed by a linear branch can be seen. Most of the separation recorded is due to plastic bending of the column face at the location of the bolt holes. The moment value of 12 kNm at which separation initiates for specimen TSAC-T-2 agrees well with the initiation of pronounced non-linear rotations of the joint as can be observed in Figure 4.14, indicating that plastic bending of the holes and Hollo-bolt sleeves contributes significantly to the plastic deformation of the whole joint.

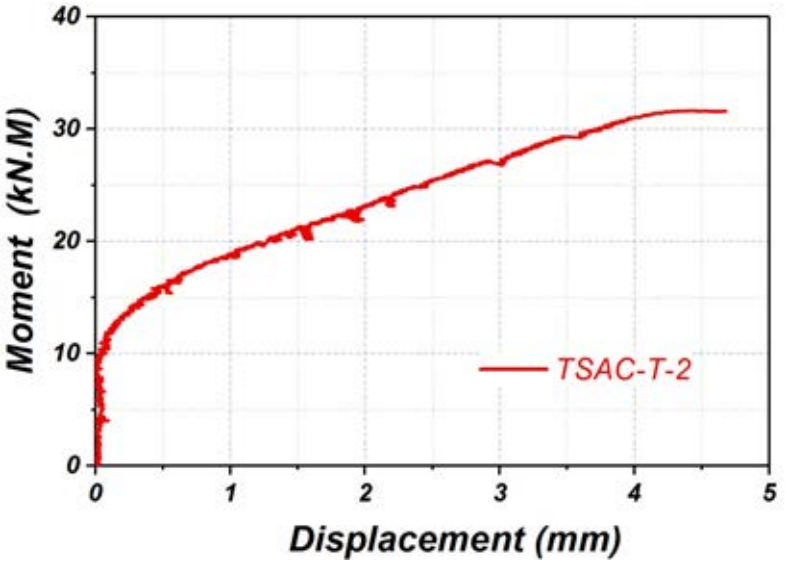

Figure 4.17 Moment vs gap opening between top cleat and column face for TSAC-T-2

In Figures 4.18(a) and 4.18(b) the development of strains in the top angle cleats connecting the tension flange of the beam to the flange of the column with increasing joint rotation is reported for specimens TSAC-T-1 and TSAC-T-2 respectively. The same sign convention as before is adopted. The evolution of strains is distinctly different for specimens TSAC-T-1 and TSAC-T-2, as the deformation modes of the angle cleats in each of the specimens are different. For both specimens high tensile strains on either side of the corner of the angle cleat (locations 2 and 3) can be observed, due to plastic bending (i.e. flattening) of the angle cleats. However, in the case of TSAC-T-1 the strains increase until the end of the test, whilst for specimen TSAC-T-2 the increase of strain in locations 2 and 3 stops at a rotation of about 60 mrad, indicating that at this rotation plastic deformations localized primarily in the bolt hole region of the column face and the bolts. A marked difference in the evolution of strains in location 4 can be observed. Since the vertical leg of the top angle cleat of TSAC-T-1 bents plastically, location 4 being on the concave side of the bent angle cleat experiences high inelastic compressive strains, whilst very small strains are recorded in the same location for specimen TSAC-T-2. Finally, very small deformations and strains are seen to develop between the bolt holes on the horizontal leg of the top angle cleat (location 1).

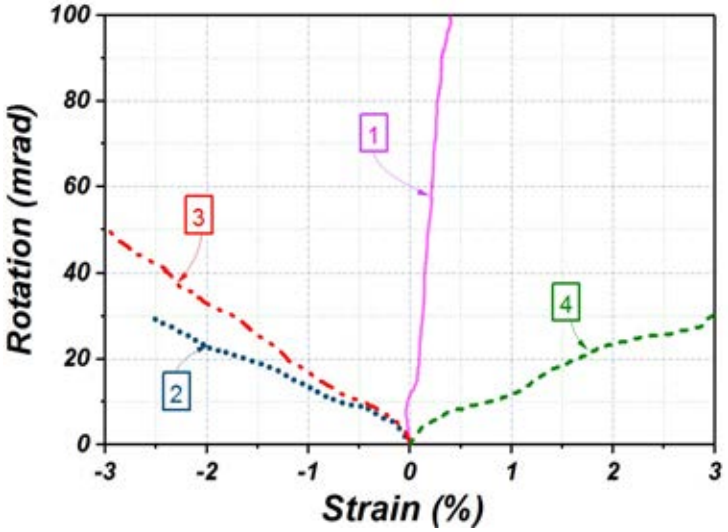

(a) Measured strains for TSAC-T-1 specimen

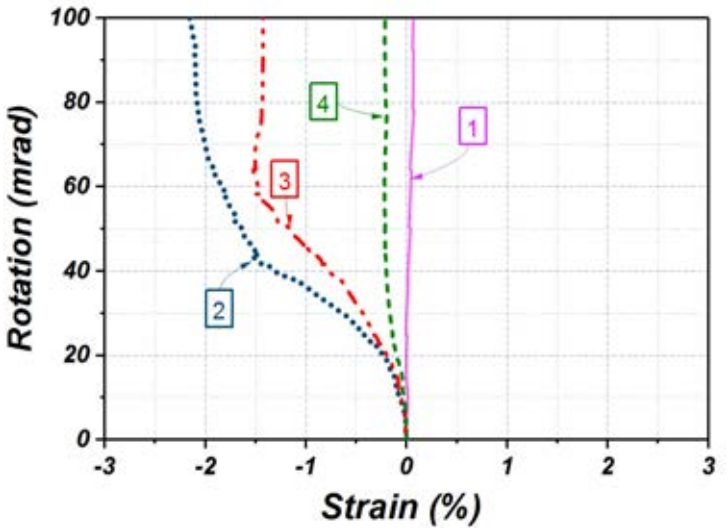

(b) Measured strains for TSAC-T-2 specimen

Figure 4.18 Strain evolution with increasing rotation for TSAC-T specimens

4.3.3 TSWAC-T

In Figure 4.19 the moment-rotation behaviour obtained from the tests on specimens TSWAC-T-1 and TSWAC-T-2 is reported. Like the TSAC-T specimens, the TSWAC-T specimens demonstrate an initially nonlinear response until all gaps between the connected parts (e.g. bolts and bolt holes) are closed. Due to the web cleats connecting the beam to the column via to additional bolt rows, the TSWAC-T specimens are seen to demonstrate superior rotational stiffness and strength compared to their TSAC-T counterparts, as

expected. Both specimens display similar overall response with the specimen employing the thicker column (TSWAC-T-1) having slightly higher stiffness but increasingly higher strength than TSWAC-T-2, as the second linear branch of the curves diverge.

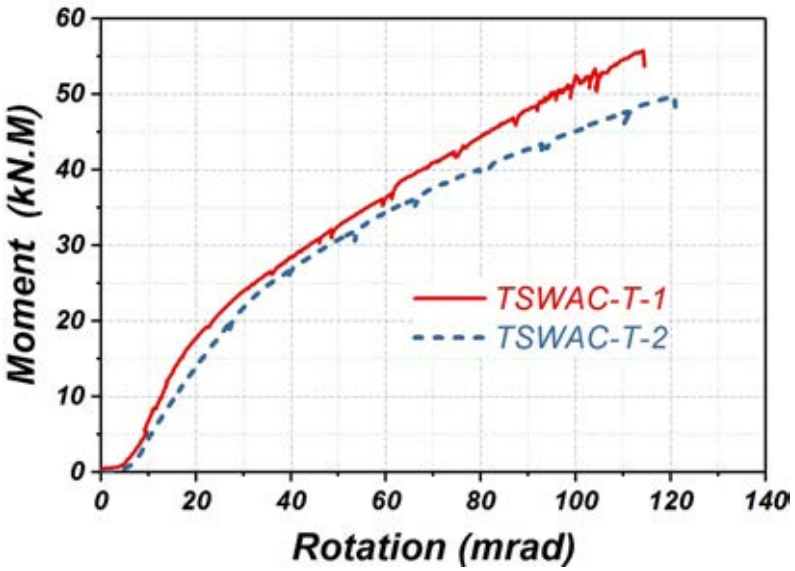

Figure 4.19 Moment-rotation response for TSWAC-T specimens

Figures 4.20(a) and 4.20(b) show the deformed configurations at the end of the tests for TSWAC-T-1 and TSWAC-T-2 respectively. Analogous observations to the ones made for the TSAC-T specimens can be made. In the case of TSWAC-T-1, due to the column face being significantly stronger and stiffer than the angle cleats, plastic deformation seems to be exclusively occurring in the top and web cleat with some bending of the seat cleat, with the remaining specimen appearing undeformed. Hence the response of specimen TSWAC-T-1 is governed by the top and web cleat, like the TSWAC-T-8 specimen reported in Chapter3. In specimen TSWAC-T-2 plastic deformations occur in the cleats, the column face and the Hollo-bolts, indicating that the joint response is the combined effect of all those components. The vertical leg of the top cleat of specimen TSWAC-T-1 shows clear signs of plastic bending at the location of the bolt row, whilst in specimen TSWAC-T-2 the tensile forces are high enough to trigger deformation of the column face and pull-out

of the bolt but not plastic bending of the much stiffer vertical leg of the top angle cleat.

(a) TSWAC-T-1: bending of top angle cleat and indentation of the sleeve of the Hollo-bolt

(b) TSWAC-T-2: deformation of angle cleats, column face and Hollo-bolts

Figure 4.20 Failure modes of TSWAC-T specimens

In Figure 4.21 the separation of the top of the end plate from the column face with increasing moment for specimen TSWAC-T-2 is shown. As before the separation is determined as the difference between the recordings of LVRTs L5 and L6 and the values recorded for the separation reflect the cumulative effect of both plastic bending of the column face and the pull-out of the bolts. No separation is observed until approximately 16 kNm, whereafter a rounded region indicating progressive loss of stiffness followed by a linear branch can be seen. Recording was terminated at 3.2 mm as the LVDT 6 ran out of stroke. Overall similar observations to the ones made for TSAC-T-2 can be made for

TSWAC-T-2. The higher moment at which the separation becomes noticeable is due to the contribution of the web cleats, which allow higher moments to be reached by the joint for the same level of tensile stresses in the top cleat.

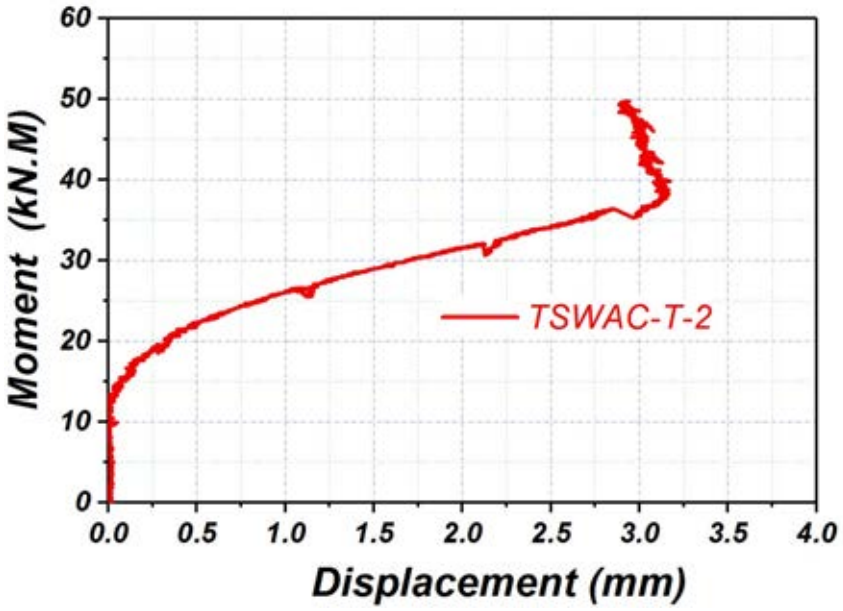

Figure 4.21 Moment vs gap opening between top cleat and column face for TSWAC-T-2

In Figures 4.22(a) and 4.22(b) the development of strains in the web cleats of the tension zone of the joint (top and web cleat) is depicted for TSWAC-T-1 and TSWAC-T-2 respectively. For both specimens, high tensile strains occur in locations 2, 3 due to bending of the top cleat with increasing rotations, whilst the strains in locations 1 and 5 are insignificant. Tensile strains are also recorded in the vicinity of the corner of the web cleat (locations 6 and 7), with specimen TSWAC-T-1 exhibiting higher strains than specimen TSWAC-T-2 in location 6, since the web cleat of TSWAC-T-1 deforms significantly more. As in the case of the TSAC-T specimens, a marked difference can be observed in the evolution of strains in location 4 for both specimens, with specimenTSWAC-T-1 experiencing high compressive strains due to bending of the vertical leg of the top cleat, whilst the strain in location 4 in specimen TSWAC-T-2 is very small. A similar trend is observed for the evolution of strains in location 8.

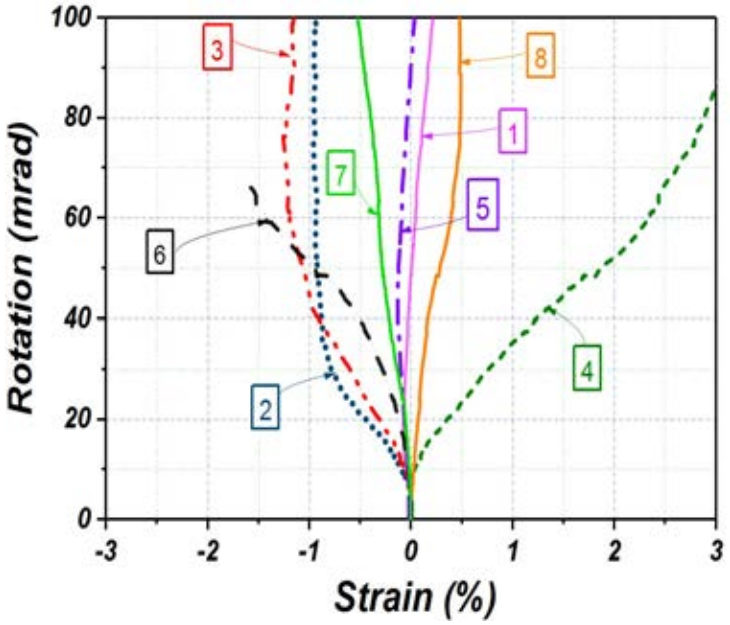

(a) (Measured strain for TSWAC-T-1 specimen

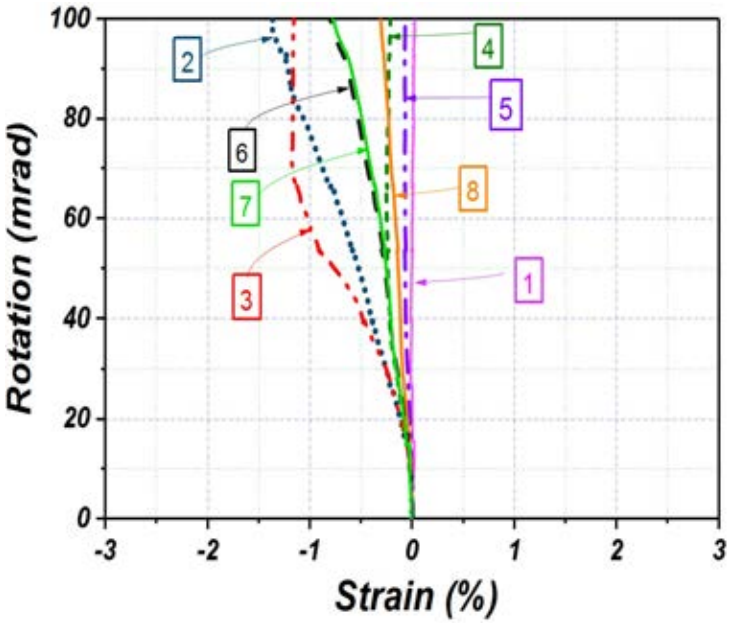

(b) Measured strain for TSWAC-T-2 specimen

Figure 4.22 Strain evolution with increasing rotation for TSWAC-T specimens

4.3.4 Key joint behaviour parameters

Table 4.3 reports a summary of key parameters pertinent to the connection response, which allows the behaviour exhibited by the tested connections to be quantified in terms of rotational stiffness and strength (plastic moment resistance), thus facilitating the

discussion and the comparison of the response of the tested joints with design predictions. The symbols used in Table 4.3 have been previously defined in Chapter 3, as have the assumptions regarding the determination of the initial rotational stiffness $S_{j,ini}$ the pseudo-plastic moment resistance $M_{j,R}$ and the reasoning for reporting $M_{j,30}$. For all specimens the maximum recorded moment $M_{j,max}$ has been reported, which is a lower bound for the actual ultimate moment that the joints could attain.

Table 4.3 Key parameters from test results

Specimen	Initial stiffness $S_{j,ini}$ (kNm/mrad)	Ultimate moment $M_{j,u}$ (kNm)	Moment at 30 mrad $M_{j,30}$ (kNm)	Plastic moment resistance $M_{j,R}$ (kNm)	Maximum recorded rotation Φ_c (mrad)
FEP-T-1	2100	46.9	26.2	27	106.4
FEP-T-2	1845	28.8	16.2	17	119.2
TSAC-T-1	712	26.0	12.7	12	126.5
TSAC-T-2	770	31.5	17.9	18	108.5
TSWAC-T-1	1421	56.7	23.1	21	114.4
TSWAC-T-2	1112	49.7	22.8	28	120.9

4.4 Comparison with analytical predictive models

After reporting the key results obtained from the experiments, design predictions for the initial rotational stiffness and strength originally developed for carbon steel joints are compared against the experimentally determined ones. Since the tests were not conducted to failure, no in-depth discussion regarding the rotation capacity can be made other than that all joint exhibited a rotation capacity far higher (more than 3 times higher) than the one stipulated for dissipative joints in structures classified as DCH according to EN 1993-1-8 (2005). A discussion on the observed failure modes is also included. As stated before the term “observed failure modes” is loosely used herein to indicate the prevailing deformation mode observed at the end of the test.

In all calculations the measured geometric and material properties are used for the joint components and all safety factors were set to unity. For specimens FEP-T-1 and TSAC-T-1 the behaviour of which is governed by bending of the end plates and angle cleats respectively, the design provisions codified in EN 1993-1-8 (2005) are used to predict the joint moment resistance, whilst for specimen TSWAC-T-1 the recommendations by Pucinotti (2001), which extend the scope of application of the EN 1993-1-8 (2005) are used as was done in Chapter 3. For specimens the response of which involves plastic bending of the column face, the design recommendations specified in SCI/BCSA (2005) have been utilized for the reasons discussed in Chapter 2.

4.4.1 Initial rotational stiffness

For the determination of initial rotational stiffness of the joints, the design equations specified in EN 1993-1-8 (2005) were used where applicable (i.e. for all components the design of which is covered by EN 1993-1-8 (2005)). The stiffness of the column face component in bending k_{cf} is determined according to Equation 4.1, which was proposed by Málaga-Chuquitaype and Elghazouli (2010) for the stiffness of the face of carbon steel SHS sections in bending.

$$k_{cf} = \frac{\pi E t_c^3}{12(1-\nu^2)0.18(\frac{b_c - t_c}{2})^2} \tag{4.1}$$

where E and ν are the Young's modulus and Poisson's ratio of the material of the column face, and b_c and t_c are the outer width and thickness of the column face respectively.

For the determination of the stiffness of the Hollo-bolts in tension the predictive model proposed by Wang et al. (2010) for Hollo-bolts has been used. The proposed

Table 4.4 Assessment of EC3 design predictions

Specimen	Initial stiffness $S_{j,ini}$ (kNm/mrad)			Moment Capacity Mj (kNm)		
	$S_{j,ini}$ (predicted)	$S_{j,ini}$ (Test)	Predicted /Test	$M_{j,R}$ (predicted)	$M_{j,R}$ (Test)	Predicted /Test
FEP-T-1	2241	2100	1.06	10	27	0.37
FEP-T-2	776	1845	0.42	7.4	17	0.44
TSAC-T-1	1500	712	2.10	6.6	12	0.55
TSAC-T-2	818	770	1.06	9.2	18	0.51
TSWAC-T-1	3161	1421	2.22	13.2	21	0.63
TSWAC-T-2	1376	1112	1.23	14.9	28	0.53
MEAN			1.35			0.50
COV			0.50			0.18

model accounts both for the axial elongation of the bolt shaft in tension according to the codified provisions and for the deformation of the flaring sleeves. Upon determination of the stiffness of all relevant components, Equation 4.2 is utilized to determine the initial rotational stiffness of the joints, where all symbols have been previously defined.

$$S_{j,ini} = \frac{Ez^2}{\sum_{i=1} \frac{1}{k_i}} \tag{4.2}$$

In Table 4.4 the predictions for the initial rotational stiffness according $S_{j,ini(pred)}$ for all tested specimens and the corresponding predicted over experimental ratios are reported. On average the predictions overestimatethe experimentally determined stiffness by 35% with a coefficient of variation of 0.50, thus indicating the inaccuracy of the stiffness predictions. Similar conclusions were reported in Chapter 3, where it was concluded that the observed discrepancies relate primarily to the inherent scatter in stiffness exhibited by bolted joints employing non-preloaded bolts, due to gaps and slips that initially occur between the connected components until contact between all connected members has been established.

4.4.2 Joint moment resistance

Using the provisions of EN 1993-1-8 (2005) and the measured $\sigma_{0.2}$ values in lieu of the yield stress of the joint components the pseudo-plastic moment resistance predictions $M_{j,R}$ determined and reported in Table 4.4 for all tested joints. As previously stated, the SCI/BCSA (2005) design equations were used for the determination of the capacity of the column face component in tension. The predicted-to-experimental ratio for the moment resistance is also reported and is on average 0.50 with a coefficient of variation 0.18. A similar level of conservatism of the EN 1993-1-8 (2005) design predictions was reported for stainless steel T-stubs in tension by Yuan et al. (2018) and for the stainless steel beam-to-column joints reported in Chapter 3, where the predicted-over-experimental resistance was 0.51 and 0.53 respectively with a coefficient of variation of 0.13 in both cases.

4.4.3 Observed failure modes

In Table 4.5 the failure modes determined according to the EN 1993-1-8 (2005) provisions are reported together with the ones observed during the tests at the maximum recorded load. In all cases the predicted failure modes, which were determined as the modes corresponding to the resistance of the weakest joint component agree well with the ones observed at the end of the test. The failure modes involved bending of an angle cleat or end plate for specimens employing a thicker column section (specimens 1) and plasticisation of the column face and or pull-out of the most highly stressed Hollo-bolts for specimens designed to precipitate bending of the column face (specimens 2), thus indicating the importance of the proportioning of the joint components for the overall response. Where mode 1 is mentioned, it refers to the deformation mode of the equivalent T-stub in tension, a matter discussed in Chapter 6.

Table 4.5 Failure modes and overstrength

Specimen	Predicted failure mode	Observed deformation mode at the end of the test	$M_{j,max}/M_{j,R}$
FEP-T-1	End plate in bending / Mode 1	End plate in bending / Mode 1	1.79
FEP-T-2	Bending of column face	Deformation/partial pull-out of Hollo-bolts	1.78
TSAC-T-1	Bending of flange cleat/Mode1	Bending of flange cleat/Mode1	2.05
TSAC-T-2	Bending of column face	Bending of column face/partial pull-out of Hollo-bolts	1.76
TSWAC-T-1	Bending of flange/Mode 1-bending of web cleat /Mode 1	Bending of flange/Mode 1-bending of web cleat /Mode 1	2.45
TSWAC-T-2	Bending of column face	Bending of column face/partial pull-out-of Hollo-bolts	2.18

In addition to the joint rotation at failure, the ratio of the maximum recorded moment resistance $M_{j,max}$ over the plastic moment resistance $M_{j,R}$, (i.e. overstrength) can be considered another quantifiable measure of ductility and is reported in Table 4.5. It can be seen that this ratio ranges from 1.76 for specimen TSAC-T-2 to 2.45 for specimen TSWAC-T-1. As previously stated, the recorded maximum moments are not the maximum achievable moments by the tested joints but a conservative lower bound. Nonetheless on average the tested specimens exhibited a recorded maximum moment twice their plastic moment resistance with a coefficient of variation of 0.14. The consistently high overstrength values together with achieved rotations in excess of 105 mrad indicate the inherent ductility of the tested stainless steel joints. Similar to the observations reported in Chapter 3, no weld fracture or crack initiation in any part of the beam, column, end plates or angle cleats was observed in any of the tests reported in this Chapter. The achieved high inelastic deformations in conjunction with the pronounced strain-hardening characteristics of austenitic stainless steels have led to an overall ductile response and significant overstrength in all tested reported in Chapters 3 and 4.

4.5 Conclusions

In this chapter six full-scale beam-to-tubular column connections employing the FEP-T, TSAC-T and TSWAC-T configurations have been reported in detail. These configurations are representative of common joint typologies employed in practice for blind bolted connections in carbon steel. The recorded moment-rotation curves, evolution of strains with increasing rotation and observed failure modes have been discussed. In all cases the joints exhibited significant inelastic deformations with recorded rotations in excess of 105 mrad, far beyond the limit of 35 mrad required for dissipative joints in structures classified as DCH (ductility class high). The achieved rotations are deemed sufficient to obtain both the initial rotational stiffness and the joint moment resistance $M_{j,R}$, whilst the rotation capacity recorded is clearly a lower bound of the available rotation capacity of the joint.

In absence of codified design recommendations for either carbon steel or stainless steel blind bolted connections, the experimentally determined initial rotational stiffness and moment resistance of the joints has been compared against the design recommendations by Elghazouli et al. (2009) for stiffness and the SCI/BCSA (2006) for the strength of the column face in bending. Both these approaches were originally developed for carbon steel joints. In all cases the predicted joint moment resistance was significantly underestimated, whilst the stiffness predictions were inaccurate. For specimens where and end plates or angle cleats were designed to be the weaker joint components (FEP-T-1, TSAC-T-1, TSWAC-T-1), almost identical conclusions to the ones reported in Chapter 3 were reached, whilst in cases where localized plastic deformations occurred at the column face, the SCI/BCSA predictions were even more conservative.

It is noteworthy that the six tests reported herein are the first to ever be conducted on stainless steel blind-bolted beam-to-column joints and as such are expected to be extensively utilized by other researchers. A FE model is developed and validated against these test data in Chapter 5, thus allowing additional structural performance data to be

generated and the response of stainless steel blind-bolted joints to be investigated on the basis of a larger pool of data.

Chapter 5

Numerical modelling and parametric studies of stainless steel beam-to-column joints

5.1 Introduction

In the third and fourth chapters twelve full scale tests on single-sided stainless steel beam-to-column joints employing both hollow and open columns have been reported in detail. Full details of the tests including general setup and instrumentation, overall moment-rotation response, initial stiffness, moment resistance, failure modes and material response of the joint components have been disclosed. Based on the obtained results, the design provisions of EN 1993-1-8 (2005), which are assumed to be applicable for both carbon steel and stainless steel (EN 1993-1-4+A1,2015), were found to consistently underestimate the plastic moment resistance and overestimate the joint initial rotational stiffness and wrongly predict the failure mode (Elflah, et al., 2018 a). Similar observations were made for the design models proposed by SCI/BCSA (2005) and Elghazouli et al. (2010) for the prediction of the strength and stiffness of beam-to-tubular column joints respectively .

This Chapter augments the experimental work reported in Chapters 3 and 4 and reports numerical studies on the response of single-sided stainless steel beam-to-column joints under monotonic loads. The part of this Chapter concerning beam-to-open column joints has been submitted and recently accepted for publication by the Journal of Constructional Steel Research (Elflah, et al., 2018 a) and much of the wording used in the journal submission is repeated herein. Due to the procedure for modelling conventional and blind-bolted connections being essentially identical, it was decided to describe the FE studies on both in one Chapter, hence avoiding unnecessary repetitions.

Initially the development of the FE models is reported followed by the discussion on the model validation. Upon validation, in terms of the FE model to numerically replicate the experimentally obtained initial stiffness, moment resistance, failure modes and overall moment-rotation response, the FE models were used to conduct parametric studies on joint typologies similar to the ones adopted in the experimental part of the research, namely flush end plate (FEP), extended end plate (EEP), top and seat angle cleat (TSAC) and top, seat and web angle cleat (TSWAC) (Elflah, et al., 2018 a). In the nomenclature and symbols used herein, the letter "O" refers to beam-to-open column joints and the letter "T" refers to beam-to-tubular column joints (i.e. blind bolted joints). Hence, a model designated as TSAC-T, refers to top and seat angle cleat joint between a beam and a tubular column, whilst TSAC-O employs the top and seat angle cleat configuration for a connection of a beam to an open section column. The investigated parameters included bolt end and edge distances, angle cleat and end plate thickness, column flange thickness and material grade of the connected members. A total of 228 parametric studies have been performed thus providing a comprehensive database of validated FE results on the response of stainless steel joints over a wide range of structural configurations likely to be employed in practice resulting in a variety of failure modes. The generated numerical data are used to assess the applicability of the currently available design models and to develop novel design recommendations, as discussed in Chapter 6 (Elflah, et al., 2018 a).

5.2 Development of FE models

Three dimensional finite element models were developed using the general purpose FE software ABAQUS (2013). Initially the development of the models for the beam-to-open column joints is reported in detail, followed by the description of the model for the beam-to-tubular column joints. In all cases the measured geometry and material properties reported in Chapters 3 and 4 have been utilized. Since there are many similarities in the modelling of both open and tubular joints, a detailed discussion of a modelling assumption or procedure is provided only when encountered for the first time.

5.2.1 Beam-to-open column joints

The components of the connections that were explicitly simulated include the connected beam and column, the bolts, the end plate and the angle cleats. The welds between the beams and the end plates were not explicitly modelled, since their response is rigid (i.e. welds can be assumed to have infinite stiffness) and no weld failure occurred during testing. Instead, a tie constrain was defined to tie the degrees of freedom of the nodes of adjacent surfaces that were welded thus preventing separation and overlapping of the respective elements.

The geometry of the simulated joints, against which the models were validated are shown in Figure 5.1, where the symbols adopted in the parametric study reported in this Chapter are also defined. The values of the geometric dimensions defined in Figure 5.1 are given in Table 5.1 for the tested beam-to-open column specimens (Elflah, et al., 2018 a).

To reduce computational cost, the threaded geometry of the bolt shank was simplified in the simulations as a prismatic cross-section (i.e. smooth cylindrical surface) with a diameter such that the area of the modelled bolts equals the stress area of the real bolts, whilst the bolt heads and nuts were modelled as cylindrical instead of hexagonal discs.

Table 5.1 Key geometric parameters of simulated beam-to-open column joints (Elflah et al., 2018a)

Designation	Connection type	Symbols defined in Figure.5.1 (mm)								
		t_c	t_p	t_a	p_1	p_2	e_1	e_2	L_1	L_2
FEP-O	Flush end plate	12	8	-	65	65	25	-	-	-
EEP-O	Extended end plate connection	12	8	-	110	100	25	-	-	-
TSAC-O-8	Top and seat angle cleat	12	-	8	0	0	35	-	100	-
TSAC-O-10	Top and seat angle cleat	12	-	10	0	0	25	-	100	-
TSWAC-O-8	Top, seat and web angle cleat	12	-	8	0	0	35	25	100	55
TSWAC-O-10	Top, seat and web angle cleat	12	-	10	0	0	25	25	100	60

Modelling the bolt shank as prismatic and accounting for the difference between the effective area of the threaded bolt shank has been shown to yield good results in similar studies (Swanson et al., 2002 ; Bursi and Jaspart, 1998; Xu, 2000 ;Girao et al, 2006) and does not compromise the accuracy of the results, unless the bolt fails by thread stripping, a failure mode not encountered in the tests. Furthermore, the bolt head, bolt nut and washers were simplified as cylinders and were tied to the bolt shank in accordance with similar studies when simulating bolts (Swanson et al., 2002; Wang et al., 2010; Liu et al., 2012a; Liu et al., 2012b; Tizani et al., 2013; Massimo et al., 2014). No bolt preload was applied, given that in the tests the bolts were hand-tightened to obtain the snug-tight condition.

The boundary conditions employed in the FE models simulated the ones applied in the experimental study. Hence all degrees of freedom of the bottom end cross-section of the column were restrained, whilst the horizontal translation of the top end of the column in the plane of loading was also restrained. The loaded end of the beam was loaded by incrementally applying a downward displacement, whilst out of plane translations were restrained at the point of load application (Elflah, et al., 2018 a).

All modelled components were discretized with the eight-noded (hexaedron) 3D solid first-order reduced integration element C3D8R, as this element type was successfully

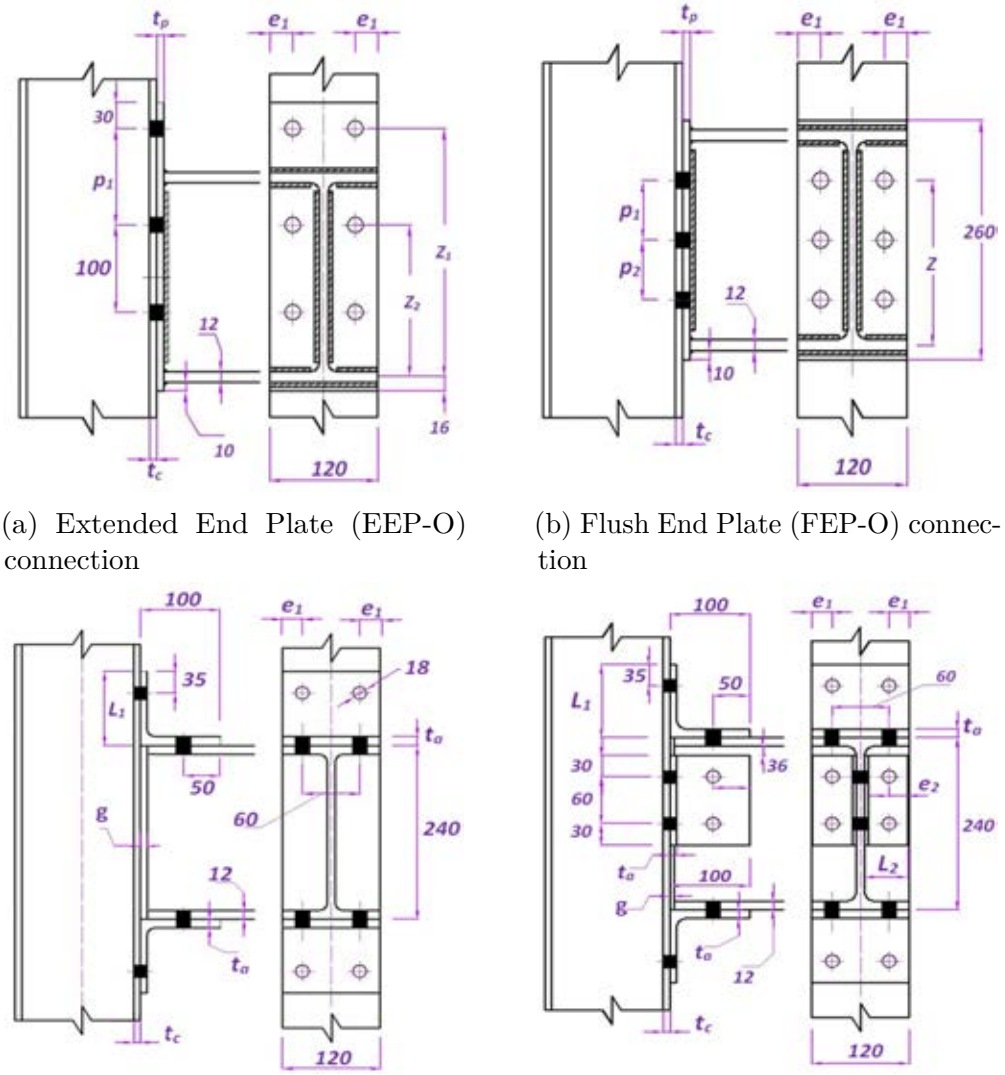

Figure 5.1 Geometric configuration of simulated beam-to-open column joints (Elflah et al., 2018a)

employed in similar previous studies (Swanson et al., 2002; Liu et al., 2012a; Liu et al., 2012b; Massimo et al., 2014). Several mesh densities were tried, and a structured mesh was employed with varying mesh density in the different parts of the model as shown below in sensitivity study. The components of the connection subjected to sharp stress gradients, such as the end plates, angle cleats and bolts, as well as the parts of the beam and the column in the vicinity of the bolt holes were discretised with a finer mesh, whilst a coarser mesh was used for the discretisation of parts of the beam and the column far from

the joint region, the response of which was predominantly elastic. At least three elements were provided through the thickness of thin-walled components such as end plates, angle cleats, flanges and webs to accurately capture their out-of-plane flexure and avoid the effect of shear locking. A minimum of 2 element has been recommended by Massimo et al. (2014) and Hongxia et al. (2008). The employed mesh density is depicted in Section 5.3 of this Chapter, where the numerically obtained failure modes are compared to the experimental ones .

Models with more refined meshes usually give more accurate results but consume more computation time. A sensitivity study has been carried out to choose an optimal mesh. Specimen FEP-O was simulated and two models were built up with different mesh sizes. Meshes for the Column, beam, endplate, the bolts and nuts were changed to investigate the effects of mesh sizes on connection behaviour. Figure 5.2 compares the two meshes. In the fine mesh (Case 1), the mesh size is approximately 4 mm for bolts and endplate and 20 mm for beam and column and 6mm within the refine region. While the typical element size in the coarse mesh (Case 2) is approximately 8 mm for bolts and endplate and 40 mm for beam and column and Table 5.2 compares the number of elements for each structural component and computation time. The moment- rotation curves for the two mesh sizes are compared in Figure 5.3. The differences between these using these two mesh sizes are relatively major and fine mesh provides a good agreement with experimental results. In order to get good results, the finer case will be adopted.

Table 5.2 Comparison of the number of elements used and computation time

component	Fine mesh (Case 1)	Coarse Mesh (Case 2)
Endplate	9560	1040
Bolt	784	256
Beam	8056	585
Column	14228	1936
Total of element	32826	3817
Computation time (min)	171 min	27 min

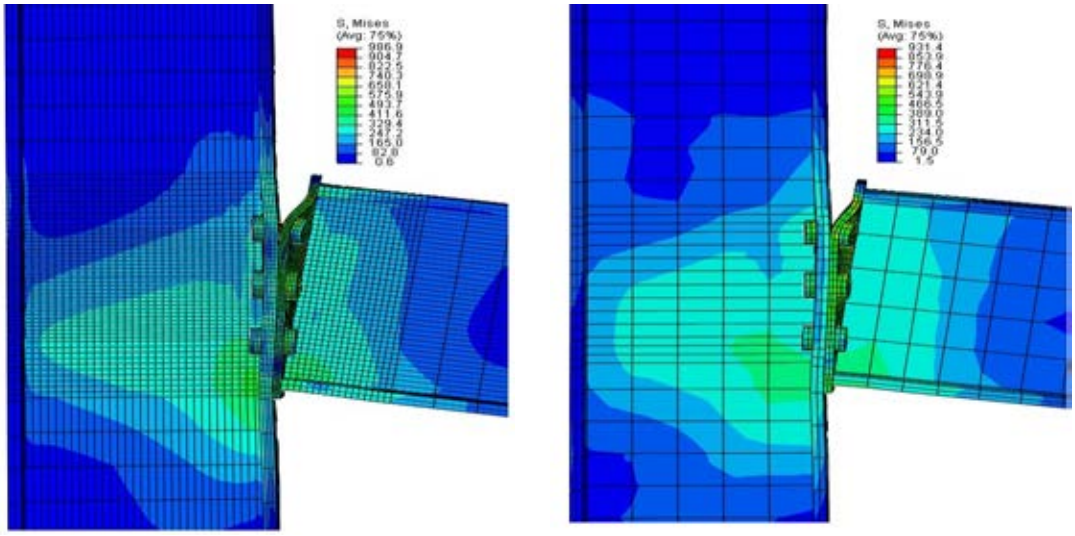

(a) FEP-O: Fine mesh (Case 1) (b) FEP-O: Coarse Mesh (Case 2)

Figure 5.2 Failure modes of FEP-O joints using two mesh sizes (Stress is Von-Mises (MPa))

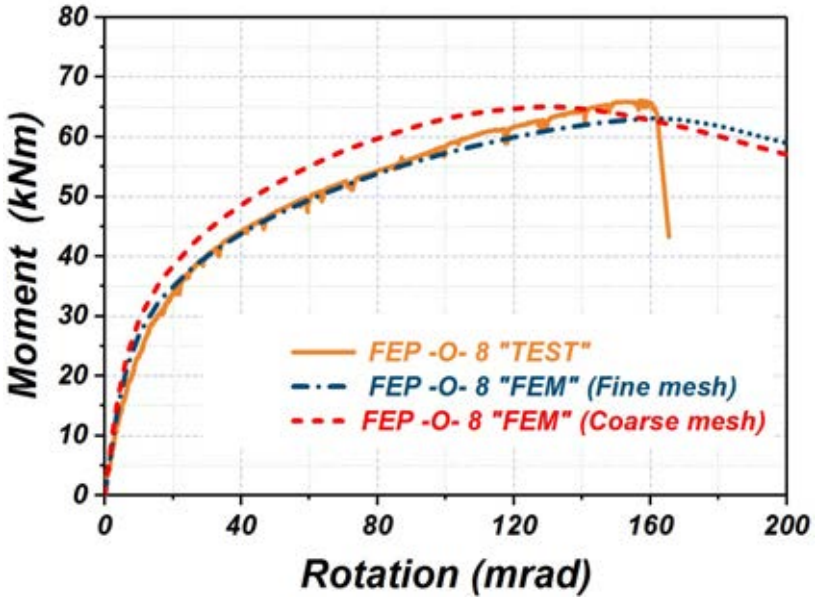

Figure 5.3 Experimental and numerical moment-rotation response using two mesh sizes for FEP-O

The contact between the various non-welded components of each joint was modelled by using the "surface to surface" contact algorithm available in ABAQUS. Surfaces discretized with course meshes were selected as master surfaces, whilst the more finely discretized surfaces were selected for salve surfaces (Liu, 2012; Xu, 2000). The contact pressure-clearance relationship was defined as "hard contact" for all cases to allow full transfer of

the compression loads and separation after contact. The penalty method with a friction coefficient of 0.3 was defined for the tangential response of all contact surfaces. This value for the friction coefficient has been employed by Wang and Wang (2016) and is within the range of usually adopted values 0.20-0.33 (Swanson et al., 2002; Liu et al., 2012a; Liu et al., 2012b; Massimo et al., 2014). Small sliding contact formulation was used at the interface between angle cleats and bolt heads, end plates and bolt heads and the seat angle cleat and the column/beam flange (Liu, 2012 ; Xu, 2000). Finite sliding contact formulation was employed for all other contact pairs (e.g. bolt shank and clearance hole), thus allowing for large slip (Elflah, et al., 2018 a).

Material nonlinearity was considered using the von Mises yield criterion coupled with isotropic hardening; hence the yield surface was assumed to expand uniformly in the stress space with increasing plastic strains. The Young's modulus values characterising the elastic material response and the stress-strain values used to define the plasticity model were derived from the experimental tests reported in Table 3-2. Since large plastic strains developed in all joints, analytical material modelling capable of approximating the material response throughout the full strain range was required (Elflah, et al., 2018 a). To this end the two-stage Ramberg-Osgood material model (Mirambell and Real, 2000; Rasmussen, 2003) was adopted. This model adopts the original Ramberg-Osgood model for stresses lower than the 0.2% proof stress and employs a similar curve thereafter until the ultimate tensile stress. The two-stage Ramberg-Osgood model was chosen over its three-stage variant (Quach et al., 2008), because it is adopted by EN1993-1-4 (2015) and is much simpler in formulation. The relevant material parameters for the analytical approximation of the material response as determined from tensile coupon testing are reported in Table 5.3, where the plastic strain at fracture is also reported and n and m are strain-hardening exponents used in the two-stage Ramberg-Osgood model. The stress and strain values obtained through analytical modelling were converted into the true

stress and logarithmic plastic strain format as required by ABAQUS (Elflah, et al., 2018 a).

Table 5.3 Material parameters adopted in FE modelling (Based on the tensile test)

Specimen	E (N/mm²)	$\sigma_{0.2}$ (N/mm²)	σ_u (N/mm²)	n	m	ε_f (%)
I-240×120×12×10 - flange	196500	248	630	5.20	2.37	66
I-240×120×12×10 - web	205700	263	651	6.70	2.41	65
Angle cleat (8 mm)	197600	280	654	12.22	2.49	55
Angle cleat (10 mm)	192800	289	656	10.62	2.54	56
End plate (6 mm)	201000	289	658	12.20	2.53	62
End plate (10 mm)	195000	276	636	11.05	2.51	51
SHS 150×150×6 - flat	189650	334	640	8.03	2.80	63
SHS 150×150×6 - corner	210420	647	795	11.00	3.83	46
SHS 150×150×10 - flat	200020	507	730	8.40	3.43	51
SHS 150×150×10 - corner	198000	608	796	4.93	3.67	47
M16 bolt (A-80)	191500	617	805	17.24	3.68	12
Sleeve of blind bolt (4 mm)	180000	381	735	5.50	2.81	32

Where E is the elastic modulus , $\sigma_{0.2}$ is 0.2% proof stress , σ_u is Ultimate tensile stress, n is Ramberg-Osgood strain hardening exponent , m is the strain-hardening coefficient and ε_f is the plastic strain at fracture

Bolt fracture occurred during testing and ultimately triggered the failure of the joints, hence failure of the bolts has to be accounted for in the numerical models. In ABAQUS, material fracture and failure can be explicitly defined for metals by defining appropriate damage initiation and damage evolution criteria, which simulates the ductile fracture of metals via void nucleation and growth (ABAQUS, 2013). However, in the absence of relevant material parameters a simplified approach was followed, according to which fracture of the components was not explicitly modelled but was indirectly defined based on the uniaxial plastic strain at fracture ε_f, which is reported in Table 5.3 for all components comprising the tested joints. Hence bolts were assumed to fail when their equivalent plastic strain obtained from the analysis reached the respective plastic strain at fracture ε_f given in Table 5.3 throughout all integration points in any given element discretising the bolt shank Geometric configuration of simulated beam-to-open column joints (Elflah et al.,

2018a). A similar approach of indirectly defining fracture via a critical strain value was successfully followed by Salih et al. (2010), where the net section failure of stainless steel bolted connections was simulated and failure was assumed when ε_f was reached, and Girao Coelho et al. (2006), who assumed that cracking occurs when the ultimate strain ε_u is reached. In this study the strain at fracture ε_f was selected over the ultimate strain ε_u as a failure criterion since it gave better results. It should be noted that in cases where the bolts were primarily loaded in tension or tension and shear, strain localisation (i.e. necking) occurred during the analysis prior to reaching the equivalent plastic strain of the bolts. Similar observations regarding the ability of FE models to reproduce ultimate deformation patterns of steel in tension based on geometric instabilities alone (i.e. without utilising material instability approaches) have previously been made for steel tensile specimens by Okazawa et al. (2002) (Elflah, et al., 2018 a).

The complex contact conditions between the various interacting parts comprising each joint led in some cases to convergence difficulties. In cases where ABAQUS/STANDARD could not converge, convergence difficulties were overcome by employing a quasi-static explicit dynamic analysis procedure using the ABAQUS/EXPLICIT solver (ABAQUS, 2013), which is well suited for highly nonlinear problems. Explicit dynamic analysis usually requires the execution of tens of thousands of computationally inexpensive increments, during which the solution is propagated form the previous step, thus avoiding convergence issues. Mass scaling was utilized to reduce computational time, whilst quasi-static response was achieved by specifying a slow displacement rate and checking that the kinetic energy was smaller than 2% of the internal energy for the greatest part of the analysis, thus ensuring that inertia effects were insignificant (ABAQUS, 2013).

5.2.2 Beam-to-tubular column joints

All modelling assumptions regarding element types, material modelling, modelling of contact, boundary conditions and analysis procedures previously reported for the simulations of the beam-to-open column joints are valid for the beam-to-tubular column joints.

There are some differences however relating to geometric modelling of the Hollo-bolts and including the effect of bolt preload. Furthermore, since flat and corner coupons extracted from the same tubular section were shown to have different material properties, material modelling of the tubular columns is also not straightforward. Following past studies on the response of stainless steel members (Gardner and Nethercot, 2004; Ashraf et al., 2006), the material properties of corner regions were assumed to extend up to 2 times the thickness into the flat region of the tubular column faces. The geometry of the modelled joints, against which the models were validated are shown in Figure 5.4, where the symbols adopted in the parametric study reported in this Chapter are also defined. The values of the geometric dimensions defined in Figure 5.4 are given in Table 5.4 for the tested beam-to-tubular column specimens and have been previously defined in Figure 4.1 .

Table 5.4 Key geometric parameters of simulated beam-to-tubular column joints

Designation	Connection type	Symbols defined in Figure.5.4 (mm)								
		t_c	t_p	t_a	p_1	p_2	e_1	e_2	L_1	L_2
FEP-T-1	Flush end plate	10	6	-	65	65	30	-	-	-
FEP-T-2	Flush end plate	6	10	-	65	65	30	-	-	-
TSAC-T-1	Top and seat angle cleat	10	-	8	0	0	30	-	100	-
TSAC-T-2	Top and seat angle cleat	6	-	10	0	0	30	-	75	-
TSWAC-T-1	Top, seat and web angle cleat	10	-	8	0	0	30	35	100	70
TSWAC-T-2	Top, seat and web angle cleat	6	-	10	0	0	30	35	100	70

All conventional metric bolts were simulated as previously described. Given the complex geometry of the Hollo-bolt and the various interacting part it comprises, a pragmatic approach was followed and the geometry of the various parts was simplified without compromising accuracy. The bolt shank was assumed to be prismatic, whilst a smooth geometry was assumed for the sleeve and the cone as well. The geometric idealization of the various components of the Hollo-bolt is shown in Figure 5.5, where the FE discretization of each component and the assembled bolt is also depicted. It can be clearly seen that a fine mesh was employed in the discretization of all components to capture the expected sharp stress gradients. Contact between the Hollo-bolt components was assumed

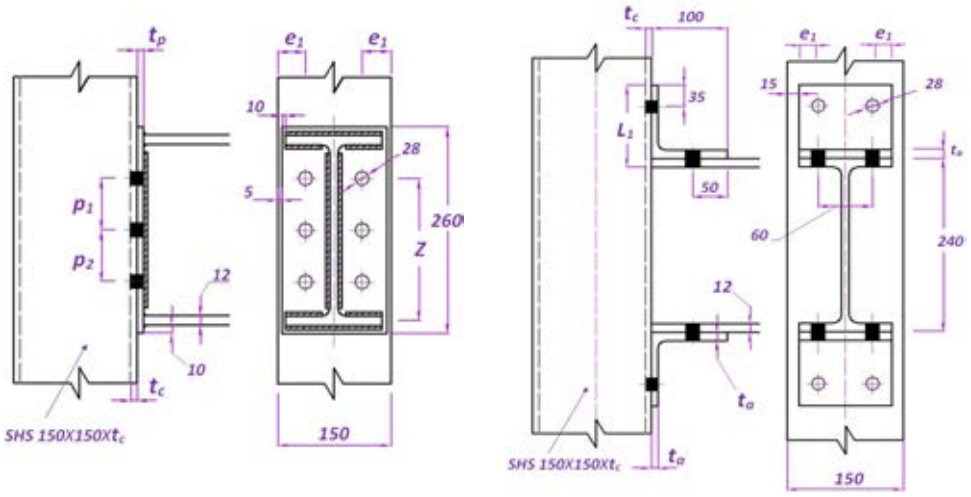

(a) Flush End Plate (FEP-T) connection

(b) Top and Seat Angle Cleat connection (TSAC-T)

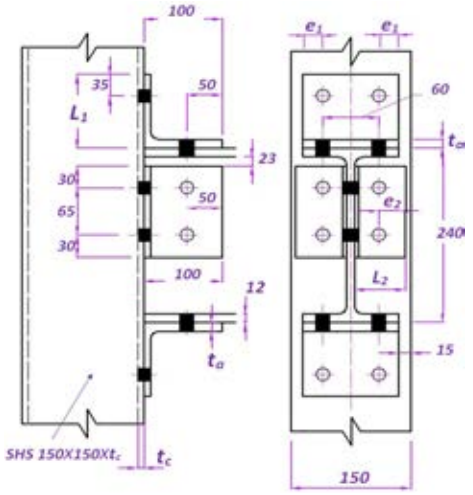

(c) Top, Seat and Web Cleat (TSWAC-T) connection

Figure 5.4 Geometric configuration of simulated beam-to-tubular column joints

and the penalty method with a friction coefficient of 0.3 was defined for the tangential response of all contact surfaces. Small sliding contact formulation was assumed at the interface between the sleeve and the cone and the sleeve and the bolt shank, since no sliding is expected or has been observed between the various parts of the Hollo-bolt. The external surface of the bolt and the internal surface of the cone were tied together via a tie constrain to simulate the clamping effect that the presence of the threads would have had and prevent any relative deformation between the cone and the shank on which it is screwed.

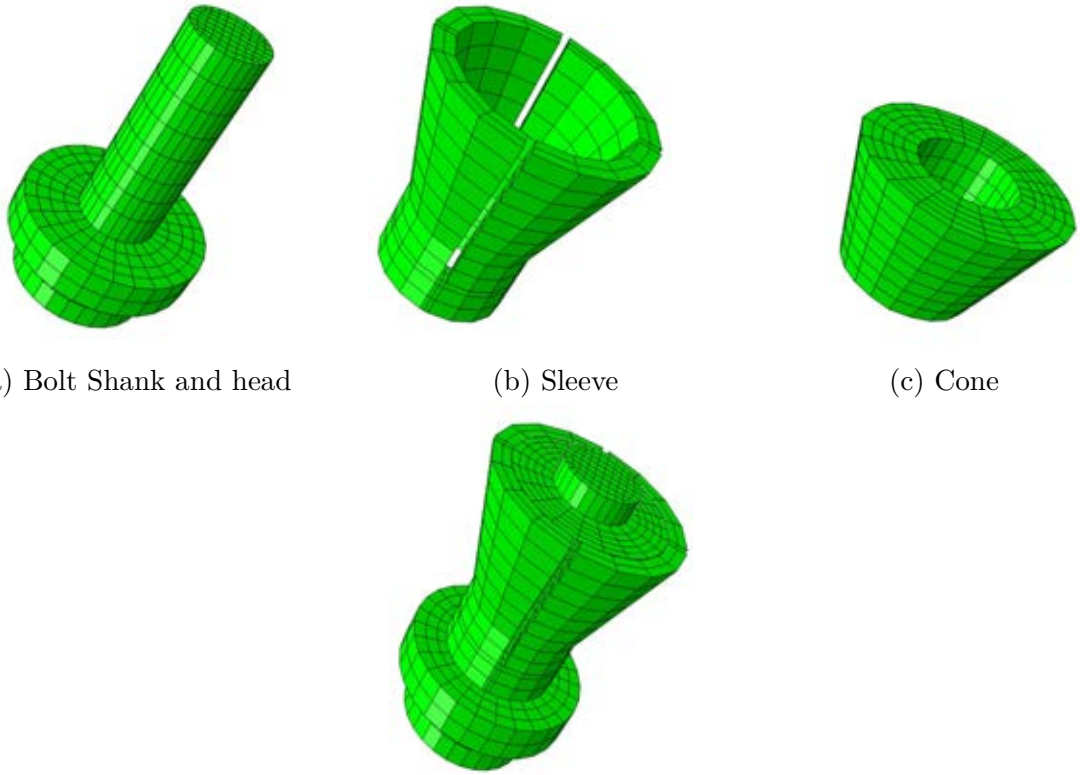

(a) Bolt Shank and head (b) Sleeve (c) Cone

(d) Assembled Hollo-bolt

Figure 5.5 Geometrical idealization and discretization of the Hollo-bolt

For simplicity and given that the focus of this research lies in the overall connection response rather than the performance of the Hollobolts, the application of the tightening torque and the plastic deformation of the sleeve from its initial undeformed to its final configuration was not explicitly modelled. Instead the final geometric configuration that the bolt sleeve assumes once the required preload value is applied has been simulated and the flaring of the sleeve was assumed to match the angle of the cone in accordance with similar studies (Wang et al., 2010; Liu et al., 2012a; Liu et al., 2012b). Not accounting for the actual deformation of the sleeve may lead to inaccuracies due to:

1. deviations of the actual geometry of the sleeve from the idealized one
2. the deformation history of the sleeve affecting its material properties.

Wang et al. (2010) conducted a sensitivity study on the effect of the actual geometry of the flaring sleeve and determined that the effect of a variation of the flaring angle of the sleeves by as much as 200 from the nominal angle of 150 does not lead to any appreciable difference in either stiffness or strength of the bolt. The effect of the plastic deformation of the sleeve on its subsequent material response may indeed be important, but past studies by Wang et al. (2010) and Liu et al. (2012a; 2012b) have indicated that satisfactory replication of experimental data can be achieved without due account of the actual stress state of the sleeve at the beginning of the simulation. This is the case for the study reported herein as will be shown in the next Section. Furthermore, the adopted material modelling only accounted for isotropic hardening and only monotonic material tests were conducted, hence the effect of deformation history of the sleeve on its material could not have been accurately captured.

Contrary to the standard bolts, which were hand-tightened, the Hollo-bolts were preloaded with a torque of 190 Nm to deform the sleeve in the desired geometric configuration and enable the blind-bolted connection to be formed according to the manufacturers guidelines (Lindapter, 2018). Hence, although the geometry of the sleeve was modelled in its final configuration, application of the preload on the bolt shank has been explicitly simulated as bolt preload has been shown to significantly affect the obtained stiffness of bolted joints (Yuan et al., 2018). To incorporate the effect of preloading in the analysis, the analysis was divided into three sequential steps, for each of which a nonlinear static analysis was performed:

1. All Hollo-bolts were pre-tensioned by using the bolt load functionality of ABAQUS (2013).

2. The length of the Hollo-bolts was fixed at the end of the first step by using “bolt length control” option.

3. A point load was applied at the end of the beam.

5.3 Validation

The numerical models were validated against the experimental results reported in Chapters 3 and 4 by comparing the numerically obtained failure modes, overall moment-rotation behaviour, initial rotational stiffness, plastic moment resistance and maximum obtained moment to the experimental ones.

5.3.1 Beam-to-open column joints

Figure 5.6 displays the experimental and numerical failure modes for FEP-O and EEP-O joints at the deformation corresponding to the maximum load. Both the test specimen and the numerical model display large inelastic deformations of similar magnitude in the column flange and the end plates. Moreover, the numerical model accurately predicted necking of the bolts in the top bolt row of FEP-O, which indicates bolt fracture, as shown in Figure 5.6 (a). The bolt plastic deformation shown in Figure 5.6 (b) is similar for both the experimental and the numerical failure modes and corresponds to combined tension and shear of the bolt .

The accuracy of the FE models for the FEP-O and EEP-O joint is demonstrated in Figure 5.7, where the experimental and numerical moment-rotation response is depicted. The numerical curves accord well with and provide a good fit to the experimental ones throughout the full range of rotations considered (Elflah, et al., 2018 a). As previously stated failure in the FE models was assumed to relate to all the integration points within an element reaching the stain at fracture ε_{f}. The numerical curves are assigned a "dash-dot-dash" linetype prior to the critical strain being reached and change to dotted lines afterwards .

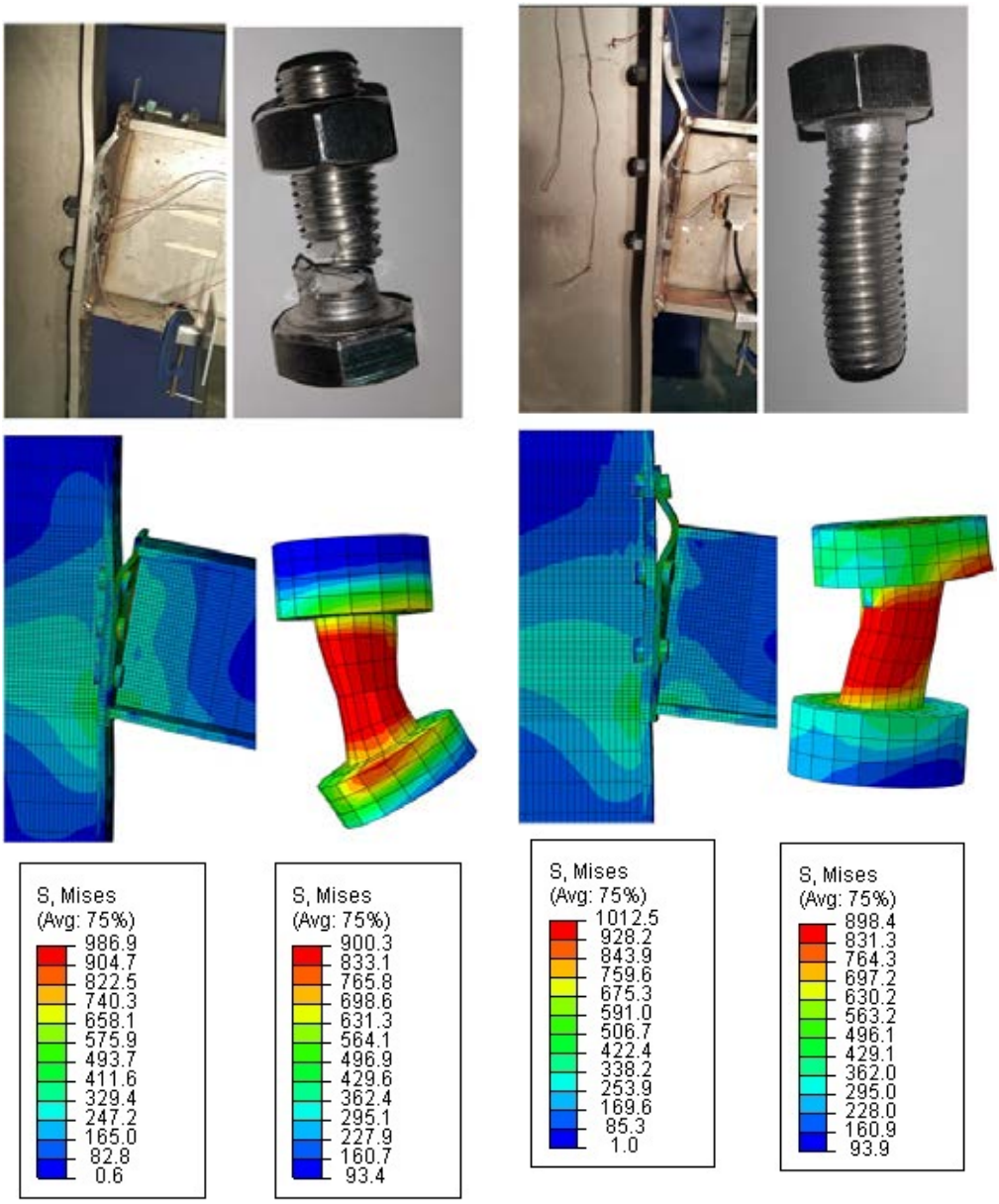

(a) FEP-O: failure mode and fractured top bolt (Stress is Von-Mises (MPa))

(b) EEP-O: connection failure mode and deformed top bolt (Stress is Von-Mises (MPa))

Figure 5.6 Experimental and numerical failure modes of FEP-O and EEP-O joints and close-up of bolt at failure (Elflah, et al., 2018 a)

The experimental and numerical failure modes and corresponding experimental and numerical moment-rotation curves are depicted for both TSAC-O and TSWAC-O joints in Figures 5.8 , 5.9 and 5.10 respectively. Once again, an excellent agreement between the experimental and numerical results can be observed in terms of failure modes and overall moment rotation response. The numerical curve for TSWAC-O-10 depicted in

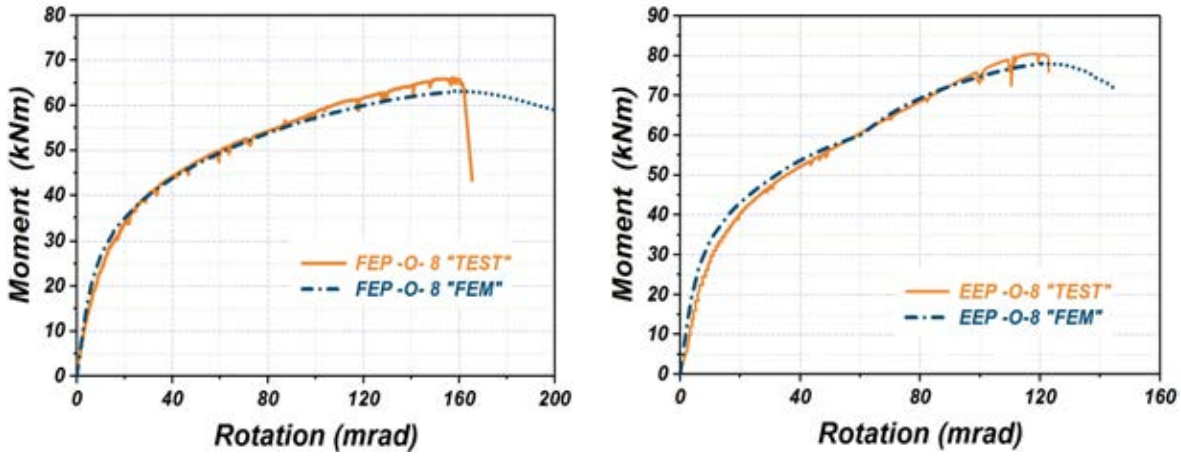

(a) FEP-O (b) EEP-O

Figure 5.7 Experimental and numerical moment-rotation response for: (a) FEP-O and (b) EEP-O (Elflah, et al., 2018 a)

Figure 5.10 (d) is plotted with a bold line until the equivalent plastic strain of the bolt reaches its limiting values, and with a dotted line thereafter. Hence it can be observed that the FE prediction for bolt failure coincides with the experimentally observed failure thus demonstrating the appropriateness of defining bolt fracture on the basis of the plastic strain at fracture ε_f .

The accuracy of the numerical models is quantified and assessed in terms of the initial rotational stiffness $S_{j,ini}$, the plastic moment resistance $M_{j,R}$, the ultimate moment resistance M_{max} and the rotation corresponding to M_{max} $\Phi_{j,u}$ in Table 5.5, where the ratio of the numerical predictions over the respective experimental values is reported. Overall, an excellent agreement between the numerical and experimental results can be observed for all joints in terms of the plastic moment resistance $M_{j,R}$ and a good agreement is obtained for the ultimate moment resistance $M_{j,max}$ and corresponding rotation $\Phi_{j,u}$, bearing in mind that these quantities are neither quantified in EN 1993-1-8 (2005) nor explicitly used in design, but nonetheless can be utilized to assess the available ductility of the connections. The stiffness is less well predicted predominantly due to poor rotational stiffness predictions for the TSAC joints and is predicted with reasonable accuracy for the end plate specimens (both FEP and EEP) and the TSWAC specimens. The observed discrepancies in the

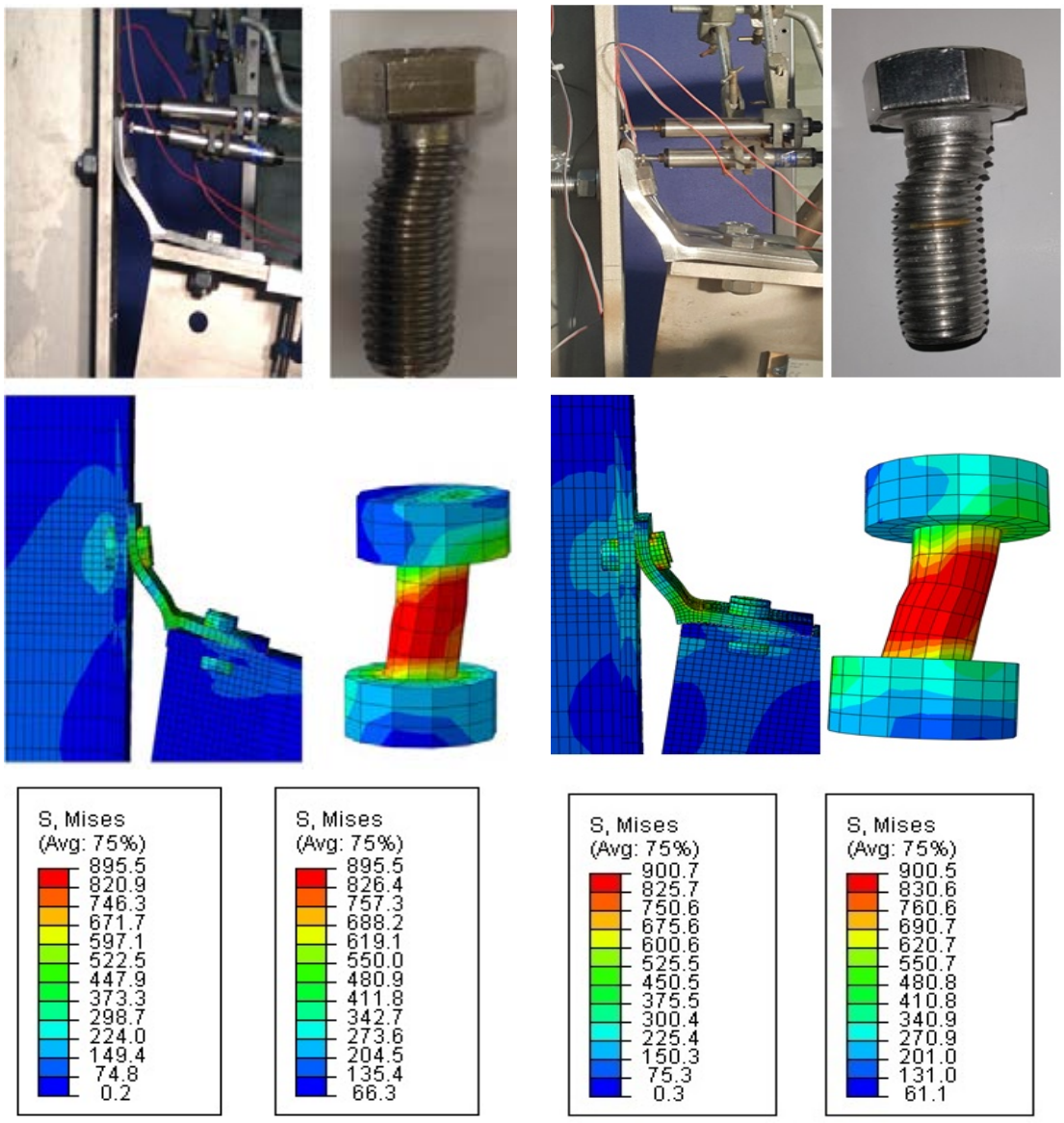

(a) TSAC-O-8: connection failure mode and bolt failure in tension and shear (Stress is Von-Mises (MPa))

(b) TSAC-O-10: connection failure mode and bolt failure in tension and shear(Stress is Von-Mises (MPa))

Figure 5.8 Experimental and numerical failure modes for TSAC-O specimens

prediction of the stiffness are arguably attributable to the gaps and slips between the various bolted components of non-preloaded bolted connections, which cannot be easily quantified or accounted for neither in numerical modelling nor in design standards (Girão and Bijlaard, 2007; Weynand, 1997; Kong and Kim, 2017; Pucinotti, 2001). Given that the initial rotational stiffness of stainless steel joints will be no different from that of carbon steel joints and that the overall connection response and failure modes are reasonably

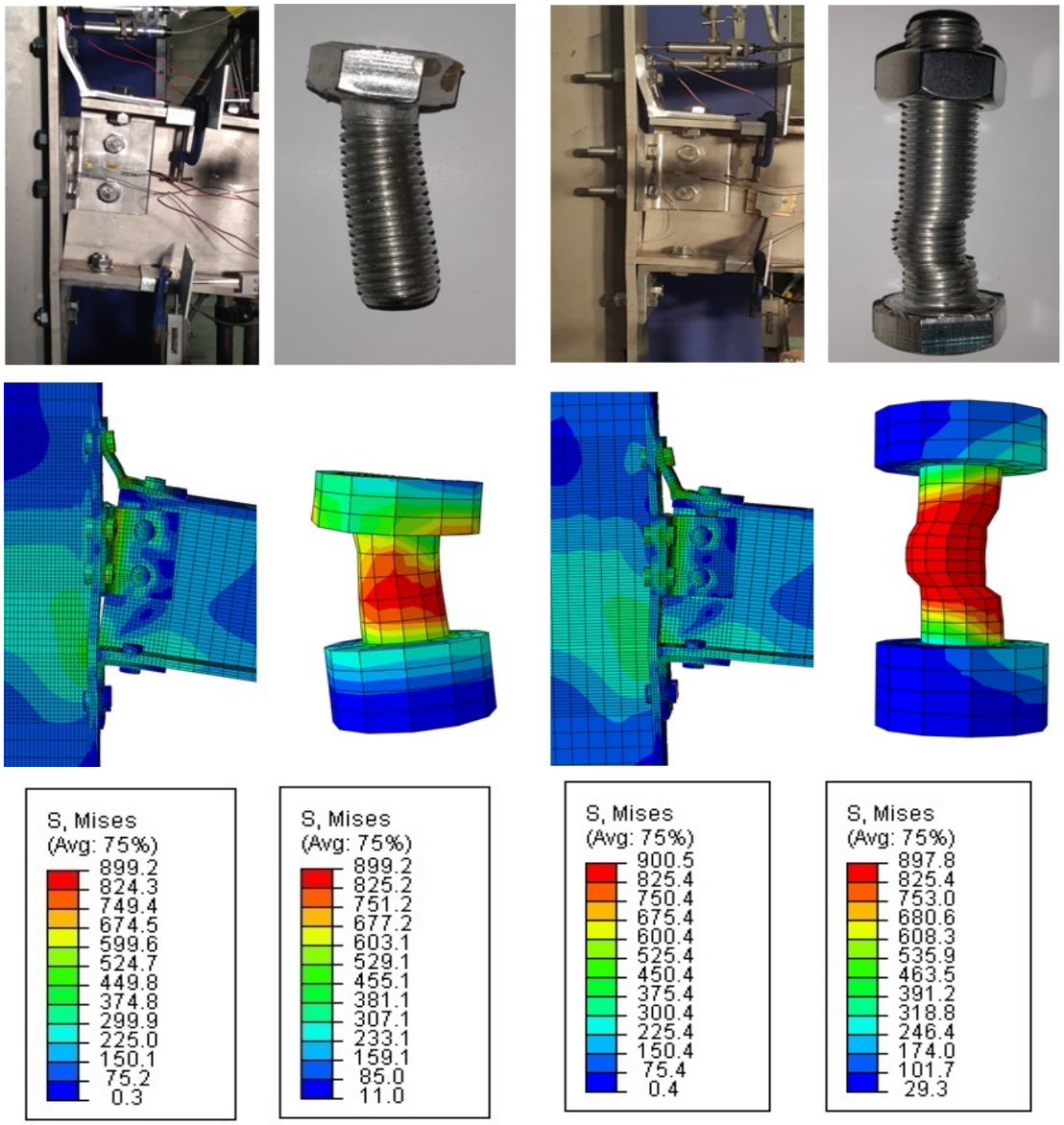

(a) TSWAC-O-8: connection failure mode and bolt failure in double shear (Stress is Von-Mises (MPa))

(b) TSWAC-O-10: connection failure mode and bolt failure in double shear (Stress is Von-Mises (MPa))

Figure 5.9 Experimental and numerical failure modes for TSWAC-O specimens

well predicted, parametric studies are conducted hereafter to generate numerical data on the basis of which the design provisions of EN 1993-1-8 (2005), particularly the plastic moment resistance $M_{j,R}$ can be assessed .

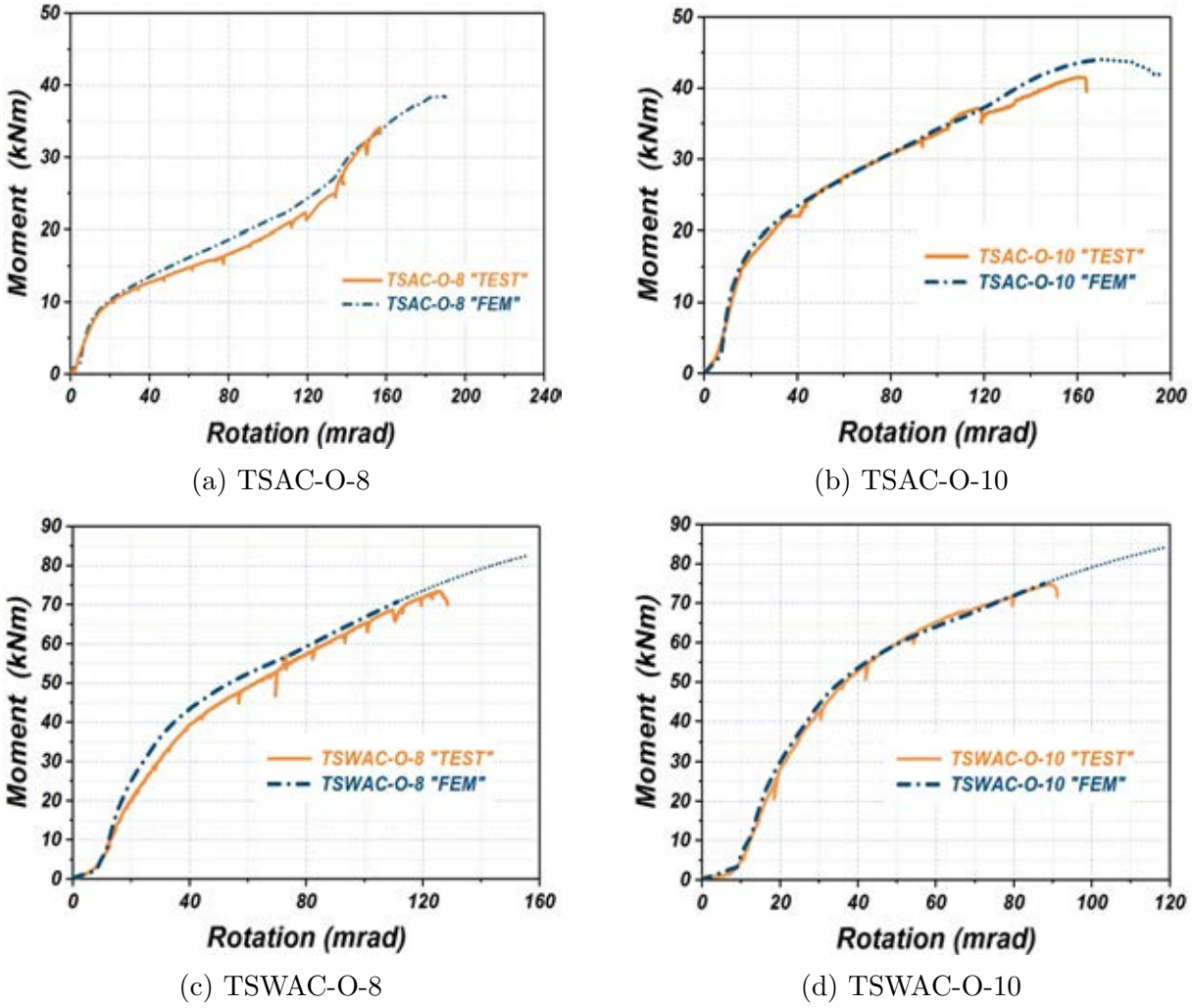

(a) TSAC-O-8 (b) TSAC-O-10

(c) TSWAC-O-8 (d) TSWAC-O-10

Figure 5.10 Experimental and numerical moment rotation response for TSAC-O and TSWAC-O specimens (Elflah, et al., 2018 a)

Table 5.5 Comparison of FE results with test results (Elflah, et al., 2018 a)

Specimen	FE/Test			
	Initial stiffness $S_{j,ini}$	Plastic Moment resistance $M_{j,R}$	Maximum moment $M_{j,MAX}$	$\Phi_{j,u}$
FEP-O	0.98	0.99	0.97	0.99
EEP-O	0.86	0.96	0.98	0.99
TSAC-O-8	2.17	1.03	1.16	1.15
TSAC-O-10	1.50	1.06	1.06	1.05
TSWAC-O -8	0.80	0.94	0.96	0.86
TSWAC-O -10	0.96	1.03	1.00	0.97
MEAN	1.21	1.00	1.02	1.00
COV	0.44	0.05	0.07	0.10

5.3.2 Beam-to-tubular column joints

Figure 5.11 shows the experimental and numerical failure modes for FEP-T-1 and FEP-T-2 joints at the deformation corresponding to the maximum load. Significant inelastic deformation of the flush end plate of FEP-T-1 can be observed in both the experimental and the numerical failure modes Figure 5.11(a), whilst the column face remains undeformed (Elflah, et al., 2018 a). Contrary, the thicker end plate of FEP-T-2 is seen to rotate but not to bend in Figure 5.11(b), whilst some deformation of the column face and the top Hollo-bolt is exhibited by both the test specimen and its numerical counterpart. Figure 5.12 shows a close-up of the regions where high inelastic deformations occur for the FEP-T specimens. A very close agreement between the deformed configuration of the 6 mm flush end plate of FEP-T-1 and the deformed shape of its numerical representation is observed.

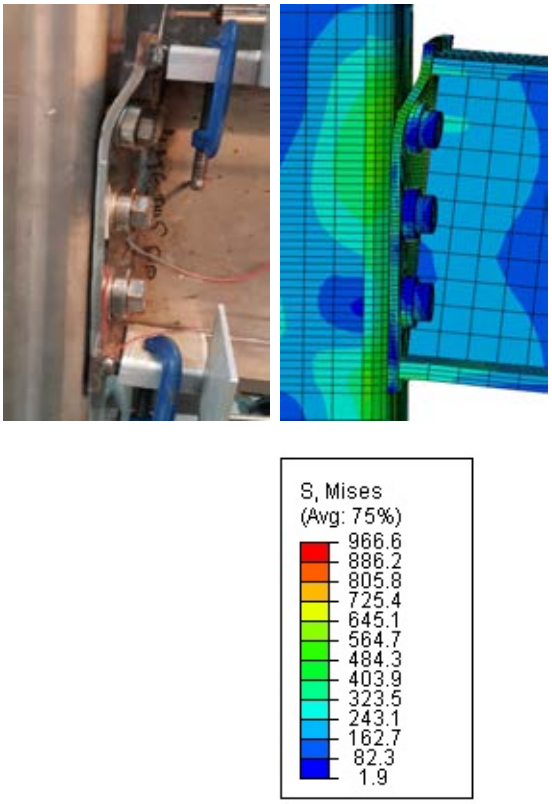

(a) FEP-T-1 (Stress is Von-Mises (MPa))

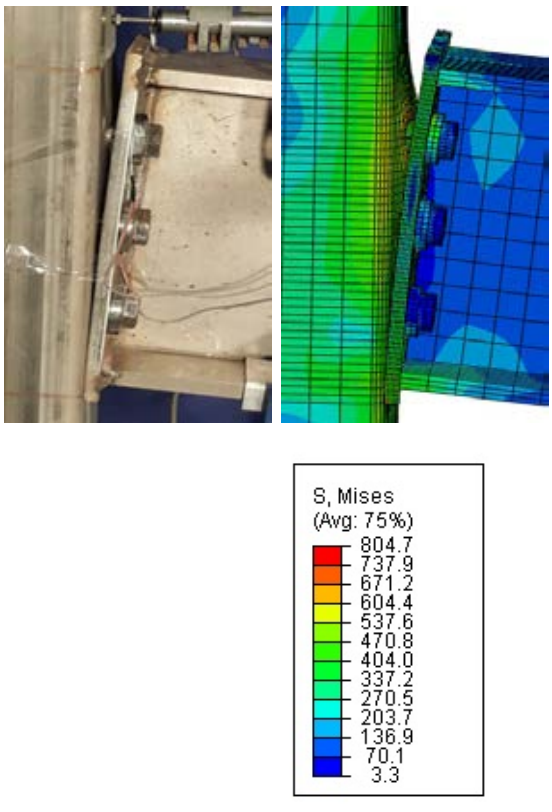

(b) FEP-T-2 (Stress is Von-Mises (MPa))

Figure 5.11 Experimental and numerical failure modes of FEP-T joints

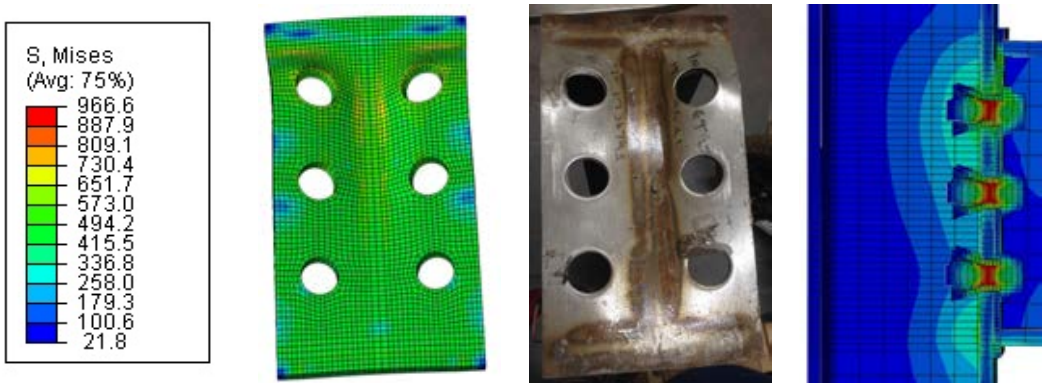

(a) FEP-T-1: deformed end plate and stress distribution in Hollo-bolts (Stress is Von-Mises (MPa))

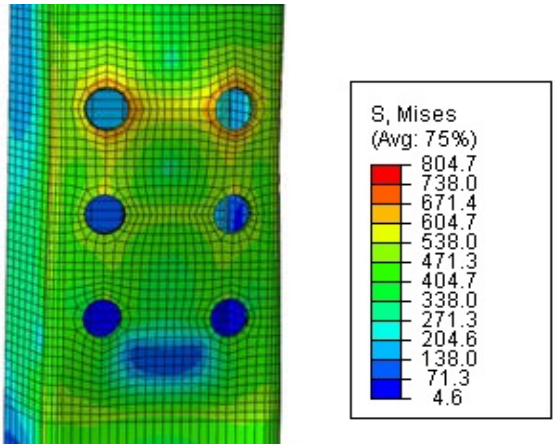

(b) FEP-T-2: deformed column face (Stress is Von-Mises (MPa))

Figure 5.12 Closeup of regions of high plastic deformations of FEP-T joints.

Finally, the accuracy of the FE models for the FEP-T joint is demonstrated in Figure 5.13, where the experimental and numerical moment-rotation response is depicted (Elflah, et al., 2018 a). A very close agreement between the experimental and the numerical curve from the onset of loading until a rotation of 70 mrad is observed for specimen FEP-T-1, whilst some divergence between the two curves is exhibited at higher rotations with the numerical model predicting higher moments. On the contrary, the numerical curve does not accurately capture the initial response of specimen FEP-T-2 and significantly underpredicts its stiffness, but the agreement between the two curves drastically improves with increasing rotations and the two curves practically coincide beyond a rotation of 20 mrad. Possible reasons for the poor prediction of the initial rotational stiffness have been discussed in detail in Chapter 3 for cases where the experimental stiffness is overestimated

by FE models. However, in this case, the rotational stiffness seems to be significantly underestimated and the discussion in Chapter 3 is not applicable. The higher rotational stiffness exhibited by the test specimen may be attributed either to experimental errors or to a higher preload accidentally applied to some of the Hollo-bolts.

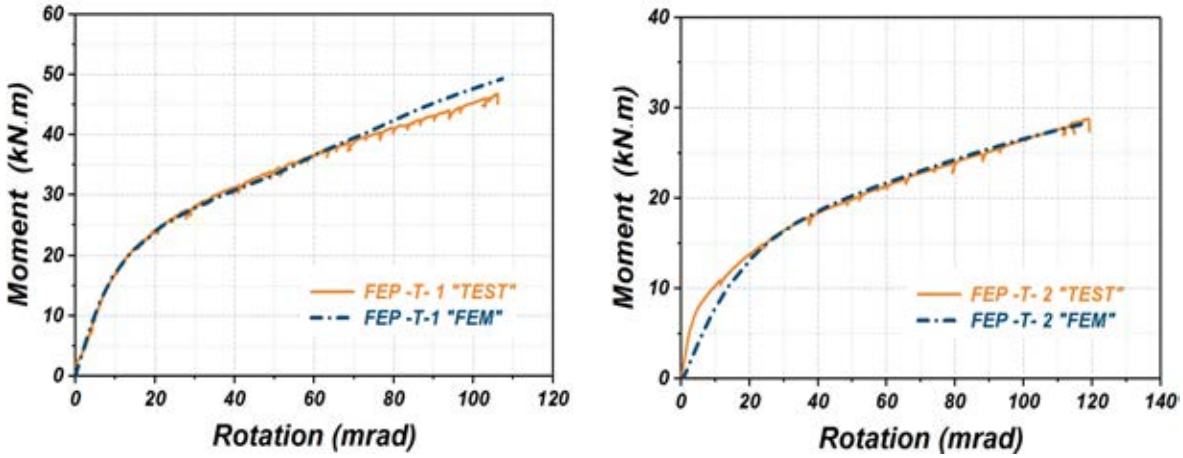

(a) FEP-T-1 (b) FEP-T-2

Figure 5.13 Experimental and numerical moment-rotation response of FEP-T joints

Figures 5.14 and 5.15 depict the experimental and numerical deformed configurations at the maximum recorded load and the experimental and numerical moment-rotation curves of the TSAC-T joints respectively. A close-up of the most heavily stressed (i.e. connecting the top cleat) Hollo-bolt shown in Figure 5.14(a) shows significant indentations in the flared sleeves of the Hollo-bolt which accord well with the stress concentration depicted in the stress contour plot of the numerical representation of the Hollo-bolt. Similarly, an identical deformation pattern of the both the angle cleats and the column face of the TSAC-T-2 specimen is observed in Figure 5.14(b). The numerical prediction of the moment-rotation curve of the TSAC-T-1 joint can be observed to coincide with the respective experimental curve in Figure 5.15 (a), whilst a slight deviation between the numerical and experimental curves of the TSAC-T-2 joint is observed in Figure 5.15 (b) for rotations higher than 90 mrad. Overall, an excellent agreement between tests and FE predictions can be observed in terms of both deformation shape and overall joint response for the TSAC-T joints.

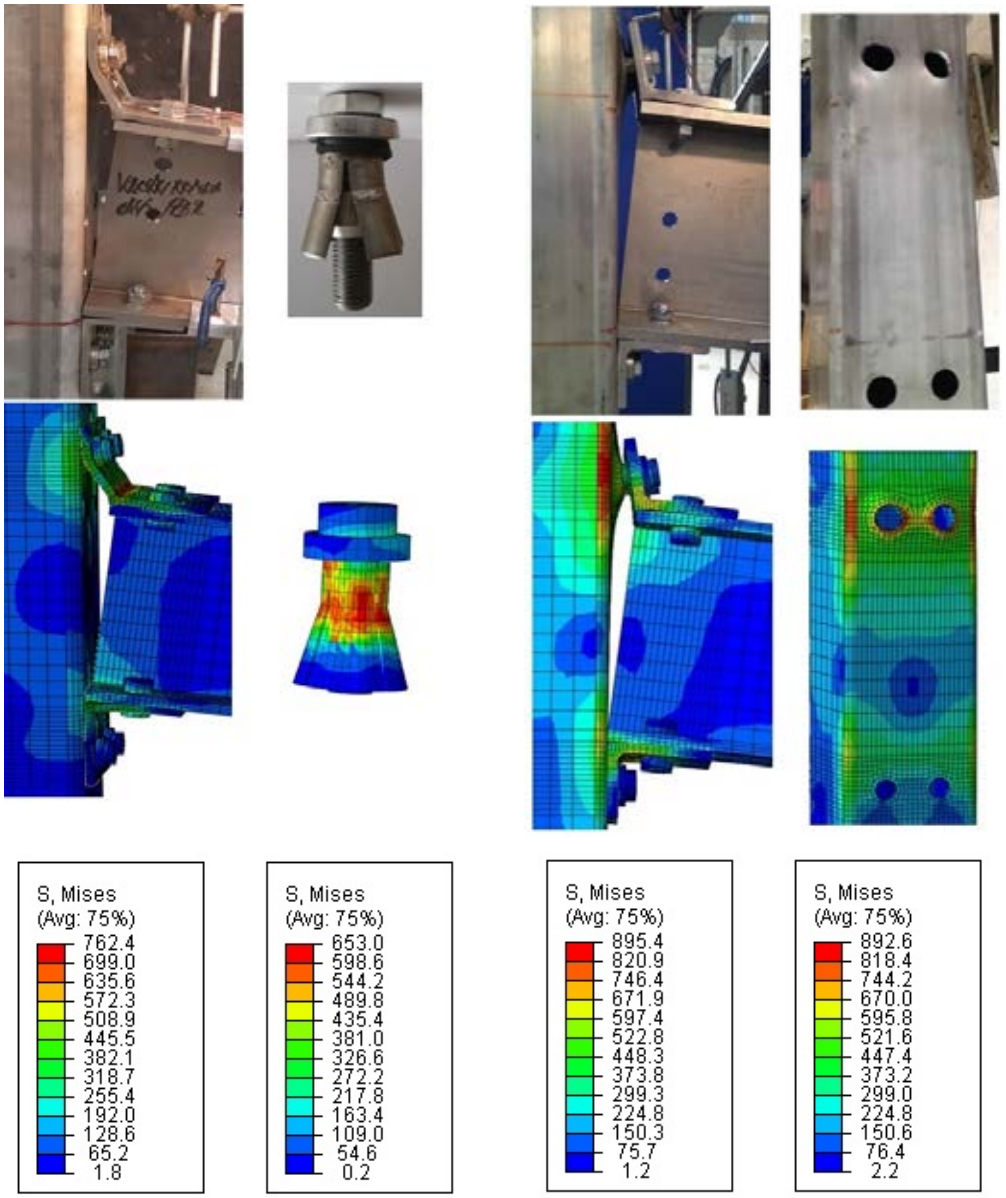

(a) TSAC-T-1: overall joint deformation and closeup of Hollo-bolt sleeve (Stress is Von-Mises (MPa))

(b) TSAC-T-2: overall joint deformation and closeup of deformed column face (Stress is Von-Mises (MPa))

Figure 5.14 Experimental and numerical failure modes of TSAC-T joints

Figures 5.16 and 5.17 depict the experimental and numerical moment-rotation curves and the experimental and numerical deformed configurations at the maximum recorded load of the TSWAC-T joints respectively. The experimental and numerical curve can be seen to almost coincide, whilst the experimental and numerically obtained deformation patterns are also identical. Similar to the TSAC-T joints, the indentations observed in

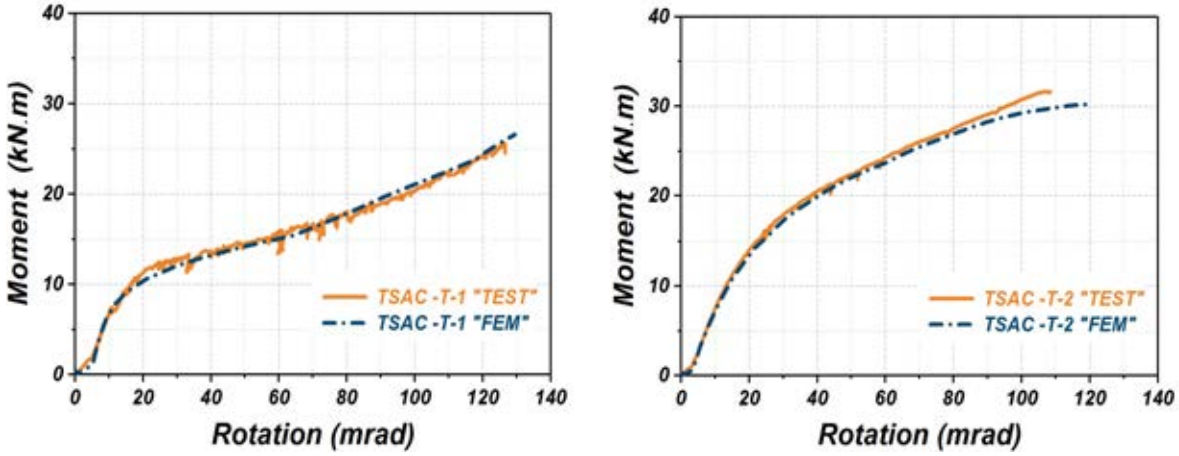

(a) TSAC-T-1 (b) TSAC-T-2

Figure 5.15 Experimental and numerical moment-rotation response of TSAC-T joints

the sleeves of the Hollo-bolt of specimen TSWAC-T-1, are reflected by a sharp stress concentration predicted by the FE model in the same rotation. Overall an excellent agreement between tests and FE predictions can be observed for the TSWAC-T joints.

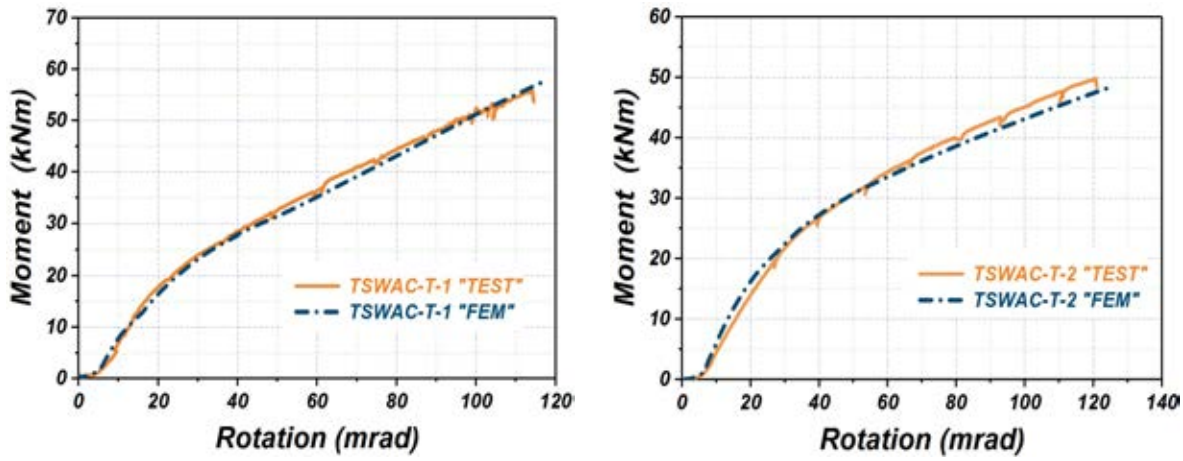

(a) TSWAC-T-1 (b) TSWAC-T-2

Figure 5.16 Experimental and numerical moment-rotation response of TSWAC-T joints.

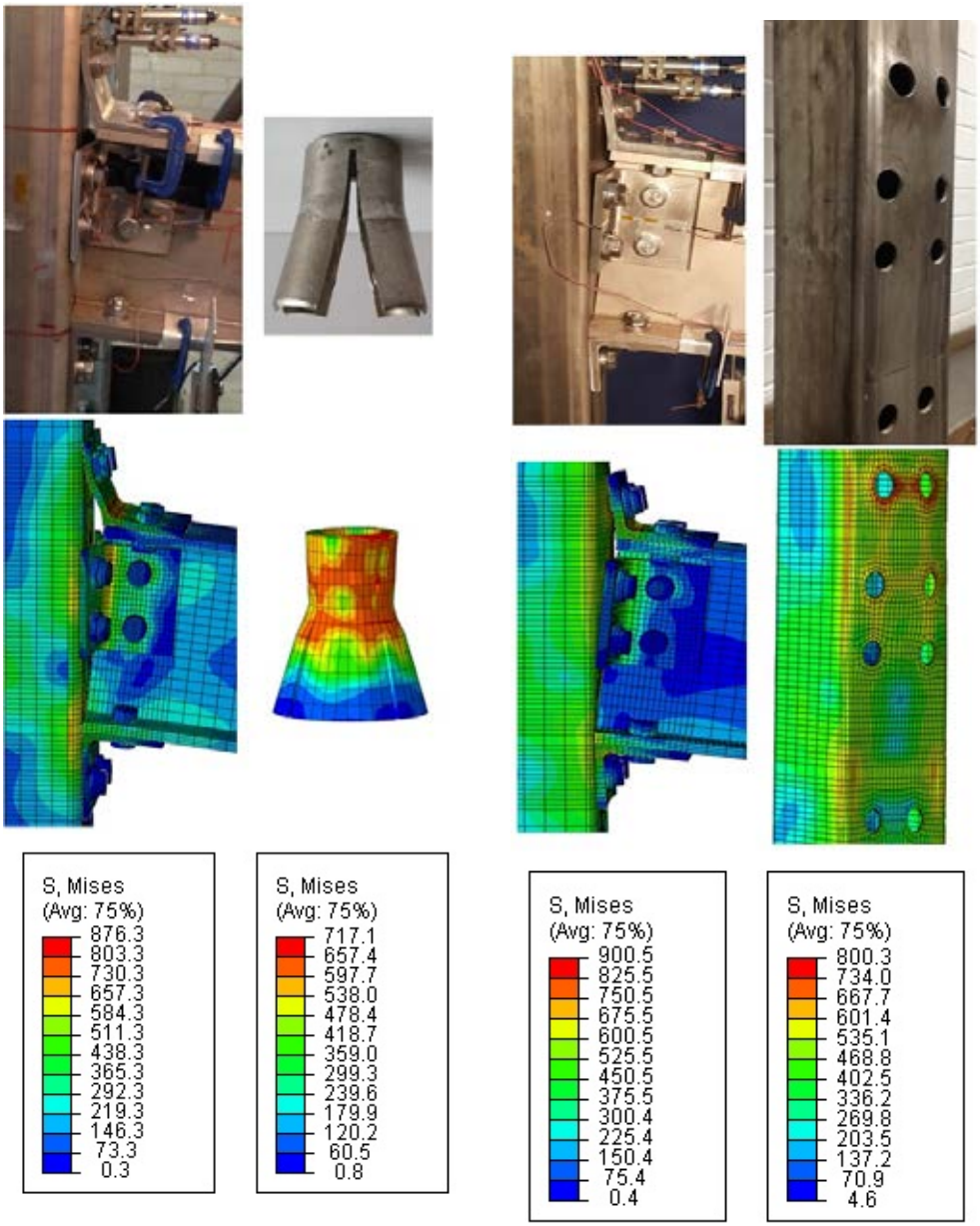

(a) TSWAC-T-1: overall joint deformation and closeup deformed Hollo-bolt sleeve (Stress is Von-Mises (MPa))

(b) TSWAC-T-2: overall joint deformation and deformed tubular column face (Stress is Von-Mises (MPa)).

Figure 5.17 Experimental and numerical failure modes of TSWAC-T joints

The accuracy of the numerical models is quantified and assessed in terms of the initial rotational stiffness $S_{j,ini}$, the plastic moment resistance $M_{j,R}$ and the maximum recorded moment at the rotation at which the tests were terminated $M_{j,max}$ in Table 5.6, where the ratio of the numerical predictions over the respective experimental values is reported. With the exception of the FEP-T-2 specimen, the initial rotational stiffness of which was

poorly predicted, a very close agreement between the experimental and the numerically determined initial rotational stiffness is observed. The reported high COV of 0.28 reduces to 0.07 if joint FEP-T-2 is not considered. The drastic improvement of the FE predictions for the tubular column joints in terms of the initial rotational stiffness compared to the respective models for the beam-to-open column joints is believed to related to the applied preload of the Hollo-bolts, which effectively removed any gaps between the various connected parts.

In terms of plastic moment resistance the FE models are seen consistently underestimate the experimental plastic moment resistance by approximately 8%. This is deemed accurate enough to proceed to parametric studies (Saliba and Gardner, 2013 and Theofanous and Gardner, 2009), given the ambiguity of the procedure by which the experimental and numerical $M_{j,R}$ is determined. Finally, the moment at the maximum applied rotation is reasonably well predicted and the accuracy of the predictions is similar to the one achieved for the beam-to-open section joints reported in Table 5.5.

Table 5.6 Comparison of FE results with test results

Specimen	FE/Test		
	Initial stiffness $S_{j,ini}$	Plastic Moment resistance $M_{j,R}$	Maximum moment $M_{j,max}$
FEP-T-1	1.06	0.93	1.09
FEP-T-2	0.40	0.88	1.03
TSAC-T-1	0.92	0.92	1.08
TSAC-T-2	0.98	0.94	0.93
TSWAC-T-1	0.98	0.95	1.07
TSWAC-T-2	1.11	0.89	0.98
MEAN	0.91	0.92	1.03
COV	0.28	0.03	0.06

5.4 Parametric studies

Upon validation of the FE models, parametric studies were performed to enable the study of the behaviour of stainless steel connections over a wide range of geometric configurations and highlight the influence of key joint details on the overall response. The joint typologies against which the FE models were calibrated, namely FEP-O, EEP-O, TSAC-O and TSWAC-O for the beam-to-open column joints and FEP-T, TSAC-T and TSWAC-T for the beam-to-tubular column joints are employed in the parametric studies (Elflah, et al., 2018 a). Moreover, the response of geometrically identical joints made in Grade EN 1.4162 (lean duplex) stainless steel is investigated. The lean duplex stainless steel grade was chosen as a representative duplex grade which displays higher strength and lower ductility than the austenitic grade. The material parameters used for the lean duplex material were taken from the material tests reported by Saliba and Gardner (2013) and Theofanous and Gardner (2010) for stainless steel I-sections and tubular (SHS) sections respectively. Hence two series of geometrically identical models were considered, one simulating the response of austenitic stainless steel and one simulating the response of lean duplex stainless steel joints, which are denoted by the letters A and L following the joint designation respectively (e.g. FEP-O-A is a flush end plate joint employing an open column section in austenitic stainless steel). All relevant symbols of the varied geometric dimensions are defined in Figures 5.1 and 5.4 for beam-to-open and beam-to-tubular column joints respectively, whilst the remaining geometric dimensions of the connected beams and columns remain identical to the ones reported Chapters 3 and 4 (Elflah, et al., 2018 a).

The parameters varied for the parametric studies of joints involving end plates (FEP or EEP) include the thickness of the column flange t_f, the thickness of the end plate t_p, the edge distance of the bolt rows from the end plate edges/column edges e_1 and the distance of the top bolt row from the centroid of the compression beam flange z as reported in in Tables 5.7 to 5.10 for FEP-O-A, FEP-O-L,FEP-T-A and FEP-T-L. Similarly, the geometric parameters varied for the EEP-O-A and EEP-O-L joints joints are defined in

Tables 5.11 and 5.12. With respect to the TSAC-O and TSAC-T specimens Tables 5.13 to 5.16 define the investigated parameters, which include the column flange thickness t_c, the angle cleat thickness t_a (both top and seat cleats were assumed to have the same geometric dimensions), the edge distance e_1 of the bolts connecting the top cleat to the column flange, the depth L_1 of the leg of the cleats parallel to the column flange and the gap g between the beam and the column flange. Similar parameters were considered for the TSWAC-O-A, TSWAC-O-L, TSWAC-T-A and TSWAC-T-L joints, the web cleat of which was kept unchanged, as shown in Tables 5.17 to and 5.20. In this case the edge distance e_1 of the bolts connecting the top angle cleat to the column flange were kept constant, whilst the edge distance e_2 of the bolts connecting the web cleats to the column flange were varied (Elflah, et al., 2018 a).

Similar to the experimental tests, the FE models exhibited large plastic deformations in the stainless steel components (i.e. column flange/face, end plates and angle cleats) with increasing loading prior to reaching the joints' ultimate failure moment. In all cases joint failure was triggered by bolt or by Hollo-bolt legs failure and pull out of bolt clearance holes, since the bolts possess markedly reduced ductility compared to the other joint components as indicated by their significantly lower plastic strain at fracture ε_f . In addition to the geometric configurations, the numerical results for $S_{j,ini}$, $M_{j,R}$, $M_{j,max}$ and $\Phi_{j,u}$ and the corresponding predictions of EN1993-1-8, (2005) for $S_{j,ini}$ and $M_{j,R}$ are also reported in Tables 5.7 to 5.20 and are discussed in the following section (Elflah, et al., 2018 a).

Table 5.7 Summary parametric studies (geometry and results) of FEP-O-A (Elflah, et al., 2018 a)

Model No	Distances according to Figure 5.1 (mm)						Initial stiffness (KNm/mrad)			Moment Capacity $M_{j,R}$ (kNm)			Maximum (FE)		Predicted failure mode	
	t_c	t_p	e_1	p_1	p_2	z	$S_{j,ini}$ (EC3)	$S_{j,ini}$ (FE)	(EC3)/ (FE)	$M_{j,R}$ (EC3)	$M_{j,R}$ (FE)	(EC3)/ (FE)	M_u (KN.m)	Φ_u (mrad)	(EC3)	(FE)
Model-1	12	8	25	65	65	179	5739	3995	1.44	18.6	40.5	0.46	63	158.5	End plate in bending / Mode 1	Bolt failure in tension
Model-2	12	14	25	65	65	179	7788	5477	1.42	28.7	56.8	0.51	69.3	77.8	Bending of column flange	Bolt failure in tension
Model-3	12	12	25	65	65	179	7406	5354	1.38	28.7	54.1	0.53	68.7	89.2	Bending of column flange	Bolt failure in tension
Model-4	12	10	25	65	65	179	6786	4948	1.37	26.4	50.4	0.52	66.1	103.9	End plate in bending / Mode 1	Bolt failure in tension
Model-5	12	6	25	65	65	179	4031	3562	1.13	10.5	26.7	0.39	60.3	201.1	End plate in bending / Mode 1	Bolt failure in tension
Model-6	12	8	35	65	65	179	7611	5806	1.31	23.7	52.9	0.45	68.7	82.1	End plate in bending / Mode 1	Bolt failure in tension
Model-7	12	8	30	65	65	179	6697	5014	1.34	20.5	48.7	0.42	66.5	111.7	End plate in bending / Mode 1	Bolt failure in tension
Model-8	12	8	20	65	65	179	4743	3816	1.24	16.5	37.8	0.44	59.6	176	End plate in bending / Mode 1	Bolt failure in tension
Model-9	12	8	15	65	65	179	3912	3353	1.17	15.3	32.5	0.47	55.6	195.1	End plate in bending / Mode 1	Bolt failure in tension
Model-10	16	8	25	65	65	179	6288	4746	1.32	18.6	45.5	0.41	65.7	134.7	End plate in bending / Mode 1	Bolt failure in tension
Model-11	14	8	25	65	65	179	6053	4674	1.3	18.6	44.2	0.42	64.8	136.7	End plate in bending / Mode 1	Bolt failure in tension
Model-12	10	8	25	65	65	179	5290	3852	1.37	18.6	41.8	0.45	60.8	162.2	End plate in bending / Mode 1	Bolt failure in tension
Model-13	8	8	25	65	65	179	4591	3650	1.26	16.1	37.5	0.43	58	175.9	Bending of column flange	Bolt failure in tension
Model-14	12	8	25	65	65	204	7585	6753	1.12	24.7	59	0.42	75.6	83	End plate in bending / Mode 1	Bolt failure in tension
Model-15	12	8	25	65	65	191.5	6554	5387	1.22	20.5	49	0.42	69.7	120.5	End plate in bending / Mode 1	Bolt failure in tension
Model-16	12	8	25	65	65	166.5	4956	3706	1.34	16.7	36	0.46	57	162.8	End plate in bending / Mode 1	Bolt failure in tension
Model-17	12	8	25	65	65	154	4245	3120	1.36	15.1	31	0.49	50.7	182.4	End plate in bending / Mode 1	Bolt failure in tension
MEAN									1.3			0.45				
COV									0.07			0.09				

Table 5.8 Summary parametric studies (geometry and results) of FEP-O-L (Elflah, et al., 2018 a)

Model No	Distances according to Figure 5.1 (mm)						Initial stiffness (KNm/mrad)			Moment Capacity $M_{j,R}$ (kNm)			Maximum (FE)		Predicted failure mode	
	t_c	t_p	e_1	p_1	p_2	z	$S_{j,ini}$ (EC3)	$S_{j,ini}$ (FE)	(EC3)/ (FE)	$M_{j,R}$ (EC3)	$M_{j,R}$ (FE)	(EC3)/ (FE)	M_u (KN.m)	Φ_u (mrad)	(EC3)	(FE)
Model-18	12	8	25	65	65	179	5838	4058	1.44	27.7	53.4	0.52	69.8	95.8	End plate in bending / Mode 1	Bolt failure in tension
Model-19	12	14	25	65	65	179	7922	5622	1.41	38.9	65.2	0.6	81.1	48	Bending of column flange	Bolt failure in tension
Model-20	12	12	25	65	65	179	7534	5431	1.39	38.9	64.5	0.6	80.3	51.1	Bending of column flange	Bolt failure in tension
Model-21	12	10	25	65	65	179	6903	5066	1.36	32.9	59.5	0.55	75.91	56.7	End plate in bending / Mode 1	Bolt failure in tension
Model-22	12	6	25	65	65	179	4100	3591	1.14	21.6	39.5	0.55	64.2	112.4	End plate in bending / Mode 1	Bolt failure in tension
Model-23	12	8	35	65	65	179	7741	5625	1.38	32.2	68.4	0.47	80.3	55.1	End plate in bending / Mode 1	Bolt failure in tension
Model-24	12	8	30	65	65	179	6812	5122	1.33	30.7	60.9	0.5	75.4	68.5	End plate in bending / Mode 1	Bolt failure in tension
Model-25	12	8	20	65	65	179	4824	3866	1.25	24.3	47.5	0.51	65.8	107	End plate in bending / Mode 1	Bolt failure in tension
Model-26	12	8	15	65	65	179	3979	3373	1.18	21.2	44.9	0.47	61.1	119.9	End plate in bending / Mode 1	Bolt failure in tension
Model-27	16	8	25	65	65	179	6396	4861	1.32	27.7	58.5	0.47	71.6	88.4	End plate in bending / Mode 1	Bolt failure in tension
Model-28	14	8	25	65	65	179	6157	4551	1.35	27.7	58.5	0.47	71.1	89.7	End plate in bending / Mode 1	Bolt failure in tension
Model-29	10	8	25	65	65	179	5381	3840	1.4	27.7	54.2	0.51	68.9	98.5	End plate in bending / mode 1	Bolt failure in tension
Model-30	8	8	25	65	65	179	4670	3750	1.25	27.7	52.3	0.53	65.1	105.2	End plate in bending / Mode 1	Bolt failure in tension
Model-31	12	8	25	65	65	204	7715	6759	1.14	33.3	71.1	0.47	86.1	42.2	End plate in bending / Mode 1	Bolt failure in tension
Model-32	12	8	25	65	65	191.5	6666	5418	1.23	30	63.8	0.47	78.4	63.4	End plate in bending / Mode 1	Bolt failure in tension
Model-33	12	8	25	65	65	166.5	5041	3764	1.34	25.5	50.2	0.51	63	109.3	End plate in bending / Mode 1	Bolt failure in tension
Model-34	12	8	25	65	65	154	4318	3170	1.36	23.4	45.1	0.52	55.8	116	End plate in bending / Mode 1	Bolt failure in tension
MEAN									1.31			0.51				
COV									0.07			0.08				

Table 5.9 Summary parametric studies (geometry and results) of FEP-T-A (Elflah, et al., 2018 a)

Model No	Distances according to Figure 5.4 (mm)						Initial stiffness (KNm/mrad)			Moment Capacity $M_{j,R}$ (kNm)			Maximum (FE)		Predicted failure mode	
	t_c	t_p	e_1	p_1	p_2	z	$S_{j,ini}$ (EC3)	$S_{j,ini}$ (FE)	(EC3)/ (FE)	$M_{j,R}$ (EC3)	$M_{j,R}$ (FE)	(EC3)/ (FE)	M_u (KN.m)	Φ_u (mrad)	(EC3)	(FE)
Model-35	10	6	30	65	65	179	2241	2221	1.01	10	25	0.4	49.3	107.2	End plate in bending / Mode 1	Bolt failure in tension
Model-36	10	14	30	65	65	179	3632	3584	1.01	23.3	57	0.41	72.4	57.6	-	Bolt failure in tension
Model-37	10	12	30	65	65	179	3522	3223	1.09	23.3	55.5	0.42	67.5	63.1	-	Bolt failure in tension
Model-38	10	10	30	65	65	179	3321	3040	1.09	23.3	47	0.49	60.9	70.6	-	Bolt failure in tension
Model-39	10	8	30	65	65	179	2943	2653	1.11	17.7	39	0.45	57	90.8	End plate in bending / Mode 1	Bolt failure in tension
Model-40	10	6	45	65	65	179	3371	2326	1.45	14	37	0.38	56.5	87.4	End plate in bending / Mode 1	Bolt failure in tension
Model-41	10	6	40	65	65	179	3020	2251	1.34	12.4	31	0.4	52.7	91	End plate in bending / Mode 1	Bolt failure in tension
Model-42	10	6	35	65	65	179	2589	2113	1.23	10.3	25	0.41	50.1	95.4	End plate in bending / Mode 1	Bolt failure in tension
Model-43	10	6	25	65	65	179	1874	1909	0.98	9	21	0.43	46.3	115.7	End plate in bending / Mode 1	Bolt failure in tension
Model-44	14	6	30	65	65	179	3632	2985	1.22	10	25	0.4	50.4	95.8	End plate in bending / Mode 1	Bolt failure in tension
Model-45	12	6	30	65	65	179	3006	2730	1.1	10	24	0.42	50.8	101.9	End plate in bending / Mode 1	Bolt failure in tension
Model-46	8	6	30	65	65	179	1418	1580	0.9	10	22	0.45	45.7	121.5	End plate in bending / Mode 1	Bolt failure in tension
Model-47	6	6	30	65	65	179	694	1046	0.66	7.4	18	0.41	36.4	137.1	-	Bolt failure in tension
Model-48	10	6	30	65	65	199	2906	3350	0.87	12.8	38	0.34	55.5	66.2	End plate in bending / Mode 1	Bolt failure in tension
Model-49	10	6	30	65	65	189	2562	2656	0.96	11.3	29	0.39	52.7	89.7	End plate in bending / Mode 1	Bolt failure in tension
Model-50	10	6	30	65	65	169	1974	1802	1.1	9.2	21	0.44	46.2	124.1	End plate in bending / Mode 1	Bolt failure in tension
Model-51	10	6	30	65	65	159	1729	1525	1.13	8.6	18.5	0.46	44	147	End plate in bending / Mode 1	Bolt failure in tension
MEAN									1.07			0.42				
COV									0.17			0.09				

Table 5.10 Summary parametric studies (geometry and results) of FEP-T- L (Elflah, et al., 2018 a)

Model No	Distances according to Figure 5.4 (mm)						Initial stiffness (KNm/mrad)			Moment Capacity $M_{j,R}$ (kNm)			Maximum (FE)		Predicted failure mode	
	t_c	t_p	e_1	p_1	p_2	z	$S_{j,ini}$ (EC3)	$S_{j,ini}$ (FE)	(EC3)/ (FE)	$M_{j,R}$ (EC3)	$M_{j,R}$ (FE)	(EC3)/ (FE)	M_u (KN.m)	Φ_u (mrad)	(EC3)	(FE)
Model-52	10	6	30	65	65	179	2280	2227	1.02	18.1	29	0.62	47.3	78.5	End plate in bending / Mode 1	Bolt failure in tension
Model-53	10	14	30	65	65	179	3694	3587	1.03	40.2	57	0.71	71.5	50.1	End plate in bending / Mode 3	Bolt failure in tension
Model-54	10	12	30	65	65	179	3582	3407	1.05	38.3	55	0.7	68.4	51.8	End plate in bending / Mode 2	Bolt failure in tension
Model-55	10	10	30	65	65	179	3378	3044	1.11	32.4	59.5	0.55	62.1	55.7	End plate in bending / Mode 2	Bolt failure in tension
Model-56	10	8	30	65	65	179	2994	2650	1.13	27.6	46	0.6	53.8	62.6	End plate in bending / Mode 2	Bolt failure in tension
Model-57	10	6	45	65	65	179	3428 a	2759	1.24	25.4	45	0.56	60.4	68	End plate in bending / Mode 1	Bolt failure in tension
Model-58	10	6	40	65	65	179	3072	2632	1.17	22.5	37	0.61	54.1	70.8	End plate in bending / Mode 1	Bolt failure in tension
Model-59	10	6	35	65	65	179	2634	2296	1.15	18.7	33	0.57	50.2	73.3	End plate in bending / Mode 1	Bolt failure in tension
Model-60	10	6	25	65	65	179	1906	2071	0.92	16.4	26	0.63	44.6	84.7	End plate in bending / Mode 1	Bolt failure in tension
Model-61	14	6	30	65	65	179	3694	3161	1.17	18.1	32	0.57	48.7	72.4	End plate in bending / Mode 1	Bolt failure in tension
Model-62	12	6	30	65	65	179	3058	2742	1.12	18.1	30	0.6	49.2	78.1	End plate in bending / Mode 1	Bolt failure in tension
Model-63	8	6	30	65	65	179	1443	1594	0.91	18.1	25	0.72	46.6	89.6	End plate in bending / mode 1	Bolt failure in tension
Model-64	6	6	30	65	65	179	706	899	0.79	15.3	22	0.7	38.6	101.6	-	Bolt failure in tension
Model-65	10	6	30	65	65	199	2956	2917	1.01	23.3	42	0.55	56.3	51.8	End plate in bending / Mode 1	Bolt failure in tension
Model-66	10	6	30	65	65	189	2606	2726	0.96	20.5	34	0.6	50.6	65	End plate in bending / Mode 1	Bolt failure in tension
Model-67	10	6	30	65	65	169	2008	1851	1.08	16.8	26	0.65	44.3	90.7	End plate in bending / Mode 1	Bolt failure in tension
Model-68	10	6	30	65	65	159	1758	1570	1.12	15.6	22	0.71	40.8	99.9	End plate in bending / Mode 1	Bolt failure in tension
MEAN									1.07			0.42				
COV									0.17			0.09				

Table 5.11 Summary parametric studies (geometry and results) of EEP-O-A (Elflah, et al., 2018 a)

Model No	Distances according to Figure 5.1 (mm)						Initial stiffness (KNm/mrad)			Moment Capacity $M_{j,R}$ (kNm)			Maximum (FE)		Predicted failure mode	
	t_c	t_p	e_1	p_1	z_1	z_2	$S_{j,ini}$ (EC3)	$S_{j,ini}$ (FE)	(EC3)/ (FE)	$M_{j,R}$ (EC3)	$M_{j,R}$ (FE)	(EC3)/ (FE)	M_u (KN.m)	Φ_u (mrad)	(EC3)	(FE)
Model-69	12	8	25	110	284	174	9394	5201	1.8	27.2	43.8	0.62	78.1	120.5	End plate in bending / Mode 1	Bolt failure in tension
Model-70	12	14	25	110	284	174	12872	8130	1.58	44.5	75.5	0.59	91.3	79.5	Bending of column flange	Bolt failure in tension
Model-71	12	12	25	110	284	174	12189	7498	1.62	41.2	70.9	0.58	86.2	86.4	Bending of column flange	Bolt failure in tension
Model-72	12	10	25	110	284	174	11122	6715	1.65	38.4	58.5	0.66	82.1	101.4	End plate in bending / Mode 1	Bolt failure in tension
Model-73	12	6	25	110	284	174	6649	4268	1.55	15.3	26.2	0.58	76.4	141.3	End plate in bending / Mode 1	Bolt failure in tension
Model-74	12	8	35	110	284	174	12541	6740	1.86	35.5	55.2	0.64	75.9	84.9	End plate in bending / Mode 1	Bolt failure in tension
Model-75	12	8	30	110	284	174	11005	6126	1.8	30.3	47.5	0.64	77.6	102.4	End plate in bending / Mode 1	Bolt failure in tension
Model-76	12	8	20	110	284	174	7649	4973	1.54	23.3	40.2	0.58	76.6	135.6	End plate in bending / Mode 1	Bolt failure in tension
Model-77	12	8	15	110	284	174	6485	4421	1.47	23	35.3	0.65	73.8	147.1	End plate in bending / Mode 1	Bolt failure in tension
Model-78	16	8	25	110	284	174	10175	6117	1.66	27.2	44.5	0.61	78.3	104.2	End plate in bending / Mode 1	Bolt failure in tension
Model-79	14	8	25	110	284	174	9839	5920	1.66	27.2	44.5	0.61	78.7	110.1	End plate in bending / Mode 1	Bolt failure in tension
Model-80	10	8	25	110	284	174	8760	5168	1.69	27.2	42.2	0.64	75	129.9	End plate in bending / Mode 1	Bolt failure in tension
Model-81	8	8	25	110	284	174	7775	4605	1.68	24.6	39.7	0.62	70.8	139.4	Bending of column flange	Bolt failure in tension
Model-82	12	8	25	80	269	189	9433	7434	1.25	30.4	59.2	0.51	87.6	104.8	End plate in bending / Mode 1	Bolt failure in tension
Model-83	12	8	25	140	299	159	9109	4385	2.13	23.9	40.1	0.59	69.7	127.5	End plate in bending / Mode 1	Bolt failure in tension
Model-84	12	8	25	170	314	144	9011	3425	2.7	23.2	35.5	0.65	62.6	138.8	End plate in bending / Mode 1	Bolt failure in tension
MEAN									1.73			0.61				
COV									0.18			0.06				

Table 5.12 Summary parametric studies (geometry and results) of EEP-O-L (Elflah, et al., 2018 a)

Model No	Distances according to Figure 5.1 (mm)						Initial stiffness (KNm/mrad)			Moment Capacity $M_{j,R}$ (kNm)			Maximum (FE)		Predicted failure mode	
	t_c	t_p	e_1	p_1	z_1	z_2	$S_{j,ini}$ (EC3)	$S_{j,ini}$ (FE)	(EC3)/ (FE)	$M_{j,R}$ (EC3)	$M_{j,R}$ (FE)	(EC3)/ (FE)	M_u (KN.m)	Φ_u (mrad)	(EC3)	(FE)
Model-85	12	8	25	110	284	174	9555	5280	1.81	44.8	66.9	0.67	82.2	78.9	End plate in bending / Mode 1	Bolt failure in tension
Model-86	12	14	25	110	284	174	13093	8245	1.59	63.8	99.8	0.64	104	33.1	Bending of column flange	Bolt failure in tension
Model-87	12	12	25	110	284	174	12399	7612	1.63	62.2	93.4	0.67	99	38.7	Bending of column flange	Bolt failure in tension
Model-88	12	10	25	110	284	174	11313	6822	1.66	57.7	83.2	0.69	90.6	47.9	End plate in bending / Mode 1	Bolt failure in tension
Model-89	12	6	25	110	284	174	6763	4360	1.55	27.5	43.1	0.64	73.9	86.6	End plate in bending / Mode 1	Bolt failure in tension
Model-90	12	8	35	110	284	174	12756	6839	1.87	57.8	78.8	0.73	80.1	40.5	End plate in bending / Mode 1	Bolt failure in tension
Model-91	12	8	30	110	284	174	11194	6216	1.8	51.2	75.4	0.68	79.8	62.4	End plate in bending / Mode 1	Bolt failure in tension
Model-92	12	8	20	110	284	174	7780	5068	1.54	38.6	65.2	0.59	80.8	94.8	End plate in bending / Mode 1	Bolt failure in tension
Model-93	12	8	15	110	284	174	6596	4508	1.46	34.8	54.2	0.64	79.5	116.7	End plate in bending / Mode 1	Bolt failure in tension
Model-94	16	8	25	110	284	174	10350	6226	1.66	44.8	69.2	0.65	82.6	77.9	End plate in bending / Mode 1	Bolt failure in tension
Model-95	14	8	25	110	284	174	10008	6018	1.66	44.8	69.2	0.65	82.6	79.7	End plate in bending / Mode 1	Bolt failure in tension
Model-96	10	8	25	110	284	174	8910	5252	1.7	44.8	65.9	0.68	80.5	82.4	End plate in bending / Mode 1	Bolt failure in tension
Model-97	8	8	25	110	284	174	7908	4694	1.68	38.1	62.5	0.61	75.5	91.38	Bending of column flange	Bolt failure in tension
Model-98	12	8	25	80	269	189	9595	7572	1.27	47.3	88.4	0.54	94.9	57	End plate in bending / Mode 1	Bolt failure in tension
Model-99	12	8	25	140	299	159	8910	4453	2	38.6	58.5	0.66	71.7	95.7	End plate in bending / Mode 1	Bolt failure in tension
Model-100	12	8	25	170	314	144	7908	3491	2.27	34.8	52.5	0.66	63	106.5	End plate in bending / Mode 1	Bolt failure in tension
MEAN									1.70			0.65				
COV									0.13			0.07				

Table 5.13 Summary parametric studies (geometry and results) of TSAC-O-A (Elflah, et al., 2018 a)

Model No	Distances according to Figure 5.1 (mm)					Initial stiffness (KNm/mrad)			Moment Capacity $M_{j,R}$ (kNm)			Maximum (FE)		Predicted failure mode	
	t_c	t_a	e_1	L_1	g	$S_{j,ini}$ (EC3)	$S_{j,ini}$ (FE)	(EC3)/ (FE)	$M_{j,R}$ (EC3)	$M_{j,R}$ (FE)	(EC3)/ (FE)	M_u (KN.m)	Φ_u (mrad)	(EC3)	(FE)
Model-101	12	10	25	100	0	2591	1011	2.56	11.1	21.8	0.51	44.1	170.3	Bending of flange cleat / Mode 1	Bolt failure in tension and shear
Model-102	12	14	25	100	0	3544	1624	2.18	23.7	36.9	0.64	48.8	100	Bolt failure in shear	Bolt failure in tension and shear
Model-103	12	12	25	100	0	3160	1370	2.31	17.3	31.4	0.55	46.3	131.4	Bending of flange cleat / Mode 1	Bolt failure in tension and shear
Model-104	12	8	25	100	0	1807	571	3.17	6.6	11.7	0.56	41.7	210	Bending of flange cleat / Mode 1	Bolt failure in tension and shear
Model-105	12	10	35	100	0	2596	949	2.74	11.1	22.4	0.49	43.6	166.6	Bending of flange cleat / Mode 1	Bolt failure in tension and shear
Model-106	12	10	15	100	0	2564	954	2.69	11.1	20.1	0.55	42.4	165.5	Bending of flange cleat / Mode 1	Bolt failure in tension and shear
Model-107	16	10	25	100	0	2634	1.024	2.57	11.1	22.1	0.5	44.2	166.1	Bending of flange cleat / Mode 1	Bolt failure in tension and shear
Model-108	14	10	25	100	0	2616	1.004	2.61	11.1	21.4	0.52	44	167.8	Bending of flange cleat / Mode 1	Bolt failure in tension and shear
Model-109	10	10	25	100	0	2551	976	2.61	11.1	21.4	0.52	44.4	176.1	Bending of flange cleat / Mode 1	Bolt failure in tension and shear
Model-110	8	10	25	100	0	2477	929	2.67	11.1	19.8	0.56	44.1	190.8	Bending of flange cleat / Mode 1	Bolt failure in tension and shear
Model-111	12	10	25	75	0	2879	1608	1.79	21.6	33.2	0.65	48.8	107.5	Bolt failure in shear	Bolt failure in tension and shear
Model-112	12	10	25	125	0	1796	645	2.78	7.8	14.2	0.55	43.7	230.3	Bending of flange cleat / Mode 1	Bolt failure in tension and shear
Model-113	12	10	25	140	0	1145	461	2.48	6.2	8.9	0.7	42.5	268	Bending of flange cleat / Mode 1	Bolt failure in tension and shear
Model-114	12	10	25	100	3	2591	661	3.92	11.1	21.8	0.51	43.7	169.1	Bending of flange cleat / Mode 1	Bolt failure in tension and shear
Model-115	12	10	25	100	6.5	2019	631	3.2	8.7	17.8	0.49	43.4	173.5	Bending of flange cleat / Mode 1	Bolt failure in tension and shear
Model-116	12	10	25	100	9	2019	598	3.38	8.7	16.4	0.53	42.9	172.1	Bending of flange cleat / Mode 1	Bolt failure in tension and shear
MEAN								2.73			0.55				
COV								0.18			0.11				

Table 5.14 Summary parametric studies (geometry and results) of TSAC-O-L (Elflah, et al., 2018 a)

Model No	Distances according to Figure 5.1 (mm)					Initial stiffness (KNm/mrad)			Moment Capacity $M_{j,R}$ (kNm)			Maximum (FE)		Predicted failure mode	
	t_c	t_a	e_1	L_1	g	$S_{j,ini}$ (EC3)	$S_{j,ini}$ (FE)	(EC3)/ (FE)	$M_{j,R}$ (EC3)	$M_{j,R}$ (FE)	(EC3)/ (FE)	M_u (KN.m)	Φ_u (mrad)	(EC3)	(FE)
Model-117	12	10	25	100	0	2774	1198	2.31	20.3	33.4	0.61	44.3	128.8	Bolt failure in shear	Bolt failure in tension and shear
Model-118	12	14	25	100	0	3826	1821	2.1	23.7	36.5	0.65	50.8	57.6	Bolt failure in shear	Bolt failure in tension and shear
Model-119	12	12	25	100	0	3404	1613	2.11	23.6	37.4	0.63	47.6	84	Bolt failure in shear	Bolt failure in tension and shear
Model-120	12	8	25	100	0	1914	768	2.49	12	17.5	0.69	40.7	175.7	Bending of flange cleat / Mode 1	Bolt failure in tension and shear
Model-121	12	10	35	100	0	2780	1161	2.39	20.3	33.4	0.61	44.2	127.5	Bolt failure in shear	Bolt failure in tension and shear
Model-122	12	10	15	100	0	2744	1202	2.28	20.3	33.4	0.61	43.3	132.1	Bolt failure in shear	Bolt failure in tension and shear
Model-123	16	10	25	100	0	2823	1241	2.27	20.3	34	0.6	44.9	141.8	Bolt failure in shear	Bolt failure in tension and shear
Model-124	14	10	25	100	0	2803	1251	2.24	20.3	34	0.6	44.7	135.6	Bolt failure in shear	Bolt failure in tension and shear
Model-125	10	10	25	100	0	2729	1189	2.29	20.3	33.2	0.61	44.9	136.1	Bolt failure in shear	Bolt failure in tension and shear
Model-126	8	10	25	100	0	2647	1140	2.32	20.3	33	0.61	45.4	157.1	Bolt failure in shear	Bolt failure in tension and shear
Model-127	12	10	25	75	0	3132	1828	1.71	21.6	34.2	0.63	51	70.4	Bolt failure in shear	Bolt failure in tension and shear
Model-128	12	10	25	125	0	1885	820	2.29	14.3	19.1	0.75	43.6	213.6	Bending of flange cleat / Mode 1	Bolt failure in tension and shear
Model-129	12	10	25	140	0	1186	580	2.04	11.4	15.9	0.72	41.3	246.6	Bending of flange cleat / Mode 1	Bolt failure in tension and shear
Model-130	12	10	25	100	3	2774	1162	2.38	20.3	33	0.61	44.4	147.2	Bolt failure in shear	Bolt failure in tension and shear
Model-131	12	10	25	100	6.5	2138	1126	1.89	15.9	29.4	0.54	44.1	149.9	Bending of flange cleat / Mode 1	Bolt failure in tension and shear
Model-132	12	10	25	100	9	2138	1041	2.05	15.9	28.5	0.56	43.5	146.3	Bending of flange cleat / Mode 1	Bolt failure in tension and shear
MEAN								2.2			0.63				
COV								0.09			0.09				

Table 5.15 Summary parametric studies (geometry and results) of TSAC-T- A (Elflah, et al., 2018 a)

Model No	Distances according to Figure 5.4 (mm)					Initial stiffness (KNm/mrad)			Moment Capacity $M_{j,R}$ (kNm)			Maximum (FE)		Predicted failure mode	
	t_c	t_a	e_1	L_1	g	$S_{j,ini}$ (EC3)	$S_{j,ini}$ (FE)	(EC3)/ (FE)	$M_{j,R}$ (EC3)	$M_{j,R}$ (FE)	(EC3)/ (FE)	M_u (KN.m)	Φ_u (mrad)	(EC3)	(FE)
Model-133	10	8	30	100	0	1500	705	2.13	6.6	11	0.6	26.6	129.5	Bending of flange cleat/ Mode1	Bolt failure in tension and shear
Model-134	10	14	30	100	0	2597	1499	1.73	22.7	31	0.73	41.6	78.2	Bending of flange cleat/ Mode1	Bolt failure in tension and shear
Model-135	10	12	30	100	0	2373	1342	1.77	17.3	24.5	0.71	37	86.1	Bending of flange cleat/ Mode1	Bolt failure in tension and shear
Model-136	10	10	30	100	0	2027	1145	1.77	11.1	16	0.69	32.2	108	Bending of flange cleat/ Mode1	Bolt failure in tension and shear
Model-137	10	6	30	100	0	844	468	1.8	3.4	5.5	0.62	24.2	145	Bending of flange cleat/ Mode1	Bolt failure in tension and shear
Model-138	10	8	40	100	0	1500	608	2.47	6.6	11	0.6	25.5	130.5	Bending of flange cleat/ Mode1	Bolt failure in tension and shear
Model-139	10	8	20	100	0	1500	644	2.33	6.6	11	0.6	24.9	125	Bending of flange cleat/ Mode1	Bolt failure in tension and shear
Model-140	14	8	30	100	0	1785	708	2.52	6.6	11.5	0.57	26	123.7	Bending of flange cleat/ Mode1	Bolt failure in tension and shear
Model-141	12	8	30	100	0	1679	677	2.48	6.6	11.5	0.57	26.6	129.4	Bending of flange cleat/ Mode1	Bolt failure in tension and shear
Model-142	8	8	30	100	0	1205	590	2.04	6.6	11.5	0.57	25.5	130.3	Bending of flange cleat/ Mode1	Bolt failure in tension and shear
Model-143	6	8	30	100	0	770	479	1.61	6.6	10	0.66	23.3	137	Bending of flange cleat/ Mode1	Bolt failure in tension and shear
Model-144	10	8	30	75	0	1876	1250	1.5	11.9	17	0.7	30.8	72.3	Bending of flange cleat/ Mode1	Bolt failure in tension and shear
Model-145	10	8	30	125	0	937	550	1.7	4.8	6.5	0.74	24.7	178.7	Bending of flange cleat/ Mode1	Bolt failure in tension and shear
Model-146	10	8	30	140	0	570	378	1.51	3.8	5.5	0.69	21	210	Bending of flange cleat/ Mode1	Bolt failure in tension and shear
Model-147	10	8	30	100	3	1500	606	2.48	6.6	11	0.6	25.2	134.9	Bending of flange cleat/ Mode1	Bolt failure in tension and shear
Model-148	10	8	30	100	6.5	1500	579	2.59	6.6	10.2	0.65	24.7	134.1	Bending of flange cleat/ Mode1	Bolt failure in tension and shear
Model-149	10	8	30	100	9	1500	514	2.92	6.6	9.5	0.69	24.2	135.4	Bending of flange cleat/ Mode1	Bolt failure in tension and shear
MEAN								2.08			0.65				
COV								0.21			0.09				

Table 5.16 Summary parametric studies (geometry and results) of TSAC-T- L (Elflah, et al., 2018 a)

Model No	Distances according to Figure 5.4 (mm)					Initial stiffness (KNm/mrad)			Moment Capacity $M_{j,R}$ (kNm)			Maximum (FE)		Predicted failure mode	
	t_c	t_a	e_1	L_1	g	$S_{j,ini}$ (EC3)	$S_{j,ini}$ (FE)	(EC3)/ (FE)	$M_{j,R}$ (EC3)	$M_{j,R}$ (FE)	(EC3)/ (FE)	M_u (KN.m)	Φ_u (mrad)	(EC3)	(FE)
Model-150	10	8	30	100	0	1593	760	2.1	12	16	0.75	27.3	98.2	Bending of flange cleat/ Mode1	Bolt failure in tension and shear
Model-151	10	14	30	100	0	2793	1580	1.77	23.7	35	0.68	45.2	57	Bending of flange cleat/ Mode1	Bolt failure in tension and shear
Model-152	10	12	30	100	0	2549	1446	1.76	23.6	31	0.76	42.3	65.4	Bending of flange cleat/ Mode1	Bolt failure in tension and shear
Model-153	10	10	30	100	0	2169	1238	1.75	20.3	26	0.78	35.4	82.6	Bending of flange cleat/ Mode1	Bolt failure in tension and shear
Model-154	10	6	30	100	0	844	513	1.72	6.3	10	0.63	22.7	119.1	Bending of flange cleat/ Mode1	Bolt failure in tension and shear
Model-155	10	8	40	100	0	1593	875	1.82	12	15.5	0.77	27.1	108.9	Bending of flange cleat/ Mode1	Bolt failure in tension and shear
Model-156	10	8	20	100	0	1593	875	1.82	12	15.5	0.77	26.4	102	Bending of flange cleat/ Mode1	Bolt failure in tension and shear
Model-157	14	8	30	100	0	1911	851	2.25	12	16	0.75	27	100.5	Bending of flange cleat/ Mode1	Bolt failure in tension and shear
Model-158	12	8	30	100	0	1792	826	2.11	12	16	0.75	26.8	101.8	Bending of flange cleat/ Mode1	Bolt failure in tension and shear
Model-159	8	8	30	100	0	1269	691	1.54	12	15.6	0.77	25.5	100	Bending of flange cleat/ Mode1	Bolt failure in tension and shear
Model-160	6	8	30	100	0	801	563	1.42	12	14.5	0.83	25.5	114.2	Bending of flange cleat/ Mode1	Bolt failure in tension and shear
Model-161	10	8	30	75	0	2032	1251	1.62	21.5	27	0.8	33.8	57.6	Bending of flange cleat/ Mode1	Bolt failure in tension and shear
Model-162	10	8	30	125	0	976	566	1.72	8.7	11	0.79	24.5	153.7	Bending of flange cleat/ Mode1	Bolt failure in tension and shear
Model-163	10	8	30	140	0	587	344	1.71	7	9	0.78	25.7	202.4	Bending of flange cleat/ Mode1	Bolt failure in tension and shear
Model-164	10	8	30	100	3	1593	750	2.12	12	17	0.71	24.8	104.7	Bending of flange cleat/ Mode1	Bolt failure in tension and shear
Model-165	10	8	30	100	6.5	1593	750	2.12	12	15	0.8	24.3	106.2	Bending of flange cleat/ Mode1	Bolt failure in tension and shear
Model-166	10	8	30	100	9	1593	750	2.12	12	14	0.86	24.3	105.4	Bending of flange cleat/ Mode1	Bolt failure in tension and shear
MEAN								2.08				0.65			
COV								0.21				0.09			

Table 5.17 Summary parametric studies (geometry and results) of TSWAC-O- A (Elflah, et al., 2018 a)

Model No	Distances according to Figure 5.1 (mm)							Initial stiffness (KNm/mrad)			Moment Capacity $M_{j,R}$ (kNm)			Maximum (FE)		Predicted failure mode	
	t_c	t_a	e_1	e_2	L_1	L_2	g	$S_{j,ini}$ (EC3)	$S_{j,ini}$ (FE)	(EC3)/ (FE)	$M_{j,R}$ (EC3)	$M_{j,R}$ (FE)	(EC3)/ (FE)	M_u (KN.m)	Φ_u (mrad)	(EC3)	(FE)
Model-167	12	10	25	25	100	60	0	6140	2879	2.13	30.3	53.2	0.57	75	87.7	Angle cleat bending / Mode 1	Web bolt failure in shear
Model-168	12	14	25	25	100	60	0	7368	3680	2	55.8	67.3	0.8	91.1	81.6	Bending of column flange	Web bolt failure in shear
Model-169	12	12	25	25	100	60	0	6855	3179	2.16	47.3	59.5	0.8	83.5	85.2	Bending of column flange	Web bolt failure in shear
Model-170	12	8	25	25	100	60	0	4673	2390	1.96	16.7	41.6	0.41	63.4	95.5	Angle cleat bending / Mode 1	Bolt failure in tension and shear
Model-172	12	10	25	30	100	60	0	5636	2673	2.11	26	53.5	0.49	75.1	79.6	Angle cleat bending / Mode 1	Web bolt failure in double shear
Model-173	12	10	25	20	100	60	0	6308	2915	2.16	38.2	47.8	0.81	83.5	85.2	Bolt failure in shear	Web bolt failure in double shear
Model-174	16	10	25	25	100	60	0	6260	2673	2.34	30.3	55.97	0.55	75.9	85.1	Angle cleat bending / Mode 1	Web bolt failure in double shear
Model-175	14	10	25	25	100	60	0	6174	2917	2.12	30.3	55.7	0.55	74.8	84.3	Angle cleat bending / Mode 1	Web bolt failure in double shear
Model-176	10	10	25	25	100	60	0	5761	2867	2.01	30.3	45.4	0.67	75.7	100.6	Bending of column flange	Web bolt failure in double shear
Model-177	8	10	25	25	100	60	0	5257	2668	1.97	28.7	49.8	0.59	72.1	107.8	Bending of column flange	Web bolt failure in double shear
Model-178	12	10	25	25	75	60	0	5284	4009	1.32	38.8	62.9	0.63	84	72.1	Bending of column flange	Web bolt failure in double shear
Model-179	12	10	25	25	125	60	0	6455	2398	2.69	29.5	47.5	0.63	65.6	91.6	Angle cleat bending / Mode 1	Web bolt failure in double shear
Model-180	12	10	25	25	140	60	0	7192	2259	3.18	30.4	43.8	0.71	61.7	96.5	Angle cleat bending / Mode 1	Web bolt failure in double shear
Model-181	12	10	25	25	100	60	3	6026	2854	2.11	30.3	49.9	0.62	74.5	76.7	Angle cleat bending / Mode 1	Web bolt failure in double shear
Model-182	12	10	25	25	100	60	6.5	4665	2747	1.7	19.7	39.7	0.51	49.9	43.9	Angle cleat bending / Mode 1	Bottom bolt failure in shear
Model-183	12	10	25	25	100	60	9	4665	2647	1.76	19.7	39.9	0.51	50.5	52.7	Angle cleat bending / Mode 1	Bottom bolt failure in shear
MEAN										2.11			0.61				
COV										0.19			0.19				

Table 5.18 Summary parametric studies (geometry and results) of TSWAC-O- L (Elflah, et al., 2018 a)

Model No	Distances according to Figure 5.1 (mm)							Initial stiffness (KNm/mrad)			Moment Capacity $M_{j,R}$ (kNm)			Maximum (FE)		Predicted failure mode	
	t_c	t_a	e_1	e_2	L_1	L_2	g	$S_{j,ini}$ (EC3)	$S_{j,ini}$ (FE)	(EC3)/ (FE)	$M_{j,R}$ (EC3)	$M_{j,R}$ (FE)	(EC3)/ (FE)	M_u (KN.m)	Φ_u (mrad)	(EC3)	(FE)
Model-184	12	10	25	25	100	60	0	6628	2952	2.25	50.18	60.8	0.83	78.7	73.1	Angle cleat bending / Mode 1	Web bolt failure in shear
Model-185	12	14	25	25	100	60	0	8136	3435	2.37	80.8	78.4	1.03	92.1	68.8	Bending of column flange	Web bolt failure in shear
Model-186	12	12	25	25	100	60	0	7561	3202	2.36	66	71.9	0.92	87.1	70.4	Bending of column flange	Web bolt failure in shear
Model-187	12	8	25	25	100	60	0	5102	2476	2.06	29.6	51.5	0.57	68.7	78.6	Angle cleat bending / Mode 1	Bolt failure in tension and shear
Model-189	12	10	25	30	100	60	0	6175	2968	2.08	46.1	68.4	0.67	76.6	62.7	Angle cleat bending / Mode 1	Web bolt failure in shear
Model-190	12	10	25	20	100	60	0	6958	2760	2.52	52.3	56.8	0.92	81.2	81.7	Angle cleat bending / Mode 1	Web bolt failure in shear
Model-191	16	10	25	25	100	60	0	6900	3020	2.28	50.2	71.4	0.7	79.1	64.9	Angle cleat bending / Mode 1	Web bolt failure in shear
Model-192	14	10	25	25	100	60	0	6800	2922	2.33	50.2	69.4	0.72	79	68.7	Angle cleat bending / Mode 1	Web bolt failure in shear
Model-193	10	10	25	25	100	60	0	6319	2731	2.31	50.2	53.7	0.93	77.5	83.5	Bending of column flange	Web bolt failure in shear
Model-194	8	10	25	25	100	60	0	5740	2516	2.28	49.1	49.8	0.99	71.7	87.3	Bending of column flange	Web bolt failure in shear
Model-195	12	10	25	25	75	60	0	5845	3903	1.5	65.6	68.8	0.95	59.7	86.4	Bending of column flange	Web bolt failure in shear
Model-196	12	10	25	25	125	60	0	7080	2376	2.98	48.4	53.1	0.91	71.3	80.4	Angle cleat bending / Mode 1	Web bolt failure in shear
Model-197	12	10	25	25	140	60	0	7903	2250	3.51	49.6	53.9	0.92	69.2	85	Angle cleat bending / Mode 1	Web bolt failure in shear
Model-198	12	10	25	25	100	60	3	6628	2924	2.27	50.2	53.8	0.93	75.3	57.9	Angle cleat bending / Mode 1	Web bolt failure in shear
Model-199	12	10	25	25	100	60	6.5	5069	2821	1.8	34.8	43.7	0.8	53.7	37.9	Angle cleat bending / Mode 1	Bottom bolt failure in shear
Model-200	12	10	25	25	100	60	9	5069	2747	1.85	34.8	43.5	0.8	53.4	43.2	Angle cleat bending / Mode 1	Bottom bolt failure in shear
MEAN										2.3			0.85				
COV										0.2			0.15				

Table 5.19 Summary parametric studies (geometry and results) of TSWAC-T- A (Elflah, et al., 2018 a)

Model No	Distances according to Figure 5.4 (mm)						Initial stiffness (KNm/mrad)			Moment Capacity $M_{j,R}$ (kNm)			Maximum (FE)		Predicted failure mode	
	t_c	t_a	e_1	e_2	L_1	L_2	$S_{j,ini}$ (EC3)	$S_{j,ini}$ (FE)	(EC3)/ (FE)	$M_{j,R}$ (EC3)	$M_{j,R}$ (FE)	(EC3)/ (FE)	M_u (KN.m)	Φ_u (mrad)	(EC3)	(FE)
Model-201	10	8	30	35	65	100	3161 a	1421	2.22	13.2	20	0.66	57.6	116.7	Bending of flange cleat/ Mode1	Bolt failure in tension and shear
Model-202	10	12	30	35	65	100	4288 a	1997	2.15	38.7b	45	0.86	75.5	102	-	Bolt failure in tension and shear
Model-203	10	10	30	35	65	100	3860 a	1882	2.05	24.1	35	0.69	68.5	111.2	Bending of flange cleat/ Mode1	Bolt failure in tension and shear
Model-204	10	6	30	35	65	100	2088 a	1284	1.63	6.5	12	0.55	53.2	130.9	Bending of flange cleat/ Mode1	Bolt failure in tension and shear
Model-205	10	8	30	40	65	100	3268 a	1405	2.33	15.8	21	0.75	58.1	112.2	Bending of flange cleat/ Mode1	Bolt failure in tension and shear
Model-206	10	8	30	30	65	100	3012 a	1424	2.12	11.7	18	0.65	55.2	121	Bending of flange cleat/ Mode1	Bolt failure in tension and shear
Model-207	14	8	30	35	65	100	4328 a	1899	2.28	13.2	21	0.63	57.7	108.5	Bending of flange cleat/ Mode1	Bolt failure in tension and shear
Model-208	12	8	30	35	65	100	3842 a	1757	2.19	13.2	21	0.63	59	115.1	Bending of flange cleat/ Mode1	Bolt failure in tension and shear
Model-209	8	8	30	35	65	100	2283 a	1304	1.75	13.2	22	0.6	56.7	122.9	Bending of flange cleat/ Mode1	Bolt failure in tension and shear
Model-210	6	8	30	35	65	100	1306 a	1064	1.23	13.2	25	0.53	50.7	146.3	Bending of flange cleat/ Mode1	Bolt failure in tension and shear
Model-211	10	8	30	35	65	75	3398 a	2108	1.61	16.4	25	0.66	55.2	83.3	Bending of flange cleat/ Mode1	Bolt failure in tension and shear
Model-212	10	8	30	35	65	125	3048 a	1204	2.53	12.9	19	0.68	50.9	116.8	Bending of flange cleat/ Mode1	Bolt failure in tension and shear
Model-213	10	8	30	35	65	140	3175 a	1204	2.64	13.2	18	0.73	47.2	116.2	Bending of flange cleat/ Mode1	Bolt failure in tension and shear
MEAN									2.05			0.66				
COV									0.19			0.13				

Table 5.20 Summary parametric studies (geometry and results) of TSWAC-T- L (Elflah, et al., 2018 a)

Model No	Distances according to Figure 5.4 (mm)						Initial stiffness (KNm/mrad)			Moment Capacity $M_{j,R}$ (kNm)			Maximum (FE)		Predicted failure mode	
	t_c	t_a	e_1	e_2	L_1	L_2	$S_{j,ini}$ (EC3)	$S_{j,ini}$ (FE)	(EC3)/ (FE)	$M_{j,R}$ (EC3)	$M_{j,R}$ (FE)	(EC3)/ (FE)	M_u (KN.m)	Φ_u (mrad)	(EC3)	(FE)
Model-215	10	8	30	35	65	100	3353	1474	2.27	27.1	33	0.82	61.0	98.9	Bending of flange cleat/ Mode1	Bolt failure in tension and shear
Model-216	10	12	30	35	65	100	4583	2006	2.28	62.1	50	1.24	74.9	74.8	-	Bolt failure in tension and shear
Model-217	10	10	30	35	65	100	4116	1840	2.24	48.1	42	1.14	69.2	81.6	Bending of flange cleat/ Mode1	Bolt failure in tension and shear
Model-218	10	6	30	35	65	100	2192	1337	1.64	13.4	20	0.67	56.7	116.6	Bending of flange cleat/ Mode1	Bolt failure in tension and shear
Model-219	10	8	30	40	65	100	3471	1437	2.42	32.4	34	0.95	62.3	99.5	Bending of flange cleat/ Mode1	Bolt failure in tension and shear
Model-220	10	8	30	30	65	100	3190	1493	2.14	23.8	28	0.85	63.4	116.0	Bending of flange cleat/ Mode1	Bolt failure in tension and shear
Model-221	14	8	30	35	65	100	4661	1929	2.42	27.1	30	0.90	62.7	96.2	Bending of flange cleat/ Mode1	Bolt failure in tension and shear
Model-222	12	8	30	35	65	100	4111	1744	2.36	27.1	30	0.90	61.5	96.1	Bending of flange cleat/ Mode1	Bolt failure in tension and shear
Model-223	8	8	30	35	65	100	2396	1351	1.77	27.1	32	0.85	59.8	102.1	Bending of flange cleat/ Mode1	Bolt failure in tension and shear
Model-224	6	8	30	35	65	100	1355	1099	1.23	27.1	33	0.82	57.3	122.0	Bending of flange cleat/ Mode1	Bolt failure in tension and shear
Model-225	10	8	30	35	65	75	3276	2015	1.63	33.5	40	0.84	62.4	80.1	Bending of flange cleat/ Mode1	Bolt failure in tension and shear
Model-226	10	8	30	35	65	125	3345	1302	2.57	26.3	27	0.98	58.4	109.5	Bending of flange cleat/ Mode1	Bolt failure in tension and shear
Model-227	10	8	30	35	65	140	3648	1340	2.72	27.1	26	1.04	54.5	108.9	Bending of flange cleat/ Mode1	Bolt failure in tension and shear
MEAN									2.13			0.92				
COV									0.20			0.16				

5.5 Results and discussion

5.5.1 Flush end plate (FEP) connections

The geometry of the simulated joints and the obtained results are reported in Tables 5.7 to 5.10 for the models employing austenitic (FEP-O-A and FEP-T-A) and lean duplex (FEP-O-L and FEP-T-L) material properties respectively. Figures 5.19 and 5.21 depict the obtained moment-rotation (M-Φ) curves of the modelled FEP-O-A and FEP-T-A joints for different end plate thicknesses tp (Figures 5.18 (a) and 5.20 (a)), edge plate distances e_1 (Figures 5.18 (b) and 5.20 (b)), column flange thicknesses t_c (Figures 5.18 (c) and 5.20 (c)) and distances of the top bolt row from the centroid of the compression beam flange z (Figures 5.18 (d) and 5.20 (d)). As expected, increasing the lever arm z, or increasing the edge distance e_1, leads to a marked increase of both the strength and the stiffness of the connections. Increasing the end plate thickness t_p also increases the strength and the stiffness of the FEP-O-A and FEP-T-A joints by increasing the resistance of the equivalent T-stub (Zoetemeijer, 1974). However, the effect is less pronounced as increasing the end plate thickness beyond a certain value (beyond 12 mm for the parameter range considered herein, as shown in Figures 5.18 (a) and 5.20 (a)), shifts the failure mode to the column flange, which becomes the weakest component of the connection. Similarly, increasing the column flange thickness t_f beyond 12 mm has a limited effect on the strength and stiffness as the end plate is already the weakest component of the joint, whilst decreasing it more drastically affects the joint response, by shifting the failure mode from “end plate in bending” to “column flange in bending”. In all cases, an increase in strength is accompanied by a corresponding decrease in the rotation at which the ultimate moment occurs (Elflah, et al., 2018 a)

Similar observations can be made for the lean duplex models FEP-O-L and FEP-T-L, the response of which is shown in Figures 5.19 and 5.21. Comparing the response of the models with different materials, it can be concluded that the lean duplex joints exhibit

higher strength but lower ductility compared to their austenitic stainless steel counterparts. This can be attributed to the increased strength of the various components due to the higher material proof stresses. Since lean duplex stainless steel reaches higher stresses at lower strains compared to austenitic stainless steel, the rotation at which the bolt force capacity is reached decreases, hence, bolt failure and overall joint failure is triggered at smaller rotations. Similar observations were made in (Girão Coelho et al., 2004a), where geometrically identical T-stubs were experimentally verified to have higher resistance and lower deformation capacity for higher steel grades (Elflah, et al., 2018 a).

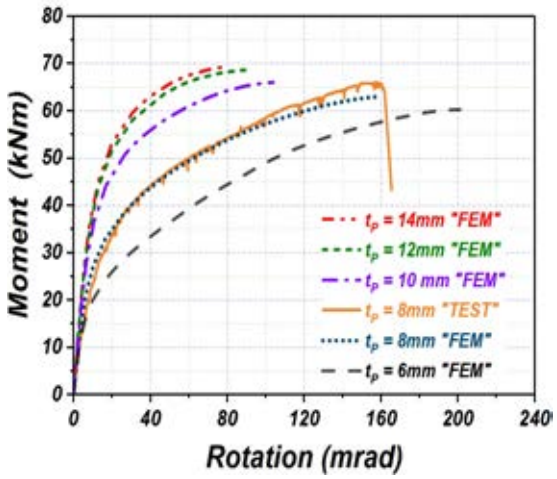

(a) M-Φ curves for different plate thicknesses t_p

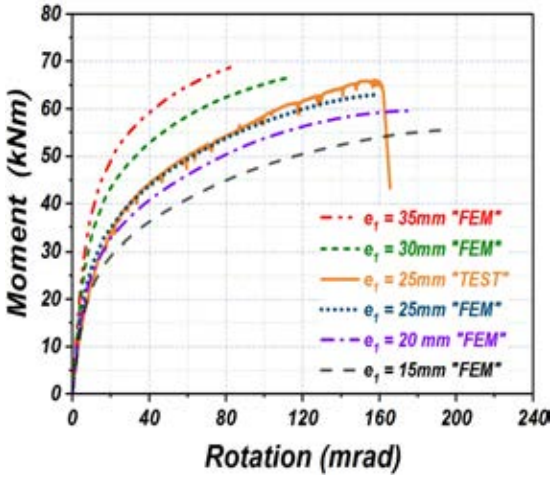

(b) M-Φcurves for different bolt edge distances e_1

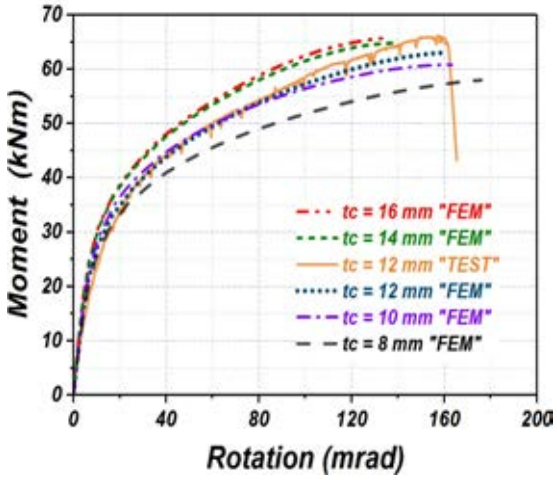

(c) M-Φ curves for different column flange thicknesses t_c

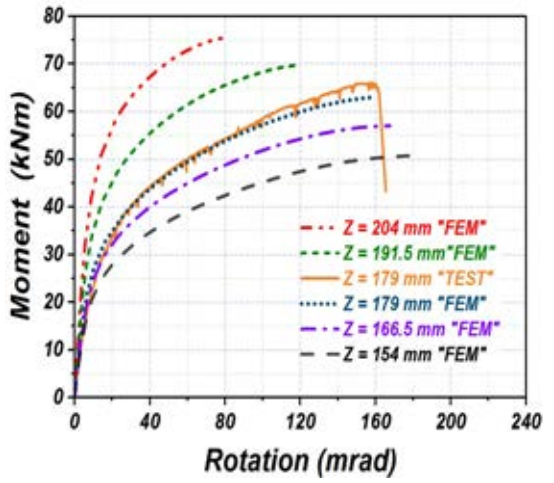

(d) M-Φ curves for different values of the lever arm z

Figure 5.18 Parametric study for FEP-O-A connections (Elflah, et al., 2018 a)

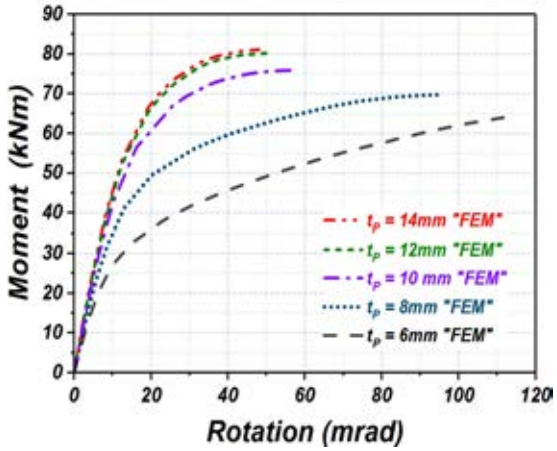

(a) M-Φ curves for different plate thicknesses t_p

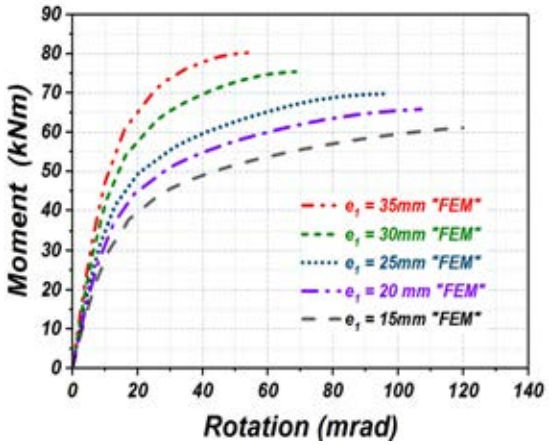

(b) M-Φcurves for different bolt edge distances e_1

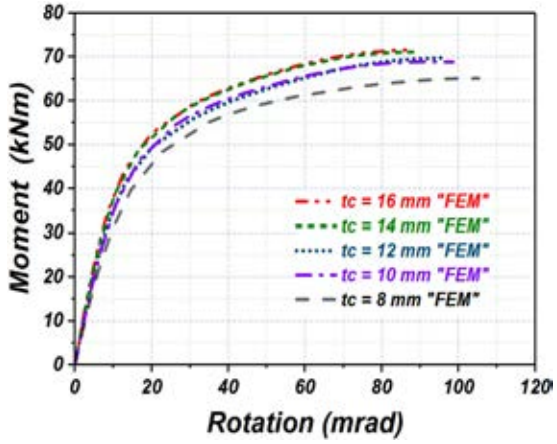

(c) M-Φ curves for different column flange thicknesses t_c

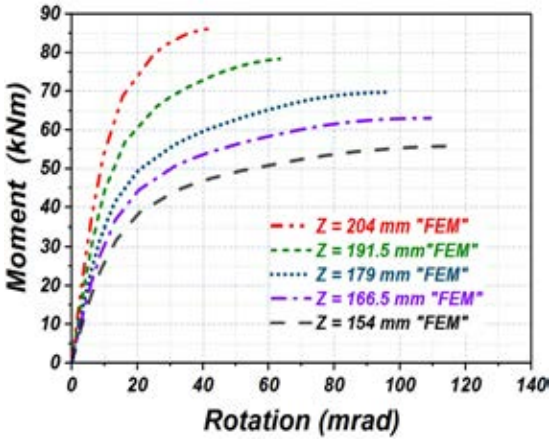

(d) M-Φ curves for different values of the lever arm z

Figure 5.19 Parametric study for FEP-O -L connections (Elflah, et al., 2018 a)

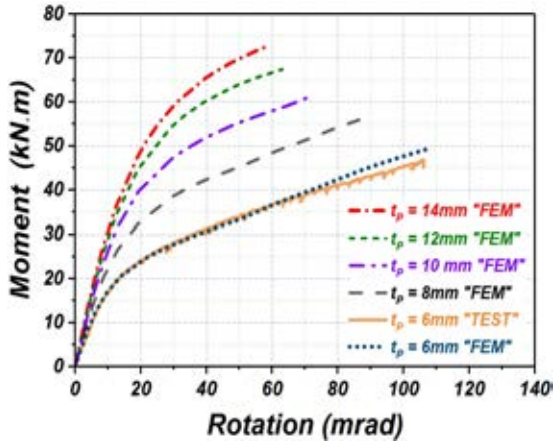

(a) M-Φ curves for different plate thicknesses t_p

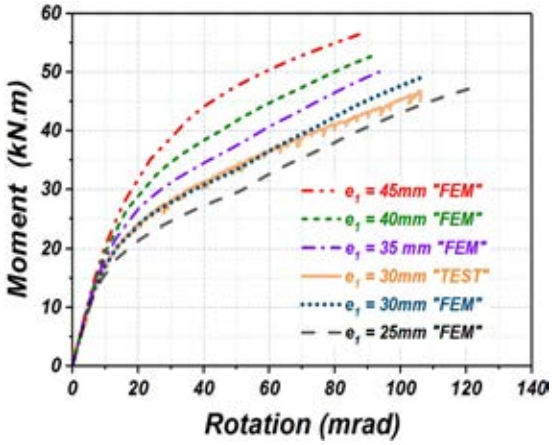

(b) M-Φcurves for different bolt edge distances e_1

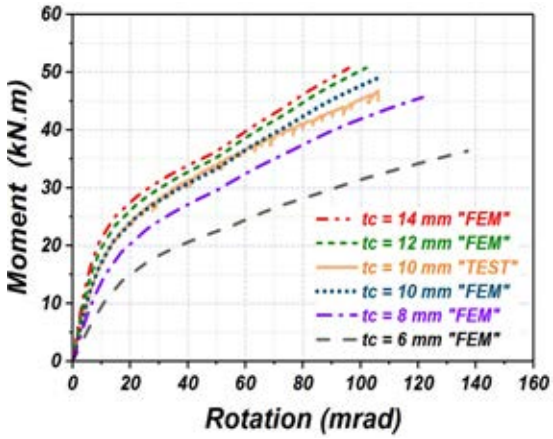

(c) M-Φ curves for different column flange thicknesses t_c

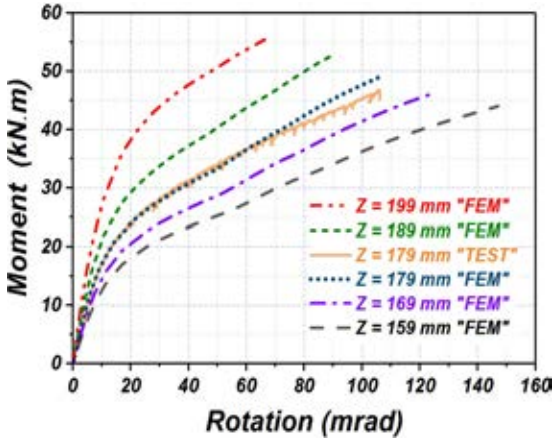

(d) M-Φ curves for different values of the lever arm z

Figure 5.20 Parametric study for FEP-T -A connections

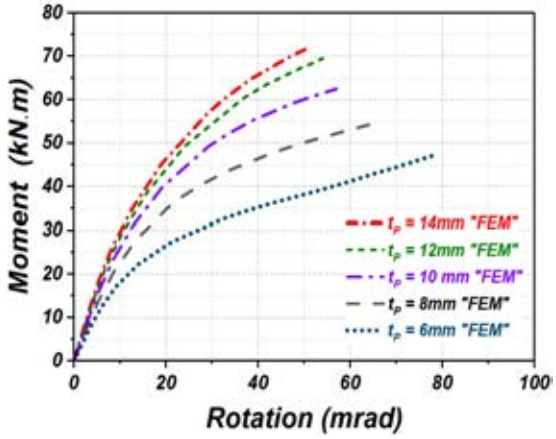

(a) M-Φ curves for different plate thicknesses t_p

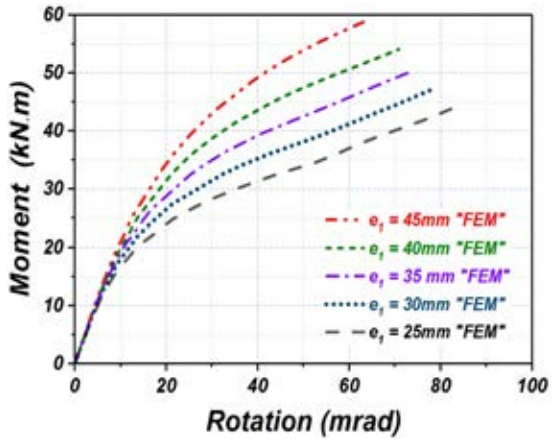

(b) M-Φcurves for different bolt edge distances e_1

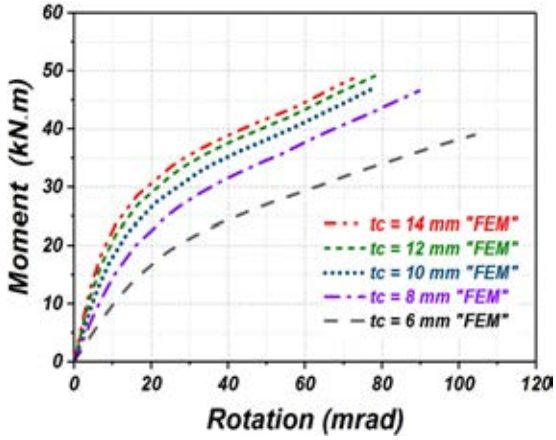

(c) M-Φ curves for different column flange thicknesses t_c

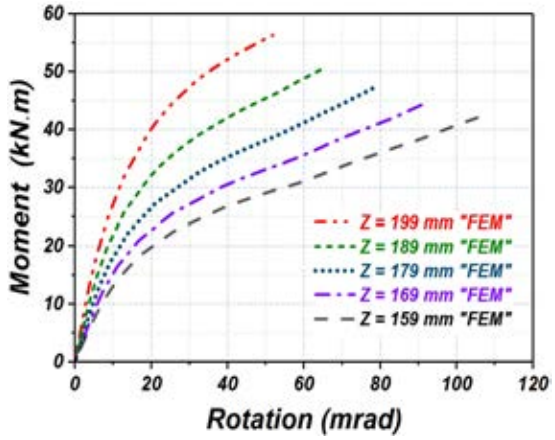

(d) M-Φ curves for different values of the lever arm z

Figure 5.21 Parametric study for FEP-T -L connections

5.5.2 Extended end plate (EEP) connections

The geometry of the simulated joints and the obtained results are reported in Tables 5.11 and 5.12 for the models employing austenitic (EEP-O-A) and lean duplex (EEP-O-L) material properties respectively. Figures 5.22 and 5.23 display the M-Φ response of the modelled joints for various geometric configurations. In general, the same remarks made for the FEP-O connections apply, as increasing the plate thickness, increasing the edge distance and decreasing bolt distance from the compression flange of the beam lead to enhanced strength and stiffness but reduced ductility, whilst the effect of the flange thickness is less pronounced. Moreover, the lean duplex stainless steel joints (EEP-O-L) display higher strength but lower ductility compared to geometrically identical joint in austenitic stainless steel (EEP-O-A) as previously discussed (Elflah, et al., 2018 a).

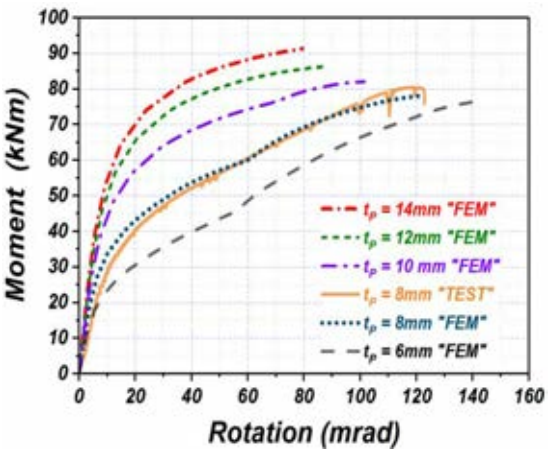

(a) M-Φ curves for different plate thicknesses t_p

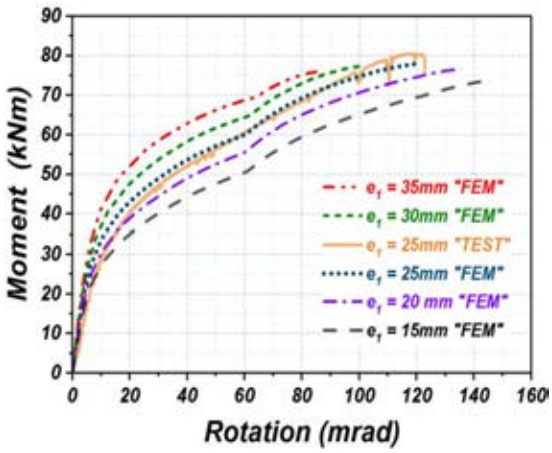

(b) M-Φcurves for different bolt edge distances e_1

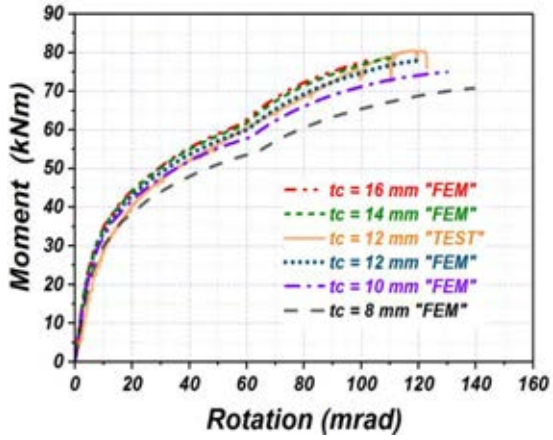

(c) M-Φ curves for different column flange thicknesses t_c

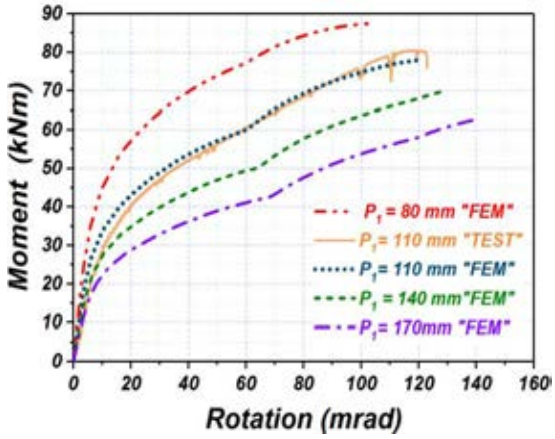

(d) M-Φ curves for different spacing of the first bolt row p_1

Figure 5.22 Parametric study of EEP-O-A connections (Elflah, et al., 2018 a)

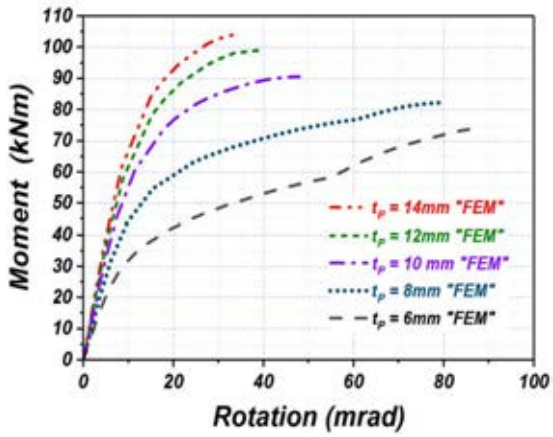

(a) M-Φ curves for different plate thicknesses t_p

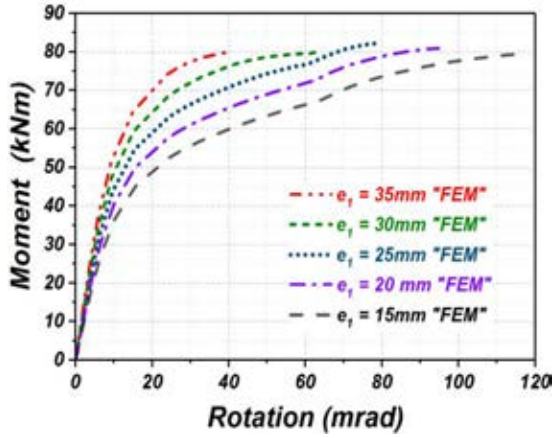

(b) M-Φcurves for different bolt edge distances e_1

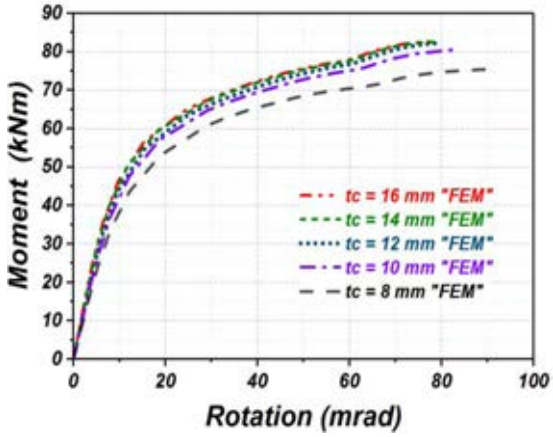

(c) M-Φ curves for different column flange thicknesses t_c

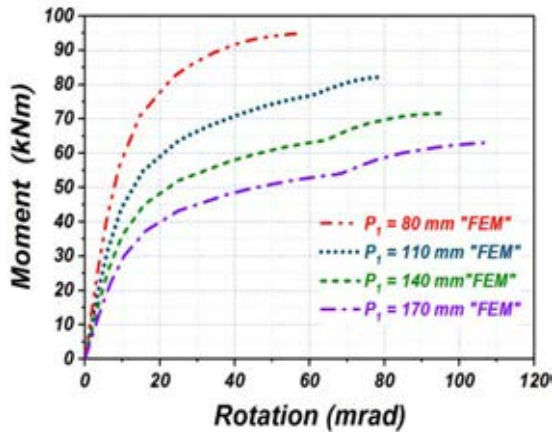

(d) M-Φ curves for different spacing of the first bolt row p_1

Figure 5.23 Parametric study of EEP-O-L connections
Parametric study of EEP-O-L connections (Elflah, et al., 2018 a)

5.5.3 Top and seat angle cleat (TSAC) connections

The geometry of the simulated joints and the obtained results are reported in Tables 5.13 to 5.16 for the models employing austenitic (TSAC-O-A and TSAC-T-A) and lean duplex (TSAC-O-L and TSAC-T-L) material properties respectively. Figures 5.25 to 5.28 depict the effect of the investigated parameters on the joint M-Φ response. From Figures 5.25 (a) and 5.27 (a) it can be observed that increasing the angle thickness significantly enhances both the strength and the stiffness of the TSAC joints, but leads to a drop in the rotation at ultimate moment $\Phi_{j,u}$, since the thicker and hence stiffer angles transfer a higher tensile force and cause bolt failure at smaller deformations compared to the thin ones. This can be clearly observed in Figure 5.24, where the failure modes of two TSAC-O joints with different angle thicknesses are shown. Both joints ultimately fail by tensile fracture of the bolts connecting the top angle cleat to the column face. However, the joint with the thicker angle cleat transmits high tensile forces to the top bolts at relatively small rotations, whereas the thinner angle cleat (t_a=8 mm) undergoes significant inelastic bending of the top angle cleat, which is almost flattened prior to causing bolt fracture. The effect of flattening due to large inelastic bending of the top cleat is shown in the lower curve of Figure 5.25 (a), where an increase of the joint stiffness can be observed at large rotations, arguably due to the angle cleat transmitting forces primarily in tension instead of bending. Similarly to the angle cleat thickness, the length L_1 of the angle cleat leg parallel to the column flange also has a marked effect on the response, with increasing leg lengths leading to smaller angle cleat resistances and hence smaller moment capacities and more flexible response (Elflah, et al., 2018 a).

On the other hand changing the column flange/face thickness t_c does not have any noticeable effect on the joint response as shown in Figure 5.25 (c), since the column flange/face remains significantly stiffer and stronger than the angle cleat for the range of parameters considered for the open section (Elflah, et al., 2018 a). However, for the TSAC-T-A joints, which employ a thin tubular column (t_c=6 mm) changing the angle

cleat thickness shifts the failure mode from the cleat to the column face, thus resulting in different response. The effect of bolt edge distance e_1 (Figures 5.25 (d) and 5.27 (d)) is negligible since, contrary to the end plate connections, the edge distance does not affect the effective leg of the equivalent T-stub, which is in agreement with the design provisions of EN 1993-1-8(2005) (Elflah, et al., 2018 a).

Finally the effect of the gap g between the beam and the column does not seem to have significant influence on the joint response for the range of parameters considered, with decreasing gap leading to slightly stiffer response. This is because in all cases considered herein, bending of the top cleat dominates the response. Similar observations can be made for TSAC-O-L and TSAC-T-L joints, as shown in Figures 5.26 and 5.28. As before, the increase in the nominal yield strength leads to higher moments and stiffer response but reduced ductility (Elflah, et al., 2018 a).

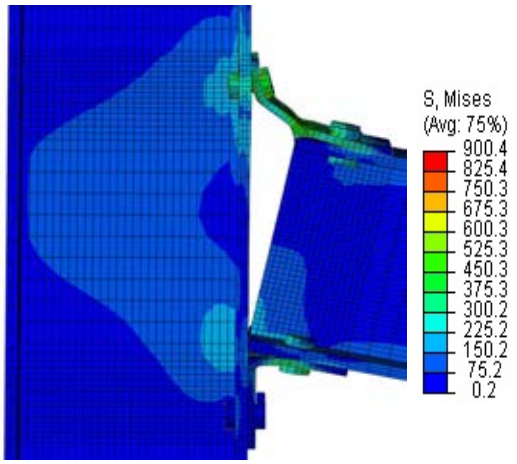

(a) TSAC-O-A (ta = 8mm) (Stress is Von-Mises (MPa))

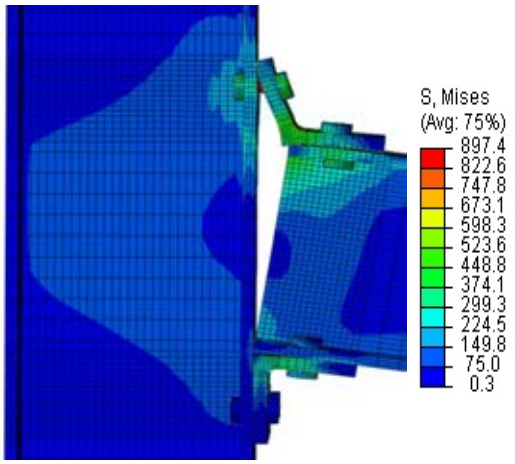

(b) TSAC-O-A (ta = 14 mm) (Stress is Von-Mises (MPa))

Figure 5.24 Failure modes of TSAC joints with different angle thicknesses

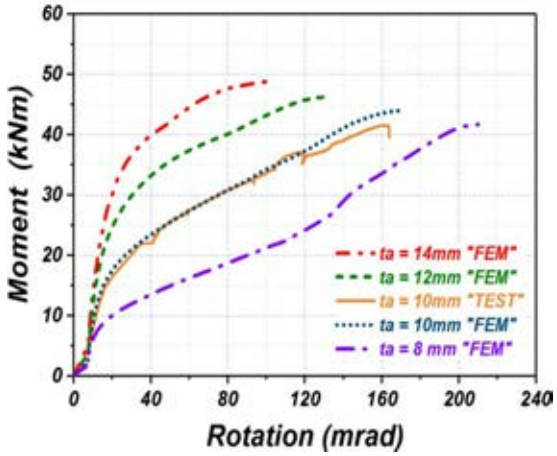

(a) M-Φ curves for different angle cleat thicknesses t_a

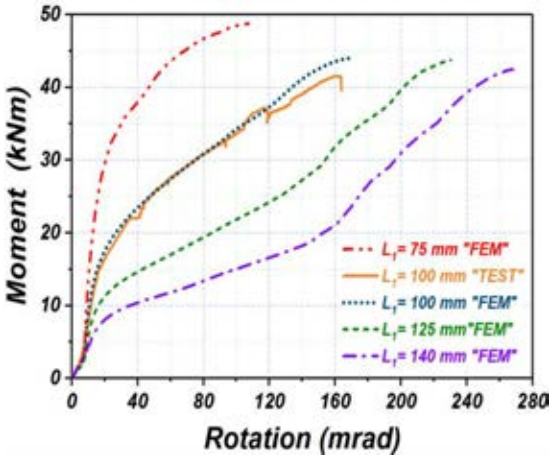

(b) M-Φ curves for different lengths L_1 of the connected angle cleats

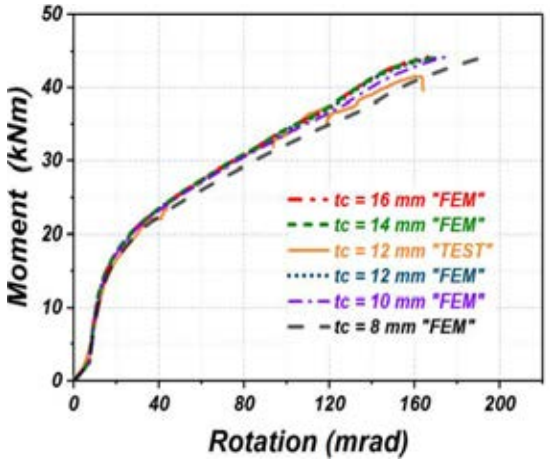

(c) M-Φ curves for different column flange thicknesses t_c

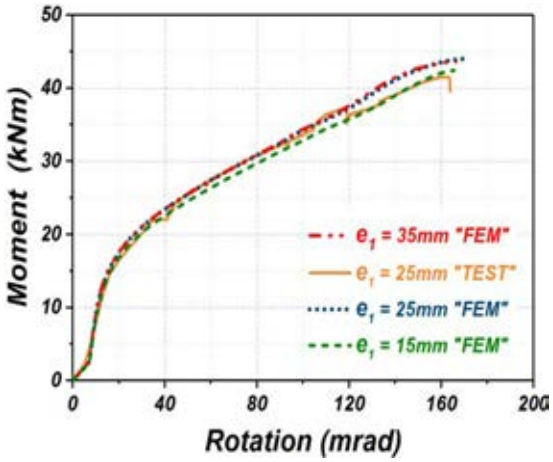

(d) M-Φ curves for different bolt edge distances e_1

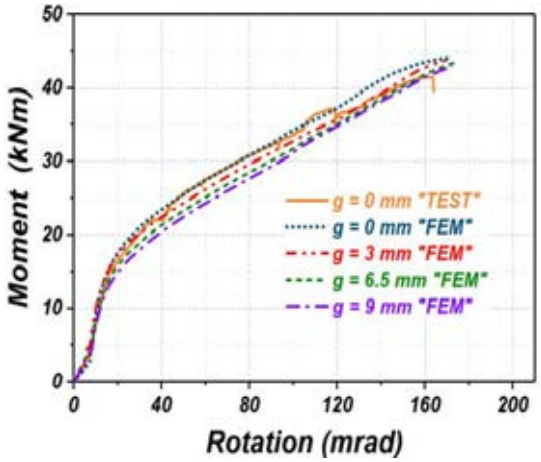

(e) M-Φ curves for different gap distances g between the beam and the column

Figure 5.25 Parametric study of TSAC-O-A connections (Elflah, et al., 2018 a)

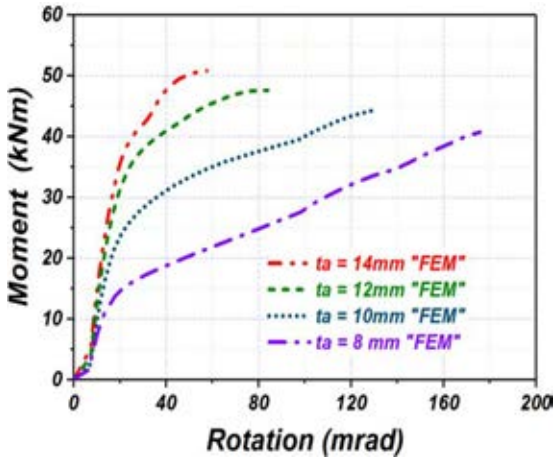

(a) M-Φ curves for different angle cleat thicknesses t_a

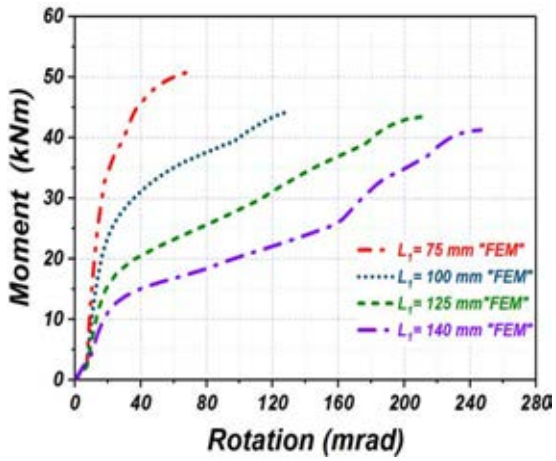

(b) M-Φ curves for different lengths L_1 of the connected angle cleats

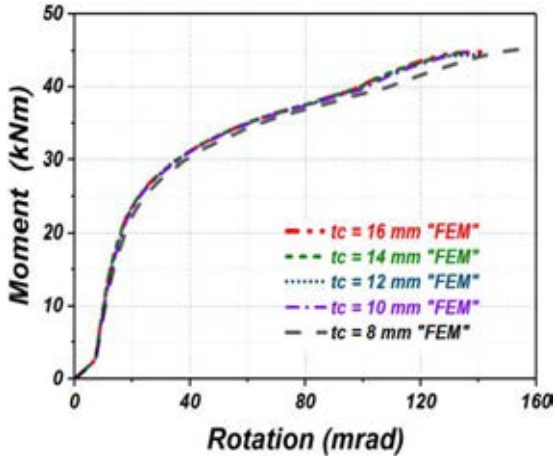

(c) M-Φ curves for different column flange thicknesses t_c

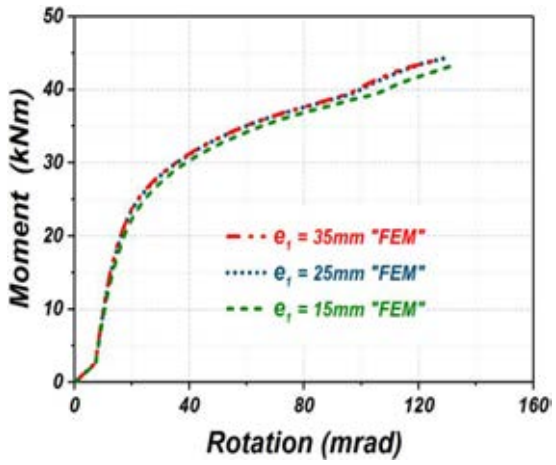

(d) M-Φ curves for different bolt edge distances e_1

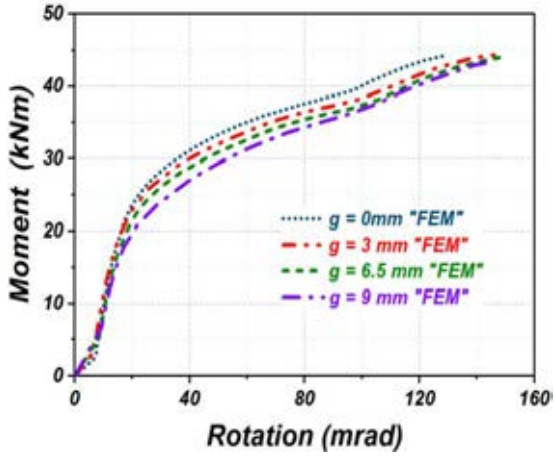

(e) M-Φ curves for different gap distances g between the beam and the column

Figure 5.26 Parametric study of TSAC-O-L connections (Elflah, et al., 2018 a).

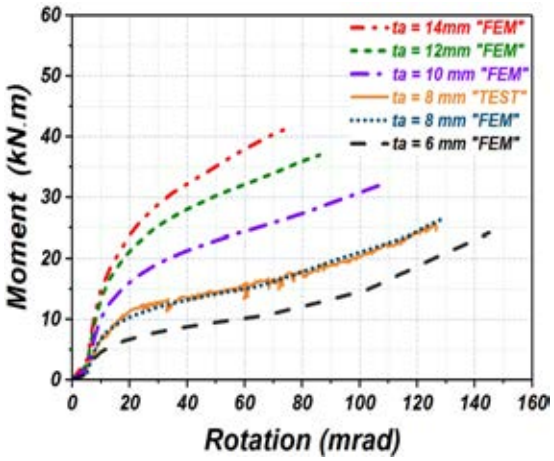

(a) M-Φ curves for different angle cleat thicknesses t_a

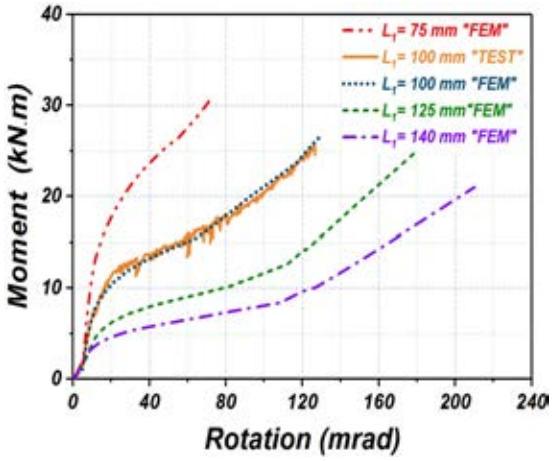

(b) M-Φ curves for different lengths L_1 of the connected angle cleats

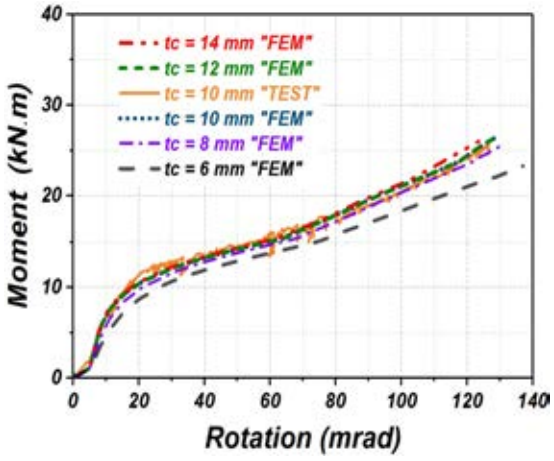

(c) M-Φ curves for different column flange thicknesses t_c

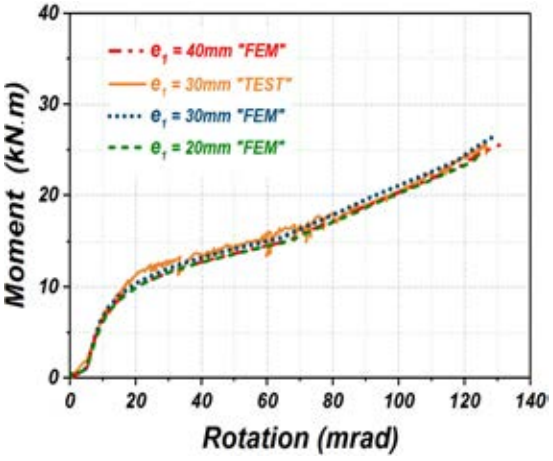

(d) M-Φ curves for different bolt edge distances e_1

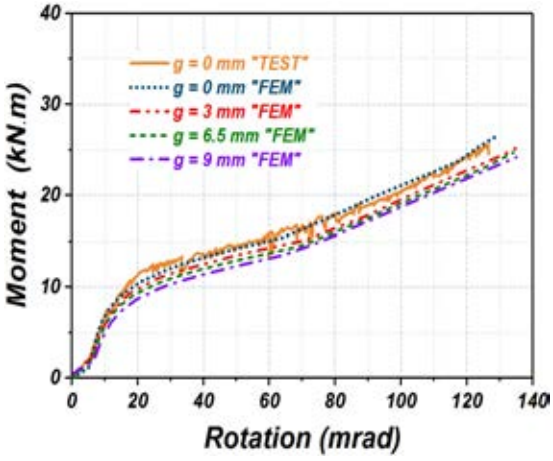

(e) M-Φ curves for different gap distances g between the beam and the column

Figure 5.27 Parametric study of TSAC-T-A connections

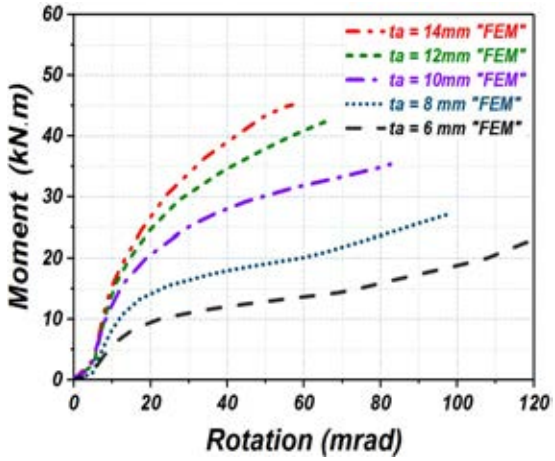

(a) M-Φ curves for different angle cleat thicknesses t_a

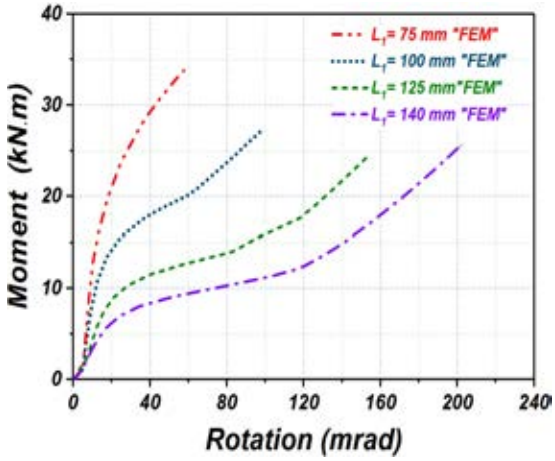

(b) M-Φ curves for different lengths L_1 of the connected angle cleats

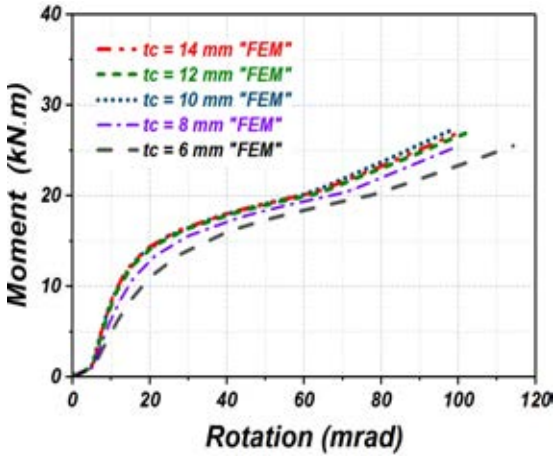

(c) M-Φ curves for different column flange thicknesses t_c

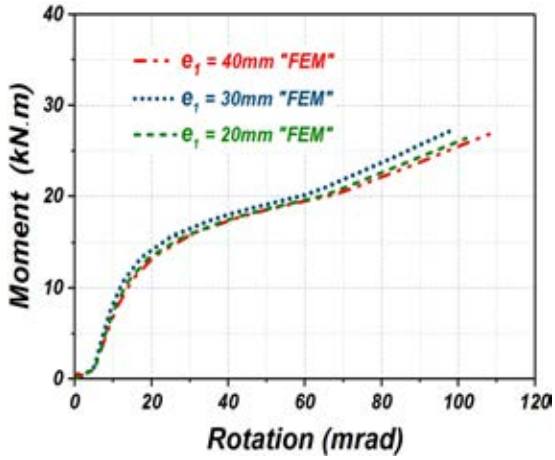

(d) M-Φ curves for different bolt edge distances e_1

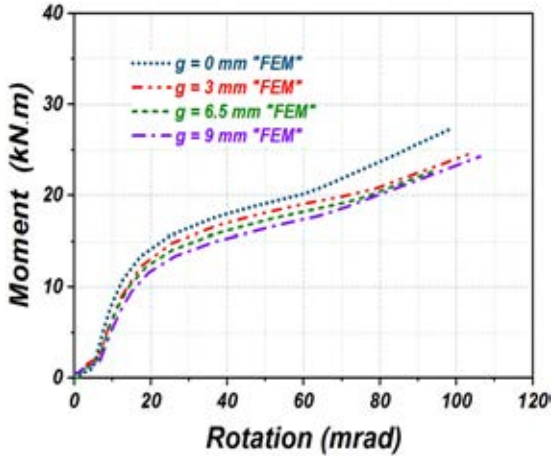

(e) M-Φ curves for different gap distances g between the beam and the column

Figure 5.28 Parametric study of TSAC-T-L connections

5.5.4 Top, seat and web cleat (TSWAC) connections

In Tables 5.17 to 5.20 the results of the parametric study for TSWAC-O-A, TSWAC-T-A, TSWAC-O-L and TSWAC-T-L are reported, whilst Figures 5.30 to 5.33 shows the effect of varying geometric parameters on the joint response. The comments regarding the effects of the angle cleat thickness t_a and the angle cleat leg L_1 on the joint response made for the TSAC-O and TSAC-T joints are also valid for the TSWAC-O and TSWAC-T joints. Given that e_1 did not seem to have any effect on the behaviour of the TSAC-O and TSAC-T joints this parameter was not considered for TSWAC-O or TSWAC-T joints and the edge distance e_2 of the bolts connecting the web cleats to the column flange was varied instead. Due to the presence of the web cleats higher moment and an overall stiffer response are obtained (Elflah, et al., 2018 a). Moreover, the behaviour of the connection is no longer dominated by the top cleat response, which leads to non-negligible effects of changing the edge distance e_2 of and flange thickness t_f, with the exception of TSWAC-T joints employing the smallest column thickness (6 mm), the failure of which is governed by flexure of the column face. contrary to the TSAC specimens, where almost all of the plastic deformations were localised in the top angle cleat. The effect of the bending of the column flange can be deduced by observing the failure modes shown in Figures 5.24 and 5.29 (a) for a TSAC-O and TSWAC-O configuration respectively. In Figure 5.24, the column flange remains almost unreformed as the top angle cleat is significantly weaker and hence attracts all the plastic deformation, whereas some flexure of the column flange can be seen in Figure 5.29 (a). Therefore increasing the flange thickness or reducing the bolt edge distance e_2 leads to an increased strength and stiffness (Elflah, et al., 2018 a).

Contrary to the TSAC-O specimens, the gap g between the beam and the column was observed in this case to have a very strong influence on the joint ultimate moment, ductility and failure mode. When there is no gap between the beam and the columns, compression is transmitted from the beam bottom flange to the column via contact, whereas by shifting the beam away from the column, shear forces are developing on the bolts connecting the

beam bottom flanges to the seat angle cleats. This has a small effect on the joint stiffness but a marked effect on the observed failure mode as shown in Figure 5.29, where the deformed shape at failure of a TSWAC-O joint without gap (g=0) and a TSWAC-O joint with a 9mm gap (g=9 mm) is depicted. In the latter case significant shear stresses are acting on the bolts connecting the seat cleat to the beam bottom flange, which may fail in single shear prior to tensile fracture of the bolts connecting the top and web cleats to the column flange, as clearly shown in Figure 5.29 (c), which shows a section through a plane containing the bolts, hence allowing the stress field in the bolts to be observed. Premature bolt failure leads to a reduced strength and stiffness with increasing gap distance g (Elflah, et al., 2018 a).

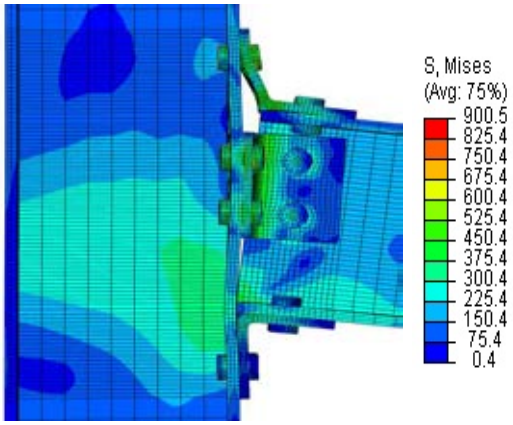

(a) TSWAC (g = 0 mm) (Stress is Von-Mises (MPa))

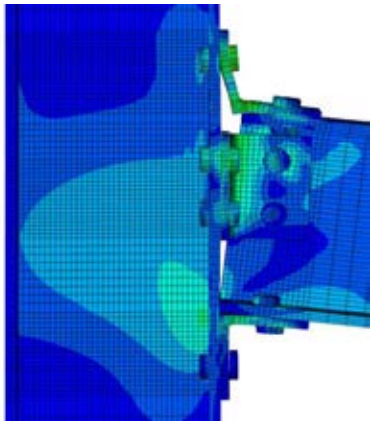

(b) TSWAC (g = 9 mm))Stress is Von-Mises (MPa))

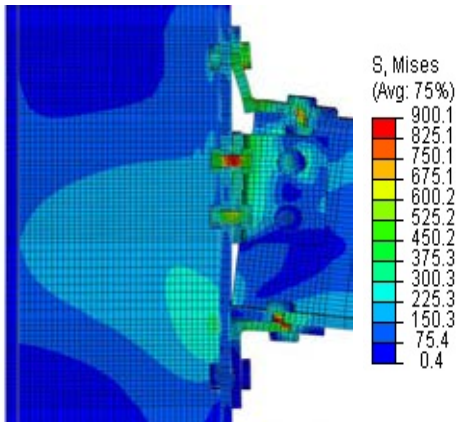

(c) TSWAC (g = 9 mm) (Stress is Von-Mises (MPa))

Figure 5.29 Effect of gap g on failure mode (Elflah, et al., 2018 a)

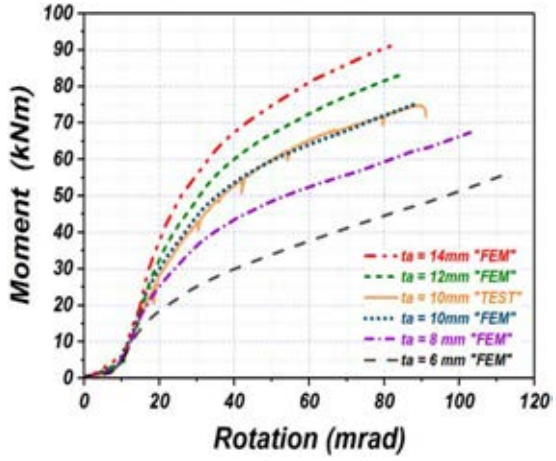

(a) M-Φ curves for different angle cleat thicknesses t_a

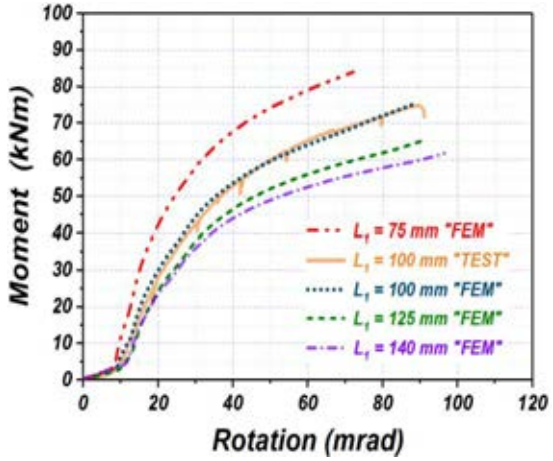

(b) M-Φ curves for different lengths L_1 of the connected angle cleats

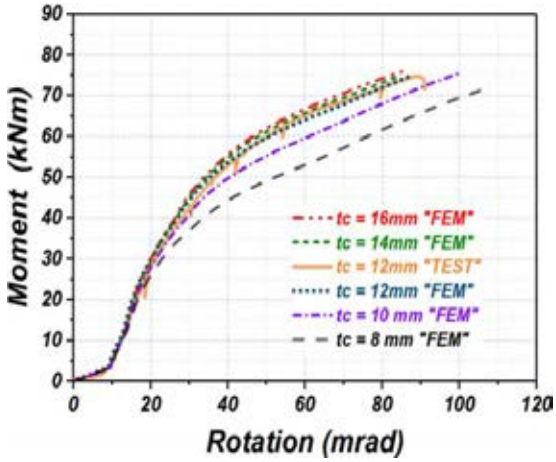

(c) M-Φ curves for different column flange thicknesses t_c

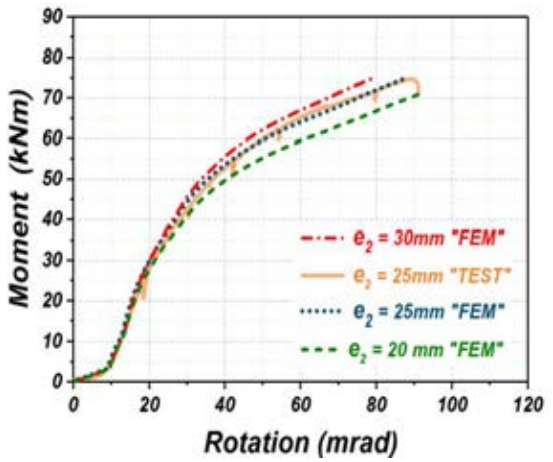

(d) M-Φ curves for different bolt edge distances e_2

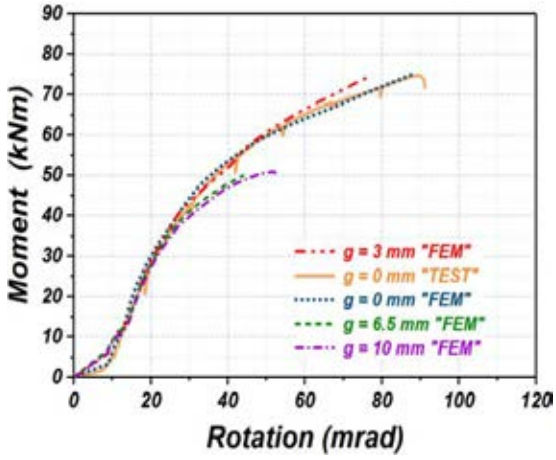

(e) M-Φ curves for different gap distances g between the beam and the column

Figure 5.30 Parametric study of TSWAC-O-A connections (Elflah, et al., 2018 a)

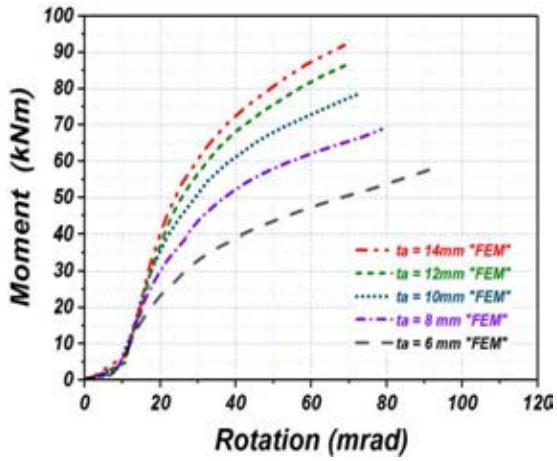

(a) M-Φ curves for different angle cleat thicknesses t_a

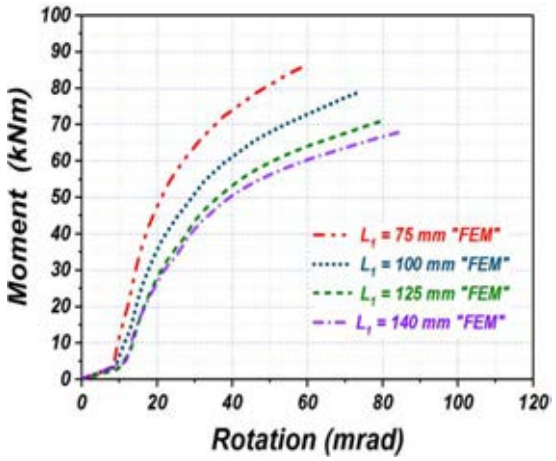

(b) M-Φ curves for different lengths L_1 of the connected angle cleats

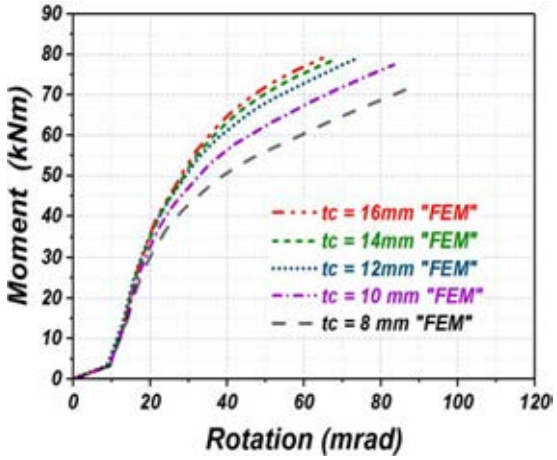

(c) M-Φ curves for different column flange thicknesses t_c

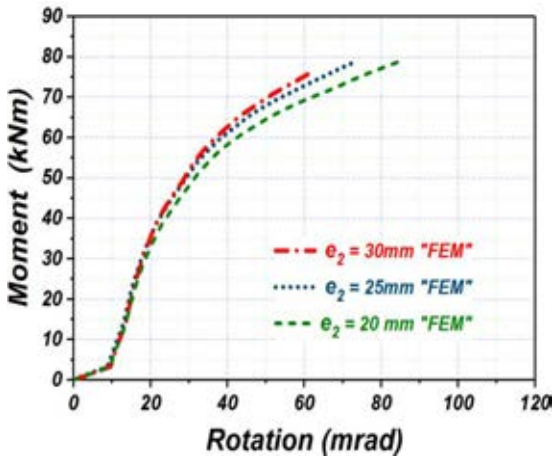

(d) M-Φ curves for different bolt edge distances e_2

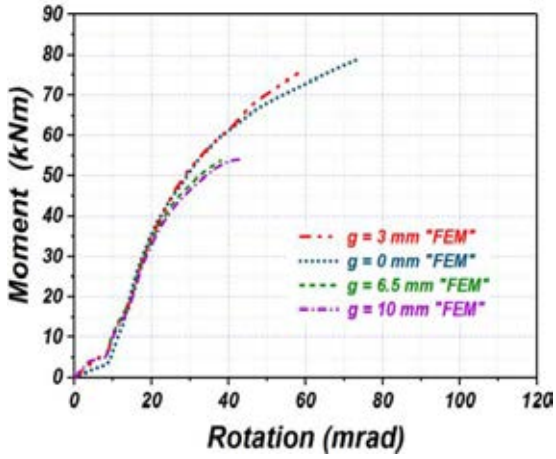

(e) M-Φ curves for different gap distances g between the beam and the column (Elflah, et al., 2018 a)

Figure 5.31 Parametric study of TSWAC-O-L connections

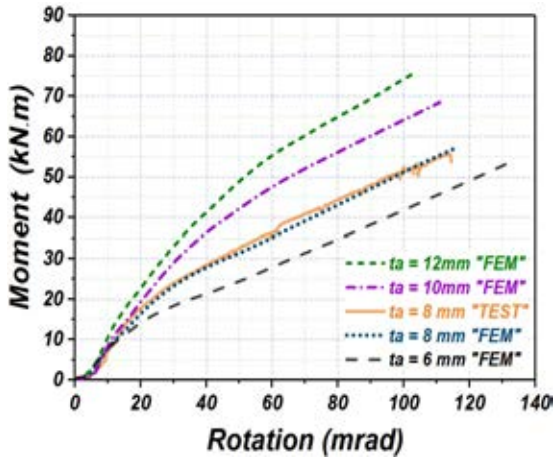

(a) M-Φ curves for different angle cleat thicknesses t_a

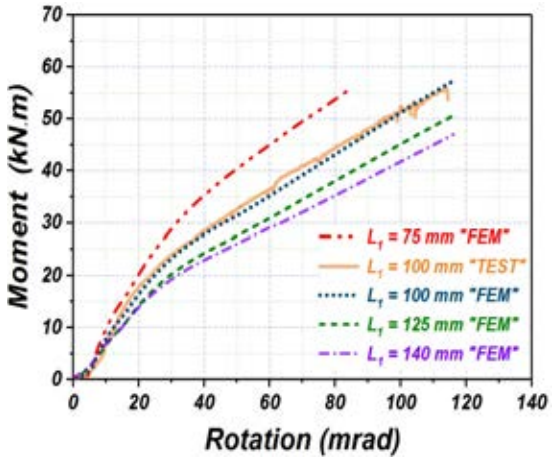

(b) M-Φ curves for different lengths L_1 of the connected angle cleats

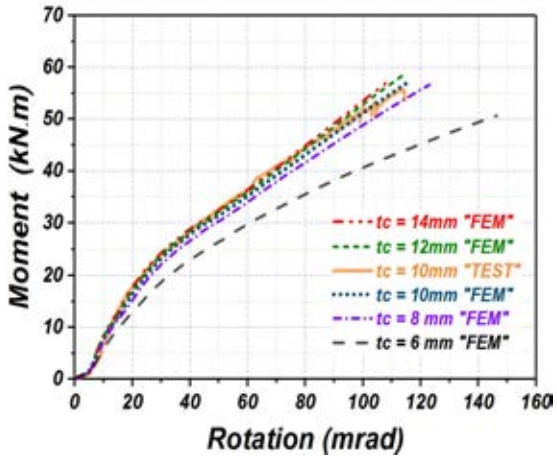

(c) M-Φ curves for different column flange thicknesses t_c

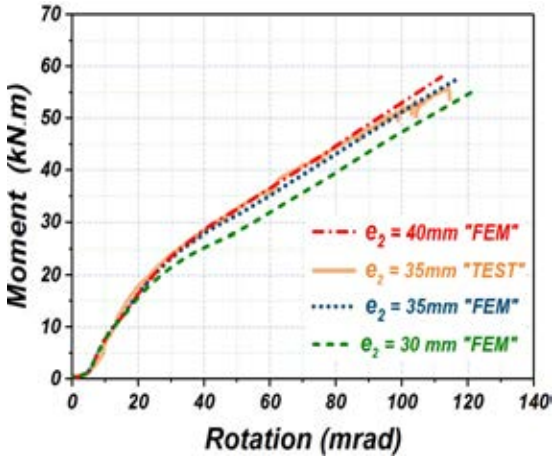

(d) M-Φ curves for different bolt edge distances e_2

Figure 5.32 Parametric study of TSWAC-T-A connections

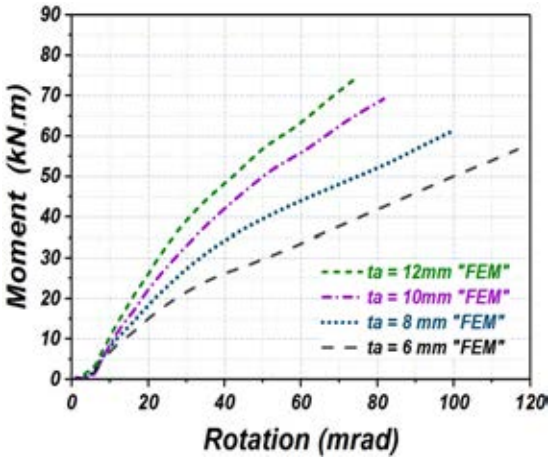

(a) M-Φ curves for different angle cleat thicknesses t_a

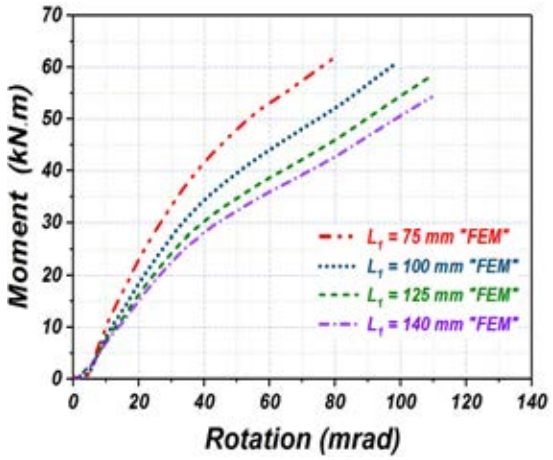

(b) M-Φ curves for different lengths L_1 of the connected angle cleats

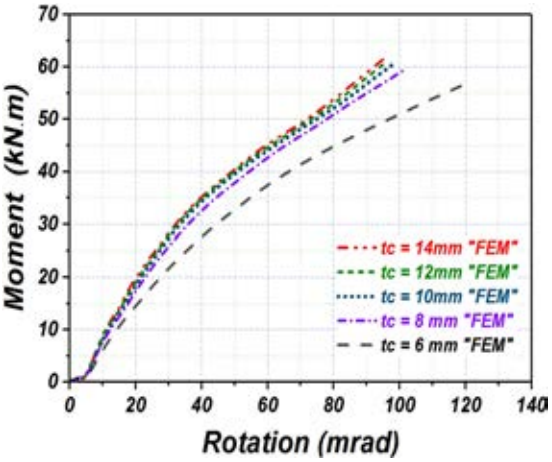

(c) M-Φ curves for different column flange thicknesses t_c

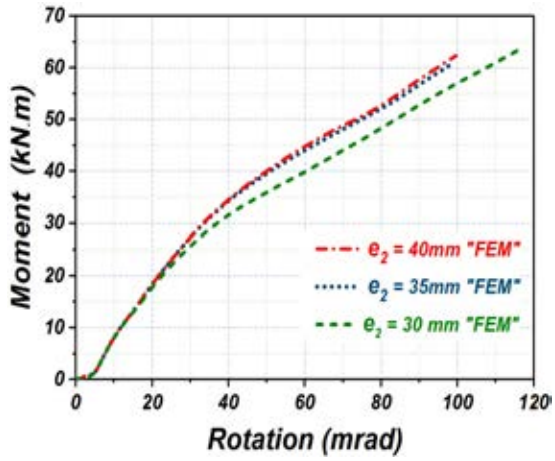

(d) M-Φ curves for different bolt edge distances e_2

Figure 5.33 Parametric study of TSWAC-T-L connections

5.6 Assessment of design provisions

In Tables 5.7 to 5.20 the average value and coefficient of variation of the EN 1993-1-8 (2005) predictions over the numerical ones in terms of initial rotational stiffness $S_{j,ini}$ and plastic moment resistance $M_{j,R}$ is given (Elflah, et al., 2018 a).

5.6.1 Open beam-to-open column joints

For open column joints, the stiffness is consistently over-predicted by about 50% for FEP-O and EEP-O joints for both stainless steel grades considered whilst for TSAC-O and TSWAC-O joints the over predictions are even more severe. These findings are in agreement with similar conclusions on the accuracy of the stiffness predictions of EN1993-1-8, (2005) as discussed in chapter 3 relate predominantly to uncertainties regarding tolerances and contact between the various components inherent in non-preloaded bolted connections (Elflah, et al., 2018 a).

In terms of the plastic moment resistance, in all cases the Eurocode model yields significantly conservative results. The ratio of the codified over the numerical moment resistance of the FEP-O -A and EEP-O-A joints is 0.45 and 0.61 respectively, whilst the corresponding values for the FEP-O -L and EEP-O-L joints are 0.51 and 0.65. In all cases the coefficient of variation is reasonably small (ranging from 0.06 to 0.09), thus indicating constituently conservative design predictions. With regard to the TSAC-A and TSAC-L joints the respective values are 0.55 and 0.63 with coefficients of variation equal to 0.09 and 0.11 respectively. Finally the moment resistance of the TSWAC joints is also under-predicted (0.61 for TSWAC-A and 0.85 for TSWAC-L) respectively, however the scatter of the predictions is in this case higher (0.15 and 0.19 respectively) (Elflah, et al., 2018 a).

5.6.2 Open beam-to-Tubular column joints

For tubular column joints, due to the absence of codified provisions for the calculation of the stiffness and strength of the column face component, the SCI (2014) model was adopted for the determination of the resistance of the columns face, whilst its stiffness was calculated based on the Equation proposed by Elghazouli et al. (2010) as mentioned in Chapter 4. The stiffness is well predicted for FEP-T joints for both stainless steel grades considered whilst for the TSAC-T and TSWAC-T joints the stiffness is over-predicted.

In terms of the plastic moment resistance, in all cases the Eurocode model yields significantly conservative results. The ratio of the codified over the numerical moment resistance of the FEP-T-A joints is 0.42, whilst the corresponding values for the FEP-T-L joints are 0.60. In all cases the coefficient of variation is reasonably small (ranging from 0.09 to 1.00), thus indicating consistently conservative design predictions. With regard to the TSAC-1-A and TSAC-T-L joints the respective values are 0.65 and 0.76 with coefficients of variation equal to 0.07 and 0.09 respectively. Finally, the moment resistance of the TSWAC-T joints is also under-predicted (0.66 for TSWAC-T-A and 0.92 for TSWAC-T-L) respectively, however the scatter of the predictions is in this case higher (0.13 and 0.16 respectively) (Elflah, et al., 2018 a).

Overall it can be observed that the conservatism is higher for austenitic stainless steel joints compared to their lean duplex counterparts. This is due to the higher ductility and strain hardening characteristics of the austenitic stainless steels. Moreover, the conservatism seems to be higher for joints exhibiting more ductile behaviour (higher rotation values at failure) compared to joints failing at smaller rotations (e.g. TSWAC-O-L). These observations agree well with the ones based on the test results alone in Chapters 3 and 4 (Elflah, et al., 2018 a).

The significant strain-hardening exhibited by stainless steels has been shown to lead to higher cross-section capacities compared to the codified ones (Gardner and Theofanous, 2008) for stocky stainless steel cross-sections, which can reach stresses higher than the nominal yield stress if they do not buckle locally. This is more pronounced in the case of connections, provided that their response is governed by a ductile failure mode such as bending of the end plate, angle cleat or column flange, since the critical components are either in bending or in tension and hence only material ductility limits the level of strain-hardening that can be attained. Based on the above observations the development of a design model in agreement with the observed structural response is warranted (Elflah, et al., 2018 a).

5.7 Concluding remarks

FE models has been developed and validated against the experimental data reported in Chapters 3 and 4. A comprehensive parametric study was conducted and the structural response of 132 beam-to-open column joints and 96 beam-to-tubular column joints has been obtained numerically (Elflah, et al., 2018 a).

Based on the numerical results the effect of key geometric parameters on the joint response has been investigated and the design provisions codified in EN1993-1-8 (2005) were assessed. In all cases, the strength and ductility of the simulated joints was limited by the failure of the bolts, as, due to the high ductility and pronounced strain-hardening of the all other joint components, the moment resistance of the joints was increasing with increasing deformation until bolt fracture occurred. However, despite bolt failure being brittle, the overall joint response was in most cases ductile as bolt failure occurred after the development of significant inelastic deformations in other joint components (end plates, flange and web angle cleats, column face of tubular columns, column flange of I-section columns) (Elflah, et al., 2018 a).

The effect of the adopted stainless steel grade on the joint response has also been studied and it was established that lean duplex stainless steel joints exhibit higher strength but lower ductility than geometrically identical austenitic joints. The plastic moment resistance was found to be underestimated on average by 44% and 34% for austenitic and lean duplex beam-to-open column joints and by 42% and 24% for austenitic and lean duplex beam-to-tubular column joints (Elflah, et al., 2018 a). It is noted that ferritic stainless steels have not been considered in the parametric studies. This is because their ductility and strain-hardening characteristics is inferior to the ones exhibited by the austenitic and duplex grades and resembles more the ones of carbon steel. Hence it is expected that the carbon steel design guidance for steel connections (EN 1993-1-8, 2005) will provide less conservative results for ferritic stainless steel joints. The study of ferritic stainless steel joints is one of the recommended topics for future research .

The development of a novel method to determine the moment resistance of stainless steel T-stubs and tubular column face in bending incorporating the effect of strain-hardening is warranted and is discussed in the following Chapter. Essentially the method adopts the component based approach of EN1993-1-8 (2005) and uses a continuous strength (e.g. T-stubs), where a high level of strain-hardening is to be expected. (Elflah, et al., 2018 a)

Chapter 6

Simplified mechanical model and design recommendations

6.1 Introduction

The experimental and numerical investigations on stainless steel joints reported in the previous Chapters demonstrated that strength predictions according to EN 1993-1-8 (2005) systematically underestimate the plastic moment resistance of the joints, for both open and tubular columns. Given the high initial cost of stainless steel, the development of a design model for stainless steel joints in line with the observed structural response is needed. Moreover, given the significant ductility exhibited by all tested specimens, the design model should ideally simulate the full range of the moment-rotation response of stainless steel joints until the failure load and provide some quantifiable measure of the rotation capacity of the joints. In this Chapter the development of a simplified mechanical model for the moment–rotation relationship of stainless steel joints within the framework of the component method of EN 1993-1-8 (2005) is reported. The model relies on a simplified representation of stainless steels' material response with due consideration of ductility and strain-hardening, which informs the predictive equations defining the response of key joint components (Elflah et al, 2018 a,b).

Based on the results reported in Chapters 3-5, significant inelastic deformations occurred in the end plates, angle cleats and column flanges. These components are idealized in the calculations according to EN 1993-1-8 (2005) as equivalent T-stubs, as shown in Figure 6.1 and as previously reported account for most of the recorded plastic deformation in the tested joints. For this reason, before proposing predictive models for the response of the full-scale stainless steel beam-to-column joints, an analytical model predicting the structural response of stainless steel T-stubs in tension up to failure is proposed following a review of past research on the response of steel T-stubs in tension (Elflah et al, 2018 a,b).

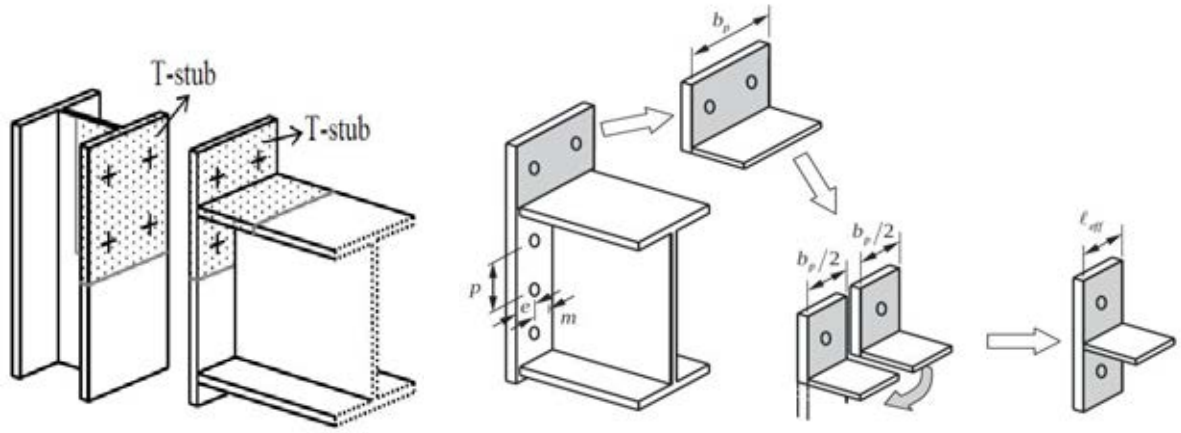

Figure 6.1 Idealised T-stub in an end plate connection after Girao et al. (2004 a) and Jaspart and Weynand (2016

6.2 Past research on the response of T-stubs in tension

Zoetemeijer (1974) was the first to idealise the response of the tension side of bolted beam-to-column joints as a T-stub loaded in tension. He reported relevant experimental tests and studied analytically the response of steel T-stubs, identifying 3 distinct failure modes and proposing relevant design equations, hence characterising the response of one of the most critical components of a joint prior to the development of the component

method. Figure 6.2 depicts the 3 failure modes relevant to a T-stub in tension and the corresponding bending moment and shear force diagrams. According to his analysis, a T-stub can fail in 3 discrete modes:

i Mode 1 (collapse mechanism B in Figure 6.2): the bolts are strong enough to allow the formation of two plastic hinges on either side of the T-stub web prior to bolt fracture. Failure is assumed to occur once a mechanism forms in the flange, even though strain-hardening allows higher forces to be achieved. In EN 1993-1-8 (2005) this failure mode is termed "complete yielding of the flange" or "Mode 1".

ii Mode 2 (collapse mechanism A a. in Figure 6.2): the bolts fail in tension after the formation of one plastic hinge at the flange to web junction of the T-stub but prior to the formation of the complete mechanism corresponding to Mode 1. In EN 1993-1-8 (2005) this failure mode is termed "bolt failure with yielding of the flange"or"Mode 2".

iii Mode 3: (collapse mechanism A b. in Figure 6.2): the bolts fail in tension prior to the flange yielding. This is simply called "bolt failure" or "Mode 3" in Eurocode terminology.

The failure load for each of the three modes is calculated according to the provisions of EN 1993-1-8 (2005), which are based on the models shown in Figure 6.2. Equations (6.1-6.4) have been extracted from EN 1993-1-8 (2005) and define the resistance of the T-stub for each of the 3 failure modes. The smaller resistance value governs and is assumed to reflect the capacity of the T-stub in tension.

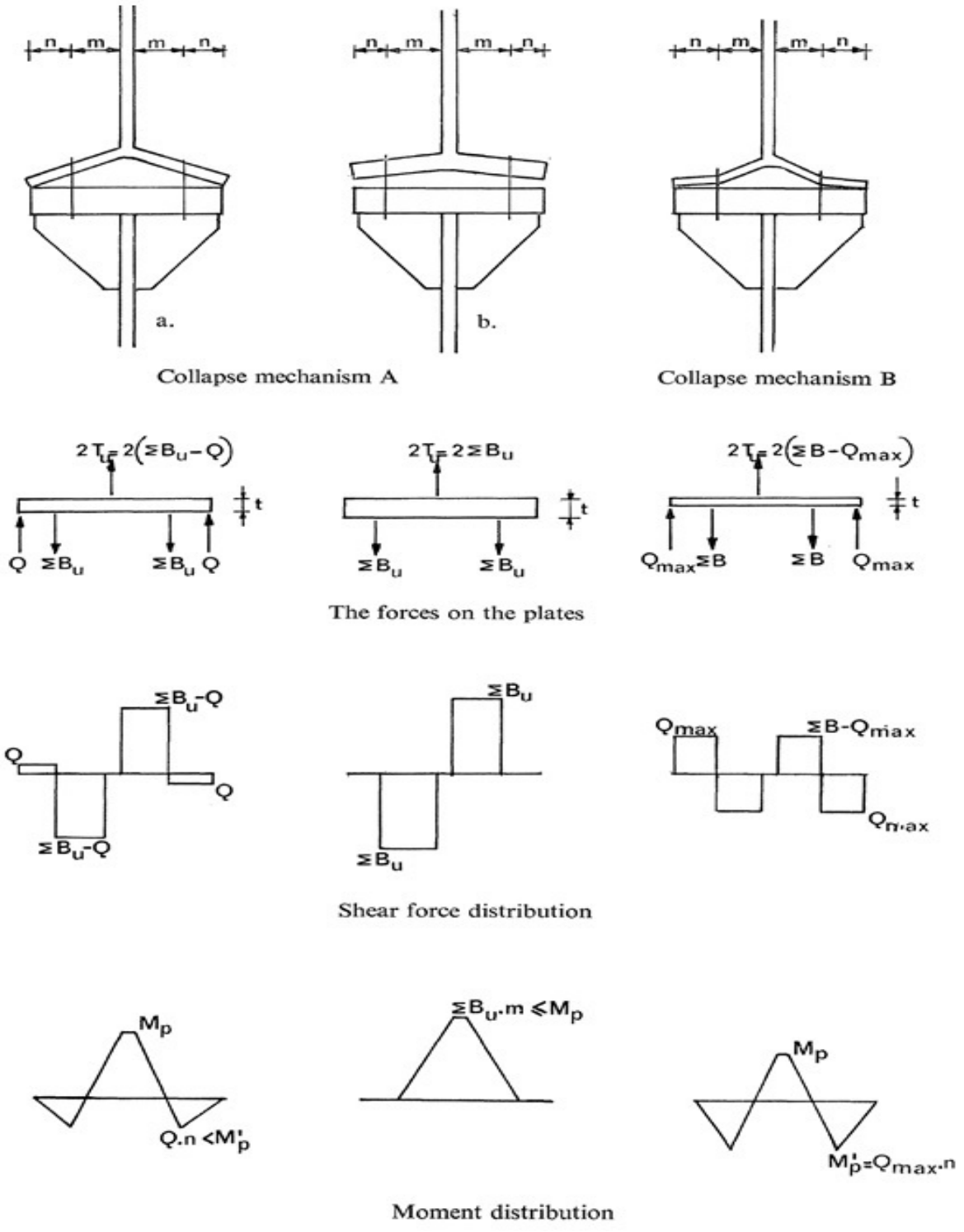

Figure 6.2 The three failure modes, free body diagrams, bending moment diagrams and shear force diagrams of an idealized T-stub in tension (Zoetemeijer, 1974)

i) For Mode 1:

$$F_{T,1,Rd} = \frac{4M_{pl,1,Rd}}{m} \qquad \text{Method 1} \tag{6.1}$$

$$F_{T,1,Rd} = \frac{(8n - 2e_w)M_{pl,1,Rd}}{2mn - e_w(m+n)} \qquad \text{Alternative method (2)} \tag{6.2}$$

ii) For Mode 2:

$$F_{T,2,Rd} = \frac{2M_{pl,2,Rd} + n\Sigma F_{t,Rd}}{m+n} \tag{6.3}$$

iii) For Mode 3:

$$F_{T,3,Rd} = \Sigma F_{t,Rd} \tag{6.4}$$

where the alternative method for the resistance corresponding to mode 1 accounts more accurately for the effect of the washers distribution of forces below the washers and is an elaboration of the original expression (method 1) proposed by Zoetemeijer (1974). The alternative method results in slightly higher and more accurate plastic resistance predictions and will be used herein (Zoetemeijer, 1974). All symbols used in Equations 6.1 to 6.3 and Figure 6.2 are compatible with the ones in EN 1993-1-8 (2005) and defined below .

- B_u is ultimate tensile load of the bolts fitted at one side of aT-stub to column connection
- T_u is half of the ultimate tensile load applied to a T-stub to column connection
- $F_{T,Rd}$ is the design tension resistance of a T-stub flange
- Q is the prying force
- Q_{max} maximum value of the prying action
- $F_{t,Rd}$ (or B in Figure 6.2) is the design tension resistance of a bolt
- $M_{pl,1,Rd} = 0.25.t_f^2.\sigma_y.b_{eff,1}$

- $M_{pl,2,Rd} = 0.25.t_f^2.\sigma_y.b_{eff,2}$
- $b_{eff,1}$ is the effective length of the T-stub for mode 1
- $b_{eff,2}$ is the effective length of the T-stub for mode 2
- σ_y is the yield strength of the T-stub
- $e_w = d_w/4$
- t_f is the flange thickness of the T-stub
- d_w is the diameter of the washer, or the width across points of the bolt head or nut, as relevant.
- m and n are indicated in Figure 6.3

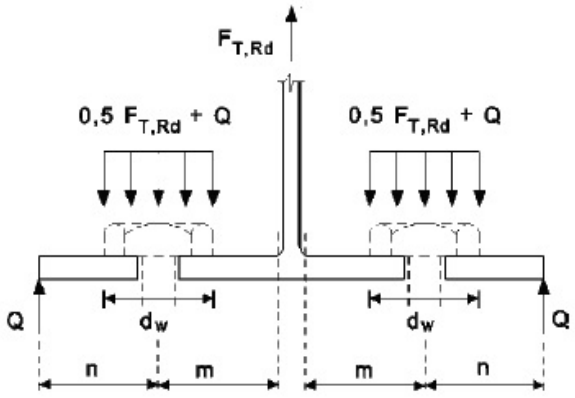

Figure 6.3 Definition of symbols for the application of the EN 1993-1-8 (2005) design equations

According to this design model, which underpins all structural design codes for steel connections, the failure mode depends on the relative strength of the bolts compared to the strength of the T-stubs. Strong bolts connecting thin plates allow complete yielding of the flange, which is the most ductile of the 3 failure modes, whilst mode 3 is typical of stiff plates connected with weaker bolts and is the least ductile of the 3 failure modes of a T-stub. Mode 2 lies in-between the two extreme cases. According to the assumptions

on which the T-stub model is based the effect of shear forces on the bolts is ignored and the bolts are assumed to be loaded concentrically in tension. In reality, due to the changing contact conditions, and depending on the deformability of the T-stub, the bolts are subjected to eccentric tension (i.e. tension and bending) and shear forces; however these effects only become significant at large deformations. Furthermore, it is assumed that complete yielding of the flange (Mode 1) leads to failure, even though in reality the T-stub can take additional loading until either the bolts or the T-stub fractures. This was acknowledged by Zoetemeijer (1974) who intended his model to provide a safe lower bound to the T-stub resistance.

A key parameter affecting the response of bolted T-stubs in tension is the development of prying forces (i.e. contact forces developing between the edges of the T-stub and the component on which it is bolted with increasing T-stub deformation. Early studies and predictive models for prying forces were reported by Douty and McGuire (1965), Nair et al. (1974) and Agerskov (1976, 1977). The effect of bolt preload on the behaviour of T-stubs was experimentally studied by Faella, et al. (1998), who reported the behaviour of T-stubs assemblies involving snug-tightened and pretensioned bolts. They concluded that the effect of bolt pretension is significant on the stiffness but not on the strength of T-stubs in tension.

More complicated T-stub arrangements were experimentally tested by Swanson and Leon (2000), who reported 48 tests on T-stubs involving bolts in both the flange and the web of the T-stub and investigated several failure modes. The structural behaviour of a T-stub configuration with 4 bolts per row, an arrangement representative of the T-stub components of larger beam-to-column joints, was investigated by Chasten et al (1992), who proposed an analytical method to determine the prying force value and its location. More recently Massimo et al. (2014) conducted 3 tests on T-stubs with 3 bolts per row in tension and validated an FE model against the obtained data. They developed a design method based on yield line analysis which provided safe estimations of the T-stub

resistance compared to the experimental and numerical results by 8% on average. Tests on stainless-steel T-stubs with 4 bolts per bolt row were also reported by Yuan et al. (2018). Since none of the tests reported in this thesis involves 4 bolts per row, such configurations are not considered any further.

Departing from approximations of the plastic collapse load of T-stubs, several researchers attempted to determine the full load-deformation response of bolted steel T-stubs in tension. Piluso et al., (2001a) proposed a theoretical model based on a multilinear approximation of the material response of steel and a rational cross-section analysis and determined the moment-curvature response at the location of the potential plastic hinges. By integrating over the T-stub length they converted the curvature into rotation and determined the load-deformation response of a T-stub in tension. Their analytical model was verified via comparisons with test data (Piluso et al., 2001b). Swanson and Leon (2001) proposed an alternative model which accounted for non-linear material properties, decreasing stiffness of the bolt with increasing applied tension and the gradual formation of plastic hinges. Their approach is based on an incremental iterative procedure which does lend itself to hand calculations.

Beg, et al. (2002) investigated the deformation capacity of moment resisting connections and proposed simple design expressions for the deformation capacity of all main joint components including the T-stub. Their approach for the T-stub relies upon an ultimate strain ε_u that a steel T-stub can reach in bending (ε_u=0.2 was assumed in their study for carbon steel) and the assumption that all deformation is localized in the location of the plastic hinges, the length of which was assumed equal to their thickness. The later assumption does not allow for the effect of the spread of deformations throughout the T-stub (in plastic zones rather than plastic hinges) on the overall deformations T-stub deformation thus compromising the accuracy of the predictions. However, their model provides reasonable accurate ultimate deformation predictions without the need for cum-

bersome integrations, thus making the proposed design method appealing and suitable for hand calculations. Therefore, the design model proposed by Beg et al. (2004) is adapted to stainless steel as discussed hereafter.

6.3 A simple design model for stainless steel T-stubs

6.3.1 Available test data

Yuan et al. (2018) reported the only available experimental tests on stainless steel T-stubs in tension. Their experimental data are utilized herein to develop a predictive method for stainless-steel T-stubs in tension, which is extended to beam-to-column joints. The reader is referred to Yuan et al. (2018) for a complete description of the experimental tests, the material properties of the constituent elements and a discussion of the test results.

Table 6-1 in conjunction with Figure 6-4 gives a summary of the geometric configurations and the material grades of the tested specimens. Both austenitic and duplex grades were considered, whilst the thickness of the T-stub flanges, the bolt diameter and the bolt preload were varied. Three specimen configurations were investigated, out of which two are utilized herein and are displayed in Figure 6-4. The third configuration involved 4 bolts per bolt row and is beyond the scope of the present study. The applied preload as previously discussed and verified by Yuan et al. (2018) did affect the initial stiffness but not the strength of the T-stubs. Furthermore, given that all tested T-stubs failed after significant inelastic deformations were obtained, the effect of the preload on the ultimate deformation is assumed negligible.

6.3.2 Determination of plastic resistance $\mathbf{F_{j,R}}$

The plastic resistance of all tested T-stub connections was obtained according to EN 1993-1-8 (2005), using the measured $\sigma_{0.2}$ values in place of the yield strength for the

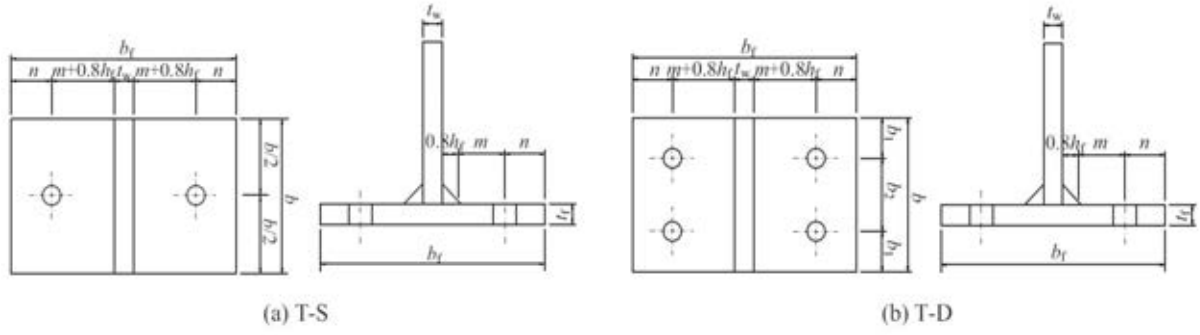

Figure 6.4 Geometric configuration of T-stub specimens (extracted from Yuan et al., 2018)

Table 6.1 Comparison of experimental results for plastic resistance for EC3 and CSM predictions and measured test values (Yuan et al. 2018)

Specimen	Material	bolt	d_b	n	m	b_1	b_2	b	b_f	t_f=t_w	h_f	Bolt preload (kN)
S1	EN 1.4301	A4-70	16	50	50.2	-	-	120	222	11.85	6	59.1
S2	EN 1.4301	A4-80	12	35	65.2	-	-	120	222	11.85	6	27.5
S3	EN 1.4462	A4-80	16	50	50.2	-	-	90	222	12.58	6	58.3
S4	EN 1.4462	A4-80	12	50	53	-	-	120	222	7.72	5	21.3
S5	EN 1.4462	A4-80	16	50	53	-	-	90	222	7.72	5	59.1
S6	EN 1.4301	A4-80	12	50	53	-	-	120	222	7.85	5	30.6
S7	EN 1.4462	A4-80	16	50	53	-	-	120	222	7.72	5	56.9
S8	EN 1.4301	A4-70	16	50	50.2	-	-	90	222	11.85	6	56.2
S9	EN 1.4301	A4-80	12	35	65.2	-	-	120	222	11.85	6	1.3
D1	EN 1.4301	A4-70	16	50	50.2	40	70	150	222	11.85	6	44.3
D2	EN 1.4301	A4-80	12	35	65.2	40	70	150	222	11.85	6	29.1
D3	EN 1.4462	A4-70	16	35	68	40	70	150	222	7.72	5	53.1
D4	EN 1.4462	A4-70	16	35	65.2	40	70	150	222	12.58	6	48
D5	EN 1.4462	A4-70	16	50	50.2	40	70	150	222	12.58	6	45.2
D6	EN 1.4301	A4-80	16	35	65.2	40	70	150	222	11.85	6	45.8
D7	EN 1.4301	A4-80	12	35	65.2	28	54	110	222	11.85	6	29.4
D8	EN 1.4301	A4-80	12	35	65.2	40	70	150	222	11.85	6	1.8

relevant components (Elflah et al, 2018 a). It should be noted that the plastic strength does not refer to the ultimate strength but to the predicted plastic strength according to EC3 and the experimentally measured plastic strength are reported in Table 6-2, as is the ratio of the predicted results to measured values. The plastic strength $F_{j,R}$ were determined in accordance with Chapters 3 and 4. As expected, all Eurocode predictions are conservative with an average ratio of predicted over experimental plastic resistance of

0.69 and a standard deviation of 0.10. As mentioned in previous chapters, these results indicate that the Eurocode consistently underestimated the capacity of stainless steel connections for every T-stub connection tested by Yuan, et al., (2018) (Elflah et al, 2018 a).

Table 6.2 Comparison of experimental results by Yuan, et al., (2018) and predicted plastic resistances according to EC3 and CSM values

Specimen	The plastic resistance $F_{j.R}$ (kN)				
	$F_{j,R}$ (TEST)	$F_{j,R}$ (EC3)	$F_{j,R}$ (CSM)	EC3/TEST	CSM/TEST
S1	153.0	106.5	138.1	0.70	0.90
S2	93.0	65.7	76.9	0.70	0.83
S3	179.0	141	147.5	0.78	0.82
S4	100.0	77.6	80.0	0.77	0.80
S5	88.0	62.9	70.5	0.71	0.80
S6	66.0	44.7	65.8	0.68	1.00
S7	112.0	83.8	94.0	0.76	0.84
S8	145.0	79.9	117.8	0.55	0.81
S9	93.0	65.7	76.9	0.71	0.83
D1	225.0	133.2	196.4	0.59	0.87
D2	150.0	99.9	127.6	0.67	0.85
D3	103.0	81.9	91.9	0.80	0.89
D4	254.0	191.6	210.7	0.75	0.83
D5	340.0	248.7	272.7	0.73	0.80
D6	175.0	102.6	151.3	0.59	0.86
D7	109.0	73.2	108.0	0.67	0.99
D8	155.0	99.9	127.6	0.64	0.82
Mean				0.69	0.86
COV				0.10	0.07

Similar observations regarding the conservatism of the EC3 design approach have been made in the past for stainless steel structural components. The design predictions of EN 1993-1-4 (2015) were observed to be overly conservative for stocky stainless steel components, such restrained beams and stub columns (Gardner and Theofanous, 2008; Afshan and Gardner, 2013). This was attributed to the pronounced strain-hardening exhibited by stainless steel stocky members, which is not accounted for in current design guidance as the maximum attainable stress is limited to the nominal yield strength $\sigma_{0.2}$.

To this end the Continuous Strength Method (CSM) was developed (Gardner and Nethrcrot, 2004; Ashraf et al., 2006; Gardner 2008; Gardner and Theofanous, 2008; Afshan and Gardner, 2013; Liew and Gardner, 2015), which allows a rational exploitation of strain-hardening in the design procedure through the adoption of a bilinear elastic-linear hardening representation of the material response. In the case of stub columns and restrained beams for which the method was originally developed, the occurrence of local buckling limits the maximum attainable strain by the cross-section and the CSM employs an empirical relationship to relate the slenderness of the cross-section to be designed to the maximum attainable strain. In the case of a T-stub in tension the exploitation of strain-hardening is not limited by anything other than material ductility.

The effect of strain-hardening can be accounted for in design by allowing moments higher than M_{pl} to be attained in the locations of the plastic hinges. To this end the CSM bilinear material model (Afshan and Gardner, 2013), shown in Figure 6-5 is adopted. The elastic branch of the stress-strain curve is assumed valid until the nominal yield strength σ_y=$\sigma_{0.2}$ is reached. Equation 6.5 defines the slope of the strain-hardening branch of the curve, E_{sh} as a function of the nominal yield stress $\sigma_{0.2}$, the corresponding elastic strain ε_y=$\sigma_{0.2}$/E, the ultimate tensile stress σ_u and the strain at ultimate stress ε_u. The strain at ultimate stress ε_u can be obtained from Equation 6.6, as proposed by Rasmussen (2003). Hence the stress corresponding to any strain value in the strain-hardening region of the curve is obtained from Equation 6.7.

$$E_{sh} = \frac{\sigma_u - \sigma_{0.2}}{0.16\varepsilon_u - (\varepsilon_y)} \tag{6.5}$$

$$\varepsilon_u = 1 - \frac{\sigma_{0.2}}{\sigma_u} \tag{6.6}$$

$$\sigma_{csm} = \sigma_{0.2} + E_{sh}\varepsilon_y\left(\frac{\varepsilon_{csm}}{\varepsilon_y} - 1\right) \tag{6.7}$$

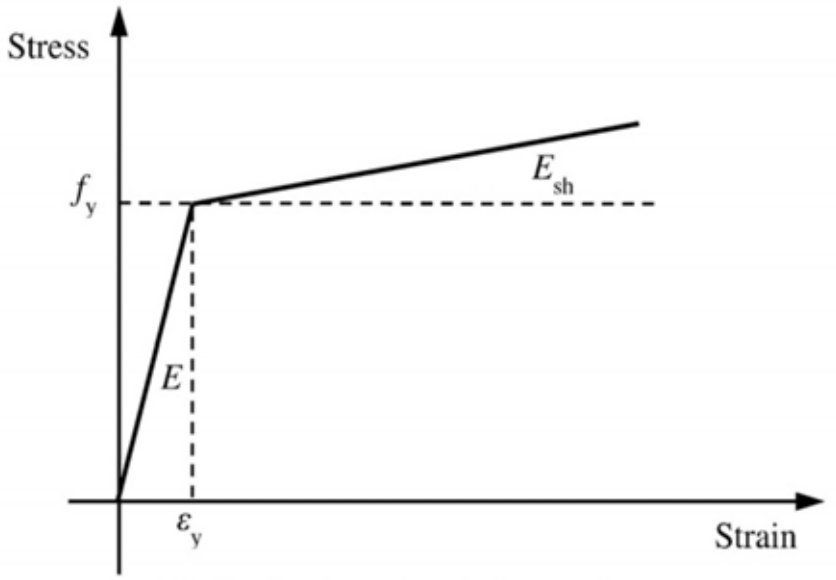

Figure 6.5 Elastic-linear hardening approximation of stainless steel material response (Yun and Gardner, 2017)

The symbols used in Figure 6.5 and Equations 6.5 to 6.7 are :

- E_{sh}, for strain hardening slope
- E, for young's modulus
- ε_u, for strain at ultimate tensile stress
- ε_y, for yield strain
- ε_{csm}, for strain at CSM predicted failure stress
- σ_u, for ultimate tensile stress
- $\sigma_{0.2}$, for 0.2% proof stress
- σ_{csm}, for CSM predicted failure stress

It should be noted that according to the original derivation of the CSM two strain limits are imposed on the maximum strain up to which strain-hardening can be exploited. The first limit is set to$15\varepsilon_y$ and relates to the EN 1993-1-4 (2015) minimum ductility requirements for structural stainless steels. This limit is deemed overly conservative as all

tested stainless steel material coupons both reported in this and other studies achieved strain values far beyond $15\varepsilon_y$. Therefore, it is recommended herein that this limit is relaxed to $30\varepsilon_y$. The second limits is equal to $0{,}1\varepsilon_u$ and relates to the ensuring that the actual stress value is not overpredicted by the bilinear approximation of the curved material response. To maintain consistency with the CSM predictions for the design of cross-sections, this limit is kept unchanged.

The plastic strength of a bolted T-stub connection can be obtained according to equations 6.2-6.4 using the moment resistance M_{CSM} in place of M_{pl}. The predicted strength $F_{j,R\ (csm)}$ based on the CSM together with the corresponding predicted-over-experimental plastic strength ratio has been obtained for all tested T-stubs and is reported Table 6.2. The experimentally obtained plastic resistance values are underestimated by the CSM compliant design approach on average by 14% with a standard deviation of 7% with none of the predicted values being lower than the experimental one. This constitutes a massive improvement over the EN 1993-1-8 (2005) design predictions; the average predicted-to-experimental ratio has increased by 23% and the corresponding standard deviation has decreased by 32%. Hence it is recommended that the CSM compliant bilinear material modelling as described herein be used to determine the plastic resistance capacity of stainless steel T-stubs, termed F_{CSM}.

6.3.3 Deformation response until F_{CSM}

In the previous subsection the determination of the plastic resistance of a T-stub F_{CSM} allowing for material strain-hardening was reported. In order to obtain a comprehensive description of the joint behaviour, the full load-deformation response is required. To this end extensive use of the EN 1993-1-8 (2005) provisions is made so that the proposed design model is in accordance with procedures with which engineers are familiar.

According to the experimental load-deformation graphs reported by Yuan et al. (2018), in all cases the initial response of the T-stubs in tension is linear elastic, followed by a curved transition region in the vicinity of the plastic resistance $F_{j,R}$ indicating extensive yielding of the flanges of the T-stub. The reported load-deflection behaviour resembles the idealized moment-rotation behaviour of steel joints, as shown in Figure 6-6.

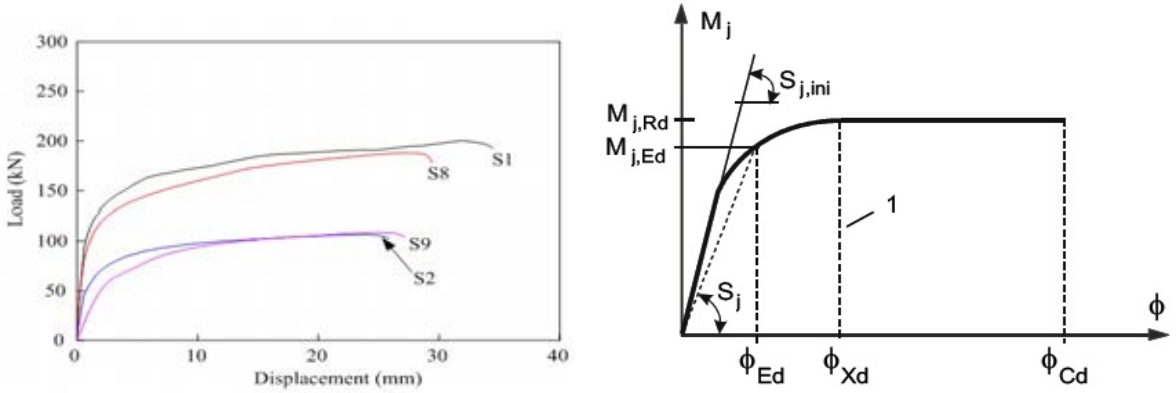

(a) Load-deflection curves (Yuan et al., 2018)

(b) Moment-rotation curve (EN1993-1-8 (2005)

Figure 6.6 Experimental and idealized load-deformation curves for a steel joint.

The symbols used in Figure 6.6 are :

- S_j, for initial rotational stiffness of the joint
- $M_{j,Rd}$, for the design moment resistance of the joint
- $M_{j,Ed}$, for the bending moment of the joint
- Φ_{Cd}, for the design rotation capacity
- Φ_{Xd}, for the rotation at which $M_{j,Ed}$ first reaches $M_{j,Rd}$
- Φ_{Ed}, for the corresponding rotation at the bending moment $M_{j,Ed}$

Based on the observed analogy the following procedure is recommended for the determination of the load-deformation response of T-stubs, which inspired by clause 5.1.2(4) and Table 5.2 of EN 1993-1-8 (2005):

- For loads F $\leq$(2/3)F_{CSM}: assume elastic behaviour, the initial elastic stiffness $S_{j,ini}$ defines the response up to a deformation equal to (2/3)$F_{CSM}/S_{j,ini}$

- For loads (2/3)F_{CSM}<F $\leq$ F_{CSM}: the initial elastic stiffness S_j in this region is obtained from $S_{j,ini}$ divided by the stiffness modification coefficient η which for all cases considered herein is equal to 2 (EN 1993-1-8 , 2005). Hence the predicted displacement δ_{CSM} at F_{CSM} is given by Equation 6.8 and is twice the displacement corresponding to the end of the elastic regime.

$$\delta_{csm} = \left(\frac{4F_{CSM}}{3S_{j,ini}}\right) \tag{6.8}$$

6.3.4 Ultimate response of T-stubs in tension

The ultimate load F_u at which failure occurs is obtained from Equations 6.2-6.4 for each of the 3 failure modes with the ultimate moment M_u being use in place of the plastic moment M_{pl}, where M_u is given by Equation 6.9.

$$M_u = 0.25.t_f^2.\sigma_u.b_{eff} \tag{6.9}$$

b_{eff} being the effective length of the T-stub (equal to the tested length for the T-stubs considered herein) and σ_u being the ultimate tensile stress.

The corresponding displacement at maximum load δ_u is obtained from the following equations according to Beg et al. (2004):

$$\text{For mode 1:} \qquad \delta_u = 2.\varepsilon_u.m \tag{6.10}$$

$$\text{For mode 2:} \qquad \delta_u = 0.1.l_b\left(1 + 2(\frac{m}{n})\right) \tag{6.11}$$

$$\text{For mode 3:} \qquad \delta_u = 0.1.l_b \tag{6.12}$$

where m and n defined in Figure 6.3 and l_b being the bolt length.

Hence, based on the above analysis the load-deformation response of T-stubs in approximated by a trilinear curve as shown in Figure 6.7.

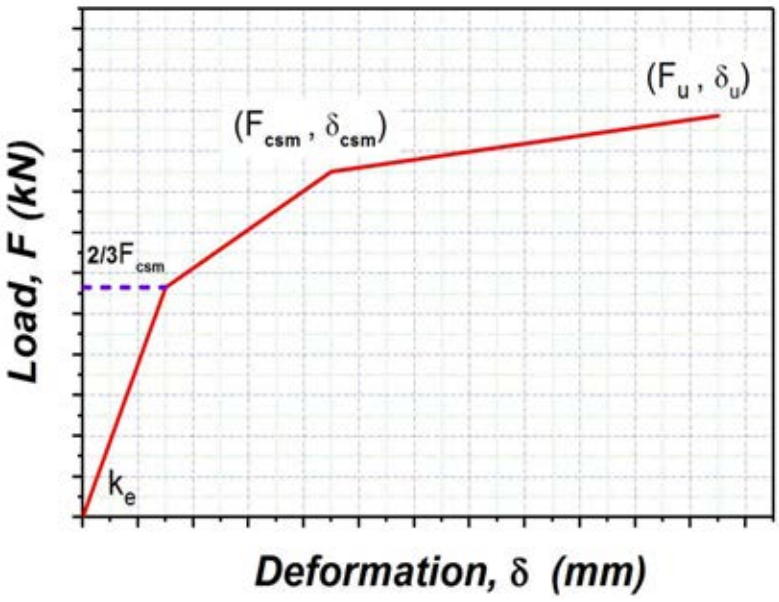

Figure 6.7 Tri-linear approximation of load-deformation response of T-stubs

6.3.5 Model validation

In Table 6.3 the predicted ultimate forces F_u and corresponding deformations δ_u are compared against the experimentally determined ones. On average the deformations are reasonably well-predicted but the standard deviation is rather high. This is not surprising considering all the assumptions involved in the model which include the prediction of the material strain at ultimate load ε_u, neglecting the effect of shear forces and eccentric tension on the bolt stiffness and hence the overall response and assuming that all deformation is localized in the plastic hinges of the T-stub thereby neglecting the deformations extending beyond them. Nonetheless the predictive model provides a reasonable estimation for the maximum deformation that a T-stub can reach with a maximum over-prediction of 30% for specimen D2.

Table 6.3 Comparison of the model predictions with the experimental results at ultimate load

Specimen	Predicted Failure mode	Ultimate load F_u (kN)			Ultimate deformation δ_u(mm)		
		F_u (pred)	F_u (Test)	pred/Test	δ_u (pred)	δ_u (Test)	pred/Test
S1	2	164	200.2	0.82	18.6	31.8	0.59
S2	2	103	106.8	0.96	29.23	23.9	1.22
S3	2	158	198.4	0.8	18.82	21.5	0.88
S4	2	84	108.9	0.77	18.01	19.7	0.91
S5	1	84	161.6	0.52	26.84	29.2	0.92
S6	2	84	104.3	0.8	18.05	26	0.69
S7	1	112	175.2	0.64	26.84	28.9	0.93
S8	2	149	188	0.79	18.6	27.3	0.68
S9	2	103	108.9	0.94	29.23	25	1.17
D1	2	282	367.5	0.77	18.6	28.7	0.65
D2	2	160	179.1	0.89	29.23	22.5	1.3
D3	1	110	260.9	0.42	34.44	33.6	1.03
D4	2	228	312.5	0.73	29.57	25.4	1.16
D5	2	290	382.5	0.76	18.82	26	0.72
D6	2	227	306.6	0.74	29.23	31.4	0.93
D7	2	140	174.3	0.8	29.23	25.8	1.13
D8	2	160	181.6	0.88	29.23	25.3	1.16
Mean				0.77			0.95
COV				0.14			0.21

The predicted ultimate force F_u is under-predicted by 23% on average, whilst the corresponding standard deviation is 0.14. However there seems to be a dependency of the accuracy of the predictions on the failure mode with the 3 specimens predicted to fail in failure mode 1 being severely under predicted, whilst for the remaining ones the predictions are more accurate. The mean ratio of the predicted over experimental ultimate load is 0.53 and 0.82 for specimens failing in mode 1 and mode 2 respectively with the corresponding standard deviations being 0.07 and 0.11. Thus the model seems to provide excellent still safe predictions for the specimens failing in mode 2 whilst the predictions deteriorate for mode 1. This may be attributed to the higher plastic deformations occurring for mode 1 which lead to a significant deformation of the parts of the T-stub lying between the bolt lines and the stem. With increasing deformation this parts of the T-stub are able to resist loads via tension, whilst the model (and all relevant models in the literature) assume that loads are solely resisted by bending. This argument is supported by Figure 6-8, where the ratio of the predicted over experimental ultimate force $F_{u,pred}/F_{u,Test}$ is plotted against the ratio of the predicted ultimate force for mode 2 over the ultimate force for mode 1. All points on the left hand side of the vertical line passing though one are predicted to fail in mode 2, whilst the ones on the right hand side are predicted to fail in mode 1. Hence with increasing importance of mode 1(i.e. with increasing deformation of the T-stub), the quality of the predictions deteriorates.

The previous discussion clearly shows the limitations of the model. However, the ultimate load F_u and corresponding deformation δ_u are not to be utilised as a design resistance for a T-stub under normal design conditions but as an estimate of the ultimate load and corresponding deformation capacity that the joint can resist under extreme conditions leading to excessive deformations of the connections. Design for such conditions, which in most cases are hard to predict or quantify, may relate to the loss of a column due to impact or blast and is beyond the scope of this thesis. In any case the proposed equations provide on average safe estimations for the ultimate response of T-stubs. Finally, in Figures 6-9

to 6-26 the predicted trilinear response of the T-stubs using the aforementioned model is plotted together with the experimental curves.

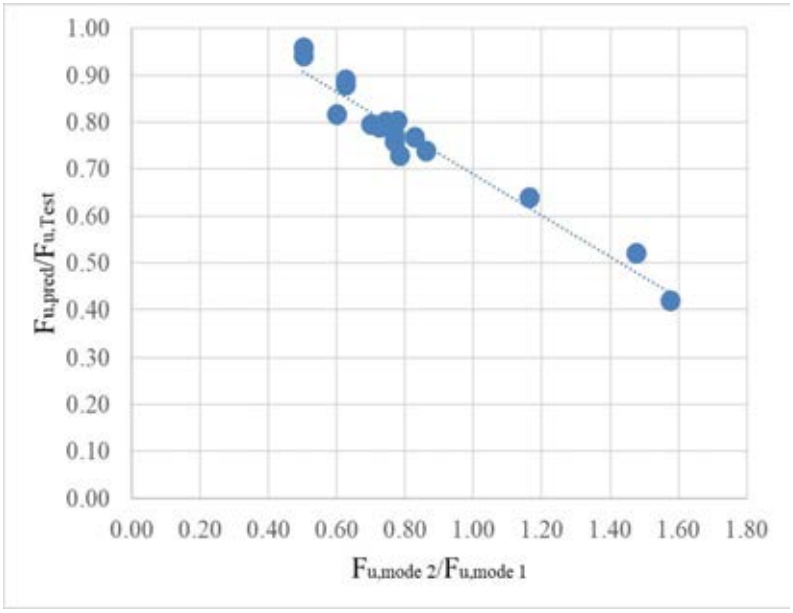

Figure 6.8 Dependency of prediction accuracy on predicted failure mode

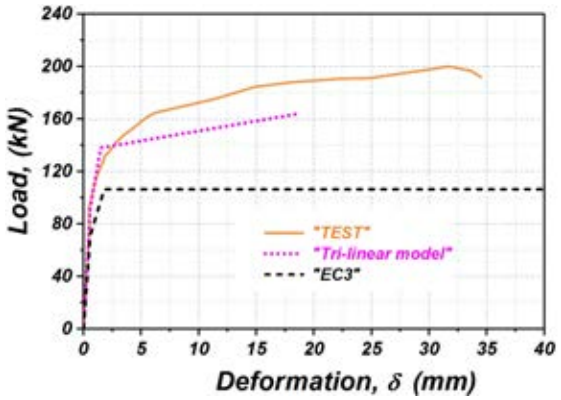

Figure 6.9 F-δ curves of experimental results, EC3 and new model predictions for S1 specimen

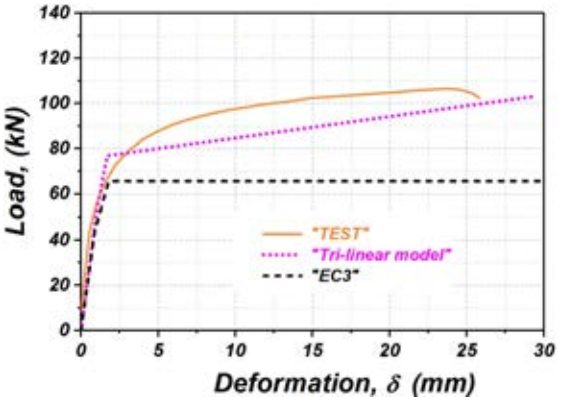

Figure 6.10 F-δ curves of experimental results, EC3 and new model predictions for S2 specimen

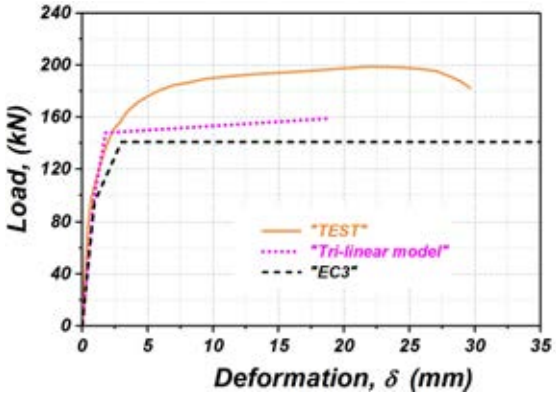

Figure 6.11 F-δ curves of experimental results, EC3 and new model predictions for S3 specimen

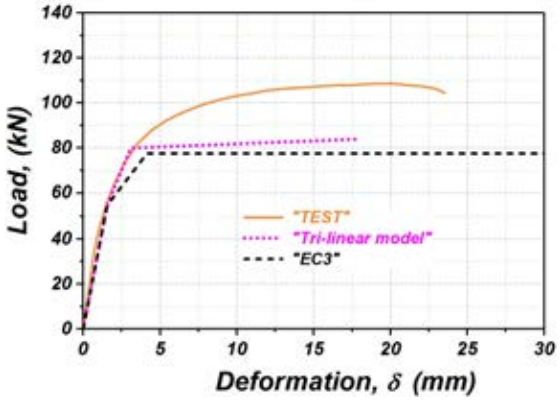

Figure 6.12 F-δ curves of experimental results, EC3 and new model predictions for S4 specimen

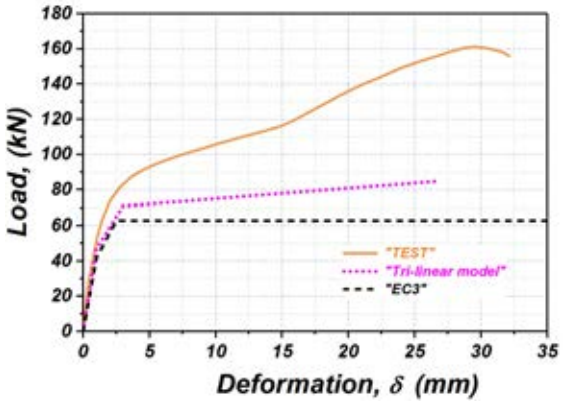

Figure 6.13 F-δ curves of experimental results, EC3 and new model predictions for S5 specimen

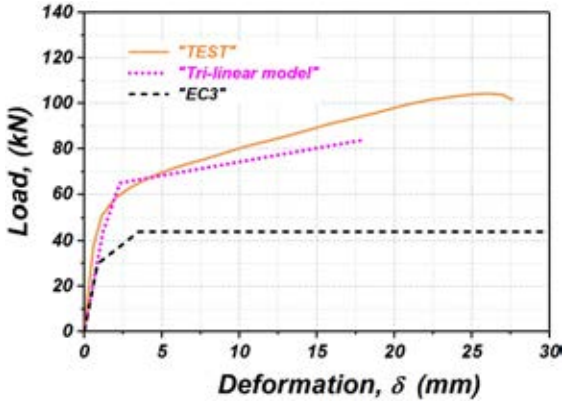

Figure 6.14 F-δ curves of experimental results, EC3 and new model predictions for S6 specimen...

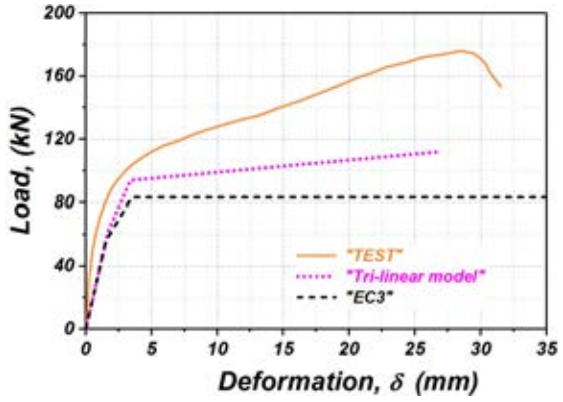

Figure 6.15 F-δ curves of experimental results, EC3 and new model predictions for S7 specimen

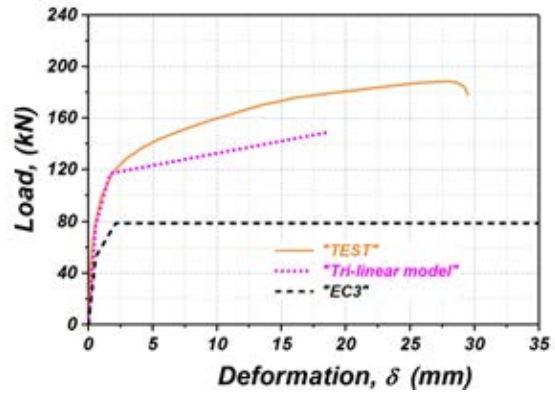

Figure 6.16 F-δ curves of experimental results, EC3 and new model predictions for S8 specimen

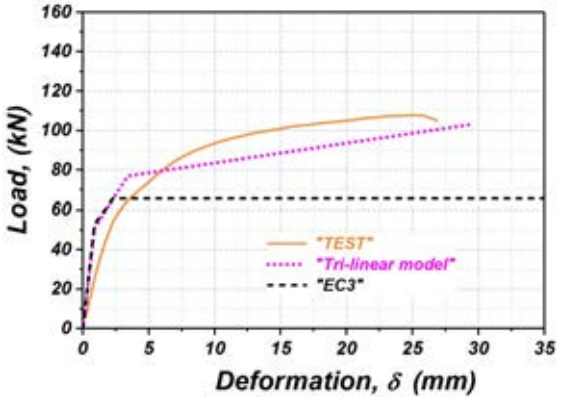

Figure 6.17 F-δ curves of experimental results, EC3 and new model predictions for S9 specimen

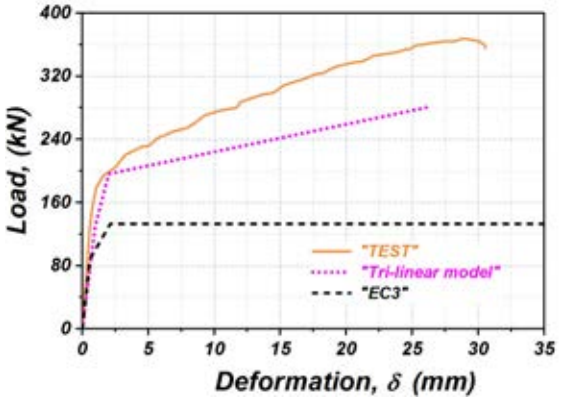

Figure 6.18 F-δ curves of experimental results, EC3 and new model predictions for D1 specimen

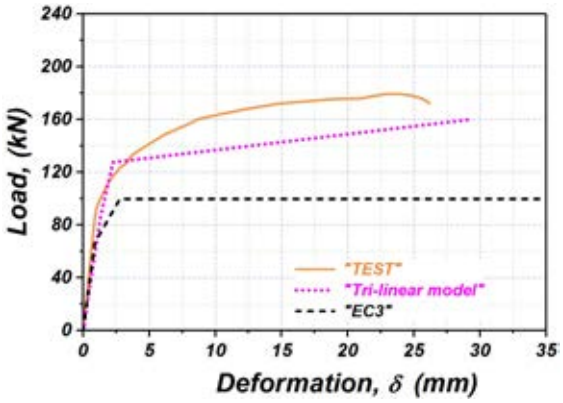

Figure 6.19 F-δ curves of experimental results, EC3 and new model predictions for D2 specimen

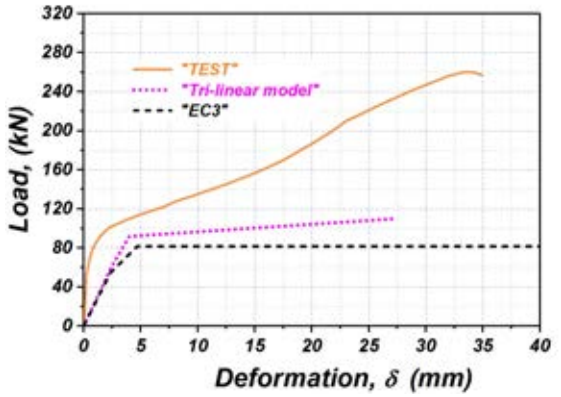

Figure 6.20 F-δ curves of experimental results, EC3 and new model predictions for D3 specimen

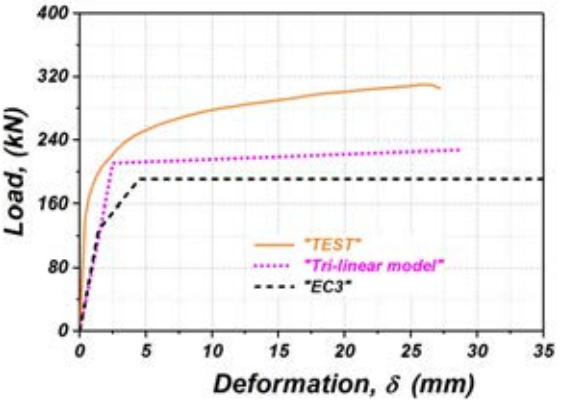

Figure 6.21 F-δ curves of experimental results, EC3 and new model predictions for D4 specimen

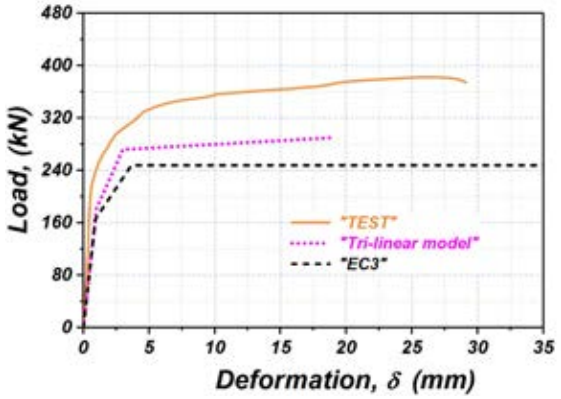

Figure 6.22 F-δ curves of experimental results, EC3 and new model predictions for D5 specimen.....

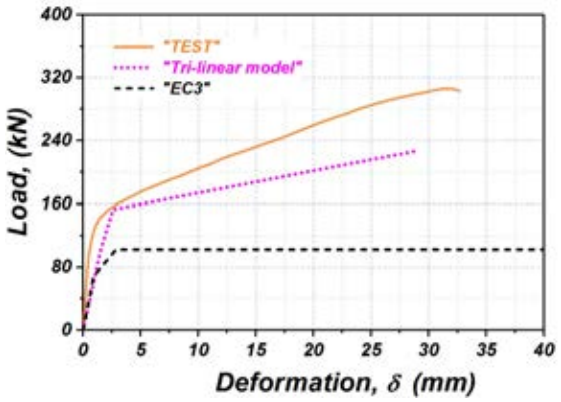

Figure 6.23 F-δ curves of experimental results, EC3 and new model predictions for D6 specimen.

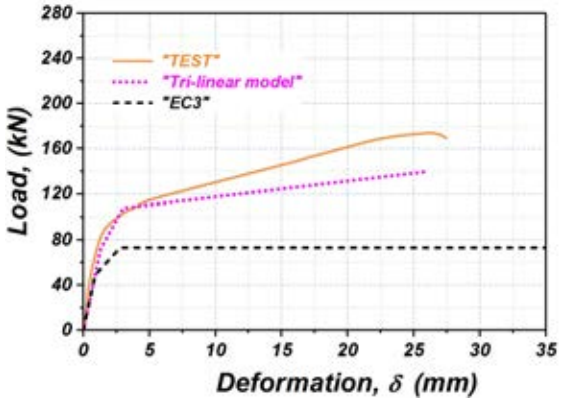

Figure 6.24 F-δ curves of experimental results, EC3 and new model predictions for D7 specimen.

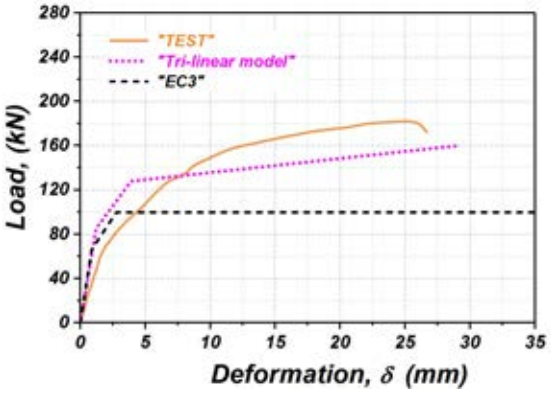

Figure 6.25 F-δ curves of experimental results, EC3 and new model predictions for D8 specimen.

6.4 Design proposals for stainless steel full-scale joints

6.4.1 Beam-to-open column joints

In the previous section a simple trilinear model was proposed for the design of stainless steel T-stubs in tension. This model can be used for the design of stainless steel beam-to-column joints where the T-stub is the component governing the response. This was the case for all tests reported in Chapter 3 and most of the numerical models, where failure and plastic deformation was localized in the angle cleats or end plates, both of which can be idealized as T-stubs. In this section the design calculations performed before to obtain the predictions according to EN 1993-1-8 (2005) are repeated with

the T-stubs being calculated according to the previously described model. The initial stiffness of the models remains unaffected and is assumed valid until 2/3 of the M_{CSM}. Equations (6.13) and (6.14) can be used to convert the T-stub predictions for force F and displacement δ into joint moment M_j and rotation Φ_j. In all cases it was verified that for the increased T-stub forces predicted by the previously described model, the remaining joint components remained elastic, hence they are not expected affect the response.

$$M_j = F.Z \tag{6.13}$$

$$\Phi_j = \delta_u/Z \tag{6.14}$$

,where z is the lever arm of the joint

In Table 6-4 the EN 1993-1-8 (2005) predictions and the predictions based on the CSM for the plastic moment resistance are compared against the experimental plastic moment of the tested joints. A significant improvement in the obtained predictions can be observed when the CSM based resistance for the T-stubs is used in the calculations with the mean predicted-to-experimental plastic resistance value increasing from 0.53 to 0.76 and the coefficient of variation decreases from 0.13 to 0.10 Similar improvements in the predictions are obtained based on the FE results.

In Table 6-5 the predicted ultimate moment $M_{u,pred}$ and corresponding rotation Φ_u are compared against the experimental results. There are no corresponding EC3 predictions in this case. It can be seen that the model provides reasonably good predictions given all the uncertainties and model simplifications involved.

Table 6.4 Comparison of EC3 and CSM predictions with experimental results for the plastic moment resistance of beam-to-open column joints

Specimen	Plastic moment resistance $M_{j,R}$ (kN.M)					
	$M_{j,R}$ (EC3)	$M_{j,R}$ (TEST)	EC3/TEST	$M_{j,R}$ (CSM)	$M_{j,R}$ (TEST)	CSM/TEST
FEP	18.6	40.0	0.47	28.0	40.0	0.70
EEP	27.2	42.0	0.65	38.0	42.0	0.90
TSAC-8	6.6	12.0	0.55	9.0	12.0	0.75
TSAC-10	11.1	23.0	0.48	16.0	23.0	0.70
TSWAC-8	19.3	39.0	0.49	29.0	39.0	0.74
TSWAC-10	30.3	55.0	0.55	43.0	55.0	0.78
Mean			0.53			0.76
COV			0.13			0.10

Table 6.5 Comparison of predictions based on the proposed model with experimental results at the ultimate moment for beam-to-open column joints

Specimen	Ultimate moment M_u (kN.M)			Ultimate rotation Φ_u (mrad)		
	M_u (Model)	M_u (TEST)	Model/TEST	Φ_u (Model)	Φ_u (TEST)	Model/TEST
FEP	60	65.4	0.92	117	157	0.75
EEP	75.4	80.4	0.94	119	119	1
TSAC-8	38.4	34.1	1.13	157	157	1
TSAC-10	45.8	41.5	1.1	156	162	0.96
TSWAC-8	70	73.3	0.95	96	125	0.77
TSWAC-10	65	74.7	0.92	98	91	1.07
Mean			0.99			0.93
COV			0.11			0.15

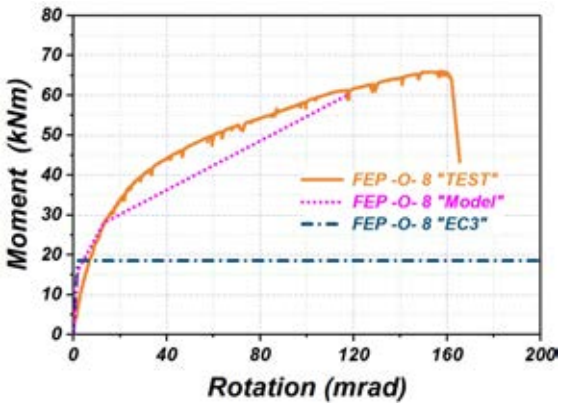

Figure 6.26 Experimental, EC3 and predicted M-Φ_u curves for specimen FEP

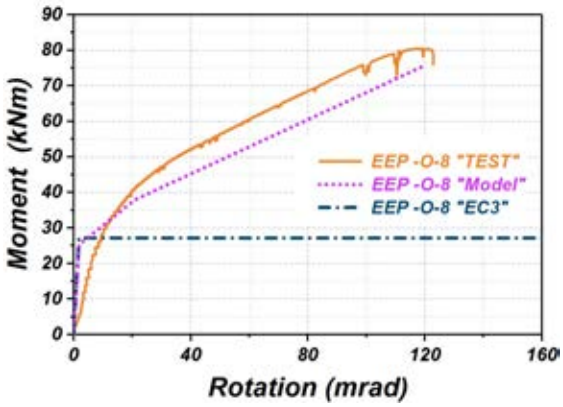

Figure 6.27 Experimental, EC3 and predicted M-Φ_u curves for specimen EEP

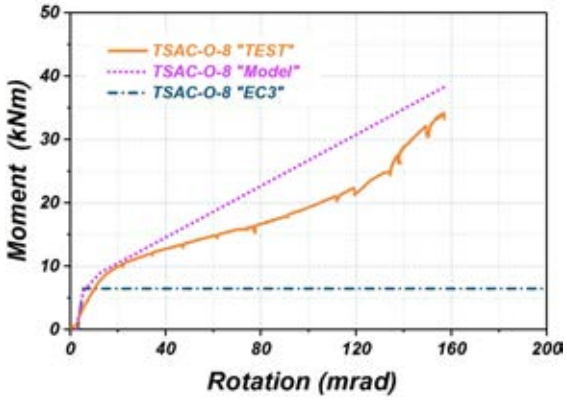

Figure 6.28 Experimental, EC3 and predicted M-Φ_u curves for specimen TSAC-8

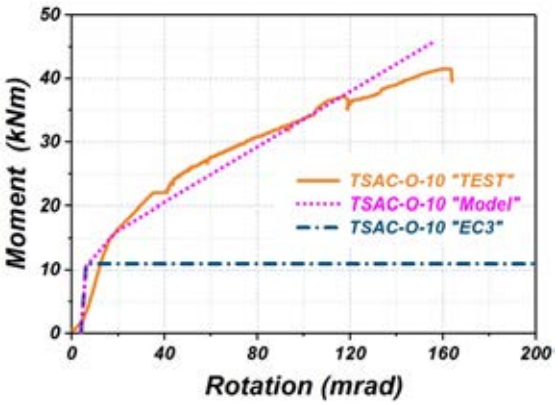

Figure 6.29 Experimental, EC3 and predicted M-Φ_u curves for specimen TSAC-10

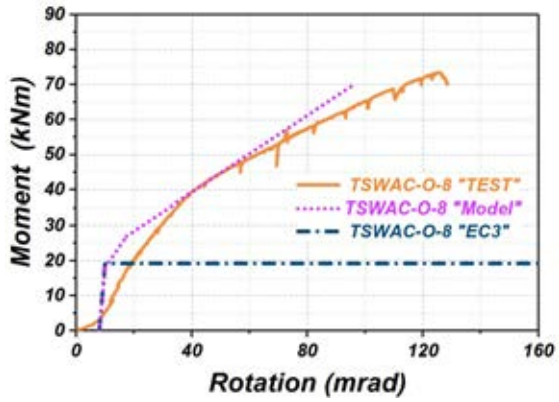

Figure 6.30 Experimental, EC3 and predicted M-Φ_u curves for specimen TSWAC-8

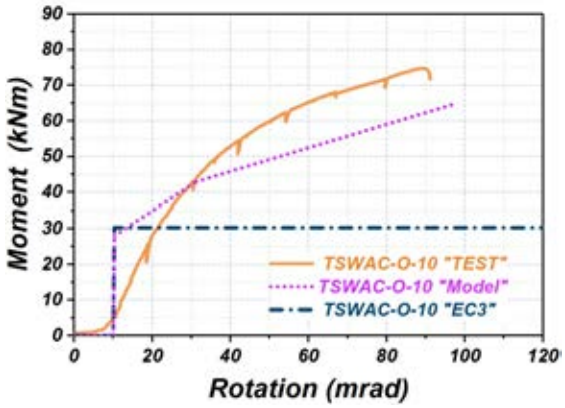

Figure 6.31 Experimental, EC3 and predicted M-Φ_u curves for specimen TSWAC-10

6.4.2 Beam-to-tubular column joints

No experimental results on components idealising the flexural response of the face of stainless steel tubular columns exist to date, hence, contrary to the beam-to-open column joints, in this case the development of a design model for this component is not currently possible. However, based on the experiments reported in Chapter 4, it was evident that high inelastic deformations developed in the tubular column faces. Limiting the maximum attainable stress to $\sigma_{0.2}$ is overly conservative. Hence, in accordance with the beam-to-open column joints, it is proposed that higher stresses are allowed in design. To this end Equations 6.5-6.7 can be utilised to obtain the stress value σ_{csm} that can be used in place of σ_y in Equation (2.1). The obtained moment predictions $M_{j,CSM}$ are compared against the experimentally obtained plastic moment resistance in Table 6-6, where the EC3

predictions are also included. As before for the beam-to-open column joints, significant improvement in terms of efficiency and consistency of the predictions can be observed for beam-to-tubular column joints.

Table 6.6 Comparison of experimental results for plastic moment resistance with EC3 and CSM predictions for open beam-to-tubular column joints

Specimen	Plastic moment resistance $M_{j,R}$ (kN.M)					
	$M_{j,R}$ (EC3)	$M_{j,R}$ (TEST)	EC3/TEST	$M_{j,R}$ (CSM)	$M_{j,R}$ (TEST)	CSM/TEST
FEP-1	10.0	27	0.37	17.0	27	0.63
FEP-2	7.4	17	0.44	13.0	17	0.76
TSAC-1	6.6	12	0.55	10.2	12	0.85
TSAC-2	9.2	18	0.51	16.1	18	0.89
TSWAC-1	13.2	21	0.63	19.0	21	0.90
TSWAC-2	14.9	28	0.53	17.0	28	0.63
Mean			0.50			0.82
COV			0.18			0.13

6.5 Concluding remarks

In this chapter the necessity to explicitly incorporate strain-hardening in the moment capacity predictions of stainless steel T-stub joints was highlighted. With the tests reported by Yuan et al. (2018) as a starting point, a design model able to predict the full load-deformation response of stainless steel T-stubs was developed. The proposed model adopts the bilinear elastic-linear hardening model for stainless steel material response also employed by the CSM (Afshan and Gardner, 2013; Liew and Gardner, 2015) and the equations proposed by Beg et al. (2004) for determining the T-stub response at ultimate load. The model provided excellent results for the plastic moment resistance of the T-stubs, far superior to the EC3 design predictions, whilst the predictions of the ultimate load F_u and corresponding deformation δ_u were less accurate, particularly for specimens failing in mode 1.

The design model for stainless steel T-stubs was utilised for the prediction of the behaviour of steel beam-to-open column joints tested in Chapter 3, since the T-stub was the component dominating the response of the joint. As before improved design predictions compared to the EN 1993-1-8 (2005) were obtained. The prediction of the full moment rotation response was also attempted and a reasonable agreement between the predicted and the experimental response was obtained. A simplified approach to account for strain-hardening in beam-to-tubular column joints by tweaking existing methods was also proposed. However, the design proposals for stainless steel beam-to-tubular column sections are less rigorous due to absence of relevant test data on the response of the column face in bending.

Chapter 7

Conclusions and suggestions for future research

7.1 Conclusions

The survey of published literature has revealed that very limited experimental and numerical research has been carried out on stainless steel beam-to- column joints with only one publication reporting experimental tests on full-scale blind-bolted connections (Tao et al., 2017) and on study reporting test results on joint components (Yuan et al. 2018). Owing to the lack of available experimental data on stainless steel connections, current design rules are based on assumed analogies with carbon steel design (EN 1993-1-8, 2005), thereby neglecting the high ductility and pronounced strain-hardening exhibited by stainless steels. Given the paramount role of connections in the behaviour of steel and stainless steel structures, the aim of this research was to address this gap in knowledge and generate much needed experimental and numerical data that would allow a better understanding of how stainless steel joints behave, the assessment of current design approaches and the formulation of novel design rules (Elflah et al, 2018 a,b).

In Chapter 3, six full scale tests on austenitic stainless steel beam-to-open column joints were reported in detail for the first time. Four joint configurations commonly employed in practice were considered and details on the failure modes and the overall moment-rotation response were provided. The effect of ductility and the accompanying strain-hardening of the critical joint components where significant plastic deformations developed was highlighted. In all cases failure of the joint was ultimately due to bolt failure, whilst all other joint components (end plates, angle cleats, column flange in bending) were observed to be too ductile to fail, contrary to similar studies on carbon steel joints, where cracking of connecting plates has been commonly observed. Comparisons with the EN 1993-1-8 (2005) design guidance, indicated that current codified design provisions underestimate the joint resistance on average by 47% due to failure to account for material strain-hardening.

A similar set of tests on six austenitic stainless steel beam-to-tubular column joints utilising the Hollo-bolt fasteners to facilitate blind-bolted connections was reported in Chapter 4. Again, this was the first set of comprehensive experimental tests to be reported on full-scale beam-to-tubular column joints. The tested specimens were designed such that different failure modes developed, thus allowing a wide range of structural responses to be experimentally studied. All specimens exhibited very high rotation capacity and their moment resistance was a lot higher to the one predicted by EN 1993-1-8 (2005), similarly to the beam-to-open column specimens.

Chapter 5 discusses in detail the development of advanced FE models able to accurately simulate the overall moment-rotation response of stainless steel beam-to-column joints and predict both the failure mode and the corresponding rotation at which it occurs. The models accounted for geometric and material nonlinearities, contact and friction, whilst a strain-based criterion was used to predict bolt fracture without the need to model it explicitly. The validated models were used to generate 228 numerical data on stainless steel joints. In addition to the effect of the joint configuration, the effect of employing a

lean duplex stainless steel grade was also studied numerically. In agreement with Chapters 3 and 4, Chapter 5 revealed the overly conservative nature of current codified design provisions. In terms of the adopted modelling assumptions the generated models can be considered standard and similar FE models have been previously developed for carbon steel joints. However, the lack of relevant test data did not allow such FE models to be deemed validated for stainless steel joints and hence therein lies the novelty and the contribution to knowledge of Chapter 5.

The consistently overly conservative predictions of EN 1993-1-8 (2005) compared to the experimental and numerical data was highlighted in Chapters 3-5 and was attributable to strain-hardening exhibited by joint components (i.e. T-stubs) undergoing large inelastic deformations. In Chapter 6 a simplified mechanical model able to account for material strain-hardening was formulated for stainless steel T-stubs in tension. The model utilises the only available set of experimental data on stainless steel T-stubs in tension reported by Yuan et al. (2018) and allows stresses higher than the nominal yield stress to be reached by imposing a maximum strain limit. A simplification of the model employing a bilinear elastic-linear hardening material representation originally developed within the framework of the Continuous Strength Method for the design of stocky stainless steel sections is also proposed and shown to yield excellent results. The model was shown to accurately predict the experimentally obtained moment-rotation response of beam-to-open section columns the response of which was governed by the T-stub. A simplified approach to account for strain-hardening in beam-to-tubular column joints by tweaking existing methods was also proposed. However the design proposals for stainless steel beam-to-tubular column sections are less rigorous due to absence of relevant test data on the response of the column face in bending.

7.2 Recommendation for future research

The literature review and research reported in this thesis have highlighted gaps in knowledge that need to be addressed so that a comprehensive design methodology for stainless steel joints can be developed. Some of the proposed future research is listed below:

1. All test data on full-scale beam-to-column joints reported herein employ austenitic stainless steel, whilst duplex stainless steel was only numerically treated. Clearly a small number of tests is required on duplex stainless steel joints to verify the validity of the obtained numerical results. Moreover no work has been reported to date on ferritic stainless steel beam-to-column joints. Due to the lower ductility and strain-hardening of ferritic stainless steel compared to the austenitic and duplex grades, special consideration for this grade is warranted. It is expected that the behaviour of ferritic stainless steel joints will lie in-between the behaviour of joints made of austenitic stainless steel and carbon steel. Hence the level of conservatism of EN 1993-1-8 (2005) for ferritic stainless steel joints needs to be studied and it has to be determined whether current carbon steel design is appropriate for ferritic stainless steel.

2. Similar to the experimental studies reported by Yuan et al. (2018) on austenitic and duplex stainless steel T-stubs in tension, a comprehensive experimental campaign on ferritic stainless steel T-stubs needs to be conducted thus augmenting the proposed joint tests on full-scale ferritic stainless steel joints.

3. In addition to the T-stub in tension, the behaviour of other joint components need to be investigated. These include the response of E-stubs in tension (i.e. idealized part of beam-to-column joints where the beam is connected on the web of the columns), the response of column web panels in shear and the response of the column web in tension and compression.

4. A comprehensive experimental campaign on T-stubs blind-bolted on tubular sections needs to be conducted to deduce the response of the tubular column face in bending and allow a design model to be formulated as was done in Chapter 6 for T-stubs in tension.

5. The effect of the employed type of fasteners on the response of the tubular column face in bending and overall joint response needs to be studied by testing similar configurations employing various types of fasteners suitable for blind-bolted connections

6. In addition to tests on stainless steel beam-to-tubular column joints employing an empty column section, connections to concrete filled stainless steel tubular sections need to be investigated thus encouraging the use of composite construction.

7. The structural behaviour of stainless steel two-sided, or even four-sided joints requires some attention particularly when failure occurs in the column region (e.g. column web panel in shear).

8. The behaviour of stainless steel structures subjected to cyclic loading needs to be investigated to ascertain the potential of stainless steel usage in seismic region. Due to the inherent ductility of stainless steel, it seems reasonable to assume that utilising stainless steel for dissipative elements/joints in earthquake resisting structures will be beneficial, but this has to be verified experimentally and numerically.

9. Design rules for stainless steel joints at elevated temperatures (i.e. in fire conditions) need to be formulated, hence relevant experimental and numerical research is warranted.

10. All the above proposed tests need to be complemented by numerical modelling and parametric studies to allow design methods to be calibrated against a large number of data encompassing several configurations likely to occur in practice.

11. Alternatively to the continuous strength approach, different reliability indices leading to different partial safety factors can be adopted for the strength of failure modes associated with different levels of available ductility. This approach would be analogous to classifying joints in discrete behavioural groups according to their available ductility. In any case a quantification of the joint ductility as limited by bolt fracture is essential in determining a limit up to which strain-hardening can be safely exploited thus allowing for higher moments to be obtained.

12. Finally, the experimental results reported in Chapters 3 and 4 and the FE study reported in Chapter 5 demonstrated that stainless steel joints exhibit very high ultimate moment resistances and excellent ductility. Even though such high rotations and moment resistances cannot be practically utilized in conventional design scenarios, the high ductility and moment resistances of stainless steel components can arguably accommodate the significant ductility demands imposed by accidental actions such as a column loss scenario (Byfield et al., 2007). Hence utilising stainless steel for joints critical components that control the response of bolted moment resisting connections such as end plates, angle cleats and bolts can arguably lead to improved robustness of steel framed structures.

Chapter 8

References

- ABAQUS (2013) Theory Manual, ver 6.13,DASSAULT SYSTÈMES SIMULIA CORP Providence, RI, USA.
- Afshan, S. and Gardner, L. (2013) The continuous strength method for structural stainless steel design. Thin-Walled Structures, 68: 42-49.
- Afshan, S., Rossi, B. and Gardner, L. (2013) Strength enhancements in cold-formed structural sections—Part I: Material testing. Journal of Constructional Steel Research, 83: 177-188.
- Agerskov, H. (1976) High-strength bolted connections subject to prying. Journal of the Structural Division, 102: (ASCE, 11840).
- Agerskov, H. (1977) Analysis of bolted connections subject to prying. Journal of the Structural Division, 103: (ASCE 13352 Proceeding).
- AISC Design Guide 27 (2013) Structural Stainless Steel. American Institute of Steel Construction.
- Al-Jabri, K.S., Davison, J.B. and Burgess, I.W. (2008) Performance of beam-to-column joints in fire—a review. Fire Safety Journal, 43: (1): 50-62.

- AS/NZS 4673 (2001) Cold-formed stainless steel structures, AS/NZS4673. Sydney: Standards Australia

- Ashraf, M., Gardner, L. and Nethercot, D. (2006) Compression strength of stainless steel cross-sections. Journal of Constructional Steel Research, 62: (1-2): 105-115.

- Augusto, H., da Silva, L.S., Rebelo, C., et al. (2016) Characterization of web panel components in double-extended bolted end-plate steel joints. Journal of Constructional Steel Research, 116: 271-293.

- Azizinamini, A., Bradburn, J. and Radziminski, J. (1985) Static and cyclic behavior of semi-rigid steel beam-column connections. University of South Carolina.

- Azizinamini, A., Bradburn, J. and Radziminski, J. (1987) Initial stiffness of semi-rigid steel beam-to-column connections. Journal of Constructional Steel Research, 8: 71-90.

- Azizinamini, A., Shekar, Y. and Saadeghvaziri, M.A. (1995) Design of through beam connection detail for circular composite columns. Engineering structures, 17: (3): 209-213.

- Baddoo, N.R., 2008. Stainless steel in construction: A review of research, applications, challenges and opportunities. Journal of Constructional Steel Research, 64(11), pp.1199-1206.

- BADDOO, N.R., BURGAN, R. and OGDEN, R.G. (1997) rchitects' guide to stainless steel , p 179. The Steel Construction Institute, 46: (1): 179.

- Bagheri Sabbagh, A., Chan, T.M. and Mottram, J.T. (2013) Detailing of I-beam-to-CHS column joints with external diaphragm plates for seismic actions. Journal of Constructional Steel Research, 88: 21-33.

- Barnett, T.C., Tizani, W. and Nethercot, D.A. (2001) The practice of blind bolting connections to structural hollow sections: A review. Steel and Composite Structures, An International Journal, 1: (1): 1-16.

- Becque, J. and Rasmussen, K.J. (2009) Experimental investigation of the interaction of local and overall buckling of stainless steel I-columns. Journal of structural engineering, 135: (11): 1340-1348.

- Beg, D., Zupančič, E. and Vayas, I. (2002) On the rotation capacity of moment connections. Proceedings of the Third European Conference on Steel Structures, Eurosteel 2002, Coimbra, vol. II., p. 967–976.

- Beg, D., Zupančič, E. and Vayas, I., 2004. On the rotation capacity of moment connections. Journal of Constructional Steel Research, 60(3-5), pp.601-620.

- BOM fastener (2018) The Highest Strength Blind Fasteners in the World https://www.afshuck.net/us/uploads/pdfs/84106 BOM Brochure 203-02-18.pdf Last accessed on April 2018.

- Bouchaïr, A., Averseng, J. and Abidelah, A. (2008) Analysis of the behaviour of stainless steel bolted connections. Journal of Constructional Steel Research, 64: (11): 1264-1274.

- Braham, M. and Jaspart, J.-P. (2004) Is it safe to design a building structure with simple joints, when they are known to exhibit a semi-rigid behaviour? Journal of Constructional Steel Research, 60: (3-5): 713-723.

- Broderick, B. and Thomson, A. (2002) The response of flush end-plate joints under earthquake loading. Journal of Constructional Steel Research, 58: (9): 1161-1175.

- BS EN 10088-4 (2009) Stainless steels. Technical delivery conditions for sheet/plate and strip of corrosion resisting steels for construction purposes. BSI.

- BS EN 10088-5 (2009) Stainless steels. Technical delivery conditions for bars, rods, wire, sections and bright products of corrosion resisting steels for construction purposes. BSI.

- BS EN ISO 6892-1 (2016) Metallic materials. Tensile testing. Method of test at ambient temperature. BSI.

- Bursi, O.S. and Jaspart, J.P., 1998. Basic issues in the finite element simulation of extended end plate connections. Computers and structures, 69(3), pp.361-382.

- Byfield, M., Mudalige, W., Morison, C., et al. (2014) A review of progressive collapse research and regulations. Proceedings of the ICE-Structures and Buildings, 167: (8): 447-456.

- Byfield, M. and Paramasivam, S. (2007) Catenary action in steel-framed buildings. Proceedings of the Institution of Civil Engineers-Structures and Buildings, 160: (5): 247-257.

- Cai, Y. and Young, B. (2014a) Behavior of cold-formed stainless steel single shear bolted connections at elevated temperatures. Thin-Walled Structures, 75: 63-75.

- Cai, Y. and Young, B. (2014b) Structural behavior of cold-formed stainless steel bolted connections. Thin-Walled Structures, 83: 147-156.

- Cai, Y. and Young, B. (2015) High temperature tests of cold-formed stainless steel double shear bolted connections. Journal of Constructional Steel Research, 104: 49-63.

- Cai, Y. and Young, B. (2016) Bearing factors of cold-formed stainless steel double shear bolted connections at elevated temperatures. Thin-Walled Structures, 98: 212-229.

- Chan, S.L. and Chui, P.P.T. (1999) "Chapter 5 - Connection behaviour and models". In Chui, S.L.C.P.T. (Ed.) Non-Linear Static and Cyclic Analysis of Steel Frames with Semi-Rigid Connections. Oxford, Elsevier Science Ltd 93-121.

- Chan, T. and Gardner, L. (2008) Compressive resistance of hot-rolled elliptical hollow sections. Engineering structures, 30: (2): 522-532.

- Chasten, C.P., Lu, L.-W. and Driscoll, G.C. (1992) Prying and shear in end-plate connection design. Journal of structural engineering, 118: (5): 1295-1311.

- Chen, W.F., 2011. Semi-rigid connections handbook. J. Ross Publishing.

- Cruz, P.J., da Silva, L.S., Rodrigues, D.S., et al. (1998) Database for the semi-rigid behaviour of beam-to-column connections in seismic regions. Journal of Constructional Steel Research, 1: (46): 233-234.

- Da Silva, L.S. (2008) Towards a consistent design approach for steel joints under generalized loading. Journal of Constructional Steel Research, 64: (9): 1059-1075.

- da Silva, L.S. and Coelho, A.G. (2001a) An analytical evaluation of the response of steel joints under bending and axial force. Computers and Structures, 79: (8): 873-881.

- Da Silva, L.S. and Coelho, A.G. (2001b) A ductility model for steel connections. Journal of Constructional Steel Research, 57: (1): 45-70.

- Da Silva, L.S., de Lima, L.R., da SVellasco, P., et al. (2004) Behaviour of flush end-plate beam-to-column joints under bending and axial force. Steel and Composite Structures, 4: (2): 77-94.

- Daniūnas, A. and Urbonas, K. (2008) Analysis of the steel frames with the semi-rigid beam-to-beam and beam-to-column knee joints under bending and axial forces. Engineering structures, 30: (11): 3114-3118.

- Davison, J., Kirby, P. and Nethercot, D. (1987) Rotational stiffness characteristics of steel beam-to-column connections. Journal of Constructional Steel Research, 8: 17-54.

- Dawe, J.L. and Grondin, G.Y. (1990) W-SHAPE BEAM TO RHS COLUMN CONNECTIONS. Canadian Journal of Civil Engineering, 17: (5): 788-797.

- De Lima, L.R.O., da Silva, L.S., Vellasco, P.d.S., et al. (2004) Experimental evaluation of extended endplate beam-to-column joints subjected to bending and axial force. Engineering structures, 26: (10): 1333-1347.

- Del Savio, A., Nethercot, D., Vellasco, P.d.S., et al. (2009) Generalised component-based model for beam-to-column connections including axial versus moment interaction. Journal of Constructional Steel Research, 65: (8-9): 1876-1895.

- Douty, R.T. and McGuire, W. (1965) High strength bolted moment connections. Journal of the Structural Division, 91: (2): 101-128.

- Elflah, M., Theofanous, M. and Dirar, S. (2018a) Behaviour of stainless steel beam-to-column joints—Part 2 : numerical modelling parametric study. Journal of Constructional Steel Research.

- Elflah, M., Theofanous, M., Dirar, S., et al. (2018b) Behaviour of stainless steel beam-to-column joints—Part 1: Experimental investigation. Journal of Constructional Steel Research.

- Elghazouli, A.Y., Málaga-Chuquitaype, C., Castro, J.M. and Orton, A.H., 2009. Experimental monotonic and cyclic behaviour of blind-bolted angle connections. Engineering Structures, 31(11), pp.2540-2553.

- Elremaily, A. and Azizinamini, A. (2001) Experimental behavior of steel beam to CFT column connections. Journal of Constructional Steel Research, 57: (10): 1099-1119.

- EN1993-1-8 (2005) Eurocode 3: Design of steel structures – Part 1-8: Design of joints. EN 1993-1-8, British Standards Institution.
- EN 1993-1-1 (2005) Eurocode 3: Design of steel structures - Part 1.1: General rules and rules for building. CEN.
- EN 1993-1-2 (2005) Eurocode 3: Design of steel structures - Part 1-2: General rules – Structural fire design. . Brussels: European Committee for Standardization.
- EN 1998-1 (2004) Eurocode 8: Design of structures for earthquake resistance - Part 1: General rules, seismic actions and rules for buildings. . British Standards Institution, CEN.
- Errera, S.J., Popowich, D.W. and Winter, G. (1974) BOLTED AND WELDED STAINLESS STEEL CONNECTIONS. ASCE J Struct Div, 100: (ST6): 1279-1296.
- ESDEP (2011) ESDEP Course. http://fgg-web.fgg.uni-lj.si/ /pmoze/ESDEP/master/wg11/l0600.htm. Last acessed on April 2018.
- Faella, C., Piluso, V. and Rizzano, G. (1998) Experimental analysis of bolted connections: snug versus preloaded bolts. Journal of structural engineering, 124: (7): 765-774.
- Feng, R. and Young, B. (2008a) Experimental investigation of cold-formed stainless steel tubular T-joints. Thin-Walled Structures, 46: (10): 1129-1142.
- Feng, R. and Young, B. (2008b) Tests of concrete-filled stainless steel tubular T-joints. Journal of Constructional Steel Research, 64: (11): 1283-1293.
- Feng, R. and Young, B. (2009) Behaviour of concrete-filled stainless steel tubular X-joints subjected to compression. Thin-Walled Structures, 47: (4): 365-374.
- Feng, R. and Young, B. (2010) Tests and behaviour of cold-formed stainless steel tubular X-joints. Thin-Walled Structures, 48: (12): 921-934.

- Feng, R. and Young, B. (2011) Design of cold-formed stainless steel tubular T-and X-joints. Journal of Constructional Steel Research, 67: (3): 421-436.
- Feng, R. and Young, B. (2013) Stress concentration factors of cold-formed stainless steel tubular X-joints. Journal of Constructional Steel Research, 91: 26-41.
- FLOWDRILL (2018) FLOWDRILL http://amr-trading.com/?page id=395. Last accessed on April 2018.
- France, J.E., Davison, J.B. and Kirby, P.A. (1999a) Strength and rotational response of moment connections to tubular columns using flowdrill connectors. Journal of Constructional Steel Research, 50: (1): 1-14.
- France, J.E., Davison, J.B. and Kirby, P.A. (1999b) Strength and rotational stiffness of simple connections to tubular columns using flowdrill connectors. Journal of Constructional Steel Research, 50: (1): 15-34.
- Gardner, L. (2005) The use of stainless steel in structures. Progress in Structural Engineering and Materials, 7: (2): 45-55.
- Gardner, L. (2008) The continuous strength method Proceedings of the Institution of Civil Engineers - Structures and Buildings 2008 161:3, 127-133.
- Gardner, L. and Baddoo, N.R. (2006) Fire testing and design of stainless steel structures. Journal of Constructional Steel Research, 62: (6): 532-543.
- Gardner, L. and Nethercot, D. (2004a) Structural stainless steel design: a new approach. Structural Engineer, 82: 21-30.
- Gardner, L. and Nethercot, D.A. (2004b) Experiments on stainless steel hollow sections—Part 1: Material and cross-sectional behaviour. Journal of Constructional Steel Research, 60: (9): 1291-1318.

- Gardner, L. and Theofanous, M. (2008) Discrete and continuous treatment of local buckling in stainless steel elements. Journal of Constructional Steel Research, 64: (11): 1207-1216.

- Gedge, G. (2008) Structural uses of stainless steel — buildings and civil engineering. Journal of Constructional Steel Research, 64: (11): 1194-1198.

- Ghobarah, A., Mourad, S. and Korol, R.M. (1996) Moment-rotation relationship of blind bolted connections for HSS columns. Journal of Constructional Steel Research, 40: (1): 63-91.

- Giakoumelis, G. and Lam, D. (2004) Axial capacity of circular concrete-filled tube columns. Journal of Constructional Steel Research, 60: (7): 1049-1068.

- Girão Coelho, A.M., Bijlaard, F.S., Gresnigt, N., et al. (2004a) Experimental assessment of the behaviour of bolted T-stub connections made up of welded plates. Journal of Constructional Steel Research, 60: (2): 269-311.

- Girão Coelho, A.M., Bijlaard, F.S. and Kolstein, H. (2009) Experimental behaviour of high-strength steel web shear panels. Engineering structures, 31: (7): 1543-1555.

- Girão Coelho, A.M. and Bijlaard, F.S.K. (2007) Experimental behaviour of high strength steel end-plate connections. Journal of Constructional Steel Research, 63: (9): 1228-1240.

- Girão Coelho, A.M., Bijlaard, F.S.K. and Simões da Silva, L. (2004b) Experimental assessment of the ductility of extended end plate connections. Engineering structures, 26: (9): 1185-1206.

- Girão Coelho, A.M., Simões da Silva, L. and Bijlaard, F.S. (2006) Finite-element modeling of the nonlinear behavior of bolted T-stub connections. Journal of structural engineering, 132: (6): 918-928.

- Gomes, F., Jaspart, J.-P. and Maquoi, R. (1996) Moment capacity of beam-to-column minor-axis joints Proceedings of the IABSE Colloquium on Semi-Rigid Structural Connections., 319-326.

- Han, L.-H., Wang, W.-D. and Zhao, X.-L. (2008) Behaviour of steel beam to concrete-filled SHS column frames: Finite element model and verifications. Engineering structures, 30: (6): 1647-1658.

- Hasan, M.J., Ashraf, M. and Uy, B. (2017) Moment-rotation behaviour of top-seat angle bolted connections produced from austenitic stainless steel. Journal of Constructional Steel Research, 136: 149-161.

- Hoang, V.-L., Demonceau, J.-F. and Jaspart, J.-P. (2014) Resistance of through-plate component in beam-to-column joints with circular hollow columns. Journal of Constructional Steel Research, 92: 79-89.

- Hoang, V.L., Demonceau, J.-F. and Jaspart, J.-P. (2013) Innovative bolted beam-to-column joints in moment resistant building frame: from experimental tests to design guidelines. Application of High Strength Steels in Seismic Resistant Structures.

- ISO, B., 898-1 (2009), Mechanical properties of fasteners made of carbon steel and alloy steel–part I, bolts, screws and studs with specified property classes–coarse thread and fine pitch thread. British Standards Institute, London, UK.

- Ivanyi, M. (2000) "Semi-Rigid Connections in Steel Frames". In Ivanyi, M. and Baniotopoulos, C. (Eds.) Semi-Rigid Joints in Structural Steelwork. Springer Vienna 1-101.

- Jaspart, J.-P. (1988) Extending of the merchant-rankine formula for the assessment of the ultimate load of frames with semi-rigid joints. Journal of Constructional Steel Research, 11: (4): 283-312.

- Jaspart, J.-P. (2000) General report: session on connections. Journal of Constructional Steel Research, 55: (1-3): 69-89.
- Jaspart, J.-P. and Maquoi, R. (1990) Guidelines for the design of braced frames with semi-rigid connections. Journal of Constructional Steel Research, 16: 319-328.
- Jaspart, J.P. and Weynand, K., 2016. Design of Joints in Steel and Composite Structures: Eurocode 3: Design of Steel Structures, Part 1-8–Design of Joints, Eurocode 4: Design of Composite Steel and Concrete Structures, Part 1-1–General Rules and Rules for Buildings. ECCS.
- Jiang, J. (2018) Behavior and Design of T-Stubs to Tubular Column Joints in Tension. BEng research project,University of Birmingham, 2018
- Kim, T.S. and Kuwamura, H. (2007) Finite element modeling of bolted connections in thin-walled stainless steel plates under static shear. Thin-Walled Structures, 45: (4): 407-421.
- Kim, T.S. and Kuwamura, H. (2011) Numerical investigation on strength design and curling effect of mechanically fastened joints in cold-formed austenitic stainless steel. Materials and Design, 32: (7): 3942-3956.
- Kim, T.S., Kuwamura, H. and Cho, T.J. (2008) A parametric study on ultimate strength of single shear bolted connections with curling. Thin-Walled Structures, 46: (1): 38-53.
- Kishi, N. and Chen, W.-F. (1986) Data base of steel beam-to-column connections. Structural Engineering Area, School of Civil Engineering, Purdue University.
- Kishi, N. and Chen, W.-F. (1990) Moment-rotation relations of semirigid connections with angles. Journal of structural engineering, 116: (7): 1813-1834.
- Kishi, N., Hasan, R., Chen, W.F., et al. (1997) Study of Eurocode 3 steel connection classification. Engineering structures, 19: (9): 772-779.

- Kong, Z. and Kim, S.-E. (2017a) Moment-rotation model of single-web angle connections. International Journal of Mechanical Sciences, 126: 24-34.
- Kong, Z. and Kim, S.E. (2017b) Moment-rotation behavior of top-and seat-angle connections with double web angles. Journal of Constructional Steel Research, 128: 428-439.
- Korol, R.M., Ghobarah, A. and Mourad, S. (1993) Blind Bolting W-Shape Beams to Hss Columns. Journal of Structural Engineering-Asce, 119: (12): 3463-3481.
- Krawinkler, H. and Mohasseb, S. (1987) Effects of panel zone deformations on seismic response. Journal of Constructional Steel Research, 8: 233-250.
- Kurobane, Y. (2004) Design guide for structural hollow section column connections. Verlag TUV Rheinland.
- Kuwamura, H. and Isozaki, A. (2002) Ultimate behavior of fastener connections of thin stainless steel plates. Study on light-weight stainless steel structures part 4. Journal of Structural and Construction Engineering, (556): 159-166.
- Kuwamura, H. and Isozaki, A. (2001a). Experimental report on strength of bolted connections in thin-walled plates. Steel Structure Laboratory. The University of Tokyo, Japan. (In Japanese).
- Lee, J., Goldsworthy, H.M. and Gad, E.F. (2010) Blind bolted T-stub connections to unfilled hollow section columns in low rise structures. Journal of Constructional Steel Research, 66: (8-9): 981-992.
- Liew, A. and Gardner, L. (2015) Ultimate capacity of structural steel cross-sections under compression, bending and combined loading. Structures, 1: 2-11.
- LINDAPTER (2018) Lindapter Hollo-Bolt. https://www.youtube.com/watch?v=b1Dfn5AU-ac. Last accessed on April 2018.

- Liu, Y. (2012) Behaviour of Beam-to-tubular Column Connections under Extreme Loading Conditions,. PhD thesis,Department of Civil and Environmental Engineering,Imperial College London, London.

- Liu, Y., Malaga-Chuquitaype, C. and Elghazouli, A.Y. (2012a) Behaviour of beam-to-tubular column angle connections under shear loads. Engineering structures, 42: 434-456.

- Liu, Y., Malaga-Chuquitaype, C. and Elghazouli, A.Y. (2012b) Response and component characterisation of semi-rigid connections to tubular columns under axial loads. Engineering structures, 41: 510-532.

- Málaga-Chuquitaype, C. and Elghazouli, A. (2010a) Behaviour of combined channel/angle connections to tubular columns under monotonic and cyclic loading. Engineering structures, 32: (6): 1600-1616.

- Málaga-Chuquitaype, C. and Elghazouli, A. (2010b) Component-based mechanical models for blind-bolted angle connections. Engineering structures, 32: (10): 3048-3067.

- Maquoi, R., Naveau, X. and Rondal, J. (1984) Column welded stud connections. Journal of Constructional Steel Research, 4: 3–26.

- Massimo, L., Gianvittorio, R., Aldina, S., et al. (2014) Experimental analysis and mechanical modeling of T-stubs with four bolts per row. Journal of Constructional Steel Research, 101: 158-174.

- Mirambell, E. and Real, E. (2000) On the calculation of deflections in structural stainless steel beams: an experimental and numerical investigation. Journal of Constructional Steel Research, 54: (1): 109-133.

- Nair, R.S., Birkomoe, P. and Munse, W.H. (1974) High strength bolts subject to tension and prying. Journal of the Structural Division, 100: (st2).

- Nethercot, D. (1985) Steel Beam to Column Connections—A Review of Test Data and Their Applicability to the Evaluation of the Joint Behaviour of the Performance of Steel Frames. CIRIA, London, England.
- Nethercot, D. and Chen, W. (1988) Effects of connections on columns. Journal of Constructional Steel Research, 10: 201-239.
- Okazawa, S., Usami, T., Noguchi, H., et al. (2002) Three-dimensional necking bifurcation in tensile steel specimens. Journal of engineering mechanics, 128: (4): 479-486.
- Pask J W Manual on connections-for beam and column construction", BCSA Publication No 9/82.
- Piluso, V., Faella, C. and Rizzano, G. (2001a) Ultimate behavior of bolted T-stubs. I: Theoretical model. Journal of structural engineering, 127: (6): 686-693.
- Piluso, V., Faella, C. and Rizzano, G. (2001b) Ultimate behavior of bolted T-stubs. II: Model validation. Journal of structural engineering, 127: (6): 694-704.
- Pitrakkos, T. (2012) The tensile stiffness of a novel anchored blind-bolt component for moment-resisting connections to concrete-filled hollow sections. University of Nottingham.
- Pucinotti, R. (2001a) Top-and-seat and web angle connections: Prediction via mechanical model. Journal of Constructional Steel Research, 57: (6): 661-694.
- Pucinotti, R. (2001b) Top-and-seat and web angle connections: prediction via mechanical model. Journal of Constructional Steel Research, 57: (6): 663-696.
- Quach, W., Teng, J.G. and Chung, K. (2008) Three-stage full-range stress-strain model for stainless steels. Journal of structural engineering, 134: (9): 1518-1527.
- Rasmussen, K.J. (2003) Full-range stress–strain curves for stainless steel alloys. Journal of Constructional Steel Research, 59: (1): 47-61.

- Roeder, C.W., Cameron, B. and Brown, C.B. (1999) Composite action in concrete filled tubes. Journal of structural engineering, 125: (5): 477-484.
- Rossi, B. (2014) Discussion on the use of stainless steel in constructions in view of sustainability. Thin-Walled Structures, 83: 182-189.
- Rossi, B., Afshan, S. and Gardner, L. (2013) Strength enhancements in cold-formed structural sections—Part II: Predictive models. Journal of Constructional Steel Research, 83: 189-196.
- Ryan, I. (1999) Development of the use of stainless steel in construction. WP 4.2, ECSC Project No. 7210-SA, 327.
- Saliba, N. and Gardner, L. (2013) Cross-section stability of lean duplex stainless steel welded I-sections. Journal of Constructional Steel Research, 80: 1-14.
- Saliba, N., Real, E. and Gardner, L. (2014) Shear design recommendations for stainless steel plate girders. Engineering structures, 59: 220-228.
- Salih, E.L., Gardner, L. and Nethercot, D.A. (2010) Numerical investigation of net section failure in stainless steel bolted connections. Journal of Constructional Steel Research, 66: (12): 1455-1466.
- Salih, E.L., Gardner, L. and Nethercot, D.A. (2011) Bearing failure in stainless steel bolted connections. Engineering structures, 33: (2): 549-562.
- Salih, E.L., Gardner, L. and Nethercot, D.A. (2013) Numerical study of stainless steel gusset plate connections. Engineering structures, 49: 448-464.
- Salih, E.L.M. (2010) Analysis and design of stainless steel bolted connections. Department of Civil and Envrinonmental Engineering Imperial College London. PhD thesis.

- Schneider, S.P. and Alostaz, Y.M. (1998) Experimental behavior of connections to concrete-filled steel tubes. Journal of Constructional Steel Research, 45: (3): 321-352.

- SCI (2014) Joints in steel construction: Simple joints to Eurocode 3. The steel construction Institution.P358.

- SCI/BCSA (2005) British Constructional Steelwork Association Joints in Steel Construction: Moment Connections. Steel Construction Institute and the British Constructional Steelwork Association (P207).

- SCI/Euro Inox (1994) Design Manual For Structural Stainless Steel.Third edition. The Steel Construction Institute and Euro Inox, Building series„ Volume 3.

- SCI/Euro Inox (2006) Design Manual For Structural Stainless Steel.Third edition. The Steel Construction Institute and Euro Inox, Building series„ Volume 3.

- SEI/ASCE-8-02 (2002) Specification for the design of cold-formed stainless steel structural members. American Society of Civil Engineers (ASCE).

- Sherman, D. and Ales, J.M. (1991) The Design of Shear Tabs With Tubular Columns. AISC Proc. National Steel Construction Conference„ pp. 23-21 to 23-14.

- Simões Da Silva, L., Santiago, A. and Vila Real, P. (2002) Post-limit stiffness and ductility of end-plate beam-to-column steel joints. Computers and Structures, 80: (5-6): 515-531.

- Soo Kim, T. and Kuwamura, H. (2007) Finite element modeling of bolted connections in thin-walled stainless steel plates under static shear. Thin-Walled Structures, 45: (4): 407-421.

- Swanson, J.A., Kokan, D.S. and Leon, R.T. (2002) Advanced finite element modeling of bolted T-stub connection components. Journal of Constructional Steel Research, 58: (5-8): 1015-1031.

- Swanson, J.A. and Leon, R.T. (2000) Bolted steel connections: tests on T-stub components. Journal of structural engineering, 126: (1): 50-56.
- Swanson, J.A. and Leon, R.T. (2001) Stiffness modeling of bolted T-stub connection components. Journal of structural engineering, 127: (5): 498-505.
- Talja, A. and Torkar, M. (2014) Lap shear tests of bolted and screwed ferritic stainless steel connections. Thin-Walled Structures, 83: 157-168.
- Tao, Z., Hassan, M.K., Song, T.-Y., et al. (2017a) Experimental study on blind bolted connections to concrete-filled stainless steel columns. Journal of Constructional Steel Research, 128: 825-838.
- Tao, Z., Hassan, M.K., Song, T.Y., et al. (2017b) Experimental study on blind bolted connections to concrete-filled stainless steel columns. Journal of Constructional Steel Research, 128: 825-838.
- Theofanous, M., Chan, T. and Gardner, L. (2009) Structural response of stainless steel oval hollow section compression members. Engineering structures, 31: (4): 922-934.
- Theofanous, M. and Gardner, L. (2010) Experimental and numerical studies of lean duplex stainless steel beams. Journal of Constructional Steel Research, 66: (6): 816-825.
- Theofanous, M., Saliba, N., Zhao, O., et al. (2014) Ultimate response of stainless steel continuous beams. Thin-Walled Structures, 83: 115-127.
- Tizani, W., Al-Mughairi, A., Owen, J.S., et al. (2013) Rotational stiffness of a blind-bolted connection to concrete-filled tubes using modified Hollo-bolt. Journal of Constructional Steel Research, 80: 317-331.
- Tizani, W. and Pitrakkos, T. (2015) Performance of T-stub to CFT joints using blind bolts with headed anchors. Journal of structural engineering, 141: (10): 04015001.

- Urbonas, K. and Daniūnas, A. (2006) Behaviour of semi-rigid steel beam-to-beam joints under bending and axial forces. Journal of Constructional Steel Research, 62: (12): 1244-1249.

- van der Merwe, P. (1987) Development of design criteria for ferritic stainless steel cold-formed structural members and connections. University of Missouri-Rolla, USA.

- Wang, J.-F., Han, L.-H. and Uy, B. (2009) Behaviour of flush end plate joints to concrete-filled steel tubular columns. Journal of Constructional Steel Research, 65: (4): 925-939.

- Wang, Z.-Y. and Wang, Q.-Y. (2016) Yield and ultimate strengths determination of a blind bolted endplate connection to square hollow section column. Engineering structures, 111: 345-369.

- Wang, Z., Tizani, W. and Wang, Q. (2010) Strength and initial stiffness of a blind-bolt connection based on the T-stub model. Engineering structures, 32: (9): 2505-2517.

- Weynand, K. (1997) Sicherheits-und Wirtschaftlichkeitsuntersuchungen zur Anwendung nachgiebiger Anschlüsse im Stahlbau. RWTH Aachen, Lehrstuhl für Stahlbau. Dissertation, Schriftenreihe Stahlbau.

- Weynand, K., Huter, M., Kirby, P., et al. (1992) SERICON Databank on Joints in Building Frames. Proceedings of the 1st COST C1 Workshop.

- Weynand, K., Jaspart, J.-P. and Steenhuis, M. (1996) "-The stiffness model of revised annex j of eurocode 3". Connections in steel structures III. Elsevier 441-452.

- White , R.N. and Fang , P.J. (1966) Framing connections for square structural tubing. Journal of the Structural Division, American Society of Civil Engineering„ 92: 175–194.

- Wilkinson, S., Hurdman, G. and Crowther, A. (2006) A moment resisting connection for earthquake resistant structures. Journal of Constructional Steel Research, 62: (3): 295-302.

- Winter, G. (1956) Tests on bolted connections in light gage steel. Journal of the Structural Division, 82: (2): 1-25.

- Xu, Y., Kasai, K. and Mao, C. (2000) Experiment and analysis of bolted semi-rigid beam-column connections Part II: 3-D finite element analysis of the connections using angles. In Proceedings of the Third International Conference: STESSA 2000; Montreal, Canada„ 207-214.

- Yang, J., Sheehan, T., Dai, X.H., et al. (2015) Experimental study of beam to concrete-filled elliptical steel tubular column connections. Thin-Walled Structures, 95: 16-23.

- Yeomans, N. (1994) I-beam/rectangular hollow section column connections using the Flowdrill system. Proceedings Sixth International Symposium on Tubular Structures, Melbourne, Australia.

- Yeomans, N. (1996) "Flowdrill jointing system: Part 2—Structural hollow section connections". CIDECT 6F-13B/96.

- Yu, H., Burgess, I., Davison, J., et al. (2008) Numerical simulation of bolted steel connections in fire using explicit dynamic analysis. Journal of Constructional Steel Research, 64: (5): 515-525.

- Yuan, H.X., Hu, S., Du, X.X., et al. (2018) Experimental behaviour of stainless steel bolted T-stub connections under monotonic loading. Journal of Constructional Steel Research.

- Yun, X. and Gardner, L., 2017. Stress-strain curves for hot-rolled steels. Journal of Constructional Steel Research, 133, pp.36-46.

- Zanon, P. and Zandonini, R. (1988) Experimental analysis of end plate connections. Proceedings of the state of the art workshop on connections and the behaviour of strength and design of steel structures, Cachan, 10: 41-51.

- Zoetemeijer, P. (1974) A design method for the tension side of statically loaded, bolted beam-to-column connections. HERON, 20 (1), 1974.